# DYNAMICS AND GEOMETRY IN ULTRACOLD ATOMS

by

**Chenwei Lv**

**A Dissertation**

*Submitted to the Faculty of Purdue University*

*In Partial Fulfillment of the Requirements for the degree of*

**Doctor of Philosophy**

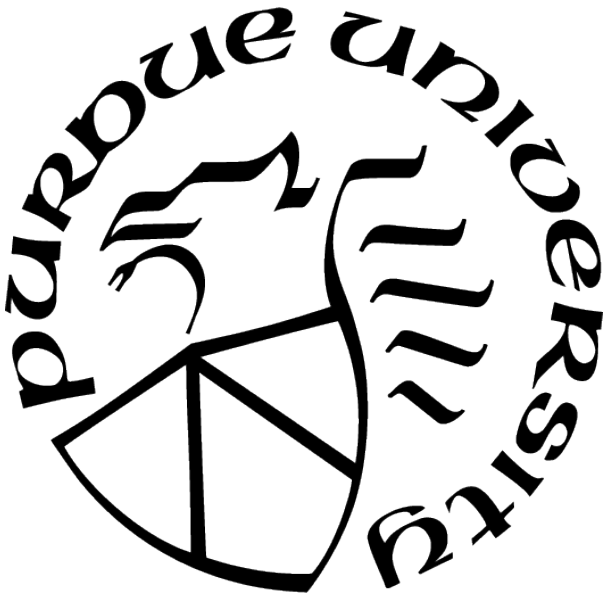


Department of Physics and Astronomy

West Lafayette, Indiana

August 2022

# THE PURDUE UNIVERSITY GRADUATE SCHOOL
# STATEMENT OF COMMITTEE APPROVAL

**Dr. Qi Zhou, Chair**

Department of Physics and Astronomy

**Dr. Christopher H. Greene**

Department of Physics and Astronomy

**Dr. Chen-Lung Hung**

Department of Physics and Astronomy

**Dr. Martin Kruczenski**

Department of Physics and Astronomy

**Approved by:**

Dr. Gabor A. Csathy

# ACKNOWLEDGMENTS

First and foremost, I would like to express my sincere gratitude to my supervisor, Professor Qi Zhou for his continuous support, patient guidance, and invaluable advice during my graduate study. His way of thinking, the logical flow, and the clarity of each detail in solving physical problems would influence and benefit me throughout my future research works.

I would also like to thank my collaborators, Changyuan Lyu, Sayan Choudhury, Mingyuan He, Professor Yangqian Yan, and Professor Ren Zhang, from whom I learned a lot regarding how theoretical research should be conducted: combining thorough theoretical calculations, concrete numerical results, and physical understanding from multiple perspectives always leads to good theoretical work.

I also wish to show my appreciation to my instructors during my graduate study and my committee members, Professor Chris Greene, Professor Martin Kruczenski, Professor Chen-Lung Hung, Professor Sergei Khlebnikov, Professor Erica Carlson, and Professor Nima Lashkari. Furthermore, I would also like to thank my undergraduate advisor Professor Renbao Liu, who led me into physics research.

Finally, I would like to express my thanks to my parents and friends for their support and understanding. Five years of graduate study has been a long but short start to theoretical work, and their support has enabled me to devote myself to my research and life down-to-earthly and to move forward with more confidence.

# TABLE OF CONTENTS

# LIST OF TABLES

# LIST OF FIGURES

# ABSTRACT

The rapid developments in technique bring simulation of quantum dynamics and precise coherence control to a new regime. The Atomic Molecular and Optical (AMO) platform provides a highly tunable means to control unitary and non-unitary time evolution. While the dissipation causes decoherence of a quantum system and is undesired in conventional understanding, manipulating dissipation in a controllable manner allows us to access a variety of peculiar non-Hermitian phenomena. This dissertation focuses on emergent geometry from $SU(1,1)$ symmetry and non-Hermitian physics, two highly entangled concepts with different realizations in the AMO system. Like $SU(2)$ symmetry, a fundamental symmetry in various physical systems, $SU(1,1)$ symmetry plays an important role in coherent control of quantum dynamics, dynamical instability, emergent curved space, and non-Hermitian phenomena. In Chapters 2 and 3, we show how different geometric structures, including hyperbolic spaces and anti-de Sitter spacetimes, are generated by $SU(1,1)$ symmetry. We also discuss several examples of coherent control of quantum systems based on their geometric representations. In Chapters 4 and 5, we move on to non-Hermitian physics. Chapter 4 discusses the quantum simulation of curved space in lattice systems. On the one hand, we demonstrate the simulation of any Riemann surfaces using a lattice system with tunable tunnelings. In particular, we consider hyperbolic spaces and show the emergences of the Efimov-like state and funneling effect on lattices. On the other hand, we build a duality between curved space and the non-Hermitian system, using a non-Hermitian generalization of the tight-binding model with chiral tunneling as an example. This duality and the highly controllable ultracold systems in laboratories allow experimentalists to simulate curved spaces using dissipation. Chapter 5 studies dissipations in ultracold molecules. While the ultracold molecules intrinsically suffer from losses caused by reaction or formation of complexes, we show that universality exists in ultracold reactive molecules. We apply contacts, a central quantity that captures many-body correlations in dilute quantum systems, to establish universal relations between various physical observables in reactive molecules. Ultracold molecules have emerged as a powerful platform in quantum simulation. The universal relations, which hold for any particle number, temperature, or interaction strength, provide physicists with a unique tool to

explore and engineer ultracold molecules. In Chapter 6, we also point out that the unit rate of reaction of ultracold molecules at a short distance amounts to a perfect event horizon. The characteristic length scale of the intermolecular potential plays the role of the horizon's radius. Therefore, the highly controllable ultracold molecules can be implemented as a simulator of black hole physics.

# 1. INTRODUCTION

Dynamical systems have attracted great attention from academia in the long history of scientific study. The Hamiltonian equation of motion was first introduced to describe dynamics in classical systems. The physical observable $v$, as a function of the canonical coordinates $q_{\mathrm{i}}$ and momenta $p_{\mathrm{i}}$, evolves according to its Poisson bracket with the system's Hamiltonian,

$$\frac{\mathrm{d}}{\mathrm{d}t}v(q_{\mathrm{i}},p_{\mathrm{i}})=\{v,H\}. \tag{1.1}$$

Canonical quantization [ ] leads to the Heisenberg equation of motion,

$$\mathrm{i}\hbar\frac{\mathrm{d}}{\mathrm{d}t}\hat{v}=[\hat{v},\hat{H}] \tag{1.2}$$

which describes the dynamics of observables in a quantum system. The Schrödinger representation, equivalent to the Heisenberg equation of motion, simplifies the dynamical problem by changing the dynamical variables into a quantum state that lives in the Hilbert space. The Schrödinger equation that describes the dynamics of the state is written as

$$\mathrm{i}\hbar\frac{\partial}{\partial t}\left|\psi\right\rangle=\hat{H}\left|\psi\right\rangle. \tag{1.3}$$

Despite its historical development, it is widely believed that quantum dynamics is more fundamental, and classical motions should be regarded as its limit as $\hbar\to 0$. On the one hand, the introduction of Hilbert space and the time evolutions as trajectories over this space have profoundly impacted people's understanding of the quantum system. Since the dynamical variables now live in the Hilbert space, the topology and geometric properties of Hilbert space influence the behavior of the quantum system. On the other hand, the linearity of Eq. ( ) provided us with a powerful group-theoretical method to characterize the system's dynamics. This dissertation focuses on the geometric properties with the group-theoretical approach. When a time-dependent Hamiltonian is considered, an initial state evolves as

$$\left|\psi(t)\right\rangle=\mathrm{e}^{-\mathrm{i}\hat{H}(t-dt)dt/\hbar}\mathrm{e}^{-\mathrm{i}\hat{H}(t-2dt)dt/\hbar}\ldots\mathrm{e}^{-\mathrm{i}\hat{H}(0)dt/\hbar}\left|\psi(0)\right\rangle=\mathcal{T}\mathrm{e}^{-\mathrm{i}\int_0^t\hat{H}(t)dt/\hbar}\left|\psi(0)\right\rangle, \tag{1.4}$$

where $\mathcal{T}$ is the time-ordering operator, $\mathcal{T}e^{-i\int_0^t \hat{H}(t)dt/\hbar} = \hat{U}(t,0)$ is the time evolution operator, or propagator. When the time-dependent Hamiltonian preserves certain symmetry, a dynamical symmetry emerges. The quantum dynamics are then mapped to the corresponding dynamical symmetry group.

### 1.1 Non-Unitary Quantum Dynamics

Inevitable system environment coupling in quantum systems causes dissipation and decoherence. Historically, the dissipation during the scattering process has been introduced by non-Hermitian Hamiltonians through the Feshbach projection approach [ ], [ ]. Developments in quantum optics have provided us with another well-established approach, the quantum master equation, that captures the dissipation and decoherence [ ]. To describe the dissipation and decoherence using the master equation, we first write the Schrödinger equation into the Liouville form

$$i\hbar\frac{\partial}{\partial t}\hat{\rho}_T = [\hat{H}_T, \hat{\rho}_T], \tag{1.5}$$

where $\hat{\rho}_T = |\psi\rangle\langle\psi|$ and $\hat{H}_T$ are the pure state density matrix and Hamiltonian of the total system, including the environment and the quantum system we want to study. All physical observables of the quantum system are only captured by a reduced density matrix which is obtained by tracing out the environment's degree of freedom in $\hat{\rho}_T$. The reduced density matrix of the quantum system, defined as $\hat{\rho} = \mathrm{Tr}_{\mathrm{env}}(\hat{\rho}_T) = \sum_n \langle n|\hat{\rho}_T|n\rangle$, where $|n\rangle$ is a set of orthogonal basis of the environment, satisfies the following equation

$$i\hbar\frac{\partial}{\partial t}\hat{\rho} = \mathrm{Tr}_{\mathrm{env}}\Big([\hat{H}_T, \hat{\rho}_T]\Big). \tag{1.6}$$

Although we arrive at a differential equation that describes the dynamics of the interested system, the solution to Eq. (  ) in general is quite involved. We, therefore, seek an approximation of Eq. (  ), which can capture the system's dynamics when certain conditions are met. The Markov approximation is a reasonable assumption in most physical systems. The Markov approximation is validated when the memory effect is negligible in the environment.

More precisely, the characteristic timescales of the decay of the environment correlation functions are much smaller than the timescale of system evolution [ ]. Under Markov approximation, the dynamical equation of $\rho$ can, in general, be written into the Markovian quantum master equation in its Lindblad form,

$$\mathrm{i}\hbar\frac{\partial}{\partial t}\hat{\rho} = [\hat{H},\hat{\rho}] + \mathrm{i}\sum\nolimits_{\mathrm{j}} \gamma_{\hat{A}_{\mathrm{j}}}\mathcal{D}_{\hat{A}_{\mathrm{j}}}(\hat{\rho}), \quad \mathcal{D}_{\hat{A}_{\mathrm{j}}}(\hat{\rho}) = \hat{A}_{\mathrm{j}}\hat{\rho}\hat{A}_{\mathrm{j}}^{\dagger} - \frac{1}{2}\{\hat{\rho},\hat{A}_{\mathrm{j}}^{\dagger}\hat{A}_{\mathrm{j}}\}, \tag{1.7}$$

where $\gamma_{\hat{A}}\mathcal{D}_{\hat{A}}$ captures the dissipation and decoherence effects introduced by the system-environment coupling. In general, a summation of a complete set of operator $\hat{A}_{\mathrm{j}}$ needs to be included. However, when the system-environment interaction is known and under certain conditions, for instance, when the system-environment coupling is either strong or weak, both $\gamma_{\hat{A}}$ and $\hat{A}$ can be explicitly evaluated.

Here, we consider a continuous $\hat{A}_{\mathrm{j}} = \hat{\psi}(x)$, which annihilates a particle at location $x$. Then the quantum master equation becomes

$$\mathrm{i}\hbar\frac{\partial}{\partial t}\hat{\rho} = [\hat{H},\hat{\rho}] + \mathrm{i}\int dx\gamma(x)\Big(\hat{\psi}(x)\hat{\rho}\hat{\psi}^{\dagger}(x) - \frac{1}{2}\{\hat{\rho},\hat{\psi}^{\dagger}(x)\hat{\psi}(x)\}\Big), \tag{1.8}$$

It is worth mention that, if the total particle number is conserved by $\hat{H}$ and the initial state has a definite particle number $N$, we can project the dynamics to the $N$ particle sector,

$$\mathrm{i}\hbar\frac{\partial}{\partial t}\hat{\rho}_N = [\hat{H},\hat{\rho}_N] + \mathrm{i}\int dx\gamma(x)\Big(-\frac{1}{2}\{\hat{\rho}_N,\hat{\psi}^{\dagger}(x)\hat{\psi}(x)\}\Big). \tag{1.9}$$

Dynamics of $\hat{\rho}_N$ is well described by a non-Hermitian Hamiltonian,

$$\hat{H}_{\mathrm{nh}} = \hat{H} - \frac{1}{2}\mathrm{i}\int dx\gamma(x)\hat{\psi}^{\dagger}(x)\hat{\psi}(x). \tag{1.10}$$

$-\mathrm{i}\gamma(x)/2$ now resembles an imaginary potential which captures the single particle loss at short times.

At high temperatures, the system environment coupling leads to rapid loss of particles and decreases in quantum coherence, such that the system quickly approaches a thermal density matrix. However, in the ultracold system, the coherence is preserved at a longer

timescale, such that the interplay between unitary evolution and decoherence becomes an important subject, motivates the studies of non-Hermitian system. We hereby introduce some intriguing properties of non-Hermitian Hamiltonian. A non-Hermitian Hamiltonian satisfies $\hat{H}_{\rm nh}^{\dagger} \neq \hat{H}_{\rm nh}$ is distinct from the Hermitian Hamiltonian we are familiar with. For instance, the eigenenergy is no longer necessarily real, and the eigenstates are no longer orthogonal to each other. Instead, we need to define the right and left eigenvectors for a non-Hermitian Hamiltonian $\hat{H}_{\rm nh}$, which satisfy

$$\hat{H}_{\rm nh} \left|\psi_{\rm R}\right\rangle = E \left|\psi_{\rm R}\right\rangle, \quad \hat{H}_{\rm nh}^{\dagger} \left|\psi_{\rm L}\right\rangle = E^{*} \left|\psi_{\rm L}\right\rangle, \tag{1.11}$$

where $*$ denotes complex conjugation. While $\hat{H}_{\rm nh}$ can be decomposited into

$$\hat{H}_{\rm nh} = \sum_{\rm j} E_{\rm j} \left|\psi_{\rm R,j}\right\rangle \left\langle\psi_{\rm L,j}\right|, \tag{1.12}$$

the orthogonal condition now involves both the left and right eigenvectors, $\langle\psi_{\rm L,i}|\psi_{\rm R,j}\rangle = \delta_{\rm ij}$. Although the non-Hermitian Hamiltonian seems can be any operator without constraints, rich physics emerges when the non-Hermitian Hamiltonian respects the PT symmetry. A non-Hermitian Hamiltonian has PT symmetry when it is invariant under a combination of parity $\mathcal{P}$ and time reversal $\mathcal{T}$ transformation. A simplest PT symmetric system is a coupled two-sites system with gain and loss on each site. The Hamiltonian of this system is written as

$$\hat{H}_{\rm PT} = \begin{pmatrix} a + {\rm i}b & g \\ g & a - {\rm i}b \end{pmatrix} = a\sigma_0 + g\sigma_x + {\rm i}b\sigma_z, \tag{1.13}$$

where $\sigma_0$ is the identity matrix and $\sigma_{x,y,z}$ are Pauli matrices. $\hat{H}_{\rm PT}$ is non-Hermitian and we can easily check its complex eigenvalues and the orthogonal conditions between left and right eigenvectors. $\hat{H}_{\rm PT}$ also exhibits PT symmetry, $(\mathcal{PT})^{-1}\hat{H}_{\rm PT}\mathcal{PT} = \hat{H}_{\rm PT}$. While $\mathcal{P} = \sigma_x$ exchanges two sites, $\mathcal{T}$ is antilinear and performs complex conjugation. PT symmetry provides

powerful constraints on the eigenenergies of the system. Suppose $|\psi\rangle$ is an eigenstate of $\hat{H}_{\rm PT}$ with eigenenergy $E$, $\mathcal{PT}|\psi\rangle$ must also be an eigenstate with eigenenergy $E^*$, according to

$$\hat{H}_{\rm PT}\mathcal{PT}|\psi\rangle = \mathcal{PT}\hat{H}_{\rm PT}|\psi\rangle\,. \tag{1.14}$$

If $\mathcal{PT}|\psi\rangle$ is the same state as $|\psi\rangle$, the eigenenergy is real $E = E^*$. We conclude PT symmetry is preserved by $|\psi\rangle$ or PT symmetry is unbroken. If these two states are different, PT symmetry is broken, and the eigenenergies come in complex conjugate pairs. In this sense, PT symmetry protects the reality of eigenenergies. PT symmetry transition only occurs when two or more eigenenergies degenerate, known as the exceptional point. Unlike degenerate eigenstates in the Hermitian system, eigenstates coalesce at an exceptional point. All these results are captured by the simplest model $\hat{H}_{\rm PT}$ in Eq. (  ), where the eigenenergies and the corresponding eigenstates are

$$E_\pm = a \pm \sqrt{g^2 - b^2}, \quad |\psi_{R,\pm}\rangle = \begin{pmatrix} b\mathrm{i} \pm \sqrt{g^2 - b^2} & g \end{pmatrix}^T. \tag{1.15}$$

While the Hamiltonian respects the PT symmetry for any $a, b$ and $g$, the system signifies the PT symmetry breaking when $g = b$.

## 1.2 Ultracold Quantum Gases

As a new phase of matter, Bose-Einstein condensate (BEC) was predicted by Einstein in 1924 based on the bosonic statistics of identical particles and realized at JILA in ultracold dilute Rb atomic cloud at 170nK using laser cooling in 1995 [ ]. In the past few decades, BEC has been realized in different atoms, molecules or quasi-particles and also in reduced dimensions [ ]–[  ]. Realizations of BEC in various systems extensively enrich the controllability of many-body quantum systems for physicists to explore coherent quantum dynamics and exotic quantum phases.

The bosonic statistics of the identical non-interacting particle leads to the boson number in a state with quantum number $v$ and energy $\epsilon_v$

$$n(\epsilon_v;\mu,T)=\frac{1}{\mathrm{e}^{(\epsilon_v-\mu)/k_BT}-1}, \tag{1.16}$$

where $\mu$ is the chemical potential, $T$ is the temperature. BEC occurs when the total boson number exceeds a temperature-dependent critical value, beyond which the ground state begins to have a macroscopic occupation, and $\mu$ becomes the ground state energy $\epsilon_0$. Since the maximal number of bosons that can be hosted in the excited states is

$$N_{\mathrm{ex}}(T_c)=\int_{\epsilon=\epsilon_0}^{\infty}g(\epsilon)n(\epsilon;\epsilon_0,T_c)d\epsilon, \tag{1.17}$$

where $g(\epsilon)$ is the density of state, characterizing the number of states within energy interval $(\epsilon,\epsilon+d\epsilon)$. For instance, the density of states for bosons in $n$-dimensional free space with volume $V$ and isotropic harmonic trap with frequency $\omega$ are

$$g_{\mathrm{nD,\,free}}(\epsilon)=\frac{V}{(2\pi)^{n/2}\Gamma(n/2)}\left(\frac{m}{\hbar^2}\right)^{\frac{n}{2}}\epsilon^{\frac{n}{2}-1},\quad g_{\mathrm{nD,\,trap}}(\epsilon)=\frac{1}{\Gamma(n)(\hbar\omega)^n}\epsilon^{n-1}, \tag{1.18}$$

respectively, where $\Gamma(x)$ denotes the Gamma function, $m$ is the boson's mass. Condensation occurs at temperature $T_c$ when the total boson number is larger than $N_{\mathrm{ex}}(T_c)$. In 3-dimensional free space and isotropic harmonic trap with frequency $\omega$, this number becomes

$$N_{\mathrm{ex,free}}(T_c)=2.61\frac{V}{\lambda_{\mathrm{th}}(T_c)^3},\quad N_{\mathrm{ex,trap}}(T_c)=1.2\left(\frac{k_BT_c}{\hbar\omega}\right)^3, \tag{1.19}$$

where $\lambda_{\mathrm{th}}(T)=\sqrt{2\pi\hbar^2/(mk_BT)}$ is the thermal de Broglie wavelength.

After the condensation, the ground state of the quantum system has a macroscopic occupation, and the coherence of the quantum state turns into the off-diagonal long-range order. It is useful to consider the zero-temperature limit where the quantum nature of the many-body system is the most profound. At zero temperature, all particles condensate

into the ground state, and we can model the quantum state of the many body system as a coherent state,

$$|\psi\rangle = \mathrm{e}^{\alpha \int d\mathbf{x}\psi_{\mathrm{gs}}(\mathbf{x})\hat{\psi}^{\dagger}(\mathbf{x})}\,|0\rangle\,, \tag{1.20}$$

where $\psi_{\mathrm{gs}}(\mathbf{x})$ is the ground state wavefunction normalized to unity, $\psi^{(\dagger)}(\mathbf{x})$ is the bosonic annihilation (creation) operator satisfying $[\psi(\mathbf{x}), \psi^{\dagger}(\mathbf{x})] = \delta(\mathbf{x}-\mathbf{x})$, and $|0\rangle$ is the many-body vacuum state. $|\alpha|^2 = N$ characterizes the total boson number. The off-diagonal term of one-body correlation function $n^{(1)}(\mathbf{x},\mathbf{y})$ characterizes quantum coherence between different locations, and it is of order $N$ even at large separation $|\mathbf{x}-\mathbf{y}|$. $n^{(1)}(\mathbf{x},\mathbf{y})$ for $|\psi\rangle$ reads

$$n^{(1)}(\mathbf{x},\mathbf{y}) = \mathrm{Tr}(\hat{\psi}^{\dagger}(\mathbf{x})\hat{\psi}(\mathbf{y})\,|\psi\rangle\,\langle\psi|) = N\psi^{*}_{\mathrm{gs}}(\mathbf{x})\psi_{\mathrm{gs}}(\mathbf{y}), \tag{1.21}$$

$n^{(1)}(\mathbf{x},\mathbf{y})|_{|\mathbf{x}-\mathbf{y}|\to\infty} \to N/V$ for BEC in free space.

We have been so far considering non-interacting bosonic gases. We will include the interaction effect in the following part of this section. Since BEC formed in laboratories is dilute such that the interaction effect is minimized, we will focus on the two-body interaction. The Schrödinger equation of two particles denoted by $\mathbf{r}_1$ and $\mathbf{r}_2$ with interaction $V(\mathbf{r}_1-\mathbf{r}_2)$ is written as

$$\left(-\frac{\hbar^2}{2m}\nabla_1^2 - \frac{\hbar^2}{2m}\nabla_2^2 + V(\mathbf{r}_1-\mathbf{r}_2)\right)\Psi(\mathbf{r}_1,\mathbf{r}_2) = E\Psi(\mathbf{r}_1,\mathbf{r}_2). \tag{1.22}$$

The Schrödinger equation can be separated into relative and center of mass motion in the absence of external trapping potential by $\Psi(\mathbf{r}_1,\mathbf{r}_2) = \psi_{\mathrm{rel}}(\mathbf{r})\Psi_{\mathrm{CM}}(\mathbf{R})$, where $\mathbf{r} = \mathbf{r}_1 - \mathbf{r}_2$, $\mathbf{R} = (\mathbf{r}_1+\mathbf{r}_2)/2$. While $\Psi_{\mathrm{CM}}(\mathbf{R})$ satisfies the Schrödinger equation of free particles with mass $2m$, the relative motion along radial direction satisfies

$$\left(-\frac{\hbar^2}{m}\frac{1}{r^2}\frac{\partial}{\partial r}\left(r^2\frac{\partial}{\partial r}\right) + \frac{\hbar^2}{m}\frac{1}{r^2}l(l+1) + V(r)\right)\psi_{\mathrm{rel}}(r) = E\psi_{\mathrm{rel}}(r). \tag{1.23}$$

We have assumed an isotropic interaction and defined $\psi_{\mathrm{rel}}(r,\theta,\varphi) = \psi_{\mathrm{rel}}(r)Y_{lm}(\theta,\varphi)$, $Y_{lm}(\theta,\varphi)$ is the spherical harmonics. The angular part leads to a centrifugal potential barrier $\frac{\hbar^2}{m}\frac{1}{r^2}l(l+1)$ for $l$-th partial wave. In the absence of two-body bound states, the finite-range inter-

action effect is purely captured by the phase shift of the asymptotic relative wavefunctions at $r \to \infty$ in different partial wave $l$. Without loss of generality, we consider the relative wave vector pointing towards the $\hat{z}$-direction. Using the partial wave expansion, the relative wavefunction of two non-interacting particles with relative $\mathbf{k} = k\hat{z}$ is written as

$$\psi_{\mathrm{rel,\,non-int}}(\mathbf{r}) = \mathrm{e}^{\mathrm{i}kz} \xrightarrow{r\to\infty} \sum_{l=0}^{\infty}(2l+1)\mathrm{i}^l \frac{\sin(kr - l\boldsymbol{\pi}/2)}{kr} P_l(\cos(\theta)) \tag{1.24}$$

where $P_l(x)$ is the Legendre polynomial of degree $l$. When the isotropic interaction is included, we have

$$\psi_{\mathrm{rel,\,int}}(\mathbf{r}) \xrightarrow{r\to\infty} \sum_{l=0}^{\infty}(2l+1)\mathrm{i}^l \mathrm{e}^{\mathrm{i}\delta_l} \frac{\sin(kr - l\boldsymbol{\pi}/2 + \delta_l)}{kr} P_l(\cos(\theta)), \tag{1.25}$$

where $\delta_l$ is the phase shift in $l$-th partial wave, which appears due to the interaction effect. A finite $\delta_l$ leads to the scattering cross section

$$\sigma = \frac{4\boldsymbol{\pi}}{k^2}\sum_{l=0}^{\infty}(2l+1)\sin^2(\delta_l), \tag{1.26}$$

characterizing the probability of elastic scattering event to happen between two particles. Because of the centrifugal barrier in higher partial wave scattering, the phase shift $\delta_l$ scales with $k$ as $k^{2l+1}$ for small $k$ at ultracold temperatures, known as the Wigner's threshold law. An explicit example showing this relation is given by a square-well interaction, where $V(r) = -\hbar^2\alpha^2/(mr_0^2)$ for $r < r_0$ and $V(r) = 0$ otherwise. In this case, the scattering phase shift becomes

$$\delta_l^{\text{square well}} = \arctan\left(\frac{\kappa \mathrm{j}_l(kr_0)\mathrm{j}_{l-1}(\kappa r_0) - k\mathrm{j}_{l-1}(kr_0)\mathrm{j}_l(\kappa r_0)}{\kappa y_l(kr_0)\mathrm{j}_{l-1}(\kappa r_0) - k y_{l-1}(kr_0)\mathrm{j}_l(\kappa r_0)}\right), \tag{1.27}$$

where $\kappa^2 = k^2 + \alpha^2/r_0^2$, $\mathrm{j}_l(x)$ and $y_l(x)$ are the $l$-th order spherical Bessel function of the first and second kind, respectively. By applying Taylor expansion to the leading order, we find

$$\delta_l^{\text{square well}}(k) = \frac{\boldsymbol{\pi}\mathrm{j}_{l+3/2}(\alpha)}{2^{2l+1}\mathrm{j}_{l-1/2}(\alpha)\Gamma(1/2+l)\Gamma(3/2+l)}(kr_0)^{2l+1}. \tag{1.28}$$

The scaling $\delta_l(k) \propto k^{2l+1}$ allows us to consider only the $s$-wave scattering in ultracold dilute Bose gases in the absence of higher partial wave resonances. While the $l$-th wave resonance occurs, for example, when the prefactor in Eq. (  ) diverges. For $s$-wave scattering, the interaction can be replaced by a zero-range contact interaction $V(r) = V_0\delta(r)$, $V_0 = 4\pi\hbar^2 a/m$ [  ]. Here we have introduced the $s$-wave scattering length $a$, which is related to the $s$-wave phase shift by $k\cot(\delta_0) = -1/a$. This effective interaction and mean-field approximation allow us to describe the condensate at ultracold temperatures.

Having introduced the zero-range effective interaction for $s$-wave scattering, we can write the Hamiltonian of the ultracold dilute Bose gases into the following form

$$\hat{H} = \int d\mathbf{x}\left(\frac{\hbar^2}{2m}\nabla\hat{\psi}^\dagger\nabla\hat{\psi} + \frac{V_0}{2}\hat{\psi}^\dagger\hat{\psi}^\dagger\hat{\psi}\hat{\psi} + V(\mathbf{x})\hat{\psi}^\dagger\hat{\psi}\right). \tag{1.29}$$

The second term captures the zero-range contact interaction. Similar to the non-interacting case, the ground state could be obtained by the mean field ansatz in writing the many-body state into a coherent state,

$$|\psi\rangle = \mathrm{e}^{\alpha\int d\mathbf{x}\psi_0(\mathbf{x})\hat{\psi}^\dagger(\mathbf{x})}\,|0\rangle\,. \tag{1.30}$$

Instead of $\psi_{\mathrm{gs}}(\mathbf{x})$ being the single particle ground state in the non-interacting case, $\Psi(\mathbf{x}) \equiv \alpha\psi_0(\mathbf{x})$ now becomes an order parameter of the condensate. The order parameter can be evaluated by the expectation value of $\hat{\psi}$, $\Psi(\mathbf{x}) = \langle\psi|\,\hat{\psi}(\mathbf{x})\,|\psi\rangle$. The expectation value of Hamiltonian is written as

$$E[\Psi] = \langle\psi|\,\hat{H}\,|\psi\rangle = \int d\mathbf{x}\left(\frac{\hbar^2}{2m}|\nabla\Psi|^2 + \frac{V_0}{2}|\Psi|^4 + V(\mathbf{x})|\Psi|^2\right). \tag{1.31}$$

Minimizing this energy functional leads to $\Psi$ of the approximated ground state.

Meanwhile, we can calculate the dynamics of the order parameter field by assuming the mean field wavefunction Eq. (  ) holds within the time interval we are interested in of

the BEC dynamics. We, therefore, have $\Psi(\mathbf{x},t) = \langle\psi(t)|\,\hat{\psi}(\mathbf{x})\,|\psi(t)\rangle$ for any $t$. Using the Heisenberg equation of motion, we can write

$$\mathrm{i}\hbar\partial_t\Psi(\mathbf{x},t) = \langle\psi|\,[\hat{\psi}(\mathbf{x},t),\hat{H}]\,|\psi\rangle = -\frac{\hbar^2}{2m}\nabla^2\Psi(\mathbf{x},t) + V_0|\Psi(\mathbf{x},t)|^2\Psi(\mathbf{x},t) + V(\mathbf{x})\Psi(\mathbf{x},t). \tag{1.32}$$

This is the Gross-Pitaevskii equation capturing the dynamics of an ultracold dilute Bose gas.

Here we take an alternative approach to capture the dynamics of interacting ultracold dilute Bose gases in free space. We first apply a Fourier transform to the field operator $\hat{\psi}(\mathbf{x}) = \frac{1}{V^{1/2}}\sum_{\mathbf{k}} \mathrm{e}^{\mathrm{i}\mathbf{k}\cdot\mathbf{x}/\hbar}\hat{a}_{\mathbf{k}}$, which transforms the Hamiltonian Eq. (  ) into

$$\hat{H} = \sum_{\mathbf{k}} \frac{\hbar^2k^2}{2m}\hat{a}^\dagger_{\mathbf{k}}\hat{a}_{\mathbf{k}} + \frac{V_0}{2V}\sum_{\mathbf{k},\mathbf{k_1},\mathbf{k_2}} \hat{a}^\dagger_{\mathbf{k_1}+\mathbf{k}}\hat{a}^\dagger_{\mathbf{k_2}-\mathbf{k}}\hat{a}_{\mathbf{k_1}}\hat{a}_{\mathbf{k_2}}. \tag{1.33}$$

The canonical commutation relation is preserved, $[\hat{a}_{\mathbf{k}},\hat{a}^\dagger_{\mathbf{k}'}] = \delta_{\mathbf{k},\mathbf{k}'}$. Instead of treating the many-body wavefunction as a coherent state during time evolution, we set the initial state as a Fock state $|N_0\rangle$ at the single-particle ground state with $\mathbf{k}=0$. When the particle number $N_0$ at the ground state is large enough, we can replace $\hat{a}_0$ and $\hat{a}^\dagger_0$ by $\sqrt{N_0}$, such that to the leading order of excitations in higher momentum states, we can write $\hat{H}$ into the Bogoliubov Hamiltonian

$$\hat{H}_{\mathrm{Bog}} = \frac{gN^2}{2V} + \sum_{\mathbf{k}\neq 0}\left(\frac{\hbar^2k^2}{2m} + V_0n_0\right)\hat{a}^\dagger_{\mathbf{k}}\hat{a}_{\mathbf{k}} + \frac{V_0n_0}{2}\sum_{\mathbf{k}\neq 0}\left(\hat{a}^\dagger_{\mathbf{k}}\hat{a}^\dagger_{-\mathbf{k}} + \hat{a}_{\mathbf{k}}\hat{a}_{-\mathbf{k}}\right), \tag{1.34}$$

where $n_0 = N_0/V$ is the particle density in the ground state. $N$ is the total particle number, which is conserved according to Eq. (  ). Diagonalizing the Bogoliubov Hamiltonian leads to the well-known Bogoliubov excitation spectrum

$$E_{\mathbf{k}} = \sqrt{\frac{\hbar^2k^2}{2m}\left(\frac{\hbar^2k^2}{2m} + 2V_0n_0\right)}, \tag{1.35}$$

which exhibits a linear dispersion relation at small momenta.

We have seen the ability to cool atoms into an ultracold regime has led to the realization of BEC and enables physicists to study intriguing quantum properties therein. On the

other hand, forming ultracold atomic gases into molecules has opened a powerful platform known as ultracold molecules. While two ultracold atoms can be brought into a weakly bounded molecular state through a Fano Feshbach resonance, a pair of Raman lasers can drive the atom pair into the molecular rovibrational ground state through an intermediate electronic excited state. Microwaves can further transfer the formed molecules between hyperfine states and the first rotational excited state, allowing full control of the hyperfine state and the realization of the ground state of ultracold molecules. Implementation of the abovementioned techniques led to the first realization of ultracold degenerate fermionic molecules in KRb at JILA by Jun Ye's group [ ].

Rovibrational ground state molecules realized in laboratories with highly controllable hyperfine degrees of freedom provide a broad range of applications in quantum chemistry, quantum simulation of exotic phases, and quantum information processing. For instance, ultracold molecules in the same or different hyperfine states satisfy different statistics when undergo two-body collisions, resulting in a centrifugal barrier in $p$-wave scattering, which suppresses chemical reactions at ultracold temperatures [ ]. While the interaction between ultracold molecules can be tuned in different means, including microwave dressing and external electric fields, various exotic quantum phases could be accessed [ ]–[ ]. The hyperfine and rotational states with long coherence times and highly tunable interactions together allow the storage and process of quantum information, making the ultracold molecules a promising candidate for the realization of quantum error-correcting codes [ ].

While ultracold molecules have emerged as a powerful platform with various applications, a grand challenge exists as chemical reactions and formation of long-lived complexes cause losses in the ultacold molecular systems [ ], [ ]. Using KRb molecules as an example, it has the exothermic tetratomic reaction channel

$$\mathrm{KRb} + \mathrm{KRb} \rightarrow \mathrm{K_2Rb_2^*} \rightarrow \mathrm{K_2} + \mathrm{Rb_2}. \tag{1.36}$$

$\mathrm{K_2Rb_2^*}$ denotes the intermediate complex, with a life-time $\tau = 2\pi\hbar\rho$ according to the Rice-Ramsperger-Kassel-Marcus theory [ ], [ ]. $\rho$ is the density of states of the intermediate complex near the incident energy. For $p$-wave scattering between KRb molecules, its life-time

is 465 ms [ ]. The molecules pair effectively leaves the system if the interested dynamics happens within a smaller timescale.

### 1.3 Curved Space

We have discussed the unitary and non-unitary quantum dynamics and provided a basic introduction to the ultracold quantum systems we are interested in. Now let's move to the geometry and curved spaces. The interest in understanding the real world through geometry can be traced back to the Platonic solid, introduced by the Greek philosopher Plato back to thousands of years ago, trying to interpret the only five regular polyhedra in three-dimensional space as classical elements forming our universe. Even earlier in history, people realized that only specific regular polygons could periodically tessellate two-dimensional surfaces. However, these discoveries about regular polyhedra and polygons will no longer be true when we turn to curved spaces.

It was not until the 19th century, after the pioneering work by Gauss in two-dimensional curved surfaces and the generalization of Riemannian geometry to higher dimensions by Riemann, that people started to obtain a powerful mathematical tool for studying the properties of curved space. The Riemannian geometry and the idea of viewing spacetime as a continuum underlie the theory of general relativity built by Einstein in the 20th century, which has become one of the most influential theories in physics. In this section, we use two-dimensional curved space as an example to introduce concepts of curved space with and without resorting to a three-dimensional embedding. We also consider quantum dynamics on these surfaces.

Surfaces in our daily life are, in general, curved. It is easy to name a few, such as the surface of a water kettle, basketball, or bagel. We can set a coordinate system to describe their surfaces. For instance, the basketball can be approximated by a sphere. By selecting the center of a sphere as the origin, its surface is described by a parameterization

$$(x(\theta,\varphi), y(\theta,\varphi), z(\theta,\varphi)) = (\sin(\theta)\cos(\varphi), \sin(\theta)\sin(\varphi), \cos(\theta)), \tag{1.37}$$

where the radius of the sphere is set to 1. While the surface is only parameterized by $\theta$ and $\varphi$, an embedding allows us to visualize this geometric object straightforwardly. Nevertheless, generalization to higher dimensions is involved since a three-dimensional curved space embedded in a four-dimensional flat space is often beyond human imagination. We, therefore, need an intrinsic description of curved space. Notice the surface is only parameterized by two parameters $(\theta, \varphi)$, it is upon the definition of distance between any two points $(\theta, \varphi)$ and $(\theta + d\theta, \varphi + d\varphi)$ that the geometry is uniquely defined. This distance, $ds$, can be directly inherited from its three dimensional embedding. We obtain

$$\begin{aligned} ds^2 =& \Big|(x(\theta + d\theta, \varphi + d\varphi), y(\theta + d\theta, \varphi + d\varphi), z(\theta + d\theta, \varphi + d\varphi)) - (x(\theta, \varphi), y(\theta, \varphi), z(\theta, \varphi))\Big|^2 \\ =& \left[\left(\frac{\partial x}{\partial \theta}\right)^2 + \left(\frac{\partial y}{\partial \theta}\right)^2 + \left(\frac{\partial z}{\partial \theta}\right)^2\right] d\theta^2 + \left[\left(\frac{\partial x}{\partial \varphi}\right)^2 + \left(\frac{\partial y}{\partial \varphi}\right)^2 + \left(\frac{\partial z}{\partial \varphi}\right)^2\right] d\varphi^2. \end{aligned} \tag{1.38}$$

For the sphere, it becomes $ds^2 = d\theta^2 + \sin^2(\theta) d\varphi^2$. In general, we have

$$ds^2 = g_{xx} dx^2 + g_{yy} dy^2 + 2 g_{xy} dx dy, \tag{1.39}$$

where $g_{\mathrm{ij}}$ is known as the metric tensor. For Euclidean space in Cartesian coordinate, the metric tensor is given by the Kronecker delta symbol $\delta_{\mathrm{ij}}$. Mathematically, Eq. ( ) is known as the induced metric on the surface $(x(\theta, \varphi), y(\theta, \varphi), z(\theta, \varphi))$. As we mentioned, while it is useful to view Eq. ( ) as a definition of distance induced from the metric of the embedded space, we can directly treat Eq. ( ) as an intrinsic definition of distance of a two-dimensional space parameterized by $x$ and $y$.

Another essential geometric object on a curved space is the connection. While physicists are used to considering scalar, vector, or tensor fields and their derivatives in a flat space, the derivative needs to be modified in a curved space. The derivative of a scalar field $\phi(x, y)$ is untouched, and a constant scalar field is defined as a scalar field that satisfies $\partial_{\mathrm{i}} \phi(x, y) = 0$,

$\mathrm{i} = x, y$. However, for a constant vector field $V^\mu(x, y)$ satisfying $\partial_x V^\mathrm{i}(x, y) = \partial_y V^\mathrm{i}(x, y) = 0$ in flat space, the partial derivatives need to be replaced by

$$\nabla_\mu V^\nu = \partial_\mu V^\nu + \Gamma^\nu_{\mu\lambda} V^\lambda, \tag{1.40}$$

in curved spaces. The Einstein summation notation has been applied. Namely, a constant vector field in a curved space satisfies $\partial_x V^\mathrm{i} + \Gamma^\mathrm{i}_{x\mathrm{j}} V^\mathrm{j} = \partial_y V^\mathrm{i} + \Gamma^\mathrm{i}_{y\mathrm{j}} V^\mathrm{j} = 0$. $\Gamma^\lambda_{\mu\nu}$, which defines constant fields, is called a connection. It is straightforward to generalize this definition to tensor fields,

$$\begin{aligned} \nabla_\sigma T^{\mu_1\mu_2\cdots}_{\nu_1\nu_2\ldots} = \partial_\sigma T^{\mu_1\mu_2\cdots}_{\nu_1\nu_2\ldots} + \Gamma^{\mu_1}_{\sigma\lambda} T^{\lambda\mu_2\ldots}_{\nu_1\nu_2\ldots} + \Gamma^{\mu_2}_{\sigma\lambda} T^{\mu_1\lambda\ldots}_{\nu_1\nu_2\ldots} + \ldots, \\ - \Gamma^\lambda_{\sigma\nu_1} T^{\mu_1\mu_2\cdots}_{\lambda\nu_2\ldots} - \Gamma^\lambda_{\sigma\nu_2} T^{\mu_1\mu_2\cdots}_{\nu_1\lambda\ldots} + \ldots. \end{aligned} \tag{1.41}$$

A connection that statisfies $\Gamma^\lambda_{\mu\nu} = \Gamma^\lambda_{\nu\mu}$ and $\nabla_\sigma g_{\mu\nu} = 0$ uniquely exists, and is termed as the Levi-Civita connection, or Christoffel connection coefficients,

$$\Gamma^\lambda_{\mu\nu} = g^{\lambda\alpha}(\partial_\mu g_{\nu\alpha} + \partial_\nu g_{\alpha\mu} - \partial_\alpha g_{\mu\nu})/2. \tag{1.42}$$

The Christoffel symbol $\Gamma^\lambda_{\mu\nu}$ defines a means to transport vectors on the curved spaces. For a free particle moving on a curved space, its velocity is necessarily a constant. Its trajectories are called geodesics denoted by $(x(t), y(t))$. Replacing $V^\mathrm{i}$ by the velocity of a free particle $(\partial_t x, \partial_t y)$, we immediately obtain the geodesic equations,

$$\begin{aligned} \frac{\partial^2 x}{\partial t^2} + \frac{\partial x}{\partial t}\left(\Gamma^x_{xx}\frac{\partial x}{\partial t} + \Gamma^x_{xy}\frac{\partial y}{\partial t}\right) + \frac{\partial y}{\partial t}\left(\Gamma^x_{yx}\frac{\partial x}{\partial t} + \Gamma^x_{yy}\frac{\partial y}{\partial t}\right) &= 0, \\ \frac{\partial^2 y}{\partial t^2} + \frac{\partial x}{\partial t}\left(\Gamma^y_{xx}\frac{\partial x}{\partial t} + \Gamma^y_{xy}\frac{\partial y}{\partial t}\right) + \frac{\partial y}{\partial t}\left(\Gamma^y_{yx}\frac{\partial x}{\partial t} + \Gamma^y_{yy}\frac{\partial y}{\partial t}\right) &= 0. \end{aligned} \tag{1.43}$$

In a compact form, it reads

$$\frac{\partial^2 x^\lambda}{\partial t^2} + \Gamma^\lambda_{\mu\nu}\frac{\partial x^\mu}{\partial t}\frac{\partial x^\nu}{\partial t} = 0. \tag{1.44}$$

Similarly, the Schrödinger equation of free quantum particle needs to be modified in curved space. Since the wavefunction is a scalar, $\partial_\nu \psi = \omega_\nu$ satisfies $\nabla_\mu \omega_\nu = \partial_\mu \omega_\nu - \Gamma^\lambda_{\mu\nu}\omega_\lambda$. We then write

$$\frac{\hbar^2}{2m}\bigg( - g^{\mu\nu}\partial_\mu\partial_\nu + g^{\mu\nu}\Gamma^\lambda_{\mu\nu}\partial_\lambda \bigg)\psi = E\psi. \tag{1.45}$$

Using the identity of Christoffel symbol $g^{\mu\nu}\Gamma^\lambda_{\mu\nu} = -\frac{1}{\sqrt{g}}\partial_\mu(\sqrt{g}g^{\lambda\mu})$, where $g = \det(g_{\mu\nu})$, $g^{\mu\nu}$ is the inverse of $g_{\mu\nu}$, we arrived at the free Schrödinger equation on curved spaces,

$$-g^{\mu\nu}\partial_\mu\partial_\nu\psi - \frac{1}{\sqrt{g}}\partial_\mu(\sqrt{g}g^{\lambda\mu})\partial_\lambda\psi = -\frac{1}{\sqrt{g}}\partial_\mu(\sqrt{g}g^{\mu\nu}\partial_\nu\psi) = \frac{2mE}{\hbar^2}\psi, \tag{1.46}$$

where $\frac{1}{\sqrt{g}}\partial_\mu(\sqrt{g}g^{\mu\nu}\partial_\nu)$ is known as the Laplace Beltrami operator. For the metric of a sphere, it becomes $\frac{1}{\sin(\theta)}\partial_\theta(\sin(\theta)\partial_\theta) + \partial^2_\varphi$. It is worth mention that, while Eq. (  ) is derived using its intrinsic property, it can also be obtained from confining the motion of a three-dimensional quantum particle onto a two-dimensional curved surface by an external potential. This physical constraint induces an extra potential on the two-dimensional curved surface that depends on both the scalar and the mean curvature [  ].

The "flatness" or holonomy of the Christoffel symbol is characterized by the Riemann curvature tensor [  ],

$$R^\beta_{\alpha\mu\nu} = \partial_\mu\Gamma^\beta_{\nu\alpha} - \partial_\nu\Gamma^\beta_{\mu\alpha} + \Gamma^\beta_{\mu\lambda}\Gamma^\lambda_{\nu\alpha} - \Gamma^\beta_{\nu\lambda}\Gamma^\lambda_{\mu\alpha}. \tag{1.47}$$

In two-dimensional surfaces, it is uniquely determined by the scalar curvature, reads $R = g^{\mu\nu}R^\lambda_{\mu\lambda\nu}$.

## 1.4 Lie Algebra and Coherent State

Lie algebra is one of the most fundamental and useful concepts in physics and mathematics. It generates the Lie group with an intrinsic geometric structure and sets the symmetry of the corresponding physical system. A Lie algebra is an abstract object which consists of two ingredients, generators and their commutators. Any generators satisfying the commutation relations form a representation of the corresponding Lie algebra. For instance, we can

consider $p$ and $q$ as two generators of a Lie algebra. Unlike ordinary variables, Lie algebra generators may not commute, $pq \neq qp$. We, therefore, use $\hat{p}$, $\hat{q}$ to distinguish them from ordinary variables. We can consider linear superposition or number multiplication of generators, which still falls in the algebra. The commutator describes the extent to of the generators do not commute with each other. Without loss of generality, we let $\hat{q}\hat{p} - \hat{p}\hat{q} = \hat{I}$, and $\hat{I}$ commutes with both $\hat{p}$ and $\hat{q}$ Then $\hat{p}$, $\hat{q}$, and $\hat{I}$ and their commutators denoted by $[\hat{q}, \hat{p}] = \hat{I}$, $[\hat{p}(\hat{q}), \hat{I}] = 0$ form the Heisenberg algebra, which is a crucial ingredient in performing the canonical quantization. One may already find a straightforward representation which acting on functions over a real line $f(x)$ as $\hat{q} = x$, $\hat{p} = -\mathrm{i}\partial_x$, $\hat{I} = \mathrm{i}$. Another explicit representation of the Heisenberg algebra is the generators of the Heisenberg group $H_3$, which read

$$\hat{q} = \begin{pmatrix} 0 & 1 & 0 \\ 0 & 0 & 0 \\ 0 & 0 & 0 \end{pmatrix}, \quad \hat{p} = \begin{pmatrix} 0 & 0 & 0 \\ 0 & 0 & 1 \\ 0 & 0 & 0 \end{pmatrix}, \quad \hat{I} = \begin{pmatrix} 0 & 0 & 1 \\ 0 & 0 & 0 \\ 0 & 0 & 0 \end{pmatrix}, \tag{1.48}$$

one can easily check the commutation relations are satisfied.

In quantum mechanics, we are familiar with angular momentum operators $\hat{S}_x$, $\hat{S}_y$ and $\hat{S}_z$. They form the $su(2)$ algebra, together with the commutation relations $[\hat{S}_\mathrm{j}, \hat{S}_k] = \mathrm{i}\epsilon_{\mathrm{j}kl}\hat{S}_l$, where $\epsilon_{\mathrm{j}kl}$ is the Levi-Civita symbol. An equally important algebra is the $su(1,1)$ algebra, where the generators $\hat{K}_0$, $\hat{K}_1$ and $\hat{K}_2$ satisfy the following commutation relation,

$$[\hat{K}_0, \hat{K}_1] = \mathrm{i}\hat{K}_2, \quad [\hat{K}_1, \hat{K}_2] = -\mathrm{i}\hat{K}_0, \quad [\hat{K}_2, \hat{K}_0] = \mathrm{i}\hat{K}_1. \tag{1.49}$$

This algebra has various representations in different physical systems. The most direct one is the generators of "rotational" symmetry of hyperbolic surfaces, similar to that of spheres. As we will show in Appendix A, $\hat{K}_0$ generates rotations of the hyperbolic surface and $\hat{K}_1$ and $\hat{K}_2$ are generators of boosts. In quantum systems, we can construct representations of $su(1,1)$ algebra similar to what we did using angular momentum operators. Namely, we define $\hat{K}_\pm = \hat{K}_1 \pm \mathrm{i}\hat{K}_2$, such that

$$[\hat{K}_+, \hat{K}_-] = -2\hat{K}_0, \quad [\hat{K}_0, \hat{K}_\pm] = \pm\hat{K}_\pm. \tag{1.50}$$

We can also define the Casimir operator of $su(1,1)$ algebra as $\hat{C} = \hat{K}_0^2 - \hat{K}_1^2 - \hat{K}_2^2$, which commutes with $\hat{K}_0$, $\hat{K}_1$ and $\hat{K}_2$. Starting from an eigenstate of $\hat{K}_0$ with eigenvalue $k$ that is annihilated by $\hat{K}_-$, we are able to construct a series of eigenstates of $\hat{K}_0$ using the raising operator $\hat{K}_+$. Unlike the angular momentum case, where such construction stops at a certain $n$ for $\hat{S}_+^n$ and leads to a negative norm state unless $k$ is an integer or half-integer, here the construction does not stop. We obtain an infinite-dimensional representation of $su(1,1)$ algebra, where

$$\hat{K}_0 \left|k, n\right\rangle = (k+n) \left|k, n\right\rangle , \quad \left|k, n\right\rangle = \sqrt{\frac{\Gamma(2k)}{\Gamma(n+1)\Gamma(2k+n)}} \hat{K}_+^n \left|k, 0\right\rangle , \tag{1.51}$$

a prefactor is included to normalize $|k, n\rangle$, and $k$ is termed as the Bargmann index [ ] as analog to the angular momentum quantum number.

The coherent state forms an overcomplete basis of the Hilbert space. The definition of a coherent state system is directly related to the Lie group. And the coherent state method is extremely effective when the interested physical system has a dynamical symmetry group as the Lie group [ ]. To be more precise, a quantum system has a dynamical symmetry if the time-dependent Hamiltonian falls into a Lie algebra such that the propagators fall into a Lie group. For example, a spin precesses in a time-dependent magnetic field and a quantum particle subjected to a harmonic potential with time-dependent frequency have dynamical groups $SU(2)$ and $SU(1,1)$, respectively. Two interacting quantum harmonic oscillators have a more complex dynamical group $SO(3,2)$. Coherent states allow us to implement the powerful group-theoretical methods in studying the dynamics in these systems.

The coherent state system is built upon a reference state $|R\rangle$. All the other quantum states of the coherent state system are obtained by acting all group elements on $|R\rangle$. For instance, if we consider the infinite dimensional representation of $su(1,1)$ algebra and set $|k, 0\rangle$ as the reference state, the coherent state system can be defined as

$$\left|\xi_0, \xi_1, \xi_2; k\right\rangle = \mathrm{e}^{-\mathrm{i}(\xi_0 \hat{K}_0 + \xi_1 \hat{K}_1 + \xi_2 \hat{K}_2)} \left|k, 0\right\rangle . \tag{1.52}$$

Nevertheless, this definition contains a redundant global phase. $|\xi_0, 0, 0\rangle$ for different $\xi_0$ represents the same quantum state $\mathrm{e}^{-\mathrm{i}\xi_0 k}\,|k, 0\rangle$. It turns out we can have a more useful parameterization of the coherent states such that this phase can be eliminated. We define

$$|\eta, \theta, \theta_0; k\rangle = \mathrm{e}^{-\mathrm{i}\theta\hat{K}_0}\mathrm{e}^{-\mathrm{i}\eta\hat{K}_1}\mathrm{e}^{-\mathrm{i}(\theta_0-\theta)\hat{K}_0}\,|k, 0\rangle\,. \tag{1.53}$$

Elimilating the global phase, the quantum state now is purely characterized by $\eta$ and $\theta$. The $SU(1,1)$ coherent state system reads

$$|\eta, \theta; k\rangle = \cosh^{-2k}(\frac{\eta}{2})\sum_{n=0}^{\infty}\sqrt{\frac{\Gamma(2k+n)}{\Gamma(n+1)\Gamma(2k)}}\Big(-\mathrm{i}\tanh\Big(\frac{\eta}{2}\Big)\mathrm{e}^{-\mathrm{i}\theta}\Big)^n\,|k, n\rangle\,. \tag{1.54}$$

We can find a one-to-one correspondence between these two parameterizations using the Baker-Campbell-Hausdorff formula [ ]. If an initial state $|k, 0\rangle$ evolves with the $SU(1,1)$ dynamical symmetry, its dynamics correspond to a trajectory on the coherent state system. We, therefore, obtain the system's dynamics using the group-theoretical approach without resorting to the time-ordered product as shown in Eq. ( ).

### 1.5 Tan's Contact in Dilute Quantum Systems

Contact is proposed by Shina Tan in the serial works [ ]. It is a central quantity that appears in ultracold dilute quantum systems where a length scale separation exists and bridges the two-body physics and the many-body environment. Here we briefly introduce the universal relations that involve contact in a bosonic system. One can refer to [ ], [ ] for a review of contacts in various systems and derivations of universal relations.

We consider a many-body bosonic system with $N$ particles. The Hamiltonian is

$$\hat{H} = \int \mathrm{d}^3\vec{r}\frac{\hbar^2}{2M}\nabla\hat{\Psi}^\dagger(\vec{r})\nabla\hat{\Psi}(\vec{r}) + \frac{1}{2}\int \mathrm{d}^3\vec{r}\,\mathrm{d}^3\vec{r}' V(|\vec{r}-\vec{r}'|)\hat{\Psi}^\dagger(\vec{r})\hat{\Psi}^\dagger(\vec{r}')\hat{\Psi}(\vec{r})\hat{\Psi}(\vec{r}') \tag{1.55}$$

The many-body wavefunction with eigenenergy $E$ is written as

$$\langle\vec{r}_1, \vec{r}_2, \ldots, \vec{r}_N|\Psi(E)\rangle = \Psi(\vec{r}_1, \vec{r}_2, \ldots, \vec{r}_N; E), \tag{1.56}$$

which is symmetric under exchange of particles. This wavefunction satisfies the many-body Schrödinger equation

$$\left(-\frac{\hbar^2}{2M}\sum_{\mathrm{i}=1}^{N}\nabla_{\mathrm{i}}^2+\sum_{\mathrm{i}>\mathrm{j}}V(|\vec{r}_{\mathrm{i}}-\vec{r}_{\mathrm{j}}|)\right)\Psi(\vec{r}_1,\vec{r}_2,\ldots,\vec{r}_N;E)=E\Psi(\vec{r}_1,\vec{r}_2,\ldots,\vec{r}_N;E). \tag{1.57}$$

The universality of the ultracold dilute quantum system comes in the behavior of many-body wavefunction when two particles are close to each other, namely,

$$\Psi(\vec{r}_1,\ldots,\vec{r}_{\mathrm{i}},\ldots,\vec{r}_{\mathrm{j}}\ldots,\vec{r}_N;E)\xrightarrow{|\mathbf{r}_{\mathrm{ij}}|\ll k_F^{-1}}\int \mathrm{d}\epsilon\psi(\mathbf{r}_{\mathrm{ij}};\epsilon)G(\mathbf{R}_{\mathrm{ij}};E-\epsilon) \tag{1.58}$$

where $k_F^{-1}$ denotes the interparticle distance, we use the notation $\mathbf{r}_{\mathrm{ij}}$ and $\mathbf{R}_{\mathrm{ij}}$ to represent $\vec{r}_{\mathrm{i}}-\vec{r}_{\mathrm{j}}$ and $\{\vec{r}_1,\ldots,\vec{r}_{\mathrm{i}}+\vec{r}_{\mathrm{j}},\ldots,\vec{r}_N\}$, respectively. $\psi(\mathbf{r}_{\mathrm{ij}};\epsilon)$ satisfies the two-body Schrödinger equation

$$\left(-\frac{\hbar^2}{M}\nabla_{\mathrm{ij}}^2+V(|\mathbf{r}_{\mathrm{ij}}|)\right)\psi(\mathbf{r}_{\mathrm{ij}};\epsilon)=\epsilon\psi(\mathbf{r}_{\mathrm{ij}};\epsilon). \tag{1.59}$$

In this limit, the two-body physics and many-body physics captured by $\psi$ and $G$ are separated.

If we assume the range $r_0$ of the interparticle interaction is much smaller than $k_F^{-1}$, from the low energy scattering theory, we obtain the behavior of many-body wavefunction within the region $r_0<|\mathbf{r}_{\mathrm{ij}}|\ll k_F^{-1}$. The threshold law allows us to focus on the $s$-wave scattering, we have

$$\Psi(\mathbf{r}_{\mathrm{ij}},\mathbf{R}_{\mathrm{ij}};E)\xrightarrow{r_0<|\mathbf{r}_{\mathrm{ij}}|\ll k_F^{-1}}\int \mathrm{d}\epsilon\left[\left(\frac{1}{|\mathbf{r}_{\mathrm{ij}}|}-\frac{1}{a}\right)+O(\epsilon)\right]Y_{00}G(\mathbf{R}_{\mathrm{ij}};E-\epsilon)+\text{other partial waves}, \tag{1.60}$$

where the $s$-wave scattering length $a$ depends on the two-body physics.

Since we consider an ultracold system and $\epsilon$ is related to its energy density, we have the length scale $\sqrt{\hbar^2/\epsilon M}\gg k_F^{-1}$. We can ignore $O(\epsilon)$ term and then obtain the asymptotic form of the $s$-wave channel wavefunction

$$\Psi_{00}(\mathbf{r}_{\mathrm{ij}},\mathbf{R}_{\mathrm{ij}};E)\xrightarrow{r_0<|\mathbf{r}_{\mathrm{ij}}|\ll k_F^{-1}}\left(\frac{1}{|\mathbf{r}_{\mathrm{ij}}|}-\frac{1}{a}\right)\frac{1}{\sqrt{4\boldsymbol{\pi}}}G(\mathbf{R}_{\mathrm{ij}};E). \tag{1.61}$$

This asymptotic form is the starting point of various universal relations. Using Eq. (  ), we obtain the asymptotic form of the density correlation function,

$$S(\vec{r}) = N(N-1)\int \mathrm{d}\mathbf{R}_{\mathrm{ij}}\left|\Psi(\vec{r},\mathbf{R}_{\mathrm{ij}})\right|^2 \xrightarrow{|\vec{r}|\to 0} N(N-1)\frac{1}{4\pi}\frac{1}{|\vec{r}|^2}\int |G(\mathbf{R}_{\mathrm{ij}};E)|^2\,\mathrm{d}\mathbf{R}_{\mathrm{ij}}. \quad (1.62)$$

The large momentum tail of momentum distribution is

$$n(\vec{k}) = N\int\prod_{m\neq \mathrm{j}}\mathrm{d}\vec{r}_m\left|\int \mathrm{d}\vec{r}_{\mathrm{j}}\Psi(\vec{r}_{\mathrm{j}},\vec{r}_{m\neq \mathrm{j}})\mathrm{e}^{-\mathrm{i}\vec{k}\cdot\vec{r}_{\mathrm{j}}}\right|^2 \xrightarrow{|\vec{k}|\to\infty} = N(N-1)\frac{4\pi}{|\vec{k}|^4}\int |G(\mathbf{R}_{\mathrm{ij}};E)|^2\,\mathrm{d}\mathbf{R}_{\mathrm{ij}}. \quad (1.63)$$

We have used the relation $\int \mathrm{d}\vec{r}\mathrm{e}^{-\lambda|\vec{r}|}\mathrm{e}^{-\mathrm{i}\vec{k}\cdot\vec{r}}\frac{1}{|\vec{r}|} = \frac{4\pi^2}{|\vec{k}|^2+\lambda^2}$. Here $|\vec{k}|\to\infty$ means $k_F \ll |\vec{k}| \ll \frac{1}{r_0}$. Another universal relation is the adiabatic relation, which can be derived from the many-body Schrödinger equation. It reads

$$\frac{\partial E}{\partial(-1/a)} = \frac{\hbar^2}{2M}N(N-1)\int |G(\mathbf{R}_{\mathrm{ij}};E)|^2\,\mathrm{d}\mathbf{R}_{\mathrm{ij}}. \quad (1.64)$$

The same factor, $G(\mathbf{R}_{\mathrm{ij}};E)$, as the many-body part of the asymptotic wavefunction, shows up in each relation. We, therefore, define the $s$-wave contact as

$$C_{00} = 4\pi N(N-1)\int |G(\mathbf{R}_{\mathrm{ij}};E)|^2\,\mathrm{d}\mathbf{R}_{\mathrm{ij}}. \quad (1.65)$$

The universal relations can be rewritten intro

$$S(\vec{r}) \xrightarrow{|\vec{r}|\to 0} \frac{1}{(4\pi)^2}\frac{C_{00}}{|\vec{r}|^2}, \quad n(\vec{k}) \xrightarrow{|\vec{k}|\to\infty} \frac{C_{00}}{|\vec{k}|^4}, \quad \frac{\partial E}{\partial(-1/a)} = \frac{\hbar^2}{8\pi M}C_{00}. \quad (1.66)$$

In general, a contact matrix could be defined if the contributions from higher partial waves need to be included [  ]. We note that the Efimov effect in the ultracold bosonic system is ignored in the derivations above. If the three-body asymptotic state is taken into account, the adiabatic relation needs to be modified and a three-body contact needs to be included [  ], [  ].

## 1.A Hyperbolic space and symmetry

This appendix introduces hyperbolic surfaces that are of fundamental importance in the following chapters. A hyperbolic surface is a two-dimensional homogeneous surface with constant negative curvature, which can be embedded as a two-dimensional surface $X^2 + Y^2 - T^2 = -R_0^2$ in a three-dimensional Minkowski spacetime $(X, Y, T)$. Let's reparameterize this surface by $(\eta, \varphi)$,

$$X = R_0 \sinh(\eta)\cos(\varphi), \quad Y = R_0 \sinh(\eta)\sin(\varphi), \quad T = R_0 \cosh(\eta). \tag{1.67}$$

Using the modified Eq. ( ) since now we have the two-dimensional surface embedded in a three-dimensional Minkowski spacetime, we find

$$\begin{aligned} ds^2 =& \left[\left(\frac{\partial X}{\partial \eta}\right)^2 + \left(\frac{\partial Y}{\partial \eta}\right)^2 - \left(\frac{\partial T}{\partial \eta}\right)^2\right] d\eta^2 + \left[\left(\frac{\partial X}{\partial \varphi}\right)^2 + \left(\frac{\partial Y}{\partial \varphi}\right)^2 - \left(\frac{\partial T}{\partial \varphi}\right)^2\right] d\varphi^2 \\ =& R_0^2 (d\eta^2 + \sinh^2(\eta) d\varphi^2). \end{aligned} \tag{1.68}$$

This is the metric of a hyperbolic space. It is invariant under boosts and rotations in the three-dimensional Minkowski spacetime according to its embedding. Its non-vanishing Christoffel symbols are $\Gamma^{\eta}_{\varphi\varphi} = -\cosh(\eta)\sinh(\eta)$ and $\Gamma^{\varphi}_{\eta\varphi} = \Gamma^{\varphi}_{\varphi\eta} = \coth(\eta)$, which lead to the scalar curvature $R = -2/R_0^2$. Usine Eq. ( ), we can write down the Schrödinger equation on this surface, reads

$$\frac{\hbar^2}{2mR_0^2}\left(-\partial_\eta^2 - \frac{1}{\sinh^2(\eta)}\partial_\varphi^2 - \coth(\eta)\partial_\eta\right)\psi = E\psi. \tag{1.69}$$

Since the hyperbolic space is infinitely large, it is desired to bring the boundary of the hyperbolic space to a finite distance. We therefore consider $\rho = \tanh(\eta/2)$, such that

$$ds^2 = \frac{4R_0^2}{(1-\rho^2)^2}(d\rho^2 + \rho^2 d\varphi^2). \tag{1.70}$$

$\eta \to \infty$ is mapped to the boundary of a unit disk. Geodesics are circles with their origins located on the boundary of the disk.

We can further reparameterize $\rho, \varphi$ into a complex number $z = x + \mathrm{i}y$, where $|z| < 1$ is defined in the unit disk.

$$ds^2 = \frac{4R_0^2}{(1-x^2-y^2)^2}(dx^2 + dy^2). \tag{1.71}$$

This metric is invariant under the Möbius transformation $z \to \tilde{z}$, where

$$\tilde{z} = \frac{\alpha z + \beta}{\beta^* z + \alpha^*} \equiv \begin{pmatrix} \alpha & \beta \\ \beta^* & \alpha^* \end{pmatrix}(z) = \mathrm{e}^{-\mathrm{i}(\xi_0(\sigma_z/2)+\xi_1(-\mathrm{i}\sigma_y/2)+\xi_2(\mathrm{i}\sigma_x/2))}(z), \tag{1.72}$$

where $|\alpha|^2 - |\beta|^2 = 1$. This transformation represents the $SU(1,1)$ group, and $\hat{K}_0 = \sigma_z/2$, $\hat{K}_1 = (-\mathrm{i})\sigma_y/2$,$\hat{K}_2 = \mathrm{i}\sigma_x/2$ satisfy the $su(1,1)$ algebra. For non-vanishing $\xi_{0,1,2}$, these transformations generate rotation, boost along $x$-direction and $y$-direction, respectively, as shown in Fig. .

Another useful coordinate system of the hyperbolic space is the Poincaré half plane. It is related to the Poincaré disk by the Cayley transform, $z \to (-\mathrm{i}z + \mathrm{i})/(z+1)$. The origin of the disk is mapped to $(0, \mathrm{i})$ on the complex plane, and the boundary circle is mapped to the real axis and the point at infinity. Under such transformation, the metric now reads

$$ds^2 = \frac{R_0^2}{y^2}(dx^2 + dy^2). \tag{1.73}$$

Clearly, this metric diverges as $y$ approaching 0, in consistent with the fact that the real axis corresponds to infinity on the hyperbolic space.

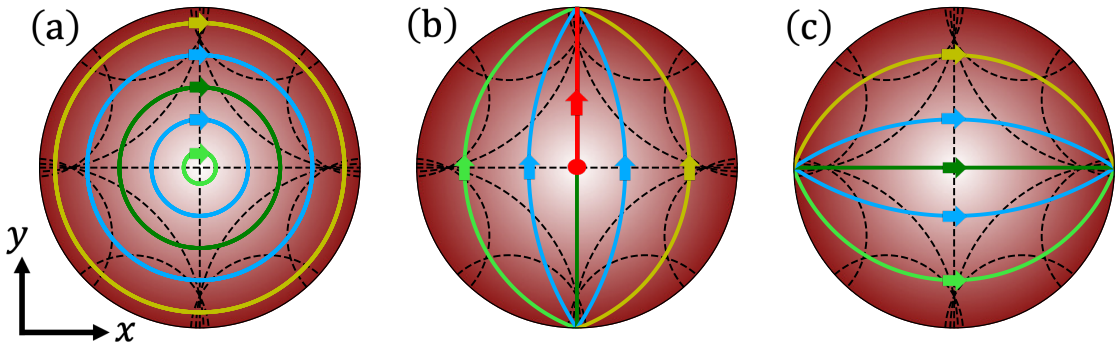


**Figure 1.1.** Trajectories of different points $z$'s under rotation (a), boost along $x$ direction (b) and boost along $y$ direction (c) on the Poincaré disk. The black dashed lines are the geodesics.

# 2. EMERGENT HYPERBOLIC SPACE IN SU(1,1) SYSTEMS AND QUANTUM CONTROL

*The contents of this chapter are based on and modified from the published articles [ ] by C. Lyu, C. Lv, and Q. Zhou, Geometrizing quantum dynamics of a Bose-Einstein condensate, Phys. Rev. Lett. 125, 253401 (2020). Copyright (2020) by the American Physical Society, and [ ] by C. Lv, R. Zhang, and Q. Zhou, SU(1,1) Echoes for Breathers in Quantum Gases, Physical Review Letters 125 (25), 253002 (2020). Copyright (2020) by the American Physical Society.*

In this chapter, we discuss the geometrization of quantum dynamics of various systems with $SU(1,1)$ dynamical symmetry. We first consider weakly interacting Bose-Einstein condensates with time-dependent interaction strength. We show that quantum dynamics in different momentum modes can be geometrized by a Poincaré disk. A single point on such a disk is an $SU(1,1)$ coherent state. In the weakly interacting bosons case, it is also a thermofield double state. The overlap between different coherent states is equal to the metric of the Poincaré disk, and stable and unstable modes are represented by closed and open trajectories. The resonant modes that follow geodesics naturally equate fundamental quantities, including the time, the length, and the temperature.

In general, quantum systems with $SU(1,1)$ dynamical symmetry generate trajectories on multiple Poincaré disks, depending on the initial state of the quantum system. The second part of this chapter studies the $SU(1,1)$ dynamical symmetry in scale-invariant quantum gases. Three-dimensional unitary fermions, two-dimensional bosons, fermions with contact interactions, and Calogero-Sutherland gases belong to this category. We will introduce $SU(1,1)$ echoes as an application of the group-theoretical method of engineering collective excitations of interacting many-body systems with $SU(1,1)$ dynamical symmetry, as well as measuring symmetry breaking perturbations.

## 2.1 Introduction

Geometries may arise as emergent phenomena in certain quantum systems. Recent decades have witnessed the emergent geometry in the AdS/CFT correspondence [ ], [ ], the ER=EPR conjecture [ ]–[ ], and scale-invariant tensor networks [ ]–[ ], where hyperbolic geometries emerge as results of strong correlations in quantum many-body systems.

In this chapter, we show that quantum dynamics of weakly interacting bosons are deeply connected to the hyperbolic geometry. We also consider the dynamics of breathers in scale-invariant quantum gases can be captured by multiple hyperbolic disks. This geometric picture provides us with new understanding of prior experimental results, including dynamical instability and breathers with certain geometric shapes. It shows that dynamical instability, a fundamental concept in various physical systems, has an underlying geometric interpretation. The dynamical instability corresponds to open trajectories that end at the boundary of the hyperbolic space. In sharp contrast, stable modes form loops.

On the other hand, our approach offers experimentalists a powerful tool to access and coherent control quantum dynamical phenomena. It delivers $SU(1,1)$ echoes to reverse quantum dynamics with $SU(1,1)$ dynamical symmetry, as analogous to spin echoes overcoming the dephasing in spin systems [ ], [ ]. Moreover, it could serve as a new framework for detecting perturbations that leads $SU(1,1)$ dynamical symmetry breaking, like utilizing spin echoes to extract useful information in interacting spins [ ]–[ ].

## 2.2 SU(1,1) Dynamical Symmetry of Weakly Interacting Bose Gas

We first consider the Bogoliubov Hamiltonian which describes weakly interacting bosons,

$$H = \sum_{\vec{k}} E_{\vec{k}} c^{\dagger}_{\vec{k}} c_{\vec{k}} + \frac{\tilde{U}}{2V} \sum_{\vec{k},\vec{k},\vec{q}} c^{\dagger}_{\vec{k}+\vec{q}} c^{\dagger}_{\vec{k}-\vec{q}} c_{\vec{k}} c_{\vec{k}}, \tag{2.1}$$

where $\tilde{U} = 4\pi\hbar^2 \frac{a_s}{M}$, $c^{\dagger}_{\vec{k}}$ ($c_{\vec{k}}$) is the creation (annihilation) operator for bosons with the momentum $\vec{k}$. $a_s(t)$ is the time-dependent scattering length. While $a_s(t) = 0$ for $t < 0$ such that the condensate is prepared at the zero momentum state, it is tuned dynamically using the magnetic or optical Feshbach resonance for $t > 0$ [ ]. Our results apply to both quenching $a_s(t) = a_s$ or an arbitrary $a_s(t)$.

Coherent dynamics can be achieved before considerable particle losses, even though a BEC with attractive interactions is not stable [ ]–[ ]. We first focus on short-time dynamics in which $N_{\vec{k}\neq 0}$, the particle number at a finite momentum, is small such that interactions

among excited atoms are negligible. The quantum dynamics is governed by $H_{\text{eff}} = \sum_{\vec{k}} H_{\vec{k}}$, where

$$H_{\vec{k}}(t) = \xi_0(\vec{k})K_0 + \xi_1(\vec{k})K_1 + \xi_2(\vec{k})K_2. \tag{2.2}$$

We have introduced the $su(1,1)$ generators in two-mode representation,

$$\begin{aligned} K_0 =& \frac{1}{2}(c^\dagger_{\vec{k}} c_{\vec{k}} + c_{-\vec{k}} c^\dagger_{-\vec{k}}) \\ K_1 =& \frac{1}{2}(c^\dagger_{\vec{k}} c^\dagger_{-\vec{k}} + c_{\vec{k}} c_{-\vec{k}}) \\ K_2 =& \frac{1}{2\mathrm{i}}(c^\dagger_{\vec{k}} c^\dagger_{-\vec{k}} - c_{\vec{k}} c_{-\vec{k}}). \end{aligned} \tag{2.3}$$

The field components that couple to the $su(1,1)$ generators are $\xi_0(\vec{k}) = 2(E_{\vec{k}} + \tilde{U}|\Psi_0|^2)$, $\xi_1(\vec{k}) = 2\,\mathrm{Re}\,U$, $\xi_2(\vec{k}) = -2\,\mathrm{Im}\,U$, $U = \tilde{U}\Psi_0^2$, and $\Psi_0 = \sqrt{N_0/V}\mathrm{e}^{\mathrm{i}\theta}$ is the condensate wavefunction. $\vec{\xi} = \{\xi_0, \xi_1, \xi_2\}$ is an external field, analogous to the magnetic field in the case of $SU(2)$, and its strength, $\xi = \sqrt{\xi_0^2 - \xi_1^2 - \xi_2^2}$, sets the energy scale. For instance, when $\xi_0^2 > \xi_1^2 + \xi_2^2$, the energy spectrum is given by $(m + 1/2)\xi$, where $m$ is an integer. The above equations show that the dynamics at different $\vec{k}$ are decoupled.

The Hamiltonian in Eq. with arbitrary choices of parameters, $\xi_{0,1,2}$ belongs to an $su(1,1)$ algebra. As such, any propagator, $P(t) = \mathcal{T}\mathrm{e}^{-\mathrm{i}\int_0^t \mathrm{d}t' H_{\vec{k}}(t')}$ is an element in $SU(1,1)$ [ ]. We, therefore, claim that the quantum dynamics has the $SU(1,1)$ dynamical symmetry [ ]–[ ]. In order to fully capture the $SU(1,1)$ dynamical group, three parameters are required and later we will show such a complete picture leads to an emergent Anti de-Sitter space. Here we consider the quotient with respect to the global $U(1)$ phase, $SU(1,1)/U(1)$, whose element is created by two operations,

$$R(\varphi_0) = \mathrm{e}^{-\mathrm{i}\varphi_0 K_0}, \quad B(\varphi_1, 0) = \mathrm{e}^{-\mathrm{i}\varphi_1 K_1}, \tag{2.4}$$

which correspond to a rotation and a boost, respectively. The group element which corresponds to a generic boost along an arbitrary direction is defined by $B(\varphi_1, \varphi_2) = \mathrm{e}^{-\mathrm{i}(\varphi_1 K_1 + \varphi_2 K_2)}$.

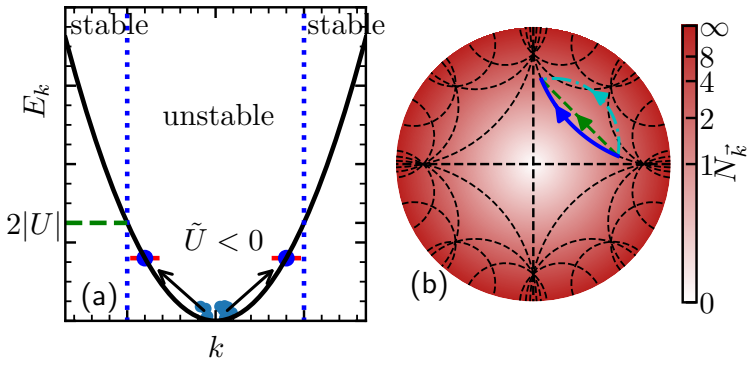


**Figure 2.1.** (a) Bosons from the condensate are scattered to states with opposite momenta through a negative interaction. Occupations in states with small kinetic energies will grow exponentially. (b) Each point on a Poincaré disk represents a TFD. The particle number or equivalently, the effective temperature, is highlighted by the color scale. Geodesics are represented by the dashed straight lines and curves. Trajectories representing dynamical evolutions of the quantum system are denoted by arrowed curves. The blue curve following the geodesic corresponds to an extreme of the time spent in quench dynamics.

Eq. parameterizes the propagators using a Poincaré disk [ ], [ ], as shown in Fig. (b). A similar approach was implemented to consider geometric phases in the adiabatic limit [ ].

To establish a one-to-one correspondence between the quantum dynamics and a Poincaré disk, we consider the vacuum as a reference state, $|\Psi(0)\rangle = |0\rangle_{\vec{k}}|0\rangle_{-\vec{k}}$, where $c_{\vec{k}}|0\rangle_{\vec{k}} = 0$. The two operators in Eq. lead to a wavefunction, $|z\rangle = R(\varphi_0)B(\varphi_1, 0)R^{\dagger}(\varphi_0)\,|\Psi(0)\rangle$, which is written as

$$|z\rangle = \sqrt{1-|z|^2}\sum_n z^n\,|n\rangle_{\vec{k}}\,|n\rangle_{-\vec{k}}\,, \tag{2.5}$$

where $z = -\mathrm{i}e^{-\mathrm{i}\varphi_0}\tanh\frac{\varphi_1}{2}$ and $|n\rangle_{\vec{k}} = c_{\vec{k}}^{\dagger n}|0\rangle/\sqrt{n!}$ denotes the Fock state. This coherent state system can be regarded as the generalized $SU(1,1)$ coherent state with the Bargmann index $k = 1/2$. The expression in Eq. is termed as a thermofield double state (TFD) state in high energy physics [ ]–[ ], [ ], [ ]. In quantum optics, this kind of two-mode squeezed state can be created through non-degenerate parametric amplification [ ]. Cre-

ating squeezed states from squeeze operators has been well studied in quantum optics [ ], and such a connection with BECs has also been recently studied [ ].

In quantum optics, it has been extensively explored how to produce squeezed states from squeeze operators [ ]. Recently, its connection with BECs has also been investigated [ ].

In TFD, we have two identical copies entangled with each other. Tracing over one copy leaves the other with a thermal density matrix,

$$\rho_{\vec{k}} = \mathrm{Tr}_{-\vec{k}} \left|z\right\rangle \left\langle z\right| = \mathcal{Z}^{-1} \sum_n \mathrm{e}^{-\frac{nE_{\vec{k}}}{k_B T}} \left|n\right\rangle_{\vec{k}} \left\langle n\right|_{\vec{k}}, \tag{2.6}$$

similar to Hawking radiation and Unruh effects [ ], [ ]. Using Eq. , we can identify the Euclidean distance to the center of the disk, $|z|$, with a temperature,

$$\tilde{T} \equiv \frac{k_B T}{E_k} = -\frac{1}{2} \ln^{-1} |z|, \tag{2.7}$$

and $\mathcal{Z} = 1 - \mathrm{e}^{-E_{\vec{k}}/k_B T}$. We, therefore, assign each point on the Poincaré disk with a temperature and the boundary circle has $T = \infty$. In quantum information, the closeness between two states is often characterized by their overlap, i.e., their fidelity [ ]. Here, the fidelity between TFDs, $F_{z,z'} = |\langle z'|z\rangle|^2$, is written as,

$$|\langle z|z'\rangle|^2 = \frac{(1-|z|^2)(1-|z'|^2)}{|1-z^* z'|^2}. \tag{2.8}$$

Consider two TFDs close to each other on the Poincaré disk, i.e., $z' = z + \mathrm{d}z$, from the above expression, we obtain

$$\mathrm{d}s^2 = 4(1 - F_{z,z+\mathrm{d}z}) = \frac{4(\mathrm{d}x^2 + \mathrm{d}y^2)}{(1-x^2-y^2)^2}, \tag{2.9}$$

which corresponds to the metric of a Poincaré disk. This definition of distance is deeply related to the adiabatic connection. The metric of a Poincaré disk can also be correlated to the complexities of the $SU(1,1)$ coherent states [ ].

## 2.3 SU(1,1) Dynamical Symmetry of Scale-Invariant Quantum Gases

In the previous section, we have found the dynamical instability of a BEC induced by quenching the scattering length, which corresponds to a particular representation of the $SU(1,1)$ group. For study in periodical driven BECs, the same representation has also been considered [ ], [ ]. In such a particular representation [ ], [ ], [ ], the Bargmann index $k$, is either a positive integer or half-integer, similar to spin systems. As we will later show, the integral or half-integral $k$ guarantees echoes with a single period. In sharp contrast, breathers in scale-invariant quantum gases correspond to a distinct representation with a continuous spectrum of $k$. Such a fundamental difference provides breathers with much richer phenomena ranging from an arbitrary multiplication of the period to dynamics with non-commensurate frequencies.

Let's introduce the $su(1,1)$ algebra in the quantum gases from its scale invariance. The Hamiltonian of scale-invariant quantum gas is written as

$$H_{\mathrm{si}} = \sum\nolimits_{\mathrm{i}} -\frac{\hbar^2}{2m}\nabla_{\mathrm{i}}^2 + \sum\nolimits_{\mathrm{i}<\mathrm{j}} V(\mathbf{r}_{\mathrm{i}} - \mathbf{r}_{\mathrm{j}}). \tag{2.10}$$

We define the scaling operator

$$K_2 = \frac{1}{4\mathrm{i}} \sum\nolimits_{\mathrm{i}} (\mathbf{r}_{\mathrm{i}} \cdot \nabla_{\mathrm{i}} + \nabla_{\mathrm{i}} \cdot \mathbf{r}_{\mathrm{i}}), \tag{2.11}$$

the scaling dimension $\Delta$ for an operator $O$ is defined as $[K_2, O] = -\mathrm{i}\Delta O$. The scale invariance of such Hamiltonian requires the interactions have the same scaling dimension $\Delta = 2$ as the kinetic term. The contact interaction in 2-D falls in this category. For contact interaction, $V(\mathbf{r}_{\mathrm{i}} - \mathbf{r}_{\mathrm{j}}) \sim g\delta(\mathbf{r}_{\mathrm{i}} - \mathbf{r}_{\mathrm{j}})$ and $\delta_{2D}(\lambda\mathbf{r}) = \lambda^{-2}\delta_{2D}(\mathbf{r})$. The inversed squared interaction considered in Calogero–Sutherland model also has this property. The fermionic system at unitary limit is also known as a scale-invariant system, where $V(\mathbf{r}_{\mathrm{i}} - \mathbf{r}_{\mathrm{j}})$ should be understood as $V(\mathbf{r}_{\mathrm{i}} - \mathbf{r}_{\mathrm{j}}) = \tilde{V}(\mathbf{r}_{\mathrm{i}} - \mathbf{r}_{\mathrm{j}})\delta_{\sigma_{\mathrm{i}} \neq \sigma_{\mathrm{j}}}$, $\sigma_{\mathrm{i}} = \uparrow, \downarrow$, $\tilde{V}$ produces a divergent scattering length.

The $su(1,1)$ symmetry appears upon introducing a harmonic potential $V_{\rm ho} = \sum_{\rm i} \frac{m}{2}\omega_0^2 |\mathbf{r}_{\rm i}|^2$. Since $[V_{\rm ho}, H_{\rm si}] \sim K_2$, and $V_{\rm ho}$ has scaling dimension $\Delta = -2$, the algebra closes and we have the $su(1,1)$ generators in two-dimensional scale-invariant many-body system defined as

$$\begin{aligned} K_0 &= \frac{1}{2}\left[\sum\nolimits_{\rm i} -\frac{1}{2}\nabla_{\rm i}^2 + \frac{1}{2}r_{\rm i}^2 + \sum\nolimits_{\rm i<j} V(\mathbf{r}_{\rm i} - \mathbf{r}_{\rm j})\right], \\ K_1 &= \frac{1}{2}\left[\sum\nolimits_{\rm i} -\frac{1}{2}\nabla_{\rm i}^2 - \frac{1}{2}r_{\rm i}^2 + \sum\nolimits_{\rm i<j} V(\mathbf{r}_{\rm i} - \mathbf{r}_{\rm j})\right], \end{aligned} \tag{2.12}$$

and $K_2$ defined in Eq. . We have chosen $l_{ho} = \sqrt{\hbar/(m\omega_0)}$ as the unit length and $\hbar\omega_0$ as the unit energy. The $su(1,1)$ algebra is then satisfied by $K_{0,1,2}$. Using the above definition, a scale-invariant quantum system confined in an isotropic harmonic trap with frequency $\kappa\omega_0$ has the Hamiltonian $H = (1+\kappa^2)K_0 + (1-\kappa^2)K_1$.

Since $H = 2K_0$ when $\kappa = 1$, its spectrum is bounded from below. For each eigenstate of $K_0$ satisfying $(K_1 - {\rm i}K_2)\,|k,0\rangle = 0$, $K_0\,|k,0\rangle = k\,|k,0\rangle$, we can define coherent states that characterized by a complex number $|z| < 1$,

$$|k,z\rangle = (1-|z|^2)^k \sum_{n=0}^{\infty} \sqrt{\frac{\Gamma(2k+n)}{\Gamma(n+1)\Gamma(2k)}} z^n\,|k,n\rangle\,, \tag{2.13}$$

The Bargmann index $k$ is also determined by the Casimir operator $C = K_0^2 - K_1^2 - K_2^2$, where $C\,|k,n\rangle = k(k-1)\,|k,n\rangle$. A single Poincaré disk is characterized by a unique $k$. $|k,n\rangle \sim (K_1 + {\rm i}K_2)^n\,|k,0\rangle$. The set of states $|k,n\rangle$ for a given $k$ is also known as conformal tower states [ ]. Since we consider a many-body system with the interaction strength could be continuously tuned, $k$ now is not necessarily integral or half-integral.

### 2.4 Quench Dynamics and Floquet Dynamics

In this section, we discuss the dynamics on the Poincaré disk, generated by quantum quench or Floquet drivings, using the weakly interacting Bose gases as an example. We first consider quenching $a_s(t)$ from zero to a finite negative value. When $E_{\vec{k}} > 2|U|$ or equivalently, $\xi^2 > 0$, the growth of $n_{\vec{k}}$ is bounded from above and is referred as to a stable mode. On the Poincaré disk, its trajectory is a closed loop, as shown in Fig. (b). When $E_{\vec{k}} = 2|U|$, $\xi$

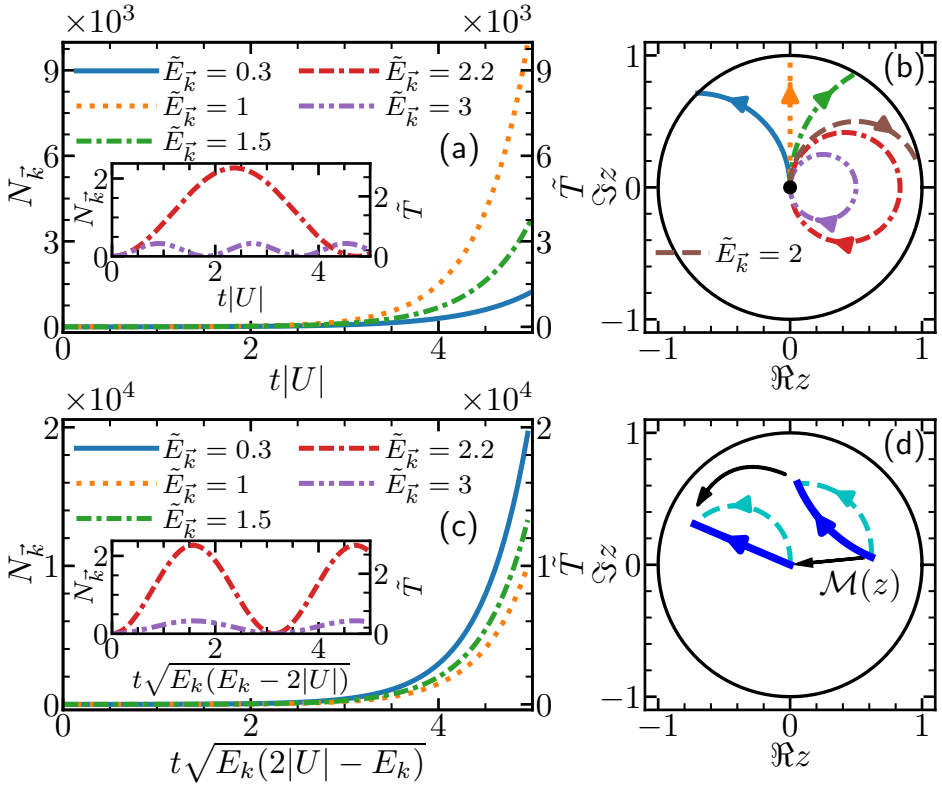


**Figure 2.2.** (a) The dependence of $N_{\vec{k}}$ (left vertical axis) and the rescaled temperature $\tilde{T}$ (right vertical axis) as a function of time. $\tilde{E}_{\vec{k}} = E_{\vec{k}}/|U|$. When $U$ is fixed, the resonant mode has the fastest growth. (b) On the Poincaré disk, the dynamics of stable(unstable) modes are mapped to closed(open) trajectories. The resonant mode follows the geodesic. (c) When $|\xi|$ is fixed, the resonant mode has the slowest growth. (d) An arbitrary initial state is mapped to the vacuum at the origin of the Poincaré disk through a Möbius transformation. The geodesic is mapped to a straight line.

vanishes and the trajectory becomes critical. When $E_{\vec{k}} < 2|U|$, i.e., $\xi^2 < 0$, the well-known dynamical instability occurs and $n_{\vec{k}}$ grows exponentially, mimicking the inflation in the early universe [ ]. Any unstable mode on the Poincaré disk corresponds to an open trajectory that extends from the origin to the circular boundary. However, because the boundary of the Poincar's disk corresponds to infinity, reaching there takes an infinity amount of time.

When $E_{\mathbf{k}} = |U|$, starting from the center of the Poincaré disk, the trajectory follows the diameter, i.e., a geodesic.

We can write the Euclidean distance to the center as

$$|z(t)| = \begin{cases} \left(1 - \frac{\xi^2}{\xi_1^2+\xi_2^2} \frac{1}{\sinh^2(\frac{|\xi|t}{2})}\right)^{-\frac{1}{2}}, & \xi^2 < 0 \\ \left(1 + \frac{\xi^2}{\xi_1^2+\xi_2^2} \frac{1}{\sin^2(\frac{|\xi|t}{2})}\right)^{-\frac{1}{2}}, & \xi^2 > 0. \end{cases} \tag{2.14}$$

From Eq. , we see that if $\xi_1^2 + \xi_2^2$ is fixed, $|z(t)|$ has the fastest growth when the system moves along the geodesic, with $\xi_0 = 0$. Under this situation,

$$|z(t)|_g = \tanh\left(\frac{|\xi|}{2}t\right). \tag{2.15}$$

Using Eq. , the length along the geodesic measured in the hyperbolic space is given by

$$\tilde{L} = \int_0^{|z(t)|_g} \frac{2\,\mathrm{d}x}{1-x^2} = |\xi|t. \tag{2.16}$$

It is worth pointing out that, if it is $|\xi|$ that is fixed, Eq. shows that the geodesic has the slowest growth among unstable modes. This conclusion is demonstrated by numerical results plotted in Fig. (c).

For off-resonant modes where $\xi_0 \neq 0$, the trajectories are no longer geodesics. However, the length along such a trajectory as a function of the time still has an expression similar to Eq. ( ) (Appendix).

The ground state is no longer a vacuum if the initial scattering length is finite. The quantum dynamics starts from a point away from the center of the Poincaré disk. A Möbius

transformation preserving the metric, $z' = \mathcal{M}(z) = \frac{\alpha z+\beta}{\beta^* z+\alpha^*}$, $\quad |\alpha|^2 - |\beta|^2 = 1$, maps the origin to any other point on the disk, therefore, all phenomena we discussed remain the same.

We now turn to periodic drivings. Consider an example,

$$H_1 = 2(E_{\vec{k}} + U)K_0 + 2UK_1, \qquad 0 < t < t_1 \tag{2.17}$$

$$H_2 = 2E_{\vec{k}}K_0, \qquad t_1 < t < T_d, \tag{2.18}$$

where the period $T_d = t_1 + t_2$. It corresponds to periodically modifying the interaction strength in Eq. . When $a_s = 0$, the propagator from $t = t_1$ to $t = T_d$ is given by Eq. , i.e., a rotation about the center of the Poincaré disk. The Floquet Hamiltonian, $\sim \log\left(\mathrm{e}^{-\mathrm{i}H_2 t}\mathrm{e}^{-\mathrm{i}H_1 t}\right)$, is tunable by changing $t_1$ or $t_2$, which allows us to manipulate both the stable and unstable modes. A quantum revival of the initial state at the end of the second period is particularly interesting. We emphasize that such a revival is accessible for any initial state, and any $H_1$ in Eq. ( ), not requiring a vacuum as the initial state nor a Hamiltonian $H_1$ satisfying the resonant condition [ ], [ ]. This revival, which is originated purely from the algebraic structure of the time-dependent Hamiltonian, can be directly implemented to other systems with $SU(1,1)$ dynamical symmetry in reversing quantum dynamics, as we will show below.

### 2.5 SU(1,1) Echoes for Breathers in Scale-Invariant Quantum Gases

Reversing quantum many-body dynamics is famously challenging because it necessitates simultaneously changing the signs of all components in the Hamiltonian and all particle dynamics. The well-established spin echoes [ ], however, have been widely employed to overcome dephasing in spin systems, providing the foundation of many modern technologies, including nuclear magnetic resonance and the central spin problem in condensed matter physics [ ], [ ], [ ].

This section will use two-dimensional Bose gases as an example to study the particular case of Floquet dynamics for systems with $SU(1,1)$ symmetry, the $SU(1,1)$ echoes that reverse collective excitation. In the study of ultracold atoms, collective excitations have

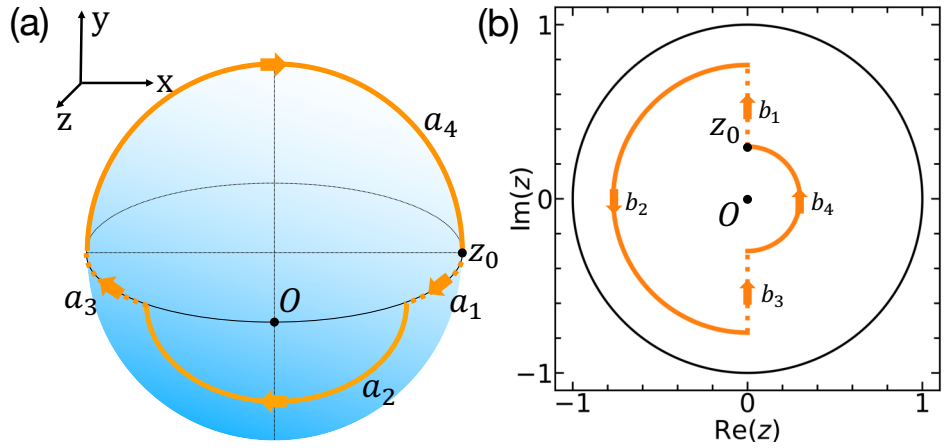


**Figure 2.3.** (a) $a_{1,2,3,4}$ denotes a spin echo. The sphere represents the Bloch sphere. The initial state is represented by $z_0$. Rotations about the $y$ axis are represented by $a_1$ and $a_3$. $\pi$-pulses about the $z$ axis are represented by $a_2$ and $a_4$. (b) $b_{1,2,3,4}$ denotes a $SU(1,1)$ echo. The unit disk represents the Poincaré disk. Boosts along a radial direction induced by the same Hamiltonian are represented by $b_1$ and $b_3$. $\pi$-rotations about the origin are represented by $b_2$ and $b_4$.

been a main and long-standing theme. [ ], [ ]–[ ]. In investigating superfluidity and hydrodynamics of interacting fermions and bosons in the past two decades, breathing modes (or breathers) have provided physicists with various valuable information [ ]–[ ]. However, once collective excitations have been generated, it is typically extremely difficult to return to the initial state. Since the relevant degrees of freedom do not obey the $su(2)$ algebra in breathers, the standard spin echoes do not apply. In the following, we consider breathers excited by a harmonic potential and implement the $SU(1,1)$ echoes to reverse collective excitations.

Breathers in quantum gases have been extensively studied following the seminal work by Pitaevskii and Rosch [ ]–[ ]. It wasn't until the ENS experiment, which discovered that the period of a breather in a harmonic trap depends on the breather's initial geometrical shape when the quantum anomaly is negligible, that the fundamental importance of initial shapes was realized [ ]. For instance, the triangular breather in a two-dimension system agrees with well-known results in harmonic traps. However, if the quantum gases has an initial disk shape, an unprecedented period multiplication occurs, quadrupling that of a triangle.

More strikingly, despite that the underlying Hamiltonian naturally determines a period, other shapes do not exhibit regular periodicities in experimentally accessible timescales. Such an observation is readily beyond understandings built upon previous works [ ]–[ ]. While the semi-classical dynamics of a triangular breather can be obtained analytically with a nice duality between hydrodynamics and the Liouville equation for ideal gases [ ], a complete picture of this remarkable ENS experiment remains open as of now. Here, we demonstrate that these extraordinary behaviors of breathers originate from an intrinsic property of representing the $su(1,1)$ algebra. In particular, the underlying algebra and the geometric representation of $SU(1,1)$ echoes allow us to infer how initial shapes of breathers lead to distinct superpositions of Poincaré disks and consequently, the revival times.

$SU(1,1)$ echoes arise from the identity,

$$\mathrm{e}^{-\mathrm{i}(\varphi_1 K_1+\varphi_2 K_2)}\mathrm{e}^{-\mathrm{i}\pi K_0}\mathrm{e}^{-\mathrm{i}(\varphi_1 K_1+\varphi_2 K_2)}\mathrm{e}^{\mathrm{i}\pi K_0}=\mathcal{I}, \tag{2.19}$$

where $\mathcal{I}$ is the identity operator, $\varphi_1$ and $\varphi_2$ are two arbitrary real numbers.

As shown in Fig. (b), $\mathcal{U}_1 = \mathrm{e}^{-\mathrm{i}\varphi_1 K_1}$ moves a given initial state along a diameter and it is then followed by a rotation $\mathcal{U}_0 = \mathrm{e}^{-\mathrm{i}\pi K_0}$. Using Eq. , we conclude $(\mathcal{U}_0\mathcal{U}_1)^2 = \mathrm{e}^{-\mathrm{i}2\pi K_0}$. Namely, the dynamics amounts a rotation of $2\pi$ about the origin on the Poincaé disk, recovers the initial state. This echo applies to any initial states on the Poincaré disk and any $\varphi_1 K_1 + \varphi_2 K_2$.

While our results are applicable to any eigenstates of a harmonic trap, we first take the initial state as the ground state of the Hamiltonian, $H_0 = 2K_0$, to illustrate our scheme. We consider a periodical driving of trapping frequency, such that the Floquet Hamiltonian is written as

$$\begin{aligned} &H_1 = (1+\kappa^2)K_0 + (1-\kappa^2)K_1, \quad nT < t < nT + t_1, \\ &H_0 = 2K_0, \qquad nT + t_1 < t < (n+1)T, \end{aligned} \tag{2.20}$$

where $n$ is a non-negative integer, and $T = t_0 + t_1$ defines a period. Within the time intervals $nT < t < nT + t_1$, the trapping frequency is $\kappa\omega_0$, where $\kappa$ could be an arbitrary

real or imaginary number. When $\kappa$ is imaginary, it corresponds to an inverted harmonic trap. Within the time intervals $nT + t_1 < t < (n+1)T$, the original trap frequency $\omega_0$ is restored. Using this time-dependent Hamiltonian, we obtain the propagator from $t = nT$ to $t = (n+2)T$, $(\mathcal{U}_0\mathcal{U}_1)^2 = (\mathrm{e}^{-\mathrm{i}H_0 t_0}\mathrm{e}^{-\mathrm{i}H_1 t_1})^2$, which can be rewritten as

$$\mathrm{e}^{-\mathrm{i}(\zeta_1+2t_0)K_0}\mathrm{e}^{-\mathrm{i}\eta_1 K_1}\mathrm{e}^{-\mathrm{i}(2\zeta_1+2t_0)K_0}\mathrm{e}^{-\mathrm{i}\eta_1 K_1}\mathrm{e}^{-\mathrm{i}\zeta_1 K_0}, \tag{2.21}$$

where $\zeta_1 = \arctan\Big(\frac{1+\kappa^2}{2\kappa}\tan\kappa t_1\Big)$ and $\eta_1 = 2\mathrm{arcsinh}\left(\frac{1-\kappa^2}{2\kappa}\sin(\kappa t_1)\right)$, the Baker-Campbell-Hausdorff formula [ ] has been implemented. When $\boldsymbol{\pi} = 2(t_0 + \zeta_1)$, or equivalently,

$$t_0 = \frac{\boldsymbol{\pi}}{2} - \zeta_1 = \frac{\boldsymbol{\pi}}{2} - \arctan\left(\frac{1+\kappa^2}{2\kappa}\tan\kappa t_1\right), \tag{2.22}$$

an echo is delivered. Under this condition, $(\mathcal{U}_0\mathcal{U}_1)^2 = \mathrm{e}^{-\mathrm{i}2\pi K_0}$. After two driving periods, the system revives with only an additional overall phase $2\boldsymbol{\pi}k$, since we consider an eigenstate of a harmonic trap with a definite $k$. Once $H_0$ and $H_1$ are fixed, tuning $t_0$ to deliver a $SU(1,1)$ echo is an analogue of adjusting the pulse's duration in creating a $\boldsymbol{\pi}$ rotation on a Bloch sphere in spin echoes.

Since $K_0 - K_1 = \sum_{\mathrm{i}} r_{\mathrm{i}}^2/2$, we can write the potential energy within the time interval $nT + t_1 < t < (n+1)T$ as $E_{\mathrm{pot}} = \langle \frac{1}{2}\sum_{\mathrm{i}} r_{\mathrm{i}}^2\rangle = \langle K_0 - K_1\rangle$. Using properties of $SU(1,1)$ coherent states, $\langle k, z|K_0|k, z\rangle = k\frac{1+|z|^2}{1-|z|^2}$, $\langle k, z|K_1|k, z\rangle = 2k\frac{\mathrm{Re}(z)}{1-|z|^2}$, we obtain,

$$E_{\mathrm{pot}} = k[1 + |z|^2 - 2\mathrm{Re}(z)]/(1 - |z|^2). \tag{2.23}$$

In the time interval $nT < t < nT + t_1$, the expectation value of $E_{\mathrm{pot}}$ is simply multiplied by $\kappa^2$. Clearly, $E_{\mathrm{pot}}$ has period $2T$. We have $k = E_g/2$, if the system is precisely prepared in the ground state of $H_0$ with energy $E_g$. The aforementioned results hold for any finite temperatures in thermal equilibrium since they are applicable to all eigenstates of the initial Hamiltonian. Under inverse temperature $\beta$, $k$ in Eq. ( ) should be replaced by $\langle K_0\rangle_{\mathrm{thermal}} = \mathrm{Tr}(K_0\mathrm{e}^{-\beta H_0})/\mathrm{Tr}(\mathrm{e}^{-\beta H_0})$.

We consider an explicit example as the two-dimensional bosons. While it is challenging to determine the exact many-body state when we consider the quantum dynamics of two

dimensional interacting bosons controlled by the $su(1,1)$ algebra, in the weakly interacting regime, such dynamics is well-captured by a Gross-Pitaevskii (GP) equation, The Gross-Pitaevskii (GP) equation,

$$\mathrm{i}\frac{\partial\Psi(\mathbf{r},t)}{\partial t}=\left(-\frac{\nabla^2}{2}+\frac{\kappa(t)^2r^2}{2}+gN|\Psi(\mathbf{r},t)|^2\right)\Psi(\mathbf{r},t), \tag{2.24}$$

well capture the dynamics in the weakly interacting regime. $\Psi(\mathbf{r},t)$ is the condensate wavefunction. where $g=4\pi a_0$ with $a_0$ being the dimensionless scattering length, $N$ denotes the boson number. We can apply an imaginary time evolution in obtaining the ground state condensate wavefunction of $H_0$. Then, we evolve the condensate according to the GP equation with $\kappa(t)$ determined by Eq. . We trace both the overlap intergral between the initial and the condensate wavefunction at time $t$, $F(t)=|\int \mathrm{d}\mathbf{r}\Psi^*(\mathbf{r},0)\Psi(\mathbf{r},t)|$, and the absolute value of the potential energy, $|E_{\mathrm{pot}}|$. Fig. shows a few typical choices and the corresponding dynamics on the Poincaé disk. (I), when we have real $\kappa$, $H_1$ corresponds to a harmonic trap with a different frequency. The field strength providing the energy scale of $H_1$ is $\xi=2\kappa$. The trajectory on the Poincaré disk follows a closed loop. (II), when the harmonic trap is turned off, $\kappa=\xi=0$. The trajectory on Poincaré disk is critical, as it travels to the boundary circle of the disk and eventually becomes tangent with it. (III), when $\kappa$ is imaginary, we have a deconfining potential pushing the BECs to expand and a purely imaginary spectrum, which denotes the quasi-normal modes. On the Poincaré disk, the system follows open trajectory towards the boundary of the disk. This result in scale-invariant quantum gases is similar to that in momentum modes of weakly interacting Bose gases we discussed in the previous section, underlies the powerful group theoretical approach. Without $H_0$, quantum dynamics governed by $H_1$ are distinct for different $\kappa$'s, nevertheless, we can always design $t_0$ and obtain revivals using $SU(1,1)$ echoes, as shown in Fig. .

When the initial state becomes a superposition of eigenstates with different $k$, we need to consider trajectories on multiple Poincaré disks in capturing the dynamics. Without loss of generality, we consider an initial state $|\Psi\rangle=\sum_{n,k}c_{nk}|k,n\rangle=\sum_k|\psi_k\rangle$, where $|\psi_k\rangle=\sum_n c_{nk}|k,n\rangle$ and $\langle\psi_{k'}|\psi_k\rangle\sim\delta_{k,k'}$. Other quantum numbers for the same $k,n$ are suppressed. Applying an an arbitrary propagator $\mathcal{U}$ in the $SU(1,1)$ group, $|\Psi\rangle$ becomes $\sum_k\mathcal{U}|\psi_k\rangle$, where

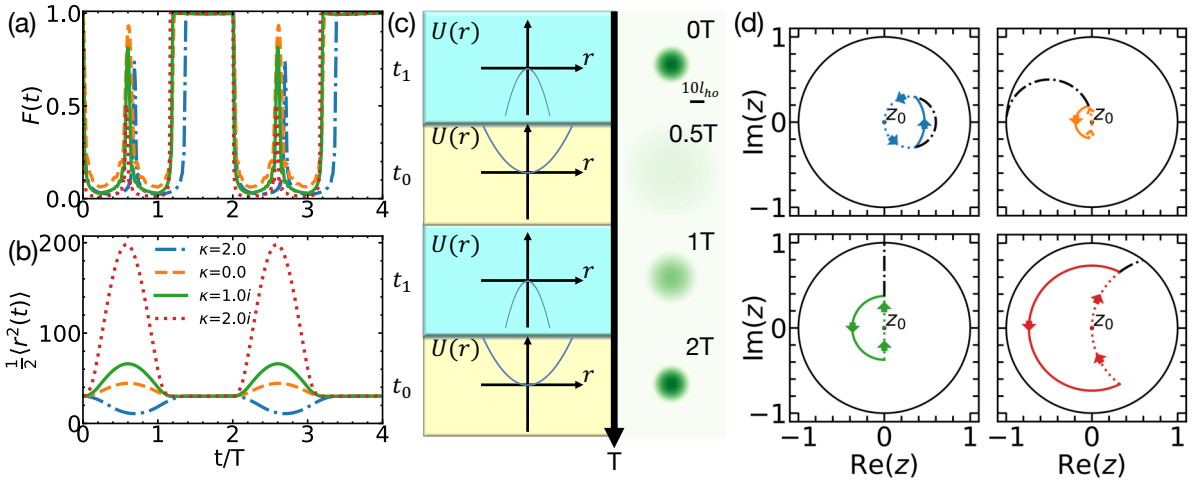


**Figure 2.4.** (a-b) $F(t)$ and $\langle r^2(t)\rangle/2$ of 2D BECs simulated by the GP equation with time-dependent $\kappa(t)$. The initial state is prepared as the ground state of the GP equation with $\kappa = 0$ using imaginary time evolution. $\kappa = 2(0)$ corresponds to a modified (vanished) trapping frequency in the time interval, $nT < t < nT + t_1$. $\kappa = \mathrm{i}, 2\mathrm{i}$ correspond to inverted harmonic traps in the time interval, $nT < t < nT + t_1$. $Ng = 25600$, $\omega_0 = 20 \times 2\pi\mathrm{Hz}$ and $t_1 = \pi/8$. $t_0$ is determined by Eq. . (c) Left panel: trapping potentials in different time intervals. Right panel: density snapshots for $\kappa = 2\mathrm{i}$ at various times. (d) Trajectories on the Poincaré disk. Dotted (solid) lines are evolutions governed by $H_1$ ($H_0$) in the periodic driving. Dot-dashed lines represent the dynamics if only $H_1$ is applied.

each $\mathcal{U}\,|\psi_k\rangle$ in the summation corresponds to an evolution on a single disk. Thus, the dynamics are superpositions of trajectories on several Poincaré disks. If an echo, $(\mathcal{U}_0\mathcal{U}_1)^2 = \mathrm{e}^{-2\mathrm{i}\pi K_0}$, acts for $m$ times on the initial state, we find

$$\mathrm{e}^{-2\mathrm{i}\pi m K_0}\,|\Psi\rangle = \sum\nolimits_{n,k} c_{nk}\mathrm{e}^{-2\mathrm{i}\pi m k}\,|k,n\rangle\,. \tag{2.25}$$

By substituting an integral over $k$ for the sum in Eq. , this initial state will include incommensurate $k$'s and the dynamics lacks a finite periodicity. Here, we only apply summation of discrete $k$'s such that the periodicity is well-defined. Since the factor $\mathrm{e}^{-2\mathrm{i}\pi m k}$ is independent of the index $n$, the return probability $P(m) = |\langle\Psi(0)|\Psi(2mT)\rangle|^2$ becomes $P(m) = \left|\sum_k \tilde{P}_k \mathrm{e}^{-2\mathrm{i}\pi m k}\right|^2$, where $\tilde{P}_k = \sum_n |c_{nk}|^2$, $\sum_k \tilde{P}_k = 1$. It is clear that $P(m) = 1$ only if for all $k$'s with a non-vanishing $c_{nk}$, $\mathrm{e}^{-2\mathrm{i}\pi m k} = \mathrm{e}^{\mathrm{i}\phi_0}$, where $\phi_0$ is a $k$-independent constant.

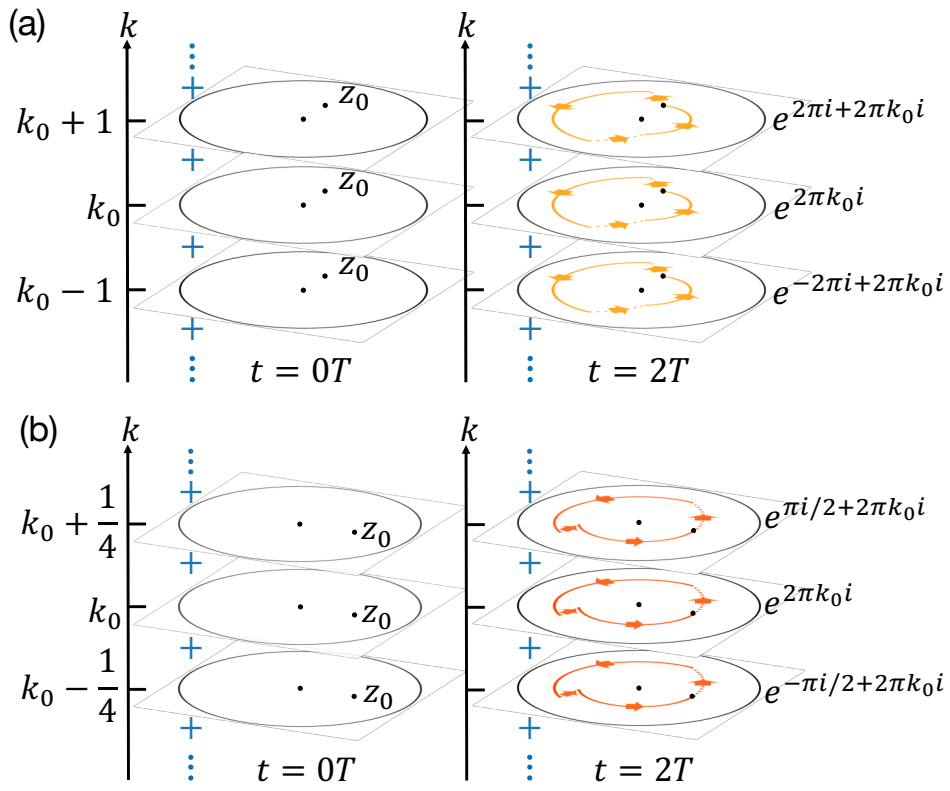


**Figure 2.5.** (a) Dynamics on different disks acquire the same phase at $t = 2T$ and the system revives. (b) Dynamics on different disks accumulate different phases and a relative phase appears at $t = 2T$. The system revives after $8T$.

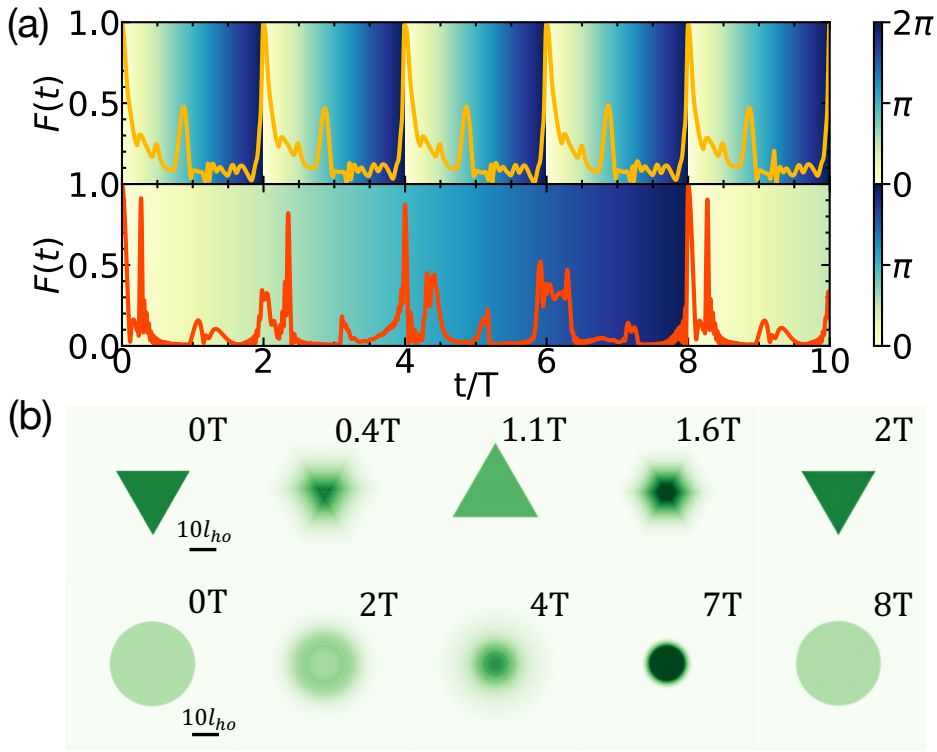


**Figure 2.6.** (a) $F(t)$ of breathers with different shapes. In numerics, we use $\omega_0 = 40 \times 2\pi\text{Hz}$, $t_1 = \pi/8$, and $\kappa = 0.5\text{i}$. $Ng = 25600$ (12800) for the triangle (disk). The time-dependent relative phase between different Poincaré disk is represented by background color. (b) condensate wavefunction at various times.

If the initial state only contains a single state $|k_0, n_0\rangle$, this condition is certainly satisfied. Clearly, it will never be satisfied if incommensurate $k$'s are included. Whereas incommensurate $k$'s does not exist when we consider excitations in momentum modes [ ], [ ], [ ], it may arise in breathers with a continuous spectrum of $k$.

Commensurate $k$'s can be represented by $k = k_0 + p/Q$, where $k_0$ is a given reference with a non-vanishing $c_{nk_0}$, $p \in \mathbb{Z}$ and $Q \in \mathbb{N}_+$ are co-prime numbers. If only commensurate $k$'s are involved in the initial state, the system revives with a period of $2QT$. As such, different superpositions of $|k, n\rangle$ in the initial state may result in distinct revival times. The period multiplies for $Q > 1$. Examples corresponding to $Q = 1$ and $Q = 4$ with revival times $2T$ and $8T$ are shown in Fig. .

We can apply the analysis above to breathers with distinct initial shapes. Such breathers are prepared as the ground states of flat-box potentials with the corresponding shapes. Since such a Hamiltonian does not commute with $K_0$, the initial state involves a superposition of multiple $|k, n\rangle$. For the triangular shape, $F(t)$ satisfies $F(t) = F(t + 2T)$. The differences between $k$'s is necessarily integral. Therefore, it has $Q = 1$ as shown in Fig. (a). For the circular shape, the revival time is $8T$ as shown in Fig. . We, therefore, conclude that the initial state must have a superposition similar to Fig. (b).

While it is the exact many-body state instead of the condensate wavefunction that evolves without the GP equation approach, the results from GP simulations are expected to serve as a good approximation in the weakly interacting limit. The specific form of the many-body state that corresponds to a given initial shape of the breather is still an intriguing unresolved problem that merits further investigation. In contrast, $c_{nk}$ can be directly evaluated in few-body systems. For example, eigenvalues of the Casimir operator are related to the angular momenta in a two-body problem. As such, the initial shape of the two-body wavefunction directly predicts the revival time (Appendix).

### 2.6 Detecting Imperfect Revivals

Similar to spin echoes, $SU(1,1)$ echoes could be implemented to detect symmetry breaking perturbations, such as an extra external potential in experiments. We have considered systems with the $SU(1,1)$ symmetry and designed echoes using the $su(1,1)$ algebra. Once a perturbation breaks the $SU(1,1)$ symmetry, the echoes will not fully recover the initial state. When interactions between spins or other effects break the $SU(2)$ symmetry, one uses the spin echo to trace these effects by measuring the imperfect revival. In this section, we consider that a static quartic $r^4$ potential exists as a non-harmonic perturbation in the trapping potential. To be specific, the Hamiltonians are given by

$$\begin{aligned} H_1 &= (1+\kappa^2)K_0 + (1-\kappa^2)K_1 + \sum_{\mathrm{i}} a_q r_{\mathrm{i}}^4, \quad nT < t < nT + t_1, \\ H_0 &= 2K_0 + \sum_{\mathrm{i}} a_q r_{\mathrm{i}}^4, \qquad nT + t_1 < t < (n+1)T, \end{aligned} \tag{2.26}$$

$a_q$ is made dimensionless with units set by $\omega_0$. Since there is no simple analytical solution, we numerically solve the GP equation,

$$\mathrm{i}\frac{\partial}{\partial t}\Psi(\mathbf{r},t)=\left(-\frac{1}{2}\nabla^2+\frac{1}{2}\kappa(t)^2r^2+a_qr^4+gN|\Psi(\mathbf{r},t)|^2\right)\Psi(\mathbf{r},t), \tag{2.27}$$

where the initial state is prepared as the ground state of $2K_0$ by an imaginary time evolution such that the system has a period of $2T$ if perfect echoes are delivered.

As shown in Fig. (a-b), for a given $a_q$, the overlap $F(2nT)$ between the wavefunction at $t=2nT$ and initial state decreases with increasing $n$. The expectation value of $r^2$ at $2nT$ also deviates from a constant. In Fig. (c-d), we explicitly show how $F(2T)$ and $\langle r^2(2T)\rangle$ change as functions of $a_q$. Thus, these revival signals allow experimentalists to trace the amplitude of the quartic potential.

Similarly, a symmetry breaking term in weakly interacting Bose gases causes the growth of particle number even the echo is applied. Here, interactions between excited particles are included. As the growth of population of the resonant mode, the dominant corrections become interactions at this mode. The Hamiltonian becomes $\tilde{H}_{\vec{k}}=H_{\vec{k}}+H'_{\vec{k}}$, where $H'_{\vec{k}}=U'(4c^\dagger_{\vec{k}}c_{\vec{k}}c^\dagger_{-\vec{k}}c_{-\vec{k}}+c^\dagger_{\vec{k}}c^\dagger_{\vec{k}}c_{\vec{k}}c_{\vec{k}}+c^\dagger_{-\vec{k}}c^\dagger_{-\vec{k}}c_{-\vec{k}}c_{-\vec{k}})$ can be rewritten as

$$H'_{\vec{k}}=6U'(K_0-2/3)^2, \tag{2.28}$$

We have chosen the initial state as the two-mode vacuum. Here, $U'=\tilde{U}/2V$. A finite $U'$ leads to a $K_0^2$ term, that breaks the $SU(1,1)$ dynamical symmetry. As a result, an $SU(1,1)$ echo can not lead to perfect revivals. In the same way that the spin echo is used to extract interactions between spins and other important information, the $SU(1,1)$ echo can then be used to measure the interactions between excited particles. Using the algebraic method, we analytically obtain the population at $t=2mT_d, m\in\mathbb{N}$,

$$N_{\vec{k}}(2mT_d)=\frac{27\cosh\left(8\tilde{U}|\Psi_0|^2t_1\right)}{16\tilde{U}^2|\Psi_0|^4}m^2U'^2. \tag{2.29}$$

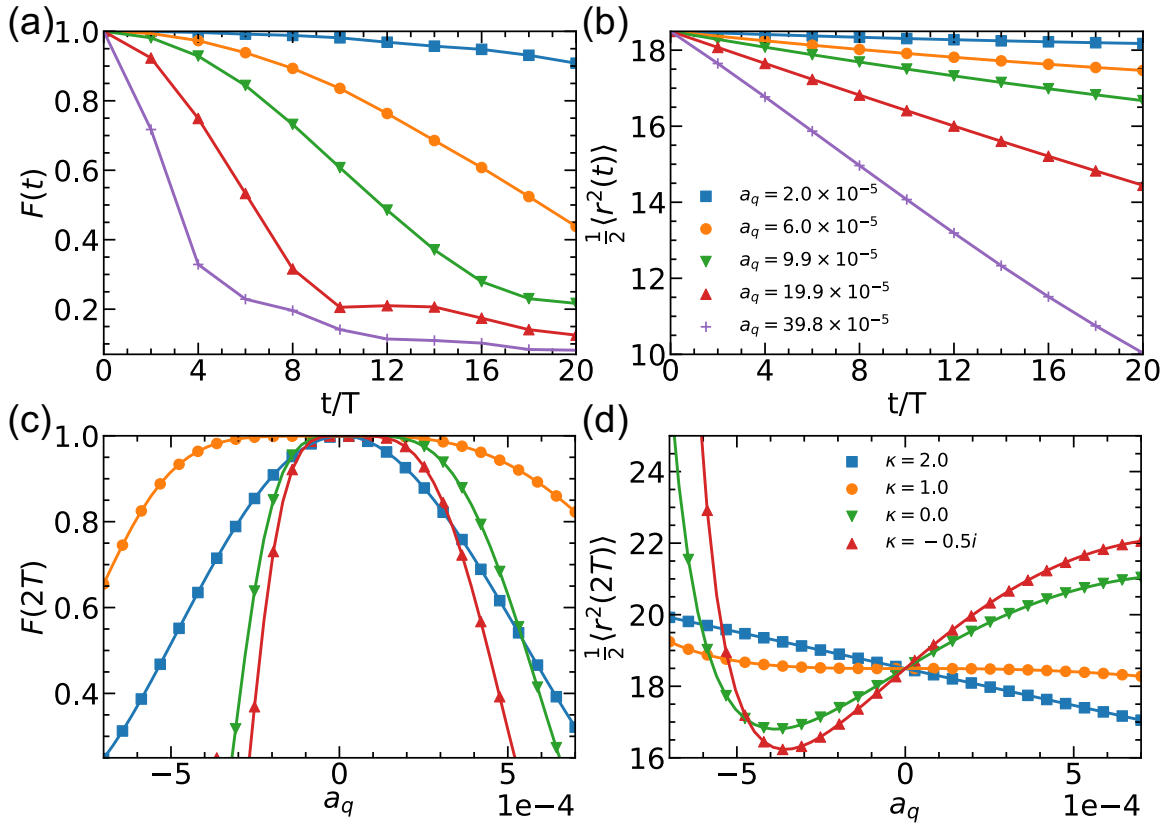


**Figure 2.7.** (a-b) Numerical results of $F(t)$ and $\langle r^2(t)\rangle/2$ of 2D BECs at stroboscopic time $2nT$ as functions of $n$ for different $a_q$'s. $Ng = 9600$, $\kappa = 2$, $\omega_0 = 20 \times 2\pi$Hz and $t_1 = \pi/8$. $t_0$ is determined by Eq. . (c-d) Numerical results of $F(t)$ and $\langle r^2(t)\rangle/2$ of 2D BECs at $t = 2T$ as functions of $a_q$ for different $\kappa$'s. $Ng = 9600$, $\omega_0 = 20 \times 2\pi$Hz and $t_1 = \pi/8$. $t_0$ for different $\kappa$ is determined by Eq. .

Confirmed by numerical calculations, Eq. shows that $N_{\vec{k}}(2mT_d)$ vanishes when $U' = 0$. If $U' \neq 0$, $N_{\vec{k}}(2mT_d)$ increases quadratically as a function of $m$, as shown in Fig.( ). Thus, the imperfect revival allows experimentalists to measure unveils $U'$. In particular, $N_{\vec{k}}(2mT_d)$ depends on $\tilde{U}|\Psi_0|^2 t_1$ exponentially. Increasing $t_1$ could further improve the precision of the measurement. Alternatively, if $U'$ is known, Eq. allows experimentalists to measure $\tilde{U}|\Psi_0|^2 t_1$ with high precision due to the exponential dependence of $N_{\vec{k}}(2mT_d)$ on this parameter.

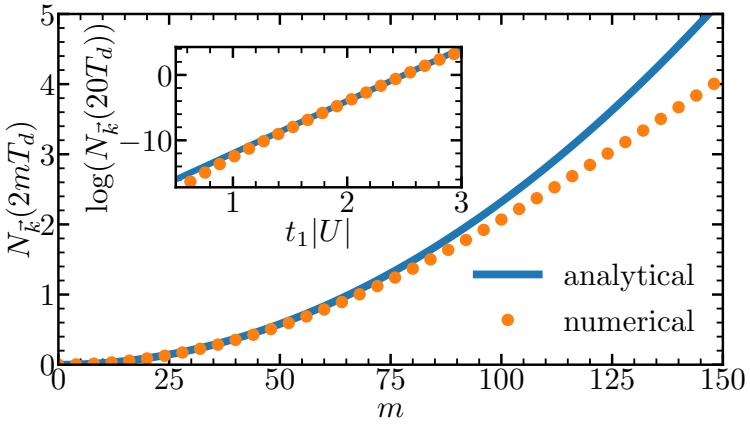


**Figure 2.8.** The particle number that is excited because of the imperfect echo at stroboscopic time $mT_d$. $U < 0$, $t_1|U| = 2.2$, $E_{\vec{k}}/|U| = 1$ and $U'/|U| = -5 \times 10^{-6}$. Inset shows the logarithm of $N_{\vec{k}}$ at $t = 20T_d$, confirming an exponential dependence of $t_1|U|$.

## 2.A Lengths of trajectories

We consider the quench dynamics where the initial state is the vacuum. The state at time $t$ is

$$|z(t)\rangle = \mathrm{e}^{-\mathrm{i}(\xi_0 K_0+\xi_1 K_1+\xi_2 K_2)t}\,|0\rangle_{\vec{k}}\,|0\rangle_{-\vec{k}} = \mathcal{U}(t)\,|0\rangle_{\vec{k}}\,|0\rangle_{-\vec{k}}\,. \tag{2.30}$$

$z(t)$ can be evaluated by writing $\mathcal{U}(t)$ in its normal ordering form [ ], and we will have

$$z(t) = -\mathrm{i}\frac{(\xi_1-\mathrm{i}\xi_2)\sin(\xi t/2)}{\xi\cos(\xi t/2)+\mathrm{i}\xi_0\sin(\xi t/2)},\ \xi=\sqrt{\xi_0^2-\xi_1^2-\xi_2^2}. \tag{2.31}$$

Therefore, the length of the trajectory as a function of $t$ on the Poincaré disk is

$$\tilde{L} = \int_0^t \sqrt{4\left|\frac{\mathrm{d}z}{\mathrm{d}t'}\right|^2 \frac{1}{(1-|z(t')|^2)^2}}\,\mathrm{d}t' = |\xi_1-\mathrm{i}\xi_2|t, \tag{2.32}$$

which holds for any $\xi_{0,1,2}\in\mathbb{R}$. Eq. ( ) reduces to $|\xi|t$ when we consider the resonance mode, where $\xi_0=0$, $|\xi|=|\xi_1-\mathrm{i}\xi_2|$, which is Eq. ( ) in the main text.

We note that, this result is not accidental. Since different trajectories here have the same $\xi_{1,2}$ but different $\xi_0$, we can apply the circuit depth, where the cost function is defined as $F[Y_\mathrm{i}]=\sqrt{Y_1^2+Y_2^2}$, in geometrizing the quantum dynamics. While the detailed calculation will be introduced in the following chapter, the resulted metric here is that of a Poincaré disk. We, therefore, conclude that trajectories of any dynamics with the same $\sqrt{\xi_1^2+\xi_2^2}$ share the same length under the metric of the Poincaré disk.

## 2.B Two unitary fermions in a harmonic trap

We consider one spin-up and one spin-down fermion in a three-dimensional harmonic trap, whose relative motion and the center of mass are decoupled. The $su(1,1)$ algebra applies to both degrees of freedom. The Hamiltonian is written as $H=H_{CM}+H_{rel}$,

$$\begin{aligned} H_{CM} &= -\frac{\hbar^2}{2M}\nabla_{\mathbf{R}}^2+\frac{1}{2}M\omega_0^2R^2,\\ H_{rel} &= -\frac{\hbar^2}{2\mu}\nabla_{\mathbf{r}}^2+\frac{1}{2}\mu\omega_0^2r^2. \end{aligned} \tag{2.33}$$

where $M = 2m$, $\mu = m/2$, $\mathbf{R} = (\mathbf{r}_1 + \mathbf{r}_2)/2$, $\mathbf{r} = \mathbf{r}_1 - \mathbf{r}_2$, $m$ is the mass of fermions. The interaction in the unitary limit is replaced by the Bethe-Peierls boundary condition of the relative motion, namely

$$\Psi_{rel}(\mathbf{r}) \underset{r\to 0}{\propto} \frac{1}{r}, \tag{2.34}$$

$\Psi_{rel}(\mathbf{r})$ is the relative wave function and $\Psi(\mathbf{R}, \mathbf{r}) = \Psi_{CM}(\mathbf{R})\Psi_{rel}(\mathbf{r})$. Since the center of mass has the same simple dynamics of a single particle in a harmonic trap, we focus on the relative motion, which has the $SU(1,1)$ generators [ ],

$$K_0^r = \frac{1}{2}\left(-\frac{1}{2}\nabla^2 + \frac{1}{2}r^2\right), \quad K_1^r = \frac{1}{2}\left(-\frac{1}{2}\nabla^2 - \frac{1}{2}r^2\right), \quad K_2^r = \frac{1}{4\mathrm{i}}\left(\mathbf{r}\cdot\nabla + \nabla\cdot\mathbf{r}\right). \tag{2.35}$$

We have chosen the harmonic length $l_{ho} = \sqrt{\hbar/(\mu\omega_0)}$ as the unit length and $\hbar\omega_0$ as the unit energy. We first evaluate the Casimir operator of the $su(1,1)$ algebra,

$$C = (K_0^r)^2 - (K_1^r)^2 - (K_2^r)^2 = \frac{L^2}{4\hbar^2} - \frac{3}{16}, \tag{2.36}$$

where $L$ is the angular momentum operator for the relative motion. $C$ has the eigenvalue $l(l+1)/4 - 3/16$ for the angular momentum eigenstate $|l, m\rangle$. Therefore we denote the eigenstate of $C$ by $|k, n; l, m\rangle$. Here $n$ is the principle quantum number, $k$ is the Casimir quantum number, $l$ and $m$ are the angular momentum and magnetic quantum number, respectively. Since $C\,|k, n; l, m\rangle = k(k-1)\,|k, n; l, m\rangle = (l(l+1)/4 - 3/16)\,|k, n; l, m\rangle$, we obtain

$$k = \frac{l}{2} + \frac{3}{4}, \quad l \geq 0; \qquad k = \frac{1}{4} \quad \text{or} \quad \frac{3}{4}, \quad l = 0, \tag{2.37}$$

where we only consider the positive discrete series for the representation of $SU(1,1)$. Using $K_-\,|k, 0; 0, 0\rangle = 0$, we find

$$\left\langle \mathbf{r}\middle|\frac{1}{4}, 0; 0, 0\right\rangle \underset{r\to 0}{\propto} \frac{1}{r}, \qquad \left\langle \mathbf{r}\middle|\frac{3}{4}, 0; 0, 0\right\rangle \underset{r\to 0}{\propto} 1. \tag{2.38}$$

We conclude that the ground state of the relative motion of two unitary fermions in the $s$-wave channel corresponds to $|1/4, n; 0, 0\rangle$. As for the center of mass, the same argument leads to $|3/4, n; 0, 0\rangle$. The spectrum of the relative motion becomes

$$E_r = l + \frac{3}{2} + 2n, \quad l \geq 1, \qquad E_r = \frac{1}{2} + 2n, \quad l = 0. \tag{2.39}$$

The dynamics on multiple Poincaré disks can be generated by choosing an initial state as a superposition of different angular momentums. For example, we consider the initial state as a mixture of $s$ and $d$-wave for their relative motion. The $s$-wave subspace has $k_s = 1/4$ and the $d$-wave subspace has $k_d = 7/4$ for any magnetic quantum number $m'$. The initial state and the state at the end of $2m$ Floquet periods are

$$\begin{aligned} |\Psi(0)\rangle &= |\Psi_{CM}\rangle \otimes \textstyle\sum_n \left( s_n \, |1/4, n; 0, 0\rangle + \sum_{m'} d_{nm'} \, |7/4, n; 2, m'\rangle \right), \\ |\Psi(2mT)\rangle &= |\Psi_{CM}\rangle \otimes \textstyle\sum_n \Big( \mathrm{e}^{-\mathrm{i}(1/4+n)2\pi m} s_n \, |1/4, n; 0, 0\rangle \\ &\qquad + \mathrm{e}^{-\mathrm{i}(7/4+n)2\pi m} \textstyle\sum_{m'} d_{nm'} \, |7/4, n; 2, m'\rangle \Big), \end{aligned} \tag{2.40}$$

respectively. Since $k_s = k_d - 3/2$, $Q = 2$, using Eq. (  ), we conclude that it takes 4 Floquet periods for the systems to recover its initial state.

If the $s$-wave scattering length vanishes, the $s$-wave subspace has $k'_s = 3/4$, while $d$-wave subspace still has $k'_d = 7/4$. Therefore, we obtain $k'_s = k'_d - 1$, $Q = 1$. It takes the same initial state 2 Floquet periods to return to the initial state.

# 3. EMERGENT SPACETIMES FROM HERMITIAN AND NON-HERMITIAN QUANTUM DYNAMICS

*The contents of this chapter are based on and modified from the article [ ] by C. Lv, and Q. Zhou, Emergent spacetimes from Hermitian and non-Hermitian quantum dynamics, arXiv preprint arXiv:2205.07429, (2022).*

In the previous chapter, we show the $su(1,1)$ dynamical symmetry gives rise to emergent hyperbolic space as a Poincaré disk. Such a geometric approach leads to the $SU(1,1)$ echo, a powerful group-theoretical method for reversing quantum dynamics in various systems. This chapter shows an Anti-de Sitter spacetime in 2+1 dimensions ($\mathrm{AdS}_{2+1}$) can emerge from any quantum system with $SU(1,1)$ dynamical symmetry, by applying the continuous circuit depth in defining the distance. The time measured in laboratories becomes either the proper time or distance, and quench dynamics now follow geodesics of $\mathrm{AdS}_{2+1}$. Such a geometric approach unifies a broad range of prototypical phenomena that appear disconnected. For instance, the light cone of $\mathrm{AdS}_{2+1}$ underlies the onsite parametric amplification, the expansions of unitary fermions released from harmonic traps, and the exceptional points representing the PT symmetry breaking in non-Hermitian systems. In practice, it provides a transparent means of optimizing quantum controls by exploiting the shortest trajectories in the emergent spacetimes. It also allows experimentalists to engineer emergent spacetimes and induce tunnelings between different $\mathrm{AdS}_{2+1}$.

## 3.1 Introduction

Though the existence of spacetime is most self-evident in conventional wisdom, studies have shown that spacetimes could arise as emergent phenomena in quantum systems. In certain strongly coupled systems, the underlying gauge theory has a gravitational counterpart with an extra dimension [ ], [ ], [ ]–[ ]. It has also been found that circuit depth, a fundamental concept in quantum computation that represents the number of steps to reach a target state, can be visualized using certain geometries [ ], [ ], [ ]–[ ]. These emergent spacetimes provide physicists not only a unique means to explore quantum systems but also a new perspective connecting multiple disciplines ranging from condensed matter physics and quantum information to high energy physics.

To derive an emergent spacetime metric from quantum dynamics, a continuous version of circuit depth is often used [ ], [ ], [ ]–[ ]. Consider quantum gates that are produced from a collection of unitary operators generated by $\{K_{\rm i}\}$, a generic expression for a gate can be written as $\mathrm{e}^{-\mathrm{i}\sum_{\rm i} Y_{\rm i}K_{\rm i}}$, where $Y_{\rm i}$ are real numbers. A sequence of gates turns a reference state, $|R\rangle$, prepared at the initial time $\tau = 0$ into a target state at time $\tau$, $|T\rangle = U|R\rangle$, where $U = \mathrm{T}\mathrm{e}^{-\mathrm{i}\int_0^\tau d\tau[\sum_{\rm i}\xi_{\rm i}(\tau)K_{\rm i}]/\hbar}$ is the propagator and T is the time-ordering operator. In a single gate operated in a time interval between $\tau$ and $\tau + d\tau$, $Y_{\rm i} = \xi_{\rm i}(\tau)d\tau/\hbar$, where $\xi_{\rm i}$ is the ith component of a field coupled to $K_{\rm i}$. The cost is written as

$$S = \int_0^\tau F[Y_{\rm i}(\tau)], \tag{3.1}$$

where $F[Y_{\rm i}]$ is a chosen function based on certain physical considerations. For instance, if $F[Y_{\rm i}] = \sum_{\rm i}|Y_{\rm i}|$, $S$ amounts to the total number of steps of all operations produced by independent $K_{\rm i}$ to reach the target state. A variety of other cost functions were considered in the literature [ ], [ ], [ ], [ ]. Viewing $S$ as a line integral, $S = \int ds$, an evolution within an infinitesimal time $d\tau$ is mapped to a line element $ds = F[Y_{\rm i}(\tau)]$, from which the corresponding metrics can be obtained.

### 3.2 Emergent $\mathbf{AdS}_{2+1}$ Spacetime

Here, we consider generators of the $SU(1,1)$ group. As we have seen, they produce Hamiltonians of a wide range of quantum systems with $SU(1,1)$ symmetry, i.e., $H(\tau) = \sum_{\rm i}\xi_{\rm i}(\tau)K_{\rm i}$, where $\xi_{\rm i}$ are real [ ], [ ], [ ], [ ], [ ]. They are also fundamental ingredients in holographic tensor networks, determining how quantum entanglement is developed with changing the length scales [ ], [ ]. Table summarizes a few examples in few-body and many-body systems, which correspond to different representations of the $SU(1,1)$ group. Their dynamics can be unified once the underlying spacetimes are unfolded. Exploiting such spacetimes delivers new quantum controls such that quantum systems can fast reach any desired target states and also allow experimentalists to create intriguing spacetimes in laboratories.

We define the cost function as

$$F[Y_{\rm i}] = \sqrt{-Y_0^2 + Y_1^2 + Y_2^2}/2, \tag{3.2}$$

where $1/2$ is included for later convenience. Such $F$ is motivated by the following observations. Consider a Hamiltonian $H(\tau) = \sum_{\rm i} \xi_{\rm i}(\tau) K_{\rm i}$, the instantaneous eigenenergies are written as $\pm(m+k)\sqrt{\xi_0^2 - \xi_1^2 - \xi_2^2}$, where $m$ is an integer, $k$ is the Bargmann index. The strength of the field coupled to $\{K_{\rm i}\}$ is thus $\xi = \sqrt{\xi_0^2 - \xi_1^2 - \xi_2^2}$, as analogous to the strength of a magnetic field coupled to a spin in the $su(2)$ case. The equally spaced instantaneous eigenenergies thus set a natural time scale $\sim \hbar/\xi$. While it certainly takes less time to reach a target state by applying a larger external field, there are always constraints on the largest possible external fields accessible in realistic experiments. As such, it is desired to consider the shortest possible time at a constant $\xi$. Meanwhile, the line element,

$$ds = \sqrt{-\xi_0^2 + \xi_1^2 + \xi_2^2}\, d\tau/(2\hbar) \tag{3.3}$$

is equivalent to the experimental time $d\tau$ once the field strength $\xi$ is fixed. We can thus directly correlate the experimental time to circuit depth and obtain the shortest possible time to achieve the target state using the information provided by the metric of the emergent spacetime. Whereas $F \geq 0$ is often chosen, here, $F$ defined in Eq.(  ) can be either real or imaginary, dependent on Sign$(\xi^2)$. This simply corresponds to whether it is spacelike or timelike in the emergent spacetime as shown later.

We consider a parameterization of the propagator $U = {\rm T} {\rm e}^{-{\rm i}\int d\tau H(\tau)/\hbar}$ with $H(\tau) = \sum_{\rm i=0}^{2} \xi_{\rm i}(\tau) K_{\rm i}$ [  ],

$$U = {\rm e}^{-{\rm i}K_0(\varphi-\psi)} {\rm e}^{-2{\rm i}K_1\eta} {\rm e}^{-{\rm i}K_0(\varphi+\psi)}, \tag{3.4}$$

where $\eta$, $\psi$ and $\varphi$ are functions of $\tau$. Since ${\rm i}\hbar\frac{dU}{d\tau}U^{-1} = \sum_{\rm i=0}^{2} \xi_{\rm i}(\tau) K_{\rm i}$, we obtain $\xi_{\rm i} = {\rm Tr}[{\rm i}\hbar\frac{dU}{d\tau}U^{-1}K_{\rm i}^{\dagger}]$, with Cartan-Killing inner product ${\rm Tr}(K_{\rm i}K_{\rm j}^{\dagger}) = \delta_{\rm ij}$ [  ]. Substituting Eq.(  ) to the right-hand side of this expression, $\xi_{\rm i}$ is expressed as a function of $\eta$, $\psi$, $\varphi$ and $d\eta/d\tau$,

**Table 3.1.** Generators of $su(1,1)$ algebra in some Hermitian and non-Hermitian systems. $a$, $b$ ($a^{(\dagger)}$, $b^{(\dagger)}$) are bosonic annihilation (creation) operators. $R$ is the hyper-radius. $s_0$ is the three-body parameter. $R$ and $\vec{r}_{\rm i}$ has the unit of harmonic length $l_0 = (\hbar/(M(0)\omega(0)))^{1/2}$. $U$ has unit $\hbar\omega(0)$. The two-body interaction satisfies $U(\lambda\vec{r}) = \lambda^{-2}U(\vec{r})$ for any $\lambda$. $S_{\rm i=0,1,2}$ are angular momentum operators.

| | $K_0$ | $K_1$ | $K_2$ |
|---|---|---|---|
| One mode squeezing | $(2a^\dagger a+1)/4$ | $(a^{\dagger 2}+a^2)/4$ | $(a^{\dagger 2}-a^2)/(4{\rm i})$ |
| Two mode squeezing | $(a^\dagger a+b^\dagger b+1)/2$ | $(a^\dagger b^\dagger+ab)/2$ | $(a^\dagger b^\dagger-ab)/(2{\rm i})$ |
| Efimov states | $\left(-\partial_R^2+R^2-(1/4+s_0^2)/R^2\right)/4$ | $\left(-\partial_R^2-R^2-(1/4+s_0^2)/R^2\right)/4$ | $(R\partial_R+1/2)/(2{\rm i})$ |
| Scale-invariant quantum systems | $\left(\sum_{\rm i}(-\nabla_{\rm i}^2+r_{\rm i}^2)+\sum_{\rm i\neq j}U(\vec{r}_{\rm i}-\vec{r}_{\rm j})\right)/4$ | $\left(\sum_{\rm i}(-\nabla_{\rm i}^2-r_{\rm i}^2)+\sum_{\rm i\neq j}U(\vec{r}_{\rm i}-\vec{r}_{\rm j})\right)/4$ | $\sum_{\rm i}\left(\vec{r}_{\rm i}\cdot\nabla_{\rm i}+\nabla_{\rm i}\cdot\vec{r}_{\rm i}\right)/(4{\rm i})$ |
| a spin in a complex magnetic field | $S_0$ | ${\rm i}S_1$ | ${\rm i}S_2$ |

$d\psi/d\tau$, $d\varphi/d\tau$. The line element in Eq.(  ) is then expressed in terms of $\eta$, $\psi$, $\varphi$ and $d\eta$, $d\psi$, $d\varphi$, and we obtain

$$ds^2 = {\rm d}\eta^2 - \cosh^2(\eta)\,{\rm d}\varphi^2 + \sinh^2(\eta)\,{\rm d}\psi^2. \tag{3.5}$$

Eq.  describes a curved spacetime with a constant negative curvature, known as the Anti-de Sitter (AdS) spacetime in (2+1) dimensions [  ]. A coordinate transformation $\eta = 2{\rm arctanh}(\rho)$ leads to

$$ds^2 = -\left(\frac{1+\rho^2}{1-\rho^2}\right)^2 {\rm d}\varphi^2 + \frac{4}{(1-\rho^2)^2}\left({\rm d}\rho^2+\rho^2\,{\rm d}\psi^2\right), \tag{3.6}$$

and brings the boundary $\eta=\infty$ to $\rho=1$ as shown in Fig.  . Starting from a reference state, which is placed at the origin, any quantum evolution governed by a Hamiltonian $H = \sum_{\rm i=0}^2 \xi_{\rm i}K_{\rm i}$ is mapped to a trajectory $(\eta(\tau),\varphi(\tau),\psi(\tau))$ in this ${\rm AdS}_{2+1}$. When $\varphi$ is constant, $ds^2 = d\eta^2 + \sinh^2(\eta)d\psi^2$, ${\rm AdS}_{2+1}$ reduces to a Poincaré disk, recovering the geometry we previously obtained about geometrizing $SU(1,1)/U(1)$ [  ].

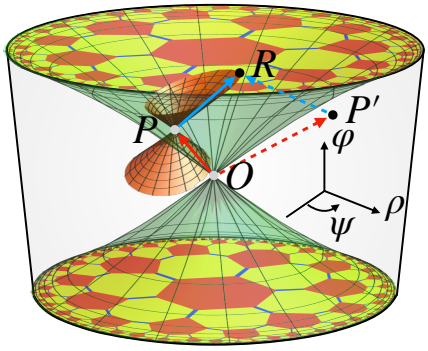


**Figure 3.1.** An $AdS_{2+1}$. Each cross section with a constant $\varphi$ is a Poincaré disk. Starting from the initial state $O$, the shortest path $OPR$ minimizes the cost or equivalently, the time spent from $O$ to $R$. $OP$ and $PR$ lay on the light cone of $O$ and $P$, respectively. A deviation from this trajectory, for instance $OPR$, where $P$ is not on the light cone of $O$, increases the cost and the time to reach the same target state $R$.

### 3.2.1 Quench dynamics as geodesics

If $\xi = 0$, from Eq.(  ), we see that this gives rise to $ds = 0$, i.e., the light cone in $AdS_{2+1}$. Using Eq.(  ), the explicit expression of the light cone can be obtained from $d\eta^2 = \cosh^2(\eta)d\varphi^2 - \sinh^2(\eta)d\psi^2$. The light cone centered at the origin is written as

$$\varphi \pm \arctan(\sinh(\eta)) = 0. \tag{3.7}$$

When $\xi^2 < 0$ ($\xi^2 > 0$), the quantum evolution is mapped to a trajectory in the spacelike (timelike) regime.

Being the local extreme of the proper time or the proper distance, geodesics distinguish themselves from other trajectories. Counterparts of geodesics in $AdS_{2+1}$ turn out to be quench dynamics, in which $\xi_{i=0,1,2}$ are time-independent constants,

$$\mathrm{Tr}\left[\frac{d}{d\tau}\left(\mathrm{i}\frac{dU}{d\tau}U^{-1}\right)K_{\mathrm{i}}^{\dagger}\right] = 0. \tag{3.8}$$

Applying the parameterization of $U$ in Eq. , we obtain

$$\begin{aligned}
\frac{d^2\varphi}{d\tau^2} &= -2\tanh(\eta)\frac{d\varphi}{d\tau}\frac{d\eta}{d\tau}, \\
\frac{d^2\eta}{d\tau^2} &= -\sinh(\eta)\cosh(\eta)\left[\left(\frac{d\varphi}{d\tau}\right)^2 - \left(\frac{d\psi}{d\tau}\right)^2\right], \\
\frac{d^2\psi}{d\tau^2} &= -2\coth(\eta)\frac{d\psi}{d\tau}\frac{d\eta}{d\tau}.
\end{aligned} \tag{3.9}$$

This is precisely geodesic equations in $\mathrm{AdS}_{2+1}$,

$$\frac{d^2x^\mu}{ds^2} = -\Gamma^\mu_{\nu\lambda}\frac{dx^\nu}{ds}\frac{dx^\lambda}{ds}, \tag{3.10}$$

which are led by the Christoffel symbols

$$\Gamma^\varphi_{\varphi\eta} = \tanh(\eta), \quad \Gamma^\eta_{\varphi\varphi} = \sinh(\eta)\cosh(\eta), \quad \Gamma^\eta_{\psi\psi} = -\sinh(\eta)\cosh(\eta), \quad \Gamma^\psi_{\eta\psi} = \coth(\eta). \tag{3.11}$$

Geodesics of $\mathrm{AdS}_{2+1}$ thus underlie quantum quench dynamics of systems with $SU(1,1)$ symmetry.

### 3.3 Applications in Various Systems

Since our results can be applied to any systems with $SU(1,1)$ symmetry, this geometrical approach provides a unified perspective to understand and explore a wide range of prototypical phenomena that appear disconnected, including but not limited to examples shown in Table . In the following discussions, we will use a few different systems to demonstrate various aspects of the emergent $\mathrm{AdS}_{2+1}$. Applications of our results to any other systems with $SU(1,1)$ symmetry are straightforward.

In the simplest representation using a single particle, $K_0$ ($K_1$) is the Hamiltonian in a harmonic (inverted harmonic) trap and $K_2$ is the scaling operator. More interesting repre-

sentations arise in Efimov states in three-body problems and interacting many-body systems. For instance, the Hamiltonian of unitary fermions in a 3D harmonic trap is written as

$$H = \sum_{\mathrm{i}} \left( -\frac{\hbar^2}{2M} \nabla_{\mathrm{i}}^2 + \frac{1}{2} M \omega^2(\tau) r_{\mathrm{i}}^2 \right) + \sum_{\mathrm{i<j}} U(\vec{r}_{\mathrm{i}} - \vec{r}_{\mathrm{j}}), \tag{3.12}$$

where $U(\vec{r})$ is the interaction giving rise to a divergent scattering length and could be implement by the Bethe-Peierls boundary condition. Without loss of generality, we have considered a time-dependent trapping frequency. Using the fourth row of Table , we see that

$$H = \hbar\omega(\tau) \left[ \left( \delta + \delta^{-1} \right) K_0 - \left( \delta - \delta^{-1} \right) K_1 \right], \tag{3.13}$$

where $\delta(\tau) = \frac{M(\tau)\omega(\tau)}{M(0)\omega(0)}$. $\omega_0 = \omega(0)$ sets the time scale of the system. We have defined the $SU(1,1)$ generators using the Hamiltonian at $\tau = 0$. The mass $M$ is fixed for unitary fermions in 3D harmonic traps, but can, in general, be tuned as a function of time. For instance, the effective mass at band bottom in an optical lattice could be tuned through a time-dependent tunnelling strength [ ]. Since $\xi_0 = \hbar\omega(\delta^{-1} + \delta)$, $\xi_1 = \hbar\omega(\delta^{-1} - \delta)$, when $\omega(\tau) = 0$, $\xi_0 = \xi_1$, and $\xi = 0$. Turning off the harmonic trap, the free expansion of unitary fermions thus corresponds to light propagating on the light cone of $\mathrm{AdS}_{2+1}$. If the system is initially prepared at the many-body ground state in a harmonic trap of a frequency $\omega_0$, the trajectory in $\mathrm{AdS}_{2+1}$ is written as $(\eta(\tau), \varphi(\tau), \psi(\tau)) = (\mathrm{arcsinh}(\omega_0\tau/2), \arctan(\omega_0\tau/2), 0)$. Correspondingly, $\langle K_0 \rangle(\tau) = (1 + \omega_0^2\tau^2/2)\langle K_0 \rangle(0)$, $\langle K_1 \rangle(\tau) = -\omega_0^2\tau^2/2\langle K_0 \rangle(0)$. The radius of the fermion cloud is then written as $\langle r^2 \rangle(\tau)/\langle r^2 \rangle(0) = 1 + \omega_0^2\tau^2$.

Similarly, dynamics in a confining (repelling) potential with a positive (negative) $\omega^2$ is mapped to trajectories in the timelike (spacetime) regime. The same conclusions also apply to other scale-invariant many-body systems [ ], [ ], [ ]–[ ].

Two-mode and one-mode squeezing in quantum optics provide alternative representations of $SU(1,1)$ group, as shown in Table [ ]. Bose-Einstein condensates with time-dependent interactions, spinor condensates with time-dependent quadratic Zeeman splitting, and fast rotating gases in the lowest Landau levels also allow experimentalists to access two-mode squeezing [ ], [ ]–[ ]. In all these systems, parametric amplifications, which are also

referred to as dynamical instability [ ], [ ]–[ ], may occur when $\xi^2 < 0$. As such, the light cone in the emergent $\mathrm{AdS}_{2+1}$ underlies the onsite of parametric amplification. The dynamically stable (unstable) regime then corresponds to the timelike (spacelike) regime. Similar conclusions hold in Floquet deformed conformal field theory, where the non-heating (heating) phase corresponds to the timelike (spacelike) regime [ ]–[ ].

Among all representations of $SU(1,1)$ group, it is worth mentioning the non-Hermitian one, as shown by the last row of Table . Since the angular momentum operators $S_{\mathrm{i}=0,1,2}$ satisfy $[S_{\mathrm{i}}, S_{\mathrm{j}}] = \mathrm{i}\epsilon_{\mathrm{ij}k}S_k$, where $\epsilon_{\mathrm{ij}k}$ is the Levi-Civita symbol, it is clear that $K_{1,2} = \mathrm{i}S_{1,2}$ and $K_0 = S_0$ transfer the $su(2)$ algebra to the $su(1,1)$ algebra. In other words, the Hamiltonian of a spin subject to a complex magnetic field, $\vec{B} = \{B_0, B_1, B_2\}$, can be written as $H(\tau) = \sum_{\mathrm{i}=0}^{2} \xi_{\mathrm{i}} K_{\mathrm{i}}$, or equivalently, $H(\tau) = \sum_{\mathrm{i}=0}^{2} B_{\mathrm{i}}(\tau) S_{\mathrm{i}}$, where $B_0 = \xi_0 \in R$ and $B_{1,2} = \mathrm{i}\xi_{1,2} \in I$. Such a Hamiltonian plays a fundamental role in non-Hermitian physics. A profound result is the existence of an exceptional point denoted by $\sum_{\mathrm{i}=0}^{2} B_{\mathrm{i}}^2 = 0$. Such an exceptional point signifies the $PT$ transition across which the energy spectrum becomes complex. It has also been widely implemented in quantum sensing [ ]–[ ].

A unique feature of the exceptional point is that eigenstates coalesce. Such coalesced eigenstates make it problematic to apply the conventional method of expanding the time-dependent wavefunction using eigenstates. Here, we see that dynamics at the exceptional point are dual to light propagating on the light cone of $\mathrm{AdS}_{2+1}$. For instance, starting from the ground state of a Hamiltonian $H = B_0 S_0$, where $B_0 \in R$, a quantum quench by suddenly turning on $B_1 = \mathrm{i}B_0$, $H = B_0(S_0 + \mathrm{i}S_1)$ accesses dynamics on the light cone. Similarly, the $PT$ symmetry broken(unbroken) phase is mapped to spacelike(timelike) regime in $\mathrm{AdS}_{2+1}$. Though circuit depth and complexity are often used in unitary evolutions of Hermitian systems, the intrinsic relation between $SU(1,1)$ and $SU(2)$ tells us they can also be implemented in non-Hermitian systems.

### 3.3.1 Minimizing transport time in quantum control

In addition to providing a new theoretical perspective to equate quantum dynamics and geometry, the emergent $\mathrm{AdS}_{2+1}$ offers experimentalists a unique means to manipulate

quantum dynamics. In quantum controls, a primary question is how to fast access a target state [ ]. Since our geometric approach has transformed time spent in laboratories to length in $\mathrm{AdS}_{2+1}$, the shortest path in such a spacetime directly unfolds the optimal choice with the least time. Though a geodesic in $\mathrm{AdS}_{2+1}$ is a local extreme, since $\mathrm{AdS}_{2+1}$ is a pseudo-Riemannian manifold, the shortest length turns out to be zero. This can be easily seen from Fig. , which shows the shortest path corresponding to a particular two-step evolution. In the first step, starting from the initial state at the origin $O$, the Hamiltonian is chosen as $\hbar\omega_0(K_0+K_1)$ and the propagator $U_{PO}=\mathrm{e}^{-\mathrm{i}(K_0+K_1)\omega_0 T_1}$ produces a trajectory on the light cone of $O$. The length of $OP$ is thus zero. After reaching a particular point $P$, the Hamiltonian is quenched to $\hbar\omega_0(K_0-K_1)$ and the propagator $U_{RP}=\mathrm{e}^{-\mathrm{i}(K_0-K_1)\omega_0 T_2}$ in the second step connecting $P$ and $R$ falls on the light cone of $P$. As such, the length in the second step also vanishes. The total length of the shortest trajectory produced by the propagator $U_{tar}=U_{RP}U_{PO}$ is hence zero.

o future analyze the shortest path, we consider a deviation of the first step, i.e., $H_1(\delta)=\hbar\omega_0\Big[(\delta^{-1}-\delta)K_0+(\delta^{-1}+\delta)K_1\Big]$ for $0<\tau<\tau_1$. We note that $\mathrm{e}^{-\mathrm{i}H_1(\delta)\tau_1/\hbar}$ becomes $U_{PO}$ as $\delta\to 0$ while keeping $\tau_1=T_1\delta$. To reach the target state, the Hamiltonian in the second step is changed to $H_2=\xi_0K_0+\xi_1K_1+\xi_2K_2$ correspondingly for $\tau_1<\tau<\tau_1+\tau_2$. To be explicit, $H_2=\frac{\mathrm{i}\hbar}{\tau_2}\log\Big(U_{\mathrm{tar}}\mathrm{e}^{\mathrm{i}H_1(\delta)\tau_1/\hbar}\Big)$. The total cost $S(\delta,\tau_1)=S_1+S_2$ can be evaluated (Supplementary Materials). Results depicted in Fig. clearly show that the cost increases when $\delta\neq 0$ and $\tau_1\neq T_1\delta$. We therefore conclude that, for any fixed field strength $\xi$, one can adjust its direction such that the trajectory approaches the shortest path $OPR$ shown in Fig. so as to minimize the time to access the target state at $R$.

Each point $(\eta,\psi,\varphi)$ in an $\mathrm{AdS}_{2+1}$ can be uniquely assigned with a wavefunction. For instance, when considering two-mode squeezing, choosing the vacuum as the origin, $(\eta,\psi,\varphi)$ is mapped to the $SU(1,1)$ coherent state [ ]

$$|\eta,\varphi,\psi\rangle=\mathrm{e}^{-\mathrm{i}\varphi}\cosh^{-1}(\eta)\sum_{n=0}^{\infty}(-\mathrm{i}\tanh(\eta)\mathrm{e}^{-\mathrm{i}(\varphi-\psi)})^n|n\rangle \tag{3.14}$$

where $|n\rangle$ denotes a Fock state with $n$ particles in each bosonic mode. $\varphi$ thus corresponds to the overall phase of the wavefunction, $\eta$ determines the average particle number $\bar{n}=$

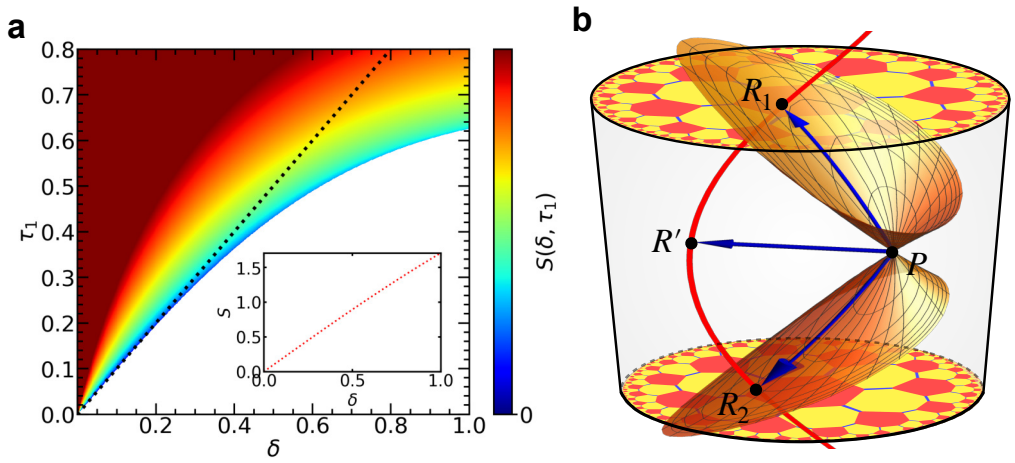


**Figure 3.2.** (a) $S(\delta, \tau_1)$ for trajectories deformed from the shortest path $OPR$. $(\tau_1 = T_1\delta, \delta = 0)$ corresponds to $OPR$ with a vanishing $S$. Representing results of a particular class of deformed trajectories. $T_1 = 1/\omega_0$, $T_2 = 2/\omega_0$ are used. (b) $PR_1$ and $PR_2$ are the shortest paths from a given initial state at $P$ to a spiral that corresponds to states with different $\varphi$. It takes longer time along any other path such as $PR$ to access the same $\eta$ and $\varphi - \psi$.

$2\sinh^2(\eta)$, and $\varphi - \psi$ gives rise to the relative phase between different Fock states. Whereas both $\eta$ and $\varphi - \psi$ can be measured in experiments, the overall phase $\varphi$ is more tricky.

We emphasize that the change of the overall phase $\varphi$ is measurable, for instance, by coupling the system to an external quantum spin-valve [ ]–[ ]. Nevertheless, it is useful to consider platforms in which the change of $\varphi$ is not easy to measure. In such a situation, states with the same $\eta$ and $\varphi - \psi$ but different $\varphi$ correspond to a spiral in $\mathrm{AdS}_{2+1}$, as shown in Fig. b. When those states cannot be distinguished in experiments, experimentalists could only access $\eta$ and $\varphi - \psi$. It is thus desirable to seek the shortest time to transport an initial state $P$ to this spiral. Since the spiral and the light cone of $P$ have two intersection points $R_1$ and $R_2$, based on the previous discussions, it takes least time to reach $R_1$ and $R_2$ by using quench dynamics represented by the arrow $PR_1$ or $PR_2$ that lies on the light cone of $P$. If one chooses a different quench dynamics such as $PR$ that corresponds to a constant $\varphi$, it takes a longer time to reach the spiral and access the same observables $\eta$ and $\varphi - \psi$.

### 3.4 Generalizations to Higher Dimensions

Similar to the conservation of the angular momentum in $SU(2)$, the eigenvalue of the Casimir operator, $C = K_0^2 - K_1^2 - K_2^2$, in $SU(1,1)$ is also conserved. In other words, each $\mathrm{AdS}_{2+1}$ spacetime emergent from quantum dynamics is characterized by a unique $C$. If we view an $\mathrm{AdS}_{2+1}$ spacetime as a universe, trajectories corresponding to quantum dynamics induced by $K_{0,1,2}$ are always confined in the same universe. Nevertheless, other operators can be introduced into the Hamiltonian such that tunnelings between different universes may occur. This can also be demonstrated using the two-mode squeezing. Any state in a single $\mathrm{AdS}_{2+1}$ can be written as

$$\begin{aligned} |\eta, \varphi, \psi; n_0\rangle =& \mathrm{e}^{-\mathrm{i}(n_0+1)\varphi} \cosh^{-(n_0+1)}(\eta) \sum_{n=0}^{\infty} \sqrt{\binom{n+n_0}{n}} \\ & \left(-\mathrm{i}\tanh(\eta)\mathrm{e}^{-\mathrm{i}(\varphi-\psi)}\right)^n |n, n+n_0\rangle \,, \end{aligned} \tag{3.15}$$

where $n_0$, the difference in the occupation numbers of these two modes, is a quantum number associated with $C$, and relates to the Bargmann index by $n_0 = 2k-1$. As particles are always created in pairs, one in mode $a$ and the other in mode $b$, $k$ is conserved in quantum dynamics induced by any $H(\tau) = \sum_{\mathrm{i}=0,1,2} \xi_{\mathrm{i}}(\tau) K_{\mathrm{i}}$ and the trajectory is confined within a single $\mathrm{AdS}_{2+1}$.

Once we add an addition operator $L$, which is outside the $su(1,1)$ algebra, to the Hamiltonian, $SU(1,1)$ symmetry is broken and $k$ is no longer conserved. The quantum system now is allowed to move along a trajectory that passes through different $\mathrm{AdS}_{2+1}$. For instance, such tunnelings between different universes can be induced by $L = (a^\dagger b - b^\dagger a)/(2\mathrm{i})$. Including $L$ gives rise to a larger dynamical group $SO(3,1)$. Nevertheless, we can still apply the previous method in obtaining a curved spacetime. We consider the propagators parameterized by $U = \mathrm{e}^{-\mathrm{i}K_0(\varphi-\psi)}\mathrm{e}^{-2\mathrm{i}K_1\eta}\mathrm{e}^{-\mathrm{i}K_0(\varphi+\psi)}\mathrm{e}^{-\mathrm{i}L\theta}$, which expands a four-dimensional subspace of the six-dimensional group manifold. We let the field coupled to $L$ be $B(\tau)$, such that $Y_3 = B(\tau)d\tau/\hbar$. If we choose a simple $F = \sqrt{-Y_0^2 + Y_1^2 + Y_2^2 + 4Y_3^2}/2$, the metric is written as

$$ds^2 = \mathrm{d}\eta^2 - \cosh^2(\eta)\,\mathrm{d}\varphi^2 + \sinh^2(\eta)\,\mathrm{d}\psi^2 + \cosh^2(2\eta)\,\mathrm{d}\theta^2. \tag{3.16}$$

Adding $L$ thus has created a higher dimensional spacetime. Whereas a fixed $\theta$ corresponds to a single $\mathrm{AdS}_{2+1}$, moving along the $\theta$ direction amounts to tunnelings between different $\mathrm{AdS}_{2+1}$ spacetimes.

### 3.A Squashed or stretched AdS, AdS black hole and soliton

While we have been focusing on an isotropic and homogeneous cost function $F$, our results can be generalized to anisotropic or non-uniform $F$ that may produce even more intriguing spacetimes, as it might be easier or more difficult to implement some gates than others in certain systems [ ]. To this end, we first consider a generalized form of the cost function $\tilde{F}_1 = \sqrt{-\lambda Y_0^2 + Y_1^2 + Y_2^2}/2$, where $\lambda \neq 1$. Similar to the $SU(2)$ case where such deformation leads to a Berger sphere [ ], [ ], we obtain a squashed or stretched $\mathrm{AdS}_{2+1}$ spacetime along timelike directions,

$$ds^2 = d\eta^2 + \sinh^2(\eta)d\psi^2 - \cosh^2(\eta)d\varphi^2 + (1-\lambda)(\sinh^2(\eta)d\psi + \cosh^2(\eta)d\varphi)^2. \tag{3.17}$$

In addition, it is of interest to explore a non-constant field strength that often leads to exotic physics. For instance, in the $SU(2)$ case, a magnetic field that varies over a sphere gives rise to 't Hooft-Polyakov monopole [ ], [ ]. Here, a non-constant field and the corresponding cost function produces intriguing spacetime metrics. We emphasize that, in addition to theoretical interest, it is an important question to consider inhomogeneous cost function, as it may become easier or harder to apply certain gates when the system evolves to a different state [ ]. For instance, in a driven BEC, all three components, $\xi_{\mathrm{i}=0,1,2}$, depend on the condensate density. Whereas the condensate density can be well approximated by a constant at small times, at large times, the occupation at excited states becomes significant such that the condensate density, as well as the field strength $\xi$, cannot be treated as a constant anymore.

As an example, we consider an inhomogeneous cost function, $\tilde{F}_2 = f^{1/2}(\eta, \psi, \varphi)F$, which corresponds to an isotropic but non-uniform field strength in the parameter space. Using the same method as presented in the main text, we obtain the following metric

$$ds^2 = f(\eta, \psi, \varphi)\left(\mathrm{d}\eta^2 - \cosh(\eta)^2\,\mathrm{d}\varphi^2 + \sinh(\eta)^2\,\mathrm{d}\psi^2\right). \tag{3.18}$$

Manipulating $f(\eta, \psi, \varphi)$ provides us with different spacetimes. For instance, when $f(\eta, \psi, \varphi) = (\rho/z_H)^2 \sinh^{-2}(\rho/z_H)$, where $\rho(\eta, \psi, \varphi) = (\cosh(\eta)\cos(\varphi) - \sinh(\eta)\sin(\psi))^{-1}$, the spacetime has an event horizon located at $z_H$. This can be seen from a coordinate transformation into the horospheric coordinates, defined as

$$\begin{aligned} \rho =& \frac{1}{\cosh(\eta)\cos(\varphi) - \sinh(\eta)\sin(\psi)}, \\ x =& \frac{\sinh(\eta)\cos(\psi)}{\cosh(\eta)\cos(\varphi) - \sinh(\eta)\sin(\psi)}, \\ t =& \frac{\cosh(\eta)\sin(\varphi)}{\cosh(\eta)\cos(\varphi) - \sinh(\eta)\sin(\psi)}, \end{aligned} \tag{3.19}$$

and the resulted metric reads

$$ds^2 = (1/z_H)^2 \sinh^{-2}(\rho/z_H)\left(-\mathrm{d}t^2 + \mathrm{d}x^2 + \mathrm{d}\rho^2\right). \tag{3.20}$$

We further consider a coordinate transformation of $\rho$, $z/z_H = \tanh(\rho/z_H)$, such that

$$ds^2 = -\left(\frac{1}{z^2} - \frac{1}{z_H^2}\right)\mathrm{d}t^2 + \frac{1}{z^2\left(1 - z^2/z_H^2\right)}\,\mathrm{d}z^2 + \left(\frac{1}{z^2} - \frac{1}{z_H^2}\right)\mathrm{d}x^2, \tag{3.21}$$

$\rho \in (0, \infty)$ is mapped to $z \in (0, z_H)$. When $z = z_H$, the speed of light vanishes as a characteristic feature of event horizon. This metric is related to that of BTZ black hole [ ],

$$ds^2 = -\left(\frac{1}{z^2} - \frac{1}{z_H^2}\right)\mathrm{d}t^2 + \frac{1}{z^2(1 - z^2/z_H^2)}\,\mathrm{d}z^2 + \frac{1}{z^2}\,\mathrm{d}x^2. \tag{3.22}$$

It is apparent that Eq.( ) and Eq.( ) become identical when $dx = 0$, i.e., for any fixed $x$. Eq.( ) is also related to the $AdS_{2+1}$ soliton metric [ ],

$$ds^2 = -\frac{1}{z^2}\,\mathrm{d}t^2 + \frac{1}{z^2(1-z^2/z_H^2)}\,\mathrm{d}z^2 + \left(\frac{1}{z^2} - \frac{1}{z_H^2}\right)\mathrm{d}x^2. \tag{3.23}$$

Eq.( ) and Eq.( ) coincide when $dt = 0$.

### 3.B Deviations from the shortest path

We consider a path $OPR$ where $P$ is no longer on the light cone. When $P$ is in the timelike regime, the Hamiltonian is written as

$$\begin{aligned} H_1 =& \Big[(\delta+\delta^{-1})K_0 - (\delta-\delta^{-1})K_1\Big]\hbar\omega_0, && 0<\tau<\tau_1, \\ H_2 =& \frac{\mathrm{i}\hbar}{\tau_2}\log\Big(\mathrm{e}^{-\mathrm{i}(K_0-K_1)\omega_0 T_2}\mathrm{e}^{-\mathrm{i}(K_0+K_1)\omega_0 T_1}\mathrm{e}^{\mathrm{i}H_1\tau_1/\hbar}\Big), && \tau_1<\tau<\tau_2. \end{aligned} \tag{3.24}$$

For any given $\delta$ and $\tau_1$, an appropriate $H_2$ defined in the above equation can be chosen such that the same target state at $R$ can be accessed at a certain time $\tau_2$. When $\delta$ decreases down to zero, the field strength remains constant. Choosing an appropriate $\tau_1$, $P$ approaches $P$ and we recover the shortest path in the limit where $\delta \to 0$.

To compute the cost $S$, or equivalently, the time spent to reach $R$ from $O$, as a function of $\delta$ and $\tau_1$, the simplest means is to implement the representation using spin-1/2 in a complex magnetic field, as shown in the last row of Table in the main text. For instance, the propagator along the shortest path can be written as $U_{OPR} = \mathrm{e}^{-\mathrm{i}\sigma_-\omega_0 T_2}\mathrm{e}^{-\mathrm{i}\sigma_+\omega_0 T_1}$, corresponding to dynamics at the exceptional points in non-Hermitian physics and the trajectory on the light cones in $AdS_{2+1}$, where $\sigma_\pm = (\sigma_x \pm \mathrm{i}\sigma_y)/2$. For generic $\delta$ and $\tau_1$, the analytical expression for the total cost reads

$$S(\delta,\tau_1)/\mathrm{i} = \omega_0\tau_1 + \left|\frac{1}{2\mathrm{i}}\log\left(\frac{f(\delta,\tau_1)-\sqrt{f(\delta,\tau_1)^2-\delta^2}}{f(\delta,\tau_1)+\sqrt{f(\delta,\tau_1)^2-\delta^2}}\right)\right|, \tag{3.25}$$

where $f(\delta,\tau_1) = [(2-\omega_0^2 T_1 T_2)\delta\cos(\omega_0\tau_1) + \omega_0(T_2+\delta^2 T_1)\sin(\omega_0\tau_1)]/2$. When $\delta \neq 0$, $S$ is finite. When $\delta$ decreases down to zero and an appropriate $\tau_1 = T_1\delta$ is chosen, $S$ approaches zero,

as we can see from Eq. (  ) $\lim_{\delta\to 0} S(\delta, T_1\delta)/\mathrm{i} = \lim_{\delta\to 0}(\omega_0 T_1 + \sqrt{\omega_0^4 T_1^3 T_2/3})\delta + O(\delta^3) = 0$. This is expected as the trajectory approaches the shortest path $OPR$.

We also consider that $P$ falls in the spacelike regime. The Hamiltonian is written as

$$\begin{aligned} H_1 =& \Big[ -(\delta - \delta^{-1})K_0 + (\delta + \delta^{-1})K_1 \Big]\hbar\omega_0, \qquad 0 < \tau < \tau_1, \\ H_2 =& \frac{\mathrm{i}\hbar}{\tau_2} \log\Big( \mathrm{e}^{-\mathrm{i}(K_0 - K_1)\omega_0 T_2} \mathrm{e}^{-\mathrm{i}(K_0+K_1)\omega_0 T_1} \mathrm{e}^{\mathrm{i}H_1\tau_1/\hbar} \Big), \qquad \tau_1 < \tau < \tau_2. \end{aligned} \tag{3.26}$$

Its total cost can be obtained by analytically continuing $\delta$ and $\tau_1$ in Eq.  to the complex domain,

$$S(\mathrm{i}\delta, \mathrm{i}\tau_1) = \omega_0\tau_1 + \left| \frac{1}{2} \log\left( \frac{f(\mathrm{i}\delta, \mathrm{i}\tau_1) - \sqrt{f(\mathrm{i}\delta, \mathrm{i}\tau_1)^2 + \delta^2}}{f(\mathrm{i}\delta, \mathrm{i}\tau_1) + \sqrt{f(\mathrm{i}\delta, \mathrm{i}\tau_1)^2 + \delta^2}} \right) \right|. \tag{3.27}$$

# 4. SYNTHETIC HYPERBOLIC SURFACES ON LATTICE SYSTEMS

*The contents of this chapter are based on and modified from the published articles [ ] by R. Zhang, C. Lv, Y. Yan, and Q. Zhou, Efimov-like states and quantum funneling effects on synthetic hyperbolic surfaces, Science Bulletin, 66(19), 1967-1972. Copyright (2021) by Science China Press., and [ ] by C. Lv, R. Zhang, Z. Zhai and Q. Zhou, Curving the space by non-Hermiticity, Nature communications, 13(1), 1-6. Copyright (2022) by The Authors.*

The preceding chapters have observed the emergent hyperbolic geometry in systems with $SU(1,1)$ dynamical symmetry, where the emergent geometries describing the quantum states offer us a powerful tool for understanding and manipulating quantum dynamics. This chapter studies synthetic curved spaces on Hermitian and non-Hermitian lattice systems. We first show that engineering lattice models with tailored inter-site tunnelings and onsite energies could provide arbitrary Riemannian surfaces with highly tunable local curvatures. Like a flat surface, discrete synthetic hyperbolic spaces on a lattice support infinitely degenerate eigenstates for any nonzero eigenenergies. Such states exhibit a discrete scaling symmetry upon a short-range boundary condition, similar to the Efimov effect. Moreover, all eigenstates are exponentially localized in the hyperbolic coordinates. Any initial wave packet travels towards a point named the funneling mouth, delivering the funneling effect, like what has been observed in non-Hermitian systems. This observation motivates us to a duality between hyperbolic space and non-Hermitian lattice system. Actually, the two-dimensional hyperbolic surfaces are dual to a prototypical non-Hermitian lattice chain named the Hatano-Nelson (HN) model [ ]. In the second part, we provide a generalized duality between non-Hermitian lattice systems and curved spaces. Such a duality unfolds deep geometric roots of non-Hermitian phenomena, delivers an unprecedented routine connecting Hermitian and non-Hermitian physics, and gives rise to a theoretical perspective reformulating our understandings of curvatures and distance.

## 4.1 Introduction

Quantum effects and a quantum mechanical interpretation of gravity have been attracting physicists' attention since the establishment of quantum mechanics. The various quantum

mechanical platforms allows quantum simulations of synthetic quantum matters [ ]–[ ]. However, the gravitational effect on quantum systems has been less investigated in laboratories due to the difficulty in creating quantum systems in curved spaces, though novel quantum phenomena that are inaccessible in flat spaces have been theoretical predicted in curved spaces [ ], [ ]–[ ]. Despite its difficulty, recent years have witnessed exciting developments in quantum simulations of curved spaces [ ]–[ ]. However, a generic scheme that simulates quantum systems in curved space with arbitrary local curvature distributions is still desired.

On the other hand, the non-Hermitian system, which is led by inevitable system environment couplings, seem to be disconnected from the curved space. While a plethora of intriguing non-Hermitian phenomena exist [ ], [ ]–[ ], and have been extensively explored in quantum sciences and technologies [ ], [ ], [ ]–[ ], [ ], [ ]–[ ], it always requires peculiar theoretical tools to study non-Hermitian physics.

In the following, we provide a lattice model for simulating arbitrary two-dimensional Riemannian surfaces. Motivated by a funneling effect on the simulated hyperbolic space, we show a duality between non-Hermitian Hamiltonians in flat spaces and their counterparts in curved spaces. This duality provides a geometric framework that explains several non-Hermitian phenomena. In practice, it not only establishes non-Hermiticity as a unique tool to simulate intriguing quantum systems in curved spaces, but also allows experimentalists to use curved spaces to explore non-Hermitian physics.

## 4.2 Simulation of Two-Dimensional Riemann Surface

Considering a two-dimensional Riemann surface, its metric, in general, is written as $ds^2 = g_{\mathrm{ij}}\mathrm{d}x^{\mathrm{i}}\mathrm{d}x^{\mathrm{j}}$. It is known that this metric can be rewritten into a conformally flat form

$$ds^2 = f(x,y)\Big(\mathrm{d}x^2 + \mathrm{d}y^2\Big) \tag{4.1}$$

under a coordinate transformation, in the two-dimensional case. As we show in the introduction chapter, the wavefunction $\Psi(x,y)$ satisfies the Schrödinger equation with replacing the Laplace operator by the Laplacian Beltrami operator. Using the metric above, we obtain

$$\frac{\hbar^2}{2m}\Big( -\frac{1}{\sqrt{g}}\sum\nolimits_{\mathrm{i}=x,y}\partial_{\mathrm{i}}\sqrt{g}g^{\mathrm{ii}}\partial_{\mathrm{i}} - \frac{\kappa}{4}\Big)\Psi(x,y) = E\Psi(x,y), \tag{4.2}$$

where $g = g_{xx}g_{yy}$, and $g_{xx} = g_{yy} = f$, $g^{xx} = g^{yy} = f^{-1}$. We have included an extra potential proportional to the Gaussian curvature $-\kappa$ [ ]. The normalization condition reads

$$\int dxdy\sqrt{g}|\Psi(x,y)|^2 = 1. \tag{4.3}$$

In order to derive the lattice model, we consider an energy functional

$$H = \frac{\hbar^2}{2m}\int dxdy\sqrt{g}\left(-\frac{1}{\sqrt{g}}\sum_{\mathrm{i}=x,y}\Psi^*\partial_{\mathrm{i}}\sqrt{g}g^{\mathrm{ii}}\partial_{\mathrm{i}}\Psi - \frac{\kappa}{4}|\Psi|^2\right), \tag{4.4}$$

which gives Eq. ( ) as the equation of motion. We then uniformly discretize the continuous model. Using $x_{\mathrm{i}+1} - x_{\mathrm{i}} = a,\ y_{\mathrm{j}+1} - y_{\mathrm{j}} = b$, the energy functional becomes

$$\begin{aligned} H = &-\frac{\hbar^2}{2ma^2}\sum_{\mathrm{i,j}}\sqrt{g_{\mathrm{i,j}}}\left[g^{xx}_{\mathrm{i,j}}\left(\Psi^*_{\mathrm{i}+1,\mathrm{j}}\Psi_{\mathrm{i,j}} + \Psi^*_{\mathrm{i,j}}\Psi_{\mathrm{i}+1,\mathrm{j}}\right) + \frac{a^2}{b^2}g^{yy}_{\mathrm{i,j}}\left(\Psi^*_{\mathrm{i,j}+1}\Psi_{\mathrm{i,j}} + \Psi^*_{\mathrm{i,j}}\Psi_{\mathrm{i,j}+1}\right)\right] \\ &+\sum_{\mathrm{i,j}}\sqrt{g_{\mathrm{i,j}}}\left[\frac{\hbar^2}{2ma^2}\left(\frac{\sqrt{g_{\mathrm{i}-1,\mathrm{j}}}}{\sqrt{g_{\mathrm{i,j}}}}g^{xx}_{\mathrm{i}-1,\mathrm{j}} + g^{xx}_{\mathrm{i,j}} + \frac{a^2}{b^2}\frac{\sqrt{g_{\mathrm{i,j}-1}}}{\sqrt{g_{\mathrm{i,j}}}}g^{yy}_{\mathrm{i,j}-1} + \frac{a^2}{b^2}g^{yy}_{\mathrm{i,j}}\right) - \frac{\hbar^2\kappa}{8m}\right]\Psi^*_{\mathrm{i,j}}\Psi_{\mathrm{i,j}} \end{aligned} \tag{4.5}$$

we have defined $\Psi_{\mathrm{i,j}} = \sqrt{ab}\Psi(\mathrm{i}a, \mathrm{j}b)$. $a$ and $b$ are the lattice constants along $x$ and $y$-direction, respectively. The normalization condition is discretized as

$$\sum_{\mathrm{i,j}}\sqrt{g_{\mathrm{i,j}}}\Psi^*_{\mathrm{i,j}}\Psi_{\mathrm{i,j}} = 1. \tag{4.6}$$

Now, we define $\varphi_{\mathrm{i,j}} = g_{\mathrm{i,j}}^{1/4}\Psi_{\mathrm{i,j}}$, such that the coefficient $\sqrt{g_{\mathrm{i,j}}}$ in the normalization of the lattice model, Eq. (  ), is absorbed. As a result, the normalization condition becomes $\sum_{\mathrm{i,j}} \varphi_{\mathrm{i,j}}^* \varphi_{\mathrm{i,j}} = 1$. Using $\varphi_{\mathrm{i,j}}$, the discretized energy functional is

$$\begin{aligned} H =& -\frac{\hbar^2}{2ma^2}\sum_{\mathrm{i,j}}\left[\frac{\sqrt{g_{\mathrm{i,j}}}g_{\mathrm{i,j}}^{xx}}{(g_{\mathrm{i+1,j}}g_{\mathrm{i,j}})^{1/4}}\left(\varphi_{\mathrm{i+1,j}}^*\varphi_{\mathrm{i,j}} + c.c\right) + \frac{a^2}{b^2}\frac{\sqrt{g_{\mathrm{i,j}}}g_{\mathrm{i,j}}^{yy}}{(g_{\mathrm{i,j+1}}g_{\mathrm{i,j}})^{1/4}}\left(\varphi_{\mathrm{i,j+1}}^*\varphi_{\mathrm{i,j}} + c.c.\right)\right] \\ &+ \sum_{\mathrm{i,j}}\left[\frac{\hbar^2}{2ma^2}\left(\frac{\sqrt{g_{\mathrm{i-1,j}}}}{\sqrt{g_{\mathrm{i,j}}}}g_{\mathrm{i-1,j}}^{xx} + g_{\mathrm{i,j}}^{xx} + \frac{a^2}{b^2}\frac{\sqrt{g_{\mathrm{i,j-1}}}}{\sqrt{g_{\mathrm{i,j}}}}g_{\mathrm{i,j-1}}^{yy} + \frac{a^2}{b^2}g_{\mathrm{i,j}}^{yy}\right) - \frac{\hbar^2\kappa}{8m}\right]\varphi_{\mathrm{i,j}}^*\varphi_{\mathrm{i,j}} \end{aligned} \tag{4.7}$$

We, therefore, obtain a second quantized Hamiltonian on a uniform lattice,

$$\hat{H} = \sum_{\mathrm{i,j}}\left[t_{\mathrm{i,j}}^x\left(a_{\mathrm{i+1,j}}^\dagger a_{\mathrm{i,j}} + a_{\mathrm{i,j}}^\dagger a_{\mathrm{i+1,j}}\right) + t_{\mathrm{i,j}}^y\left(a_{\mathrm{i,j+1}}^\dagger a_{\mathrm{i,j}} + a_{\mathrm{i,j}}^\dagger a_{\mathrm{i,j+1}}\right) + u_{\mathrm{i,j}}a_{\mathrm{i,j}}^\dagger a_{\mathrm{i,j}}\right], \tag{4.8}$$

where $a_{\mathrm{i,j}}^{(\dagger)}$ denotes the annihilation (creation) operator on site $(\mathrm{i,j})$. The parameters can be read from Eq. (  ),

$$\begin{aligned} t_{\mathrm{i,j}}^x =& -\frac{\hbar^2}{2ma^2}\frac{\sqrt{g_{\mathrm{i,j}}}g_{\mathrm{i,j}}^{xx}}{(g_{\mathrm{i+1,j}}g_{\mathrm{i,j}})^{1/4}}, \\ t_{\mathrm{i,j}}^y =& -\frac{\hbar^2}{2mb^2}\frac{\sqrt{g_{\mathrm{i,j}}}g_{\mathrm{i,j}}^{yy}}{(g_{\mathrm{i,j+1}}g_{\mathrm{i,j}})^{1/4}}, \\ u_{\mathrm{i,j}} =& \frac{\hbar^2}{2ma^2}\left(\frac{\sqrt{g_{\mathrm{i-1,j}}}}{\sqrt{g_{\mathrm{i,j}}}}g_{\mathrm{i-1,j}}^{xx} + g_{\mathrm{i,j}}^{xx} + \frac{a^2}{b^2}\frac{\sqrt{g_{\mathrm{i,j-1}}}}{\sqrt{g_{\mathrm{i,j}}}}g_{\mathrm{i,j-1}}^{yy} + \frac{a^2}{b^2}g_{\mathrm{i,j}}^{yy}\right) - \frac{\hbar^2\kappa}{8m}. \end{aligned} \tag{4.9}$$

For a Poincaré half-plane, another prototypical parameterization of hyperbolic surface, we have $f(x,y) = 1/(\kappa y^2)$ [  ]. It is related to the Poincaré disk by a coordinate transformation, which is also termed as a Cayley transformation [  ]

$$\rho e^{\mathrm{i}\theta} = -\frac{x + \mathrm{i}(y-1)}{x + \mathrm{i}(y+1)}, \tag{4.10}$$

where $(\rho, \theta)$ denote the radial and angular coordinate of a Poincaré disk. $-\kappa$ is the Gaussian curvature of the hyperbolic space.

Using the method introduced above, we find a lattice model

$$\hat{H}_{\mathrm{p}} = \sum_{\mathrm{i}=-\infty}^{\infty} \sum_{\mathrm{j}=0}^{\infty} a_{\mathrm{i,j}}^{\dagger} \left[ t_{\mathrm{j}}^{x} a_{\mathrm{i+1,j}} + t_{\mathrm{j}}^{y} a_{\mathrm{i,j+1}} + u_{\mathrm{i,j}} a_{\mathrm{i,j}} \right] + \mathrm{h.c.}, \tag{4.11}$$

where the non-uniform tunnelings are $t_{\mathrm{j}}^{x} = -\kappa \mathrm{j}^2$, $t_{\mathrm{j}}^{y} = -\kappa \mathrm{j}(\mathrm{j}+1)$, and $u_{\mathrm{i,j}} = (4\mathrm{j}^2 - 1/4)\kappa$ is an on-site potential. j starts from 0 since we consider the upper half-plane with $y > 0$. The solution, $\varphi_{\mathrm{i,j}}$, of this lattice model in Eq.(  ), directly provides the wavefunction on the Poincaré half-plane via $\Psi(x_{\mathrm{i}}, y_{\mathrm{j}}) = \varphi_{\mathrm{i,j}} g_{\mathrm{i,j}}^{-1/4}$. The non-uniform tunnelings along the i and j-direction reflect an intrinsic property of the Poincaré half-plane. While the Euclidean distance between two points is fixed, their distance under the metric of the Poincaré half-plane decreases with increasing $y$. Therefore, the tunnelings need to increase.

### 4.2.1 Scale-invariant states

Poincaré half-plane is a hyperbolic space with the $SO(2,1)$ isometric group. Especially, it is invariant under the scaling transformation, $y \to \lambda y$, $x \to \lambda x$, with $\lambda > 0$. The scaling invariance can be shown from the eigenstates in a Poincaré half-plane. Such scaling invariance also appears in the Efimov state, where three bosons interact and form bound states with discrete scaling symmetry.

To solve the eigenstates, we first write down the time-independent Schrödinger equation on the Poincaré half-plane,

$$-\kappa \left[ y^2 \left( \frac{\partial^2}{\partial x^2} + \frac{\partial^2}{\partial y^2} \right) + \frac{1}{4} \right] \Psi(x,y) = E\Psi(x,y), \tag{4.12}$$

where $y > 0$, and the normalization condition reads

$$\int_0^{\infty} \frac{dy}{\kappa y^2} \int_{-L}^{L} dx \Psi^*(x,y)\Psi(x,y) = 1. \tag{4.13}$$

We the define $\Psi(x,y)=\phi(x)\psi(y)$, where $\phi(x)=\frac{1}{\sqrt{L}}\mathrm{e}^{\mathrm{i}k_x x}$, such that motions along the $x$ and $y$-directions are separated. $\psi(y)$ satisfies

$$\frac{\partial^2}{\partial y^2}\psi(y)+\frac{1/4+E/\kappa}{y^2}\psi(y)=\epsilon\psi(y), \tag{4.14}$$

where $\epsilon=k_x^2$ depends on the wave vector $k_x$ along $x$-direction, and $k_x$ is continuous as $L$ approach infinity.

We notice that, the equation above is scale-invariant. It has the same form as the hyper-radial equation in Efimov physics [ ],

$$\frac{\partial^2}{\partial R^2}\psi(R)+\frac{1/4+s_0^2}{R^2}\psi(R)=-\tilde{E}_b\psi(R), \tag{4.15}$$

where $R$ is the hyper radius, defined by the averaged separation among particles, $s_0\approx 1.00624$ is the discrete scaling factor. $\tilde{E}_b$ is the binding energy of an Efimov state. We therefore identify $y\to R$, $E/\kappa\to s_0^2$, and $\epsilon\to-\tilde{E}_b$,

In Efimov physics, there are infinite numbers of bound states for a given $s_0$. These bound state energies satisfy the discrete scaling law, $\tilde{E}_{b,n-1}=\mathrm{e}^{2\pi/s_0}\tilde{E}_{b,n}$. From the mapping, we immediately conclude that similar behavior exists on the Poincaré half-plane. We notice that the energy of a quantum particle moving on the Poincaré half-plane is always continuous and non-negative without specifying the boundary condition, i.e., $E\geq 0$. There is only one eigenstate, $y^{1/2}$, with $E=0$. This corresponds to a divergent scaling factor. For any finite $E>0$, there are infinitely degenerate eigenstates with different $\epsilon$, due to the continuous scaling symmetry. We call it the Efimov-like eigenstates, since a discrete scaling law emerges similar to the Efimov states, once we apply a short-range boundary condition at $y=y_0$.

To be more specific, we can write down the eigenstate of Eq. ( ),

$$\psi(y)\propto\sqrt{y}K_{\mathrm{i}\sqrt{E/\kappa}}(\sqrt{\epsilon}y), \tag{4.16}$$

where $K_a(x)$ is the modified Bessel function of the second kind. In the short-range limit, we can recast the eigenstate into a more insightful form using the asymptotic form of the Bessel function, which reads,

$$\psi(y) \propto \sqrt{y}\cos\left(\sqrt{E/\kappa}\ln\frac{\sqrt{\epsilon}y}{2} + \arg\left[\Gamma(-\mathrm{i}\sqrt{E/\kappa})\right]\right), \quad \epsilon y \to 0. \tag{4.17}$$

Imposing the open boundary condition $\psi(y_0) = 0$, leads to the quantized $k_x$ and $\epsilon$ for a finite $E$. The continuous scaling symmetry becomes discrete, $\epsilon_{n-1} = \mathrm{e}^{2\pi\sqrt{\kappa/E}}\epsilon_n$. Correspondingly, $\psi_n(y) \propto \psi_{n-1}(y\mathrm{e}^{\pi\sqrt{\kappa/E}})$. Namely, the $(n-1)$-th eigenstate is transformed to the $n$-th one with the same eigenenergy $E$ by a dilation $y \to y\mathrm{e}^{\pi\sqrt{\kappa/E}}$, as shown in Fig. . Unlike Efimov state where the scaling factor is fixed by the mass ratios and particle statistics, here the scaling factor is given by the eigenenergy $E$ and the Gaussian curvature $\kappa$ and can be continuously tuned.

Since a Cayley transformation relates the Poincaré half-plane and the Poincaré disk, the eigenstates on the Poincaré disk can be directly obtained from the results of a Poincaré half-plane. We need to note that the boundary conditions should also be transformed correspondingly for such mapping to work. The boundaries with constant $y$'s on the Poincaré half-plane are transformed to horocycles, which are circles with boundaries attached to the same point on the boundary of the Poincaré disk, as shown in Fig. . The Efimov-like states emerge on the Poincaré disk only under this particular boundary condition.

By applying the discrete lattice model, we numerically solve the eigenenergies and eigenstates and then show the scaling behaviors. We demonstrate that a good agreement, as expected, supports the validity of the lattice models as discrete versions of the hyperbolic spaces in Fig. .

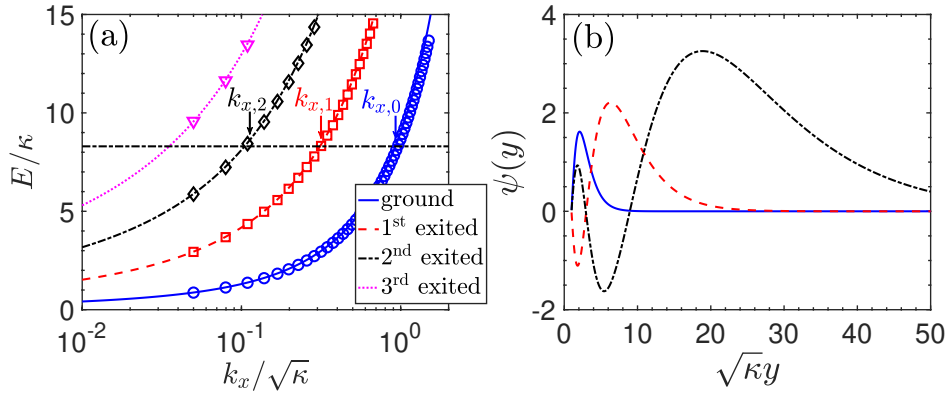


**Figure 4.1.** The states with a short-range boundary condition on Poincaré half-plane and the corresponding eigenenergies with various $k_x$. (a): Different $k_x$'s with the same $E$ exhibit discrete scaling symmetry. $k_{x,n-1}/k_{x,n} = \exp\left(\pi(\kappa/E)^{1/2}\right)$. Curves (Markers) represent eigenenergies of the continuous (discretized lattice) model. (b): Three eigenstates with the short-range boundary condition $\psi(\kappa^{-1/2}) = 0$ and the same eigenenergies $E/\kappa = 8.5$ but different $k_x$ show a discrete scaling symmetry.

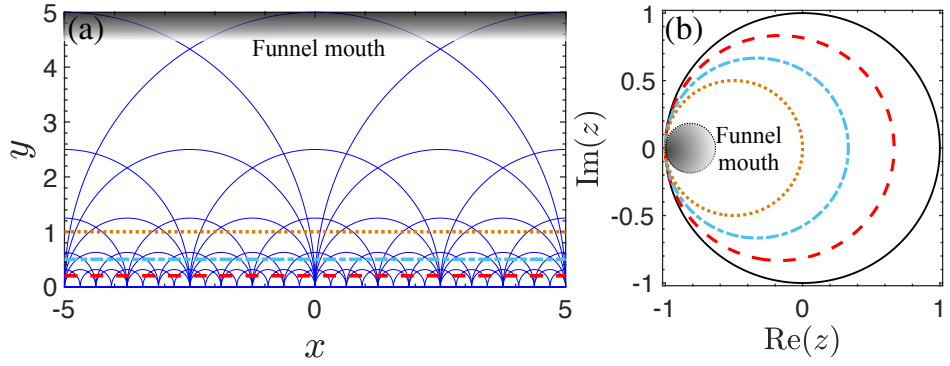


**Figure 4.2.** Location of the funneling mouth, denoted by the shaded area, on the Poincaré half-plane and disk. Lines with constant $y$'s in (a) are mapped to horocycles in (b) through a Cayley transformation shown in Eq. ( ).

### 4.2.2 Localization and quantum funneling effect

In the last section, we have shown that the eigenstate with zero energy is written as $y^{1/2}$. In fact, all eigenstates on these hyperbolic surfaces are localized in the hyperbolic coordinates. We use the Poincaré half-plane as an example. The distance from $y_0$ to $y$ is

$$s = \int_{y_0}^{y} dy \frac{1}{\sqrt{\kappa} y} = \frac{1}{\sqrt{\kappa}} \ln \frac{y}{y_0}. \tag{4.18}$$

Using $s$, we can rewritten the eigenstates as $\psi_n(s) \propto \sqrt{y_0}\mathrm{e}^{\sqrt{\kappa}s/2}K_{\mathrm{i}\sqrt{E/\kappa}}(\sqrt{\epsilon_n}y_0\mathrm{e}^{\sqrt{\kappa}s})$. When $\epsilon = 0$, it becomes $\psi_\infty(s) \propto \sqrt{y_0}\mathrm{e}^{\sqrt{\kappa}s/2}\sin\Big(\sqrt{E}s\Big)$. Therefore, a Euclidean space observer would find that all eigenstates with vanishing $k_x$ localize in $s$ to the large $s$-direction, which also corresponds to the large $y$-direction of the Poincaré half-plane. Such a localization at infinity precisely originates from the $1/y^2$ behavior of the metric of the Poincaré half-plane. A finite $\epsilon$ leads to an extra effective potential that increases exponentially in the $y$-direction, and the localization is compensated. As a result, any eigenstates decay to zero when $s \to \infty$ for any finite $\epsilon$. Nevertheless, the tendency of the localization towards infinity remains in a length scale much smaller than the characteristic length scale $\sim 1/\sqrt{\epsilon}$ of the effective potential.

Such a phenomenon is reminiscent of the funneling effects in the non-Hermitian system. In certain one-dimensional non-Hermitian systems, all eigenstates are also localized and any initial wavepacket travels towards the end where eigenstates localize [ ], [ ]. In these non-Hermitian systems, it is the chiral tunnelings that force eigenstates and wavepacket to concentrate at one end. It is also termed as "non-Hermitian skin effect" [ ]. Nevertheless, such a localization phenomenon on curved space occurs in a Hermitian system where chiral tunnelings are absent. In such systems, it is the metric that induces localization of eigenstates and the quantum funneling, as we will later show. The funneling mouth is located at $y = \infty$ on the Poincaré half-plane, and the mapping between the Poincaré half-plane and the Poincaré disk indicates the same phenomenon on the Poincaré disk. Now, the funneling mouth is located around a particular point on the boundary of the Poincaré disk, as shown by the shaded regions in Fig. . We emphasize that, in accordance with the $su(1,1)$ symmetry of the hyperbolic surface, appropriate boundary conditions can be implemented to continuously change the locations of funneling mouths.

The fact that any wavefunction is localized at one end of the system has a profound impact on quantum dynamics, which is termed as quantum funneling effect. Since any initial wavepacket, which is prepared as a linear superposition of many eigenstates, will disperse and finally become delocalized if we consider a flat and Hermitian one-dimensional system as time evolves, the localization of all eigenstates means that the final state must be a delocalized one multiply by the localization term. As a result, the final state here is localized

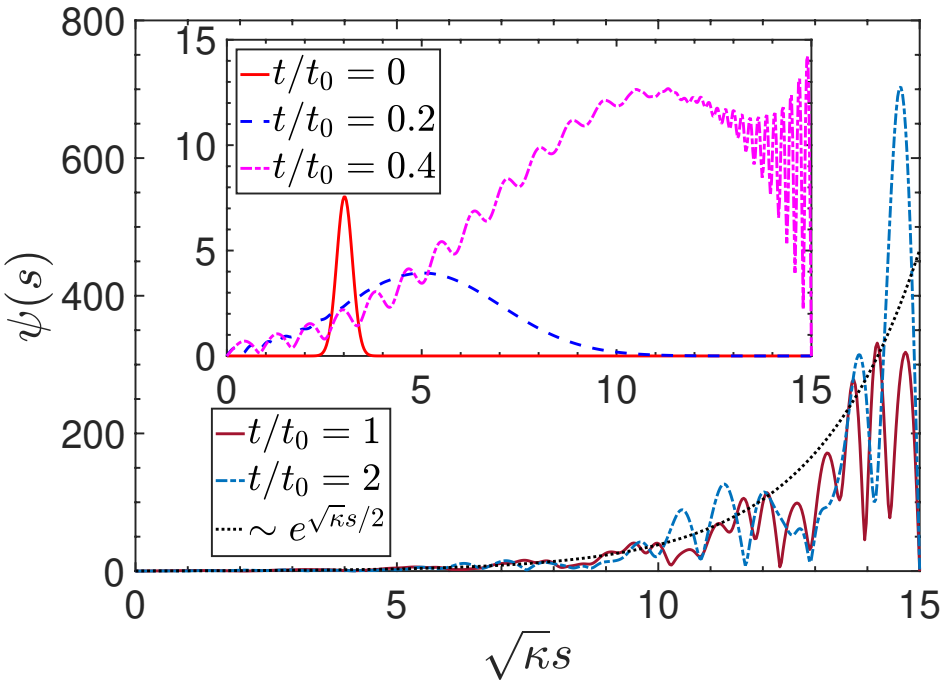


**Figure 4.3.** Quantum dynamics of a wavepacket in the Poincaré half-plane which is constant in the $x$-direction shows the funneling effect. We have transformed the $y$-coordinate into the $s$-coordinate. A localized Gaussian wavepacket (red solid curve) is prepared at $t = 0$. As time evolves, the wavepacket disperses and travels towards the funneling mouth at the large end in the $s$-direction. The wavepacket finally becomes localized at the large $s$ boundary with an exponential envelope (black dotted curve), in the long-time limit. $t_0 = 2m/(\hbar^2\kappa)$ defines the time unit.

and any initial state will travel to the localized end, which is demonstrated in Fig. . This phenomenon is analog of the funneling in a non-Hermitian system [ ].

### 4.3 Non-Hermitian Lattice Models and Their Duals in Curved Spaces

We have seen a Hermitian lattice model with tunneling strength and on-site potential in Eq. ( ) can be used to simulate any Riemann surface. Nevertheless, it is $\varphi_{\mathrm{i,j}}$ that is simulated, such that the normalization $\sum_{\mathrm{i,j}} |\varphi|^2 = 1$ is satisfied; and it is $\psi$ which localizes. Simulating $\Psi_{\mathrm{i,j}}$ directly leads to a non-Hermitian lattice model. In this section, we present

the duality between non-Hermitian lattice model and curved space using the celebrated HN model [ ]. The time-independent Schrödinger equation reads,

$$-t_R\psi_{n-1} - t_L\psi_{n+1} = E\psi_n, \quad n = 0, 1, ...N-1, \tag{4.19}$$

where $t_{R(L)}$ denotes chiral nearest-neighbor tunneling amplitudes towards right (left). In a Hermitian system, it is necessary to have $t_L = t_R^*$. Here, we no longer have such a constraint. We now apply the open boundary condition (OBC), $\psi_0 = \psi_{N-1} = 0$. The eigenstates become $\psi_n = \mathrm{e}^{n\ln(\gamma)}\sin(k_m n d)/\sqrt{(N-1)/2}$, where $d$ is the lattice constant, $k_m = m\pi/((N-1)d)$, $m = 1, 2, ...N-2$. $\gamma = \sqrt{t_R/t_L}$ characterizes the strength of non-Hermiticity. The corresponding eigenenergies read $E_m = -2\sqrt{t_L t_R}\cos(k_m d)$.

To build the duality between a lattice model and a continuous one, we consider the effective theory of Eq. ( ) near $k_m = 0$. Similar to the Hermitian lattice models, it describes the motion of a non-relativistic particle. The effective theory near $k_m = 0$ for any strength of non-Hermiticity is obtained by considering $\psi_n = \sqrt{d}\phi(s_n)\mathrm{e}^{qs_n}$, where $q = \ln(\gamma)/d = \frac{1}{2d}\ln(t_R/t_L)$ and $s_n = nd$. While $q^{-1}$ captures the localization length, $\phi(s)$ is the extension of the wavefunction $\psi_n$ with discrete supports on a continuous variable $s$, it now varies slowly with changing $s$. As such, we can apply the Taylor expansion of $\phi(s)$, $\phi(s_{n\pm1}) = \phi(s_n) \pm d\partial_s\phi + \frac{1}{2}d^2\partial_s^2\phi$. Substituting $\psi_n$ into Eq. ( ), we obtain an equation of $\phi$, $-\sqrt{t_L t_R}(2 + \partial_s^2)\phi = E\phi$. Translating back to $\psi$, the effective theory near $k_m = 0$ is

$$-\sqrt{t_L t_R}d^2\left(\partial_s^2 - 2q\partial_s + q^2 + 2/d^2\right)\psi(s) = E\psi(s). \tag{4.20}$$

This equation contents an imaginary vector potential, $A \sim \mathrm{i}q$ [ ], [ ]. Here, an imaginary vector potential curves the space, unlike a real one which amounts to a $U(1)$ gauge field. Applying a coordinate transformation $y/y_0 = \mathrm{e}^{2qs}$ and defining the effective mass $M = \hbar^2/(2\sqrt{t_L t_R}d^2)$, curvature $\kappa = 4\ln^2(|\gamma|)/d^2$, we obtain

$$-\frac{\hbar^2}{2M}\kappa\left(y^2\partial_y^2 + \frac{1}{4}\right)\psi(y) = E\psi(y), \tag{4.21}$$

**Table 4.1.** The mapping between the continuum limit of the HN model near the band bottom under OBC and the Poincaré half-plane.

| 2D Hyperbolic surface | Curvature $-\kappa$ | Energy scales $\hbar^2/(2Md^2)$ | Coordinate $y_n = y_0 e^{n\sqrt{\kappa}d}$ | Eigenfunctions $\psi(y) \propto (y/y_0)^{\frac{1}{2}} \sin\left(\frac{m\pi \ln(y/y_0)}{\ln(y_{N-1}/y_0)}\right)$ | Eigenenergies $E_m = \frac{\kappa\hbar^2 m^2\pi^2}{2M\ln(y_{N-1}/y_0)^2}$ |
|---|---|---|---|---|---|
| 1D Non-Hermitian chain | Non-Hermiticity $-4\ln^2(\lvert\gamma\rvert)/d^2$ | Tunneling strength $\sqrt{t_R t_L}$ | Lattice site $n$ | $\psi_n \propto \gamma^n \sin\left(\frac{m\pi}{N-1}n\right)$ | $\frac{E_m}{2\sqrt{t_R t_L}} = (-1 + \frac{m^2\pi^2}{2(N-1)^2} + O(\frac{m^4}{N^4}))$ |

up to a constant energy shift $-2\sqrt{t_L t_R}$. We notice that, this is exactly the time-independent Schrödinger equation on the Poincaré half plane with $k_x = 0$. A finite $k_x$ just leads to an external potential, as we have seen in the previous section. Actually, if we consider the time-independent Schrödinger equation in the hyperbolic coordinate $s$ on the Poincaré half plane and perform discretization, using $\psi$, we obtain

$$V_n\psi_n - t_R\psi_{n-1} - t_L\psi_{n+1} = E\psi_n, \tag{4.22}$$

where $V_n = a^2\sqrt{t_R t_L}\gamma^{4n}$ is the potential led by finite $k_x$. We have defined a dimensionless quantity $a^2 = 4(\ln^2|\gamma|)y_0^2 k_x^2$ that characterizes the strength of $V_n$. At the band top near $k_m = \boldsymbol{\pi}$, we have $M \to -M$, and a relativistic theory on the Poincaré half plane needs to be defined for other $k_m$'s since the dispersion is now linear.

We have summarized the mapping between these two models in Table , which serves as a dictionary translating microscopic parameters between them.

### 4.3.1 Geometric interpretations of non-Hermitian phenomena

Several peculiar non-Hermitian phenomena have a natural explanation that is provided by our duality. We first consider the orthonormal condition in a non-Hermitian system. As we have discussed, the left and right eigenvectors need to be introduced. The orthonormal condition on the Poincaré half plane with $k_x = 0$ reads

$$\int \frac{\mathrm{d}y}{\kappa y^2}\psi^*(y;k_y)\psi(y;k_y') = \mathcal{N}\delta_{k_y,k_y'}. \tag{4.23}$$

$\mathcal{N}$ is a normalization constant that can be freely chosen. The curvature-dependent factor $(\kappa y^2)^{-1}$, has a physical meaning as the width of a strip in the domain $x_0 \le x \le x_0 + L$

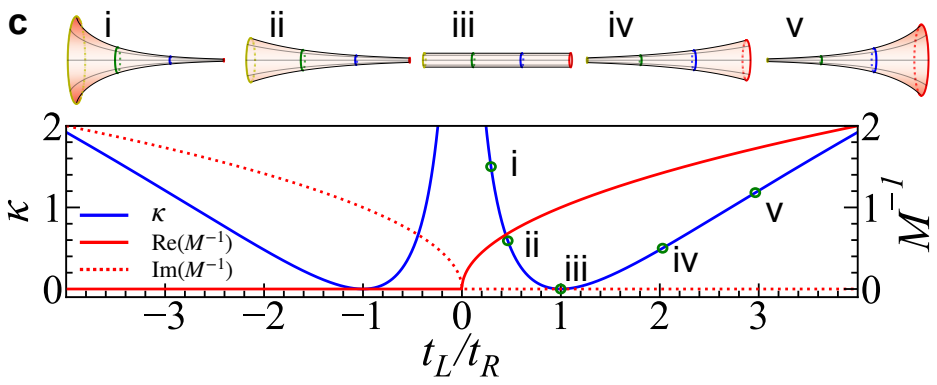


**Figure 4.4.** The curved spaces and corresponding microscopic parameters with varying $t_L$ and fixed $t_R$. The curvature $\kappa$ and inversed mass $M^{-1}$ have units $1/d^2$ and $2t_R d^2/(\hbar^2)$, respectively. In (i-v), we show the hyperbolic spaces dual to the HN model at various $t_L > 0$ using their three-dimensional embeddings. For $t_L < 0$, the pseudosphere is the same as that for $-t_L$ while the mass becomes imaginary.

decreases as $(\sqrt{\kappa}y)^{-1}$, since $L_x(y) = \int_{x=x_0}^{x_0+L} \mathrm{d}x/(\sqrt{\kappa}y) = L/(\sqrt{\kappa}y)$. Transforming into the $s$-coordinate, Eq. (  ) becomes $\int \frac{\mathrm{d}s}{\sqrt{\kappa}y_0} \mathrm{e}^{-2qs} \psi^*_{k_y}(s)\psi_{k'_y}(s) = \mathcal{N}\delta_{k_y,k'_y}$. Discretizing this equation leads to

$$\sum_n |\gamma|^{-2n} \psi^*_n(k_m)\psi_n(k_{m'}) = \delta_{k_m,k_{m'}}, \tag{4.24}$$

we have chosen $\mathcal{N} = (\sqrt{\kappa}y_0)^{-1}$. This orthonormal condition is precisely that provided by the left and right eigenvectors $\psi_L(R)$, and $|\gamma|^{-2n}$ capturing the difference between $\psi_L(R)$ defines the metric operator [  ]. This mapping, therefore, provides an explicit physical interpretation of non-Hermitian orthonormal conditions.

Secondly, the duality allows us to equate the non-Hermitian skin effect to its counterpart on the Poincaré half-plane as we have shown above. The exponential factor of eigenstates on hyperbolic spaces in the $s$-coordinate is precisely dual to the exponential localization on the HN model due to non-Hermitian chiral tunnelings.

Thirdly, the coalesce eigenstates and collapsed spectrum also admit a natural geometric interpretation. While $\kappa$ vanishes when $t_L = t_R$, $\kappa$ increases with decreasing $t_L$ for a given $t_R(> t_L)$. Therefore, the curvature of the hyperbolic space becomes larger with increasing the non-Hermiticity, as shown in Fig.  . Such changes can be visualized by embedding the hyperbolic space into a three-dimensional Euclidean space as a pseudosphere, similar to

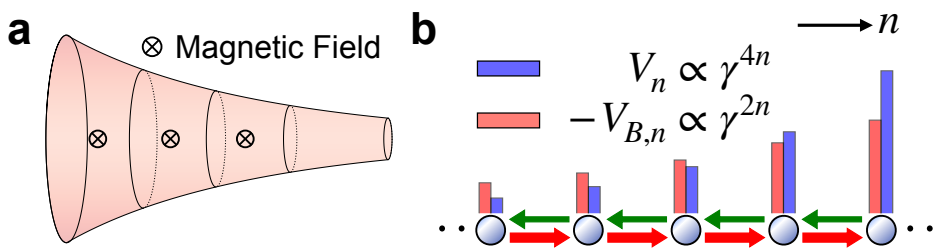


**Figure 4.5.** A hyperbolic surface threaded by uniform magnetic fluxes (a) and the non-Hermitian dual (b).

changing the radius of a sphere. This pseudosphere embedding with a negative curvature is written as

$$(u, v, w) = \frac{1}{\sqrt{\kappa}}\left((\eta - \tanh(\eta)), \frac{\cos(\varphi)}{\cosh(\eta)}, \frac{\sin(\varphi)}{\cosh(\eta)}\right). \tag{4.25}$$

where $y = r_0 \cosh(\eta)$, $x = r_0\varphi$, with $r_0$ an arbitrary constant. $\eta > 0$, $\varphi \in (-\pi, \pi)$.

As approaching the exceptional point, $t_L \to 0$ and the localization length, $1/\ln(|\gamma|)$, vanishes. All eigenstates are forced to coalesce. Since $M$ is divergent, eigenenergies also collapse to zero. With continuously decreasing $t_L < 0$, $M$ becomes imaginary and the system goes across the exceptional point, all previous results apply provided $M \to \pm iM$. Since the eigenenergy is imaginary, particles in hyperbolic spaces now are dissipative, and stationary states no longer exist.

In a non-Hermitian system with chiral tunnelings, changing the boundary condition from an open into a periodic one leads to drastic changes in the eigenstate and the spectrum. From the duality, we immediately conclude the same phenomenon in curved space. This curved space picture provides such drastic changes a physical interpretation, as we are connecting two boundaries with exponentially different radii [ ].

### 4.3.2 Non-Hermitian realization of quantum Hall states in curved spaces

In practice, this duality can be applied to the simulation of intriguing curved space phenomena using non-Hermitian systems. For example, it provides us a means to thread magnetic fluxes on a curved space in studying the gravitational responses of quantum Hall states.

as shown in Fig. . To be more precise, we consider the Poincaré half plane. Under a uniform magnetic field in the Landau gauge, we have a vector potential $\mathbf{A} = (-B/(\kappa y), 0)$ [ ]. The Schrödinger equation of a particle with a charge $-$e becomes

$$-\frac{\hbar^2}{2M}\kappa y^2\left[\left(\partial_x - \mathrm{i}\frac{\mathrm{e}B}{\hbar\kappa}\frac{1}{y}\right)^2 + \partial_y^2\right]\Psi(x,y) = E\Psi(x,y). \tag{4.26}$$

The lowest Landau level (LLL) wavefunctions are written As

$$\psi_{\mathrm{LLL}} = (2k_x)^{\frac{\mathrm{e}B}{\hbar\kappa}-\frac{1}{2}}\sqrt{\frac{\mathcal{N}\kappa}{\Gamma(2\frac{\mathrm{e}B}{\hbar\kappa}-1)L}}\mathrm{e}^{-k_x y+\mathrm{i}k_x x}y^{\frac{\mathrm{e}B}{\hbar\kappa}}, \tag{4.27}$$

where the corresponding eigenenergies, $E_{LLL} = -\frac{\hbar^2\kappa}{8M} + \frac{\hbar\mathrm{e}B}{2M}$, are independent of $k_x$. The degeneracy of the Landau levels for different $k_x$ is similar to that in a flat space. Using the method we introduced, we find the corresponding non-Hermitian systems as a HN model with an extra onsite potential. A finite magnetic field, therefore, changes $V_n$ in Eq.( ) into $V_n + V_{B,n}$ where $V_{B,n} = -ba\gamma^{2n}\sqrt{t_L t_R}$, as shown in Fig. b. $b = \mathrm{e}Bd^2/(\hbar\ln|\gamma|)$ is a dimensionless parameter that characterizes strength of $V_{B,n}$ relative to $V_n$. $y_0 k_x = a(2\ln|\gamma|)^{-1}$ is used. We also define the magnetic flux density, $\rho_\phi = \mathrm{e}B/(2\pi\hbar) = \frac{\ln|\gamma|}{2\pi d^2}b$. Similar to the well-known result of flat spaces where the location of the minimum of a harmonic potential is determined by $k_x$ in the Landau gauge, a finite $k_x$ shifts the minimum of onsite potential $V_n + V_{B,n}$.

A complete description of quantum Hall states requires its gravitational responses in curved spaces. For example, the particle density, $\rho$, differs from the magnetic flux density, $\rho_\phi$, by the local curvature [ ],

$$\rho = \nu\rho_\phi - \kappa/(4\pi), \tag{4.28}$$

where $\nu$ is the filling factor, which is $\nu = 1$ for integer quantum Hall states. Using Eq.(  ), Eq. (  ) for a hyperbolic surface can be directly proved (Appendix). The counterpart of Eq.(  ) in the non-Hermitian lattice is

$$|\gamma|^{2n} \int \mathrm{d}a \mathcal{N}_n(a,b) = b \ln(|\gamma|) - 2\ln^2(|\gamma|), \tag{4.29}$$

where $\mathcal{N}_n(a,b) = |\gamma|^{-2n}\psi_n^*\psi_n$ denotes the particle number at lattice site $n$ in the non-Hermitian system. Eq.(  ) and Eq.(  ) are equivalent if we map the magnetic flux, $\mathrm{e}B/(2\pi\hbar)$, to the ratio between onsite potentials, $b\ln(|\gamma|)/(2\pi d^2)$. The dependence of densities of quantum Hall states on curvatures is thus readily detectable using this non-Hermitian realization.

### 4.4 Generalizations to Long-Range and Non-Uniform Tunnelings

While the HN model offers a useful illustration of the duality, it is simple to apply our approach to general non-Hermitian models. We consider

$$-\sum_{m=1}^{M} t_{Rm}\psi_{n-m} - \sum_{m=1}^{M} t_{Lm}\psi_{n+m} = E\psi_n, \tag{4.30}$$

where $t_{Rm}$ and $t_{Lm}$ are tunneling amplitudes from the $(n \mp m)$th to $n$th sites. An eigenstate under OBC is written as a linear combination of $\mathrm{e}^{\mathrm{i}knd+qnd}$, where $kd \in [0, 2\pi]$ and $q$ is real. Only one $q$ dominates in the bulk. Unlike the HN model, where $q = \ln(t_R/t_L)/(2d)$ is a constant, $q$ is a function of $k$ and defines the so-called generalized Brillouin zone in the complex plane, once beyond the nearest neighbor tunnelings exist [  ], [  ], [  ], [  ], [  ]. We define $\psi(s) = \mathrm{e}^{\mathrm{i}K_0 s}\mathrm{e}^{q(K_0)s}\phi(s)$, in the vicinity of any point in the generalized Brillouin zone specified by $K_0 d \in [0, 2\pi]$, such that $\phi(s)$ changes slowly as a function of $s$. In analog to the method we applied in formulating the effective theory of the HN model, using the Taylor expansion of $\phi(s)$, we obtain

$$-\mathcal{B}(K_0)[\partial_s^2 - 2\mathcal{A}(K_0)\partial_s + \mathcal{C}(K_0)]\psi(s) = E\psi(s), \tag{4.31}$$

where $\mathcal{A}(K_0)$, $\mathcal{B}(K_0)$ and $\mathcal{C}(K_0)$ depend on $K_0$, as well as $t_{Rm}$ and $t_{Lm}$. When only $t_{R1}$ and $t_{L1}$ exist, the equation above at $K_0 = 0$ recovers Eq.(  ), and $\mathcal{A}(K_0)$ provides a constant imaginary vector potential. In the most generic case, $\mathcal{A}(K_0)$ becomes complex, whose real part, $\mathcal{A}_R(K_0)$, curves the space. Using a coordinate transformation defined by $\mathcal{A}_R(K_0)$, $y = y_0 \mathrm{e}^{2\mathcal{A}_R(K_0)s}$, we obtain a hyperbolic surface in the same means as the HN model, with the only difference that $\kappa$ now depends on $K_0$ and is written as $\kappa = 4\mathcal{A}_R^2$. Such $K_0$-dependent curvature delivers a geometric interpretation for the generalized Brillouin zone.

Whereas uniform chiral tunnelings result in a hyperbolic surface with a constant curvature, non-uniform tunnelings lead to curved spaces with inhomogeneous local curvatures. We consider non-uniform chiral tunneling amplitudes denoted by $t_{R(L),n}$,

$$-t_{R,n-1}\psi_{n-1} - t_{L,n}\psi_{n+1} = E\psi_n. \tag{4.32}$$

For slowly varying $t_{R(L),n}$, we first extend them to the continuous variables by defining $\bar{t}(s)$ and $\bar{\gamma}(s)$, where $\bar{t}(nd) = \frac{2Md^2}{\hbar^2}\sqrt{t_{R,n}t_{L,n}}$ and $\bar{\gamma}(nd) = \sqrt{t_{R,n}/t_{L,n}}$. We then introduce a slowly changing function $\phi(s) = \mathrm{e}^{\nu(s)/2}\psi(s)$ with $\nu(s) = \frac{2}{d}\int_0^s \ln(\bar{\gamma}(s))\,\mathrm{d}s$. This approach generalizes the uniform case. In the HN model, $\nu(s) = s\ln(\gamma)/d$ reduces to a linear function of $s$. Using the same procedure, we obtain

$$\frac{\hbar^2}{2M}\left(-\frac{1}{\sqrt{g}}\partial_{\mathrm{i}} g^{\mathrm{ij}}\sqrt{g}\partial_{\mathrm{j}} - \frac{\kappa}{4} + V_c\right)\Psi(x,y) = E\Psi(x,y), \tag{4.33}$$

where $g_{xx} = g_{yy} = \sqrt{g} = \bar{t}(s_y)\mathrm{e}^{-\frac{4}{d}\int_0^{s_y}\ln(\bar{\gamma}(s))\,\mathrm{d}s}$, $g_{xy} = g_{yx} = 0$, $V_c = \frac{\hbar^2}{2Md^2}\left(\frac{d}{2}\partial_s \ln\bar{\gamma}|_{s_y} - 2\right)\bar{t}(s_y)$. The inhomogeneous local curvatures becomes $\kappa(y) = \bar{t}(s_y)\left(4\ln\bar{\gamma}^2(s_y) - 2d\partial_s\ln\bar{\gamma}|_{s_y}\right)/d^2$. In these expressions, $s_y$ is obtained from $y - y_0 = \int_0^{s_y}\mathrm{d}s\mathrm{e}^{\frac{2}{d}\int_0^s \ln(\bar{\gamma}(s))\,\mathrm{d}s}/\bar{t}(s)$. When $t_{R,n}$ and $t_{L,n}$ are constants, the constant $\kappa$ of a hyperbolic surface is recovered. Changing $t_{R,n}$ and $t_{L,n}$ then tunes local curvatures. For instance, when $t_{R,n} = \frac{\hbar^2}{2Md^2}\mathrm{e}^{-\Theta(n-n^*)/(2n)}$, $t_{L,n} = \frac{\hbar^2}{2Md^2}\mathrm{e}^{\Theta(n-n^*)/(2n)}$, where $\Theta(x)$ is the Heaviside step function, the curvature vanishes everywhere except at a particular location, i.e., $\kappa \sim \delta(y - y^*)$, where $y^* = y_0 + n^*d$.

### 4.A Coupled HN chains

In addition to one dimension, many non-Hermitian models in higher dimensions can be constructed based on the HN model. For instance, 1D HN chains can be assembled through inter-chain couplings to access higher dimensional curved spaces. For instance, the lattice model with HN chains coupled vertically is illustrated in Fig. a, which reads

$$-t\Psi_{n,m+1} - t\Psi_{n,m-1} - t_R\Psi_{n-1,m} - t_L\Psi_{n+1,m} = E\Psi_{n,m}. \tag{4.34}$$

We define $\Psi(s,z)$ such that $\Psi(s_n, z_m) \equiv \Psi_{n,m}/d$, and $\Psi(s,z) = \Phi(s,z)\mathrm{e}^{qs}\mathrm{e}^{\mathrm{i}K_0 s}\mathrm{e}^{\mathrm{i}k_{z0}z}$, where $\Phi$ is slowly varying. We have applied periodical boundary condition along the $z$-direction. Near the band bottom ($K_0 = 0, k_{z0} = 0$), substituting $\Psi$ to Eq. ( ) and using the Taylor expansion of $\Phi(s,z)$, we obtain

$$\begin{aligned} -\Big[&\left(2t + t_R\mathrm{e}^{-qd} + t_L\mathrm{e}^{qd}\right) + \left(-t_R\mathrm{e}^{-qd} + t_L\mathrm{e}^{qd}\right) d\partial_s \\ &+\frac{d^2}{2}\left(t_R\mathrm{e}^{-qd} + t_L\mathrm{e}^{qd}\right)\partial_s^2 + td^2\partial_z\Big]\Phi(s,z) = E\Phi(s,z) \end{aligned} \tag{4.35}$$

A generic solution is written as $\Phi = \mathrm{e}^{\mathrm{i}k_s s}\mathrm{e}^{\mathrm{i}k_z z}$. To ensure the open boundary condition in $s$-direction and obtain an effective theory near ($K_0 = 0, k_{z0} = 0$), we require $E(k_s, 0) = E(-k_s, 0)$, which leads to $-t_R\mathrm{e}^{-qd} + t_L\mathrm{e}^{qd} = 0$. The solution gives $q = \ln\left(\sqrt{t_R/t_L}\right)/d$. For a finite $k_z$, the solution to Eq.( ) that satisfies the specified boundary conditions is written

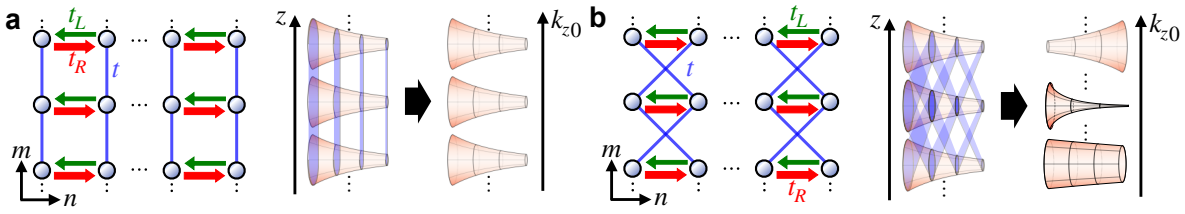


**Figure 4.6.** A set of coupled HN chains is dual to a 3D curved space. (a) The curvature of each decoupled surface remains unchanged by the vertical inter-chain couplings. (b) Inter-chain couplings fundamentally influence each curved surface, and the curvature becomes energy-dependent.

as $\mathrm{e}^{\mathrm{i}k_z z}\sin(k_s s)$. In other words, $q$ and the resultant curvature, is independent of $k_z$. After a coordinate transformation $\frac{y}{y_0}=\mathrm{e}^{2qs}$, Eq. (  ) is written as

$$-\left[2\left(t+\sqrt{t_L t_R}\right)+\sqrt{t_L t_R}d^2\kappa\left(y^2\partial_y^2+\frac{1}{4}\right)+td^2\partial_z^2\right]\Psi(y,z)=E\Psi(y,z), \tag{4.36}$$

where $\kappa=4\ln^2\left(\sqrt{\frac{t_R}{t_L}}\right)/d^2$.

In contrast, the model in Fig.  b reads

$$-t\Psi_{n-1,m-1}-t\Psi_{n+1,m-1}-t\Psi_{n-1,m+1}-t\Psi_{n+1,m+1}-t_R\Psi_{n-1,m}-t_L\Psi_{n+1,m}=E\Psi_{n,m}. \tag{4.37}$$

The slowly varying $\Phi(s,z)$ satisfies

$$\begin{aligned}-\Big[&\left(2t\mathrm{e}^{-qd}+2t\mathrm{e}^{qd}+t_R\mathrm{e}^{-qd}+t_L\mathrm{e}^{qd}\right)+\left(-2t\mathrm{e}^{-qd}+2t\mathrm{e}^{qd}-t_R\mathrm{e}^{-qd}+t_L\mathrm{e}^{qd}\right)d\partial_s\\&+\left(2t\mathrm{e}^{-qd}+2t\mathrm{e}^{qd}+t_R\mathrm{e}^{-qd}+t_L\mathrm{e}^{qd}\right)\frac{1}{2}d^2\partial_s^2+2t\left(\mathrm{e}^{qd}+\mathrm{e}^{-qd}\right)\frac{1}{2}d^2\partial_z^2\\&+t\left(\mathrm{e}^{qd}-\mathrm{e}^{-qd}\right)d^3\partial_z^2\partial_s\Big]\Phi(s,z)=E\Phi(s,z).\end{aligned} \tag{4.38}$$

For the effective theory near $(K_0=0,k_{z0}=0)$, the open boundary condition in $s$-direction requires $E(k_s,0)=E(-k_s,0)$ and $-2t\mathrm{e}^{-qd}+2t\mathrm{e}^{qd}-t_R\mathrm{e}^{-qd}+t_L\mathrm{e}^{qd}=0$. This provides us with $q=\frac{1}{d}\ln\left(\sqrt{\frac{t_R+2t}{t_L+2t}}\right)$, and

$$-\left[2\tilde{t}+\tilde{t}d^2\partial_s^2+\frac{t}{\tilde{t}}(4t+t_L+t_R)d^2\partial_z^2+\frac{t}{\tilde{t}}(t_R-t_L)d^3\partial_z^2\partial_s\right]\Phi(s,z)=E\Phi(s,z), \tag{4.39}$$

where $\tilde{t}=\sqrt{(t_R+2t)(t_L+2t)}$. When $k_z$ is finite, the solution to Eq.(  ) reads $\Phi=\mathrm{e}^{\mathrm{i}k_z z}\sin(k_s s)\mathrm{e}^{\left(\frac{t(t_R-t_L)}{2\tilde{t}^2}k_z d\right)k_z s}$. The extra exponential function gives rise to a $k_z$-dependent $q(k_z)=\frac{1}{d}\ln\left(\sqrt{\frac{t_R+2t}{t_L+2t}}\right)+\frac{td(t_R-t_L)}{2\tilde{t}^2}k_z^2$. After a coordinate transformation $\frac{y}{y_0}=\mathrm{e}^{2qs}$ and $\Phi(s,z)=\Psi(s,z)\mathrm{e}^{-qs}$, Eq. (  ) is written as

$$\begin{aligned}-\tilde{t}d^2\Bigg[&\frac{t(t_R-t_L)}{\tilde{t}^2}\partial_z^2\left(\frac{4t+t_R+t_L}{t_R-t_L}+d\sqrt{\kappa_c}\left(y\partial_y-\frac{1}{2}\right)\right)\\&+\frac{2}{d^2}+\kappa_c\left(y^2\partial_y^2+\frac{1}{4}\right)\Bigg]\Psi(y,z)=E\Psi(y,z),\end{aligned} \tag{4.40}$$

where $\kappa_c = \ln^2\left(\frac{t_R+2t}{t_L+2t}\right)/d^2$. A finite $k_z$ modifies the curvature, $\kappa_c(k_z) = \frac{1}{d^2}\ln^2\left(\frac{t_R+2t}{t_L+2t}\right) + \frac{2t(t_R-t_L)}{t^2}\log\left(\frac{t_R+2t}{t_L+2t}\right)k_z^2 + \mathcal{O}((k_z d)^4)$.

Whereas the above discussions apply to the band bottom, the effective theory can be formulated at any energies. In the lattice models, we write $\Psi_{n,m} = \psi_n \mathrm{e}^{\mathrm{i}k_{z0}md}$, and obtain

$$-2t\cos(k_{z0}d)\psi_n - t_R\psi_{n-1} - t_L\psi_{n+1} = E\psi_n, \tag{4.41}$$

and

$$-(t_R + 2t\cos(k_{z0}d))\psi_{n-1} - (t_L + 2t\cos(k_{z0}d))\psi_{n+1} = E\psi_n, \tag{4.42}$$

for Eq. (  ) and (  ), respectively. Therefore, for each $k_{z0}$, we have a dual model in the curved space. Especially, for Eq. (  ), we obtain a $k_{z0}$-dependent HN model and the corresponding curved space can be derived in the same manner as in the main text, where $\kappa = \ln^2\left(\left|\frac{t_R+2t\cos(k_{z0}d)}{t_L+2t\cos(k_{z0}d)}\right|\right)/d^2$, which is $k_{z0}$ dependent. It reduces to $\kappa_c$ if we take the limit of $k_{z0}d \to 0$.

### 4.B Gravitational responses of quantum Hall states in hyperbolic spaces

The normalized wavefunction at the lowest Landau level on a Poincaré half-plane is written as

$$\Psi_{\mathrm{LLL}}(x,y) = 2^{\alpha-1/2}k_x^{\alpha-1/2}\sqrt{\frac{\kappa\mathcal{N}}{\Gamma(2\alpha-1)L}}\mathrm{e}^{\mathrm{i}k_x x}\mathrm{e}^{-k_x y}y^{\alpha}, \tag{4.43}$$

where $\Gamma(x)$ is the Gamma function $\alpha = \frac{eB}{\hbar\kappa} > 0$, and $k_x = 2\pi n/L$. The particle density at unit filling becomes

$$\rho(x,y) = \frac{1}{\mathcal{N}}\sum_{k_x}|\Psi_{\mathrm{LLL}}|^2 = \left(\frac{4\pi}{L}\right)^{2\alpha-1}\frac{\kappa y^{2\alpha}}{\Gamma(2\alpha-1)L}\mathrm{Li}_{1-2\alpha}(\mathrm{e}^{-\frac{4\pi}{L}y}), \tag{4.44}$$

where $\mathrm{Li}_k(z) = \sum_{n=1}^{\infty} z^n/n^k$ is the polylogarithm function of order $k$. The summation is only taken from $n = 1$ to $\infty$ since the wavefunction is not normalizable and Landau levels do not exist for $n \leq 0$. In the thermodynamic limit,

$$\lim_{L\to\infty}\rho(x,y) = (4\pi)^{-1}\frac{\Gamma(2\alpha)\kappa}{\Gamma(2\alpha-1)} = \frac{eB}{2\pi\hbar} - \frac{\kappa}{4\pi}. \tag{4.45}$$

We have used $\mathrm{Li}_k(\mathrm{e}^w) = \Gamma(1-k)(-w)^{k-1} + \sum_{\mathrm{j}=0}^{\infty} \frac{\zeta(k-\mathrm{j})}{\mathrm{j}!} w^{\mathrm{j}}$, which is valid for $|w| < 2\boldsymbol{\pi}$ and $k \notin \mathbb{N}^+$. $\zeta(x)$ denotes the zeta function.

# 5. UNIVERSAL RELATIONS FOR ULTRACOLD REACTIVE MOLECULES

*The contents of this chapter are based on and modified from the published article [ ] by M. He, C. Lv, H.-Q. Lin, and Q. Zhou, Universal relations for ultracold reactive molecules, Science Advances, 6(51), eabd4699. Copyright (2020) by The Authors.*

The laboratory realization of ultracold polar molecules has pushed physics and chemistry into new realms. Polar molecules, in particular, provide chemists with unparalleled opportunities to investigate controllable chemical reactions in the ultracold regime, where quantum effects become evident. Ultracold molecules with rich internal degrees of freedom also provide a promising platform in quantum information processing. However, reactions or formations of complexes due to collisions between ultracold molecules lead to two-body loss. A key question about how two-body loss depends on quantum correlations in interacting many-body systems remains open. In this chapter, we provide a set of universal relations that correlate two-body loss to other physical observables, such as density correlation functions and momentum distribution. These relations, which hold for any arbitrary microscopic parameter, such as particle number, temperature, interaction strength, and dimensionality, reveal the critical role of contacts, a fundamental quantity of dilute quantum systems, in determining the reaction rate of quantum reactive molecules in a many-body environment.

## 5.1 Introduction

Highly controllable polar molecules in a temperature regime down to a few tens of nano-Kelvin provide scientists with a powerful apparatus to study a vast range of new quantum phenomena in quantum information processing, condensed matter physics, and quantum chemistry, such as quantum gates with fast switching times [ ], [ ], exotic quantum phases [ ]–[ ], and quantum chemical reactions [ ], [ ], [ ]–[ ]. The two-body loss is an essential ingredient leading to non-Hermitian phenomena in all these studies. Collisions between ultracold molecules may yield certain products and release energies, which allow particles to escape the traps. For example, a prototype reaction, KRb+KRb $\rightarrow$ $K_2$ + $Rb_2$, is the principal source of KRb molecule loss. Because of the rich internal degree of freedom of molecules, four-body complexes that are not detectable may also develop during

the scattering process. Such long-lived complexes also result in losses in the system of interest [ ], [ ].

Whereas chemical reactions are known for their complexities, including quantum effects imposes an even bigger challenge to both physicists and chemists. Quantitative analysis of the reactions is difficult due to the exponentially large degrees of freedom and quantum correlations built upon interactions. A standard approach is to consider two interacting particles, the reaction rate of which is trackable [ ], [ ]. When the temperature is high enough and correlations between different pairs of particles are negligible, such results are applicable in many-body systems; however, when the temperature decreases, many-body correlations become significant, and this method fails. To completely comprehend the quantum many-body effects, a theory encompassing them needs to be developed.

This chapter shows that universality exists in ultracold reactive molecules when chemical reactions are present. Contacts, the central quantity in dilute quantum systems [ ], are implemented to build universal relations between the two-body loss rate and other quantities, including the density correlation function and the momentum distribution. Previously, two-body loss of zero-range potentials hosting inelastic s-wave scatterings were correlated to the s-wave contact [ ], [ ]. Nevertheless, chemical reactions occur at a finite separation in reality. Higher-partial wave scatterings are also needed in characterizing many systems. For example, single-component fermionic KRb molecules interact with p-wave scatterings [ ], [ ]. Therefore, it is necessary to develop a theory that can be applied to all short-range reactive interactions. We will focus on single-component fermionic molecules to concretize discussions. All of our results can be directly generalized to other systems with arbitrary short-range interactions.

## 5.2 Length Scale Separation and Universal Relations

The Hamiltonian of $N$ reactive molecules is written as

$$H = \sum_{\mathrm{i}} [ -\frac{\hbar^2}{2M}\nabla_{\mathrm{i}}^2 + V_{\mathrm{ext}}(\mathbf{r}_{\mathrm{i}})] + \sum_{\mathrm{i>j}} U(\mathbf{r}_{\mathrm{i}} - \mathbf{r}_{\mathrm{j}}), \tag{5.1}$$

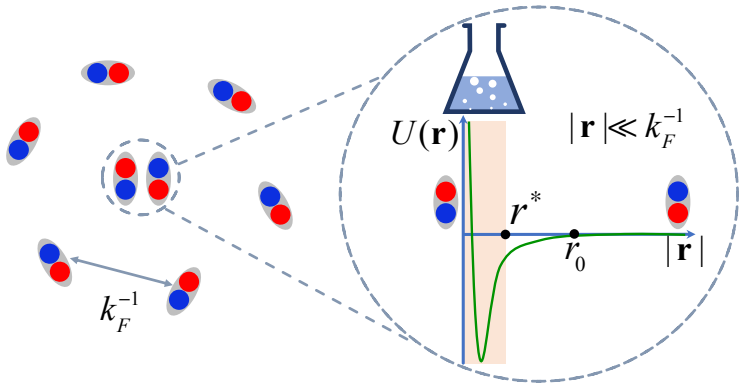


**Figure 5.1.** A length scale separation in ultracold dilute systems. Potassium (rubidium) atoms are represented by blue (red) solid spheres. Two molecules inside the dashed circle are seperated much closer than the average inter-particle spacing, $|\mathbf{r}| \ll k_F^{-1}$. A schematic of the chemical reaction is shown in the enlarged plot of the region within the dashed circle. The real (imaginary) part of the interaction, $U_R(\mathbf{r})$ ($U_I(\mathbf{r})$) is represented the green solid curve (shaded area), respectively. The reaction happens only at the shaded area where $U_I(\mathbf{r})$ is finite.

where $M$ is the molecular mass, $V_{\text{ext}}(\mathbf{r})$ and $U(\mathbf{r})$ are the external potential and a two-body interaction, respectively, as shown in Fig. . The many-body wavefunction, $\Psi(\mathbf{r}_1, \mathbf{r}_2, ..., \mathbf{r}_N)$, satisfies the time-dependent Schrödinger equation,

$$\mathrm{i}\hbar\partial_t \Psi(\mathbf{r}_1, \mathbf{r}_2, ..., \mathbf{r}_N) = H\Psi(\mathbf{r}_1, \mathbf{r}_2, ..., \mathbf{r}_N). \tag{5.2}$$

$U(\mathbf{r})$ is a short-range interaction with a characteristic length scale, $r_0$, in the absence of electric fields. When $|\mathbf{r}| > r_0$, $U(\mathbf{r}) = 0$. Chemical reactions have a finite range but happen in an even shorter length scale, $r^* < r_0$. We apply a one-channel model with a complex $U(\mathbf{r}) = U_R(\mathbf{r}) + \mathrm{i}U_I(\mathbf{r})$ in describing the chemical reaction [ ], where $U_I(\mathbf{r}) \leq 0$. When $|\mathbf{r}| > r^*$, $U_I(\mathbf{r}) = 0$. The same universal relations can also be derived using the Lindblad equation that models the losses by jump operators (Appendix A).

### 5.2.1 Length scale separation in dilute ultracold quantum system

In ultracold dilute quantum systems, the average inter-particle separation, provided by the inverse of the Fermi momentum, $k_F^{-1}$, sets the largest length scale. Universal relations are originated from a length scale separation $r^* < r_0 \ll k_F^{-1}$. When the distance between two molecules is much smaller than $k_F^{-1}$, we obtain,

$$\Psi(\mathbf{r}_1, \mathbf{r}_2, ..., \mathbf{r}_N) \xrightarrow{|\mathbf{r}_{ij}| \ll k_F^{-1}} \sum_{m,\epsilon} \psi_m(\mathbf{r}_{ij}; \epsilon) G_m(\mathbf{R}_{ij}; E - \epsilon), \tag{5.3}$$

where $\mathbf{r}_{ij} = \mathbf{r}_i - \mathbf{r}_j$ describes the relative motion between the ith and the jth molecules, and $\mathbf{R}_{ij} = \{(\mathbf{r}_i + \mathbf{r}_j)/2, \mathbf{r}_{k \neq i,j}\}$ denotes the center of mass motion and the coordinates of all other particles. In the short-range limit, the many-body wavefunction is factorized into a two-body and a many-body part. The two-body wavefunction $\psi_m(\mathbf{r}_{ij}; \epsilon)$ is in p-wave and $m = 0, \pm 1$ denotes the magnetic quantum number. $\psi_m$ is determined by the two-body Hamiltonian, $H_2 = -(\hbar^2/M)\nabla^2 + U(\mathbf{r}_{ij})$, because all other particles are far away from the chosen pair in the regime, $|\mathbf{r}_{ij}| \ll k_F^{-1}$. $E$ is the total energy of the many-body system which is conserved. The two-body colliding energy, $\epsilon = \hbar^2 q_\epsilon^2/M$, is no longer a good quantum number, and a sum shows up in Eq. (  ). Because both a continuous spectrum and discrete bound states might occur at the same time, we employ sum rather than integral notation.

From the near threshold scattering theory, we can write down the universal asymptotic wavefunction within the region $r_0 < |\mathbf{r}_{ij}| \ll k_F^{-1}$ expanded by the two-body colliding energy $\epsilon$. We define $\psi_m(\mathbf{r}_{ij}; \epsilon) = \varphi_m(|\mathbf{r}_{ij}|; \epsilon) Y_{1m}(\hat{\mathbf{r}}_{ij})$, where $Y_{1m}(\hat{\mathbf{r}}_{ij})$ is the p-wave spherical harmonics. The near threshold wavefunction is characterized by the energy dependent phase shift. Despite the fact that there are many resonances, the phase shift of scattering between KRb molecules remains a smooth function of energy due to the large average line width, which much exceeds the mean level spacing of the bound states [  ]. The phase shift, $\eta$, then has a well defined expansion, $q_\epsilon^3 \cot[\eta(q_\epsilon)] = -1/v_p + q_\epsilon^2/r_e$. Since we have reactive interaction,

both the p-wave scattering volume $v_p$ and effective range $r_\mathrm{e}$ become complex. Consequently, $\varphi_m(|\mathbf{r}_\mathrm{ij}|;\epsilon) = \varphi_m^{(0)}(|\mathbf{r}_\mathrm{ij}|) + q_\epsilon^2\varphi_m^{(1)}(|\mathbf{r}_\mathrm{ij}|) + \mathrm{O}(q_\epsilon^4)$, where

$$\varphi_m^{(0)}(|\mathbf{r}_\mathrm{ij}|) \xrightarrow{r_0<|\mathbf{r}_\mathrm{ij}|\ll k_F^{-1}} \frac{1}{|\mathbf{r}_\mathrm{ij}|^2} - \frac{1}{v_p}\frac{|\mathbf{r}_\mathrm{ij}|}{3}, \tag{5.4}$$

$$\varphi_m^{(1)}(|\mathbf{r}_\mathrm{ij}|) \xrightarrow{r_0<|\mathbf{r}_\mathrm{ij}|\ll k_F^{-1}} \frac{1}{r_\mathrm{e}}\frac{|\mathbf{r}_\mathrm{ij}|}{3} + \frac{1}{v_p}\frac{|\mathbf{r}_\mathrm{ij}|^3}{30} + \frac{1}{2}. \tag{5.5}$$

We have considered isotropic $p$-wave interactions to simplify expressions. $\varphi(|\mathbf{r}_\mathrm{ij}|) = \varphi_m(|\mathbf{r}_\mathrm{ij}|)$ and $G(\mathbf{R}_\mathrm{ij}; E-\epsilon) = G_m(\mathbf{R}_\mathrm{ij}; E-\epsilon)$. Other partial waves that do not show up in universal relations relevant for our consideration are suppressed. Using the expressions above, we are able to construct universal relations in the dilute gases.

### 5.2.2 Two-body loss rate

Using Eqs. (  ,  ,  ) and the low energy expansion, we find the decay rate,

$$\partial_t N = -\frac{\hbar}{8\pi^2 M}\sum_{\nu=1}^{3}\kappa_\nu C_\nu, \tag{5.6}$$

The three contacts $C_\nu$ are written as

$$C_1 = 3(4\pi)^2 N(N-1)\int \mathrm{d}\mathbf{R}_\mathrm{ij}|g^0|^2, \tag{5.7}$$

$$C_2 = 6(4\pi)^2 N(N-1)\int \mathrm{d}\mathbf{R}_\mathrm{ij}\mathrm{Re}(g^{0*}g^1), \tag{5.8}$$

$$C_3 = 6(4\pi)^2 N(N-1)\int \mathrm{d}\mathbf{R}_\mathrm{ij}\mathrm{Im}(g^{0*}g^1), \tag{5.9}$$

$\int d\mathbf{R}_\mathrm{ij}$ integrates over all coordinates in $\mathbf{R}_\mathrm{ij}$, and $g^s = \sum_\epsilon q_\epsilon^{2s} G(\mathbf{R}_\mathrm{ij}; E-\epsilon)$. As we will show later, $C_1$ is the contact that determines the leading term in the large momentum tail, similar to systems without losses [  ]–[  ]. $C_{2,3}$ are new quantities in systems with two-body loss, in contrast.

$\kappa_\nu$ in Eq. (  ) are microscopic parameters solely captured by the two-body physics. Using the one-channel model, we can write their explicit expressions as

$$\kappa_1 = -\frac{M}{\hbar^2}\int_0^\infty U_I(r)\left|\varphi^{(0)}(r)\right|^2 r^2\,\mathrm{d}r, \tag{5.10}$$

$$\kappa_2 = -\frac{M}{\hbar^2}\mathrm{Re}\left(\int_0^\infty U_I(r)\,\varphi^{(0)*}(r)\varphi^{(1)}(r)r^2\,\mathrm{d}r\right), \tag{5.11}$$

$$\kappa_3 = \frac{M}{\hbar^2}\mathrm{Im}\left(\int_0^\infty U_I(r)\,\varphi^{(0)*}(r)\varphi^{(1)}(r)r^2\,\mathrm{d}r\right), \tag{5.12}$$

where $r = |\mathbf{r}|$.

Equation (  ) is universal and it applies to any particle number, any short-range interaction strengths, as well as any conservative external potential. It separates $C_\nu$, which capture the many-body physics, from two-body parameters, $\kappa_\nu$, that is captured by the microscopic details of reactive interaction. Moreover, even when microscopic details of the reactive interaction, such as the exact expression of $U_{R(I)}(\mathbf{r})$, are unknown, $\kappa_\nu$ can still be accessed in systems whose $C_\nu$ are easily measurable using other universal relations (Appendix B). Eq. (  ) also applies for any finite temperatures if the reaction rate is slow compared to the time scale of establishing quasi-equilibrium. In this case, $C_\nu$ should be interpreted as their thermal averages.

We have found that $\kappa_1$ and $\kappa_2$ can be rewritten as familiar parameters. In fact, $\kappa_1 = \mathrm{Im}(v_p^{-1})$ and $\kappa_2 = \mathrm{Im}[-1/(2r_\mathrm{e})]$ (see details in Appendix B). In contrast, $\kappa_3$ is a new parameter that has not been addressed in previous works to the best of our knowledge. Similar to the effective range, $\kappa_3$ can be expressed as the difference between the realistic wavefunction at $|\mathbf{r}| < r_0$ and the extrapolation of the two-body wavefunction at $|\mathbf{r}| > r_0$ toward $|\mathbf{r}| < r_0$ (Appendix B) [  ]. Using these expressions, Equation (  ) becomes

$$\partial_t N = -\frac{\hbar}{8\pi^2 M}\left[\mathrm{Im}(v_p^{-1})C_1 - \frac{1}{2}\mathrm{Im}(r_\mathrm{e}^{-1})C_2 + \kappa_3 C_3\right]. \tag{5.13}$$

The first term in the bracket was previously derived for s-wave complex zero-range interactions, with $v_p^{-1}$ replaced by the complex s-wave scattering length [  ]. All three contacts and all three microscopic parameters are required for a generic short-range interaction, as

shown in Eqs. ( , ). These expressions allow us to directly relate the two-body loss rate to a broad range of physical quantities.

### 5.2.3 Momentum distribution

The first physical quantity we consider is the momentum distribution. Since the universal form of the short-range wavefunction and the contacts together determine the short-range behavior of the many-body wavefunction, the momentum distribution led by the universal form of the short-range wavefunction can be directly correlated with the contact. The universal behavior of momentum distribution appears when $|\mathbf{k}| \ll 1/r_0$ but much larger than all other momentum scales, including the thermal wavelength, $k_F$, and the inverses of the scattering length. The angular averaged total momentum becomes

$$n(|\mathbf{k}|) = \sum_{m=0,\pm1} \int \mathrm{d}\mathbf{\Omega} n_m(\mathbf{k}) \to \frac{C_1}{|\mathbf{k}|^2}, \tag{5.14}$$

where $\mathbf{\Omega}$ is the solid angle. The first term in Eqs. ( , ) is known once $n(|\mathbf{k}|)$ is measured. If an radio-frequency (RF) spectroscopy exists for molecules, similar to that for atoms, Eq. ( ) also indicates a universal tail in the transition rate,

$$\Gamma(\omega) \to [(\Omega_{rf} V)/(8\boldsymbol{\pi}^2)] C_1 (\hbar\omega/M)^{-1/2}, \tag{5.15}$$

where $\omega$ and $\Omega_{rf}$ is the $RF$ frequency and $RF$ Rabi frequency, respectively. $V$ denotes the system's volume. It is worth noting that, Eq. ( ) describes the leading term of the large momentum tail for atoms with elastic p-wave interactions [ ]–[ ]. We have found no connection between the subleading term $\sim |\mathbf{k}|^{-4}$ and two-body loss.

### 5.2.4 Density correlation function

The density correlation function, $S(\mathbf{r}) = \int \mathrm{d}\mathbf{R} \langle n(\mathbf{R} + \mathbf{r}/2) n(\mathbf{R} - \mathbf{r}/2) \rangle$, is another fundamentally important quantity. It measures the probability of having two particles separated by a distance $\mathbf{r}$. Using Eqs. ( , , ), $S(\mathbf{r})$ can be evaluated in the regime, $r_0 < |\mathbf{r}| \ll k_F^{-1}$.

$S(\mathbf{r})$ can be integrated over a shell with thickness $D$ to enhance the signal, which is given by $P(x,D)=\int_x^{x+D}\mathrm{d}\mathbf{r}S(\mathbf{r})$, and

$$\left.\frac{\partial P(x,D)}{\partial D}\right|_{D\to 0}=\frac{1}{16\pi^2}\Big\{C_1\frac{1}{x^2}+\frac{1}{2}C_2-\Big[2\mathrm{Re}(\frac{1}{v_p})C_1-\mathrm{Re}(\frac{1}{r_\mathrm{e}})C_2+\mathrm{Im}(\frac{1}{r_\mathrm{e}})C_3\Big]\frac{x}{3}\Big\}. \quad (5.16)$$

We have suppressed other partial waves since their contributions are provided by different spherical harmonics. Provided that $v_p$ and $r_\mathrm{e}$ are known, using the power series to fit $\partial P(x,D)/\partial D|_{D\to 0}$ measured in experiments in Eq. ( ) allows one to obtain all three contacts, $C_{1,2,3}$. Higher order terms need to be included in the expansion if these two parameters are unknown (Appendix B).

We would like to address that, equations ( , , , ) allow experimentalists to explore the role of contacts in interacting few-body and many-body systems in determining chemical reactions, despite whether correlation functions and thermodynamic quantities can be computed accurately in theories. In fact, when exact theoretical results are not accessible in the strongly interacting regime, these universal relations become most powerful.

### 5.3 Calculation With a Complex Finite Square Well Interaction

In the following, we will focus on the two-body loss rate by considering the analytical result from an explicit example. We first consider the two-body loss in a two-body quantum system and compute $\kappa$'s and contact. Then we apply the virial expansion to the second order to obtain the high temperature loss rate.

#### 5.3.1 Result from a two-body problem

We model $U(\mathbf{r})$ by two square well potentials. One is real with strength $-\tilde{U}_R$ and another is imaginary with strength $-\tilde{U}_I$. For simplicity, we set the range of both as $r_0=r^*$, such that $U(\mathbf{r})=-\tilde{U}_R-\mathrm{i}\tilde{U}_I$ when $|\mathbf{r}|\leq r_0=r^*$ and 0 elsewhere. The ratio $r_0/r^*$ does not qualitatively change any results. Fig. shows the dependency of $\kappa_{1,2,3}$ on $\tilde{U}_I$ with various fixed $\tilde{U}_R$. $\kappa_{1,2,3}=0$ in the absence of $\tilde{U}_I$. $\kappa_{1,2,3}$ change non-monotonically with increasing $\tilde{U}_I$, and all approach zero when $\tilde{U}_I$ is large, which signifies the quantum Zeno limit.

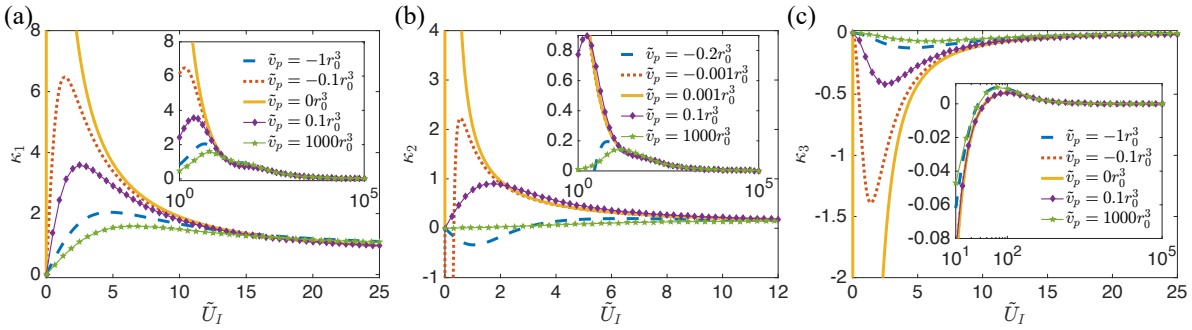


**Figure 5.2.** The three microscopic parameters as functions of the reactive interactions, $\tilde{U}_I$, which has the unit of $\hbar^2/(Mr_0^2)$. $\tilde{v}_p$ denotes the scattering volume when $\tilde{U}_I = 0$. $\kappa_{1,2,3}$ are in unit of $r_0^{-3}$, $r_0^{-1}$ and $r_0^{-1}$, respectively. The location of the maximum of $\kappa_1$ ($\kappa_3$) first approaches and then leaves the origin when $\tilde{v}_p$ crosses zero. $\kappa_1$ ($\kappa_3$) remains positive (negative). When $\tilde{U}_I$ is small, $\kappa_2$ quickly changes from positive to negative as $\tilde{v}_p$ crosses zero. All three microscopic parameters vanish in the large $\tilde{U}_I$ limit, as shown by the insets.

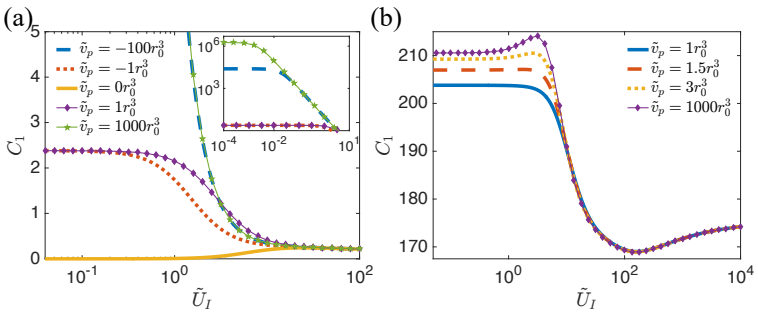


**Figure 5.3.** Contact $C_1$ in scattering and bound states of a two-body system in free space. (a) Scattering state $C_1$ with the unit $r_0^4/V$ as a function of $\tilde{U}_I$ with the unit $\hbar^2/(Mr_0^2)$, for various fixed $\tilde{v}_p$. $q_\epsilon = 0.01/r_0$. (b) Bound state $C_1$ with the unit $r_0$ as a function of $\tilde{U}_I$ with the unit $\hbar^2/(Mr_0^2)$.

**Table 5.1.** Analytical expressions for contacts $C_\nu$ of two particles in different limits. Line 1 show the results in the weakly interacting regime. Line 2 show the results at resonance. Line 3 includes the results for bound states with considering a single angular momentum $m$.

| | $C_1$ | $C_2$ | $C_3$ |
|---|---|---|---|
| $v_p \to 0_\pm$ | $12(4\pi)^3 q_\epsilon^2 \lvert v_p \rvert^2 / V$ | $2C_1 \mathrm{Re}(q_\epsilon^2)$ | 0 |
| $v_p \to \infty$ | $12(4\pi)^3 q_\epsilon^{-2} \lvert r_e \rvert^2 / V$ | $2C_1 \mathrm{Re}(q_\epsilon^2)$ | 0 |
| bound | $2(4\pi)^2 \mathrm{Re}(-r_e)$ | $2C_1 \mathrm{Re}(q_\epsilon^2)$ | $2C_1 \mathrm{Im}(q_\epsilon^2)$ |

We consider a two-body system in free space in evaluating the contacts. In such a system, $\epsilon$ in Eqs. (  ,  ,  ) becomes a good quantum number, and $G(\mathbf{R}_{ij}; E-\epsilon)$ becomes a delta function in the energy space. We consider the wavefunction, $\Psi^{[2]}(\mathbf{r}_1, \mathbf{r}_2) = \phi_c(\mathbf{R}_{12})\psi(\mathbf{r}_{12})$, for scattering states, where $\phi_c(\mathbf{R}_{12})$ is a normalized wavefunction of the center of mass and $\psi(\mathbf{r}_{12}) = \sqrt{8\pi/V}[\mathrm{i}/(\cot\eta - \mathrm{i})][\cot\eta \mathrm{j}_1(q_\epsilon|\mathbf{r}_{12}|) - n_1(q_\epsilon|\mathbf{r}_{12}|)] \sum_m Y_{1m}(\hat{\mathbf{r}}_{12})$. Fig.  shows the dependence of $C_1$ on $\tilde{U}_I$ when $\tilde{v}_p$ is fixed at various values. Bound state results with complex $\epsilon$ are also shown. $C_1$ approaches a non-zero constant in both cases with increasing $\tilde{U}_I$. Here, $C_2 = 2C_1 \mathrm{Re}(q_\epsilon^2)$. $C_3 = 0$ if a scattering state is considered. In contrast, $C_3 = 2C_1 \mathrm{Im}(q_\epsilon^2)$ for a bound state. Table.  shows the analytical results in the limits, $v_p = 0^\pm, \infty$.

**Table 5.2.** Analytical expressions for thermal averaged contacts $\langle C_\nu \rangle_T$ in different limits. The weakly interacting regime results are shown in Line 1 and 2. The results at resonance are shown in Line 3. The contributions of Bound states exist when $v_p$ is positive and are included in Line 1. $N_D$ is the number of dimers. $\lambda_T = [(2\pi\hbar^2)/(Mk_BT)]^{1/2}$ is the thermal wave length.

| $v_p$ | $\langle C_1 \rangle_T$ | $\langle C_2 \rangle_T$ | $\langle C_3 \rangle_T$ |
|---|---|---|---|
| $v_p \to 0_+$ | $72(2\pi)^4\|v_p\|^2\lambda_T^{-2}Nn$ $+2(4\pi)^2\mathrm{Re}(-r_e)N_D$ | $360(2\pi)^5\|v_p\|^2\lambda_T^{-4}Nn +$ $4(4\pi)^2\mathrm{Re}(-r_e)\mathrm{Re}(\frac{r_e}{v_p})N_D$ | $4(4\pi)^2\mathrm{Re}(-r_e)\mathrm{Im}(\frac{r_e}{v_p})N_D$ |
| $v_p \to 0_-$ | $72(2\pi)^4\|v_p\|^2\lambda_T^{-2}Nn$ | $360(2\pi)^5\|v_p\|^2\lambda_T^{-4}Nn$ | 0 |
| $v_p \to \infty$ | $24(4\pi)^2\|r_e\|^2\lambda_T^2Nn$ | $12(4\pi)^3\|r_e\|^2Nn$ | 0 |

### 5.3.2 High temperature results from virial expansion

Using the two-body results, we study a thermal gas at high temperatures with the second order virial expansion. The partition function is written as

$$Z = Z_0 + \mathrm{e}^{2\mu/(k_BT)} \sum_{E_c,n} (\mathrm{e}^{-(E_c+\epsilon_n)/(k_BT)} - \mathrm{e}^{-(E_c+\epsilon_n^0)/(k_BT)}), \tag{5.17}$$

where $\mu$ is the chemical potential, $E_c = \hbar^2K^2/(4M)$ $(K)$ is the energy (momentum) of thecenter of mass motion, and $Z_0$ is the partition function of non-interacting fermions. $\epsilon_n$ and $\epsilon_n^0$ denote the eigenenergies of the relative motion with and without interactions, respectively.

Based on results of the two-body problem, we can derive the thermal averaged contacts $\langle C_\nu \rangle_T = Z^{-1}\mathrm{e}^{2\mu/(k_BT)}(\sum_{E_c} \mathrm{e}^{-E_c/(k_BT)})(\sum_n C_\nu(\epsilon_n)\mathrm{e}^{-\epsilon_n/(k_BT)})$. Using $N = k_BT\partial_\mu \ln Z$, we obtain $\langle C_\nu \rangle_T$. Analytical expressions of $\langle C_\nu \rangle_T$ in the weakly interacting and resonance limits are shown in Table. .

In a homogenous system without bound states, we obtain,

$$\partial_t N = \frac{144\pi^2}{h}\mathrm{Im}(v_p)Nnk_BT + \frac{360\pi^2}{h}\mathrm{Im}(\frac{v_p}{v_p^*}r_\mathrm{e}^{-1})\frac{M|v_p|^2}{\hbar^2}Nnk_B^2T^2. \tag{5.18}$$

The first term in Eq. ( ) was derived in a previous work using a different approach [ ]. The second term, which leads to a different power of the dependence on $T$, as the contribution from $r_{\rm e}$, needs to be included in a complete expression.

The dependence on $T$ could be completely different as a harmonic trap may exist in experiments. In order to include the effect of an external trapping potential, we apply the local density approximation and integrate over local contacts. As a result, we find $C_\nu^{\rm trap} = [(\pi k_B T)/(M\omega^2)]^{3/2}\mathcal{C}_\nu(0)$, where $\omega$ is harmonic trapping frequency, and $\mathcal{C}_\nu(0)$ are the contact densities at the trap's center (Appendix C). Consequently,

$$\begin{aligned}\partial_t N^{\rm trap} = &\frac{18\sqrt{\pi}}{h}(M\omega^2)^{\frac{3}{2}}{\rm Im}(v_p)(N^{\rm trap})^2\frac{1}{\sqrt{k_B T}}\\ &+\frac{45\sqrt{\pi}}{h}(M\omega^2)^{\frac{3}{2}}{\rm Im}(\frac{v_p}{v_p^*}r_{\rm e}^{-1})\frac{M|v_p|^2}{\hbar^2}(N^{\rm trap})^2\sqrt{k_B T}.\end{aligned} \tag{5.19}$$

In sharp contrast to the homogeneous case, the first term now decreases with increasing $T$. When the temperature increases in a trap, the molecular cloud expands such that the total contacts and densities decrease for a fixed particle number $N$. Similarly, with increasing $T$, the second term increases linearly, which is slower than the homogenous case. Alternatively, the leading order of decay rate linearly depends on $T$ again if we consider the density at the trap's center (Appendix C).

Though a high temperature example is used in explaining Eqs. ( , , , ), we need to emphasize that these universal relations are powerful tools at any temperatures. Contacts, in particular, are no longer proportional to $N^2$ at lower temperatures, thus showing the crucial roles of many-body correlations in determining the reaction rate. For instance, contacts may be directly related to superfluid order parameters below the superfluid transition temperature [ ], [ ].

## 5.A The Lindblad equation

Simiar to the single-body dissipator which leads to an imaginary potential as we shown in the Introduction chapter, the two-body dissipator leads to an imaginary inter-particle interaction. We consider a Lindblad master equation,

$$\hbar\frac{d\rho}{dt} = -\mathrm{i}[H,\rho] + \mathcal{D}[\rho]. \tag{5.20}$$

$H$ is a Hermitian Hamiltonian. It describes the unitary time evolution. The dissipator $\mathcal{D}$ provides quantum jump and it captures the two-body inelastic collisions,

$$\begin{aligned}\mathcal{D}[\rho] = &-\int \mathrm{d}^3x_1\,\mathrm{d}^3x_2\frac{1}{2}\Gamma(|\mathbf{x_1}-\mathbf{x_2}|)\\ &\Big(2\Psi(\mathbf{x_2})\Psi(\mathbf{x_1})\rho\Psi^\dagger(\mathbf{x_1})\Psi^\dagger(\mathbf{x_2}) - \{\Psi^\dagger(\mathbf{x_1})\Psi^\dagger(\mathbf{x_2})\Psi(\mathbf{x_2})\Psi(\mathbf{x_1}),\rho\}\Big),\end{aligned} \tag{5.21}$$

$\Psi(\mathbf{x})$ satisfying $\{\Psi(\mathbf{x}),\Psi^\dagger(\mathbf{x}')\} = \delta^{(3)}(\mathbf{x}-\mathbf{x}')$ is the fermionic field operator. $(1/2)\Gamma(|\mathbf{x}_1-\mathbf{x}_2|)$ denotes a finite-range dissipation. The loss rate of the total particle number, $dN/dt = \int \mathrm{d}^3x(d/dt)\mathrm{Tr}(n(\mathbf{x})\rho)$, $n(\mathbf{x}) = \Psi^\dagger(\mathbf{x})\Psi(\mathbf{x})$, is written as

$$\begin{aligned}\frac{dN}{dt} =& -\frac{1}{\hbar}\mathrm{Tr}\Big(\int \mathrm{d}^3x\Psi^\dagger(\mathbf{x})\Psi(\mathbf{x})\int \mathrm{d}^3x_1\,\mathrm{d}^3x_2\frac{1}{2}\Gamma(|\mathbf{x}_1-\mathbf{x}_2|)\Big[2\Psi(\mathbf{x}_2)\Psi(\mathbf{x}_1)\rho\Psi^\dagger(\mathbf{x}_1)\Psi^\dagger(\mathbf{x}_2)\\ &-\{\Psi^\dagger(\mathbf{x}_1)\Psi^\dagger(\mathbf{x}_2)\Psi(\mathbf{x}_2)\Psi(\mathbf{x}_1),\rho\}\Big]\Big)\\ =&-\frac{1}{\hbar}\int \mathrm{d}^3x_1\,\mathrm{d}^3x_2\,\mathrm{d}^3x\Gamma(|\mathbf{x}_1-\mathbf{x}_2|)\mathrm{Tr}\left(\rho[\Psi^\dagger(\mathbf{x}_1)\Psi^\dagger(\mathbf{x}_2),\Psi^\dagger(\mathbf{x})\Psi(\mathbf{x})]\Psi(\mathbf{x}_2)\Psi(\mathbf{x}_1)\right)\\ =&\frac{2}{\hbar}\int \mathrm{d}^3x\,\mathrm{d}^3x'\Gamma(|\mathbf{x}'-\mathbf{x}|)\Big\langle\Psi^\dagger(\mathbf{x})\Psi^\dagger(\mathbf{x}')\Psi(\mathbf{x}')\Psi(\mathbf{x})\Big\rangle.\end{aligned} \tag{5.22}$$

For any finite range dissipator, this equation is valid. In zero-range approximation, $\Gamma = g\delta^{(3)}(\mathbf{x}-\mathbf{x}')$, the loss rate reduces to [ ], [ ], [ ]

$$\frac{dN}{dt} = \frac{2}{\hbar}g\int \mathrm{d}^3x\Big\langle\Psi^\dagger(\mathbf{x})\Psi^\dagger(\mathbf{x})\Psi(\mathbf{x})\Psi(\mathbf{x})\Big\rangle. \tag{5.23}$$

Reference [ ] considered two-component fermions and obtained $d\langle N_1\rangle/dt = d\langle N_2\rangle/dt = -[\hbar/(2\pi m)]\mathrm{Im}(1/a)C$, where $N_1$ ($N_2$) is the number of spin-up (spin-down) fermions, $a$ and $C$ denote the s-wave scattering length and the s-wave contact, respectively.

We note that Eq. ( ) is equivalent to results derived from a non-Hermitian Hamiltonian, namely, the Hamiltonian with a complex interaction as we shown in the main text, provided $U_I$ is identified with $\Gamma$. Therefore, as the probability of having more than two particles at small distances is negligible in dilute systems, universal relations obtained using the Lindblad master equation are the same as what we obtained in the main text.

### 5.B Universal relations

In the section, we provide the detailed derivations of universal relations presented in the main text. We consider a non-Hermitian many-body Hamiltonian with complex short-range interactions. The many-body time-dependent Schrödinger equation becomes

$$\mathrm{i}\hbar\partial_t\Psi(\mathbf{r}_1,\mathbf{r}_2,...,\mathbf{r}_N) = \Big[\sum_{\mathrm{i}=1}^{N}[-\frac{\hbar^2}{2M}\nabla_{\mathrm{i}}^2 + V_{\mathrm{ext}}(\mathbf{r}_{\mathrm{i}})] + \sum_{\mathrm{i}>\mathrm{j}}U(\mathbf{r}_{\mathrm{ij}})\Big]\Psi(\mathbf{r}_1,\mathbf{r}_2,...,\mathbf{r}_N). \tag{5.24}$$

#### 5.B.1 Decay rate

Net current vanishes at the boundary for any finite size system. Using the time-dependent Schrödinger equation, we obtain

$$\partial_t N = \frac{4}{\hbar}\sum\nolimits_{\mathrm{i}>\mathrm{j}}\int \mathrm{d}\mathbf{R}_{\mathrm{ij}}\,\mathrm{d}\mathbf{r}_{\mathrm{ij}}U_I(\mathbf{r}_{\mathrm{ij}})|\Psi(\mathbf{R}_{\mathrm{ij}},\mathbf{r}_{\mathrm{ij}})|^2. \tag{5.25}$$

We can also write it into a second quantization form,

$$\partial_t N = \frac{2}{\hbar}\int \mathrm{d}^3x\,\mathrm{d}^3x' U_I(|\mathbf{x}'-\mathbf{x}|)\Big\langle\Psi^\dagger(\mathbf{x})\Psi^\dagger(\mathbf{x}')\Psi(\mathbf{x}')\Psi(\mathbf{x})\Big\rangle. \tag{5.26}$$

Using Eq. (  ) in the main text, and $\epsilon\psi_m(\mathbf{r}_{\rm ij};\epsilon)=[-(\hbar^2/M)\nabla^2_{r_{\rm ij}}+U(\mathbf{r}_{\rm ij})]\psi_m(\mathbf{r}_{\rm ij};\epsilon)$, we obtain

$$\begin{aligned}
&2{\rm i}\sum\nolimits_{\rm j>i}\int {\rm d}\mathbf{R}_{\rm ij}\int_0^{r_0}{\rm d}\mathbf{r}_{\rm ij}|\Psi\left(\mathbf{R}_{\rm ij},\mathbf{r}_{\rm ij}\right)|^2U_I\left(\mathbf{r}_{\rm ij}\right)\\
&-\sum\nolimits_{\rm j>i}\int {\rm d}\mathbf{R}_{\rm ij}\int_0^{r_0}{\rm d}\mathbf{r}_{\rm ij}\Psi^*\left(\mathbf{R}_{\rm ij},\mathbf{r}_{\rm ij}\right)\sum\nolimits_{m,\epsilon}\epsilon G_m\left(\mathbf{R}_{\rm ij};E-\epsilon\right)\psi_m(\mathbf{r}_{\rm ij};\epsilon)\\
&+\sum\nolimits_{\rm j>i}\int {\rm d}\mathbf{R}_{\rm ij}\int_0^{r_0}{\rm d}\mathbf{r}_{\rm ij}\Psi\left(\mathbf{R}_{\rm ij},\mathbf{r}_{\rm ij}\right)\sum\nolimits_{m,\epsilon}\epsilon^* G^*_m\left(\mathbf{R}_{\rm ij};E-\epsilon\right)\psi^*_m(\mathbf{r}_{\rm ij};\epsilon)\\
=&\frac{\hbar^2}{M}\sum\nolimits_{\rm j>i}\int {\rm d}\mathbf{R}_{\rm ij}\int_0^{r_0}{\rm d}\mathbf{r}_{\rm ij}\left[\Psi^*\left(\mathbf{R}_{\rm ij},\mathbf{r}_{\rm ij}\right)\nabla^2_{r_{\rm ij}}\Psi\left(\mathbf{R}_{\rm ij},\mathbf{r}_{\rm ij}\right)-\Psi\left(\mathbf{R}_{\rm ij},\mathbf{r}_{\rm ij}\right)\nabla^2_{r_{\rm ij}}\Psi^*\left(\mathbf{R}_{\rm ij},\mathbf{r}_{\rm ij}\right)\right].
\end{aligned}\tag{5.27}$$

Note that, for the system with isotropic interactions $U(\mathbf{r})=U(|\mathbf{r}|)$ and $\psi_m(\mathbf{r}_{\rm ij};\epsilon)=\varphi(|\mathbf{r}_{\rm ij}|;\epsilon)Y_{1m}(\hat{\mathbf{r}}_{\rm ij})$, one has [  ]

$$v_p = \frac{r_0^3}{3}\frac{r_0\varsigma-2}{r_0\varsigma+1},\tag{5.28}$$

$$\frac{1}{r_{\rm e}} = -\frac{1}{r_0}-\frac{r_0^2}{3}\frac{1}{v_p}+\frac{r_0^5}{45}\frac{1}{(v_p)^2}-\int_0^{r_0}[\varphi^{(0)}(r)]^2r^2\,{\rm d}r,\tag{5.29}$$

where $\varsigma=\{\partial\ln[r\varphi(r;\epsilon)]/\partial r\}|_{\epsilon=0}$. Based on Eqs. (  ,  ) in the main text and Eq. (  ), we define

$$C^{ss'}_{1m}=(4\pi)^2N\left(N-1\right)\int {\rm d}\mathbf{R}_{\rm ij}g^{s*}_m g^{s'}_m,\quad g^s_m=\sum\nolimits_\epsilon q^{2s}_\epsilon G_m(\mathbf{R}_{\rm ij};E-\epsilon),\quad C_{1m}=C^{00}_{1m},\tag{5.30}$$

and obtain

$$\begin{aligned}
&\sum\nolimits_m\left[{\rm Im}\left(-v_p^{-1}\right)C_{1m}+\frac{1}{2}{\rm Im}\left(r_{\rm e}^{-1}\right)\left(C^{01}_{1m}+C^{10}_{1m}\right)-{\rm i}\kappa_3\left(C^{01}_{1m}-C^{10}_{1m}\right)+{\rm O}\left((E-E^*)^2\right)\right]\\
=&\frac{(4\pi)^2\,2M}{\hbar^2}\sum\nolimits_{\rm i>j}\int {\rm d}\mathbf{R}_{\rm ij}\int_0^{r_0}{\rm d}\mathbf{r}_{\rm ij}\left|\sum\nolimits_{m,\epsilon}G_m\left(\mathbf{R}_{\rm ij};E-\epsilon\right)\psi_m(\mathbf{r}_{\rm ij};\epsilon)\right|^2U_I\left(\mathbf{r}_{\rm ij}\right),
\end{aligned}\tag{5.31}$$

which leads to Eqs. (  ,  ,  ) in the main text,

$$\begin{aligned}\kappa_1 =&\mathrm{Im}\left(v_p^{-1}\right) = -\frac{M}{\hbar^2}\int_0^\infty \mathrm{d}r r^2\left|\varphi^{(0)}(r)\right|^2 U_I(r),\\ \kappa_2 =&\mathrm{Im}\left(-r_\mathrm{e}^{-1}/2\right) = -\frac{M}{\hbar^2}\mathrm{Re}\left(\int_0^\infty \mathrm{d}r r^2\varphi^{(0)*}(r)\varphi^{(1)}(r)U_I(r)\right),\\ \kappa_3 =&-\int_0^{r_0}\left\{\left[\mathrm{Im}\varphi^{(0)}(r)\right]^2-\left[\mathrm{Im}\tilde{\varphi}^{(0)}(r)\right]^2\right\}r^2\,\mathrm{d}r\\ =&\frac{M}{\hbar^2}\mathrm{Im}\left(\int_0^\infty \mathrm{d}r r^2\varphi^{(0)*}(r)\varphi^{(1)}(r)U_I(r)\right),\end{aligned} \tag{5.32}$$

where $\tilde{\varphi}^{(0)}(r)$ is a wave function obtained from extending the actual wave function $\varphi^{(0)}(r)$ outside the potential ($r > r_0$) into the regime $r < r_0$. We obtain Eq. (  ) in the main text,

$$\partial_t N = -\frac{\hbar}{8\pi^2 M}\Big[\mathrm{Im}(v_p^{-1})C_1 - \frac{1}{2}\mathrm{Im}(r_\mathrm{e}^{-1})C_2 + \kappa_3 C_3\Big], \tag{5.33}$$

where $C_1 = \sum_m C_{1m}$, $C_2 = 2\sum_m \mathrm{Re}(C_{1m}^{01})$ and $C_3 = 2\sum_m \mathrm{Im}(C_{1m}^{01})$. The above equation leads to Eqs. (  ,  ,  ) in the main text by considering $G_m(\mathbf{R}_{\mathrm{ij}}; E-\epsilon) = G(\mathbf{R}_{\mathrm{ij}}; E-\epsilon)$.

### 5.B.2 Momentum distribution

The momentum distribution of a many-body wavefunction is

$$n(\mathbf{k}) = \sum_{\mathrm{i}=1}^N \int \prod_{\mathrm{j}\neq\mathrm{i}} \mathrm{d}\mathbf{r}_\mathrm{j} \left| \int \mathrm{d}\mathbf{r}_\mathrm{i} \Psi(\mathbf{r}_1, \mathbf{r}_2, ..., \mathbf{r}_N)\, \mathrm{e}^{-\mathrm{i}\mathbf{k}\cdot\mathbf{r}_\mathrm{i}}\right|^2, \tag{5.34}$$

similar to systems with real interactions [  ]. Using the asymptotic form, we obtain

$$n(\mathbf{k}) \xrightarrow{k_F \ll |\mathbf{k}| \ll r_0^{-1}} \frac{C_1}{3|\mathbf{k}|^2}\sum_m |Y_{1m}(\hat{\mathbf{k}})|^2, \tag{5.35}$$

which leads to

$$n(|\mathbf{k}|) = \int \mathrm{d}\mathbf{\Omega} n(\mathbf{k}) = \frac{C_1}{|\mathbf{k}|^2}. \tag{5.36}$$

### 5.B.3 Density correlations

In the second quantized form, the density correlation function is written as $S(\mathbf{r}) = \int \mathrm{d}\mathbf{R}\langle n(\mathbf{R}+\mathbf{r}/2)n(\mathbf{R}-\mathbf{r}/2)\rangle$. It can be rewritten into

$$S(\mathbf{r}) = N(N-1)\int \left(\prod\nolimits_{k\neq \mathrm{i,j}} \mathrm{d}\mathbf{r}_k\right) \left|\Psi\left(\mathbf{r}_1, ..., \mathbf{r}_\mathrm{i} = \mathbf{R}+\frac{\mathbf{r}}{2}, ..., \mathbf{r}_\mathrm{j} = \mathbf{R}-\frac{\mathbf{r}}{2}, ..., \mathbf{r}_N\right)\right|^2, \quad (5.37)$$

using the many-body wavefunction. In the regime, $r \ll k_F^{-1}$, we have

$$\begin{aligned} S(\mathbf{r}) =& N(N-1)\int \mathrm{d}\mathbf{R}_\mathrm{ij} \sum_m |Y_{1m}(\hat{\mathbf{r}})|^2 \\ & \left[|\varphi_m^{(0)}(r)|^2|g_m^{(0)}|^2 + \varphi_m^{(0)}(r)\varphi_m^{(1)*}(r)g_m^{(1)*}g_m^{(0)} + \varphi_m^{(1)}(r)\varphi_m^{(0)*}(r)g_m^{(0)*}g_m^{(1)}\right], \end{aligned} \quad (5.38)$$

where $r = |\mathbf{r}|$. The integral over a shell allows us to obtain

$$\begin{aligned} P(x,D) = \int_x^{x+D} \mathrm{d}\mathbf{r} S(\mathbf{r}) =& \frac{1}{(4\pi)^2}\sum_m \int_x^{x+D} r^2\,\mathrm{d}r \\ & \left[\varphi_m^{(0)}(r)\varphi_m^{(0)*}(r)C_{1m} + \varphi_m^{(0)}(r)\varphi_m^{(1)*}(r)C_{1m}^{10} + \varphi_m^{(1)}(r)\varphi_m^{(0)*}(r)C_{1m}^{01}\right]. \end{aligned} \quad (5.39)$$

Using Eqs. ( , ) in the main text, we obtain

$$\begin{aligned} \left.\frac{\partial P(x,D)}{\partial D}\right|_{D\to 0} =& \frac{1}{16\pi^2}\left\{C_1\frac{1}{x^2} + C_2\frac{1}{2} + \left[-2\mathrm{Re}(\frac{1}{v_p})C_1 + \mathrm{Re}(\frac{1}{r_\mathrm{e}})C_2 - \mathrm{Im}(\frac{1}{r_\mathrm{e}})C_3\right]\frac{x}{3}\right. \\ & \left. + \left[-\frac{2}{3}\mathrm{Re}(\frac{1}{v_p})C_2 - \mathrm{Im}(\frac{1}{v_p})C_3\right]\frac{x^3}{5} + \left[\frac{C_1}{|v_p|^2} - \mathrm{Re}(\frac{1}{v_p^* r_\mathrm{e}})C_2 + \mathrm{Im}(\frac{1}{v_p^* r_\mathrm{e}})C_3\right]\frac{x^4}{9} - \frac{C_2}{90|v_p|^2}x^6\right\}. \end{aligned} \quad (5.40)$$

Eq. ( ) in the main text is recovered in the first line. Higher order terms are included in the second line. Fitting the first line with the experimental data readily allows one to obtain the three contacts $C_\nu$ provided $v_p$ and $r_\mathrm{e}$ are known. In the case where $v_p$ and $r_\mathrm{e}$ are unknown, the fitting prefactors of the second line are then required.

### 5.C Reactive molecules in a harmonic trap

The density of the reactive molecules can be well approximated by $n = \exp[\mu/(k_B T)]\lambda_T^{-3}$ in the high temperature regime. We apply the local density approximation in the presence of an external potential, by replacing the chemical potential $\mu$ with the local chemical potential $\mu(\mathbf{r}) = \mu(0) - V_{\rm ext}(\mathbf{r})$. For a harmonic trap, $V_{\rm ext}(\mathbf{r}) = (1/2)M\omega^2(x_1^2 + x_2^2 + x_3^2)$, $\omega$ is the harmonic frequency. The local density now becomes $n(\mathbf{r}) = \exp[\mu(\mathbf{r})/(k_B T)]\lambda_T^{-3}$. The chemical potential at the trap's center, $\mu(0)$, is fixed by the total particle number, $\int d^3 r n(\mathbf{r}) = N^{\rm trap}$. Applying this approach, we find the density at the trap's center $n(0) = [(2\pi k_B T)/(M\omega^2)]^{-3/2} N^{\rm trap}$. Integrating the local contacts provides the total contacts,

$$\langle C_\nu^{\rm trap}\rangle_T = \mathcal{C}_\nu(0)\int {\rm e}^{-2V_{\rm ext}(\mathbf{r})/(k_B T)}\,{\rm d}\mathbf{r} = \left(\frac{\pi k_B T}{M\omega^2}\right)^{3/2}\mathcal{C}_\nu(0). \tag{5.41}$$

where $\mathcal{C}_\nu = \langle C_\nu/V\rangle_T$ is the contact density of $\nu$th contact at the center of the trap. If the decay rate at the center of the trap $\tilde{\beta}$, which satisfies

$$\partial_t n(0) = -\tilde{\beta} n^2(0), \tag{5.42}$$

is considered, one has

$$\tilde{\beta}\Big|_{v_p\to 0}(T) = 36\sqrt{2}\pi^2 d_h^3 \frac{\hbar\omega}{h}\left|\frac{v_p}{d_h^3}\right|^2\left[{\rm Im}\left(\frac{d_h^3}{v_p}\right)k_F^2 d_h^2\frac{T}{T_F} - \frac{5}{2}{\rm Im}\left(\frac{v_p}{v_p^*}\frac{d_h}{r_{\rm e}}\right)k_F^4 d_h^4\frac{T^2}{T_F^2}\right], \tag{5.43}$$

$$\tilde{\beta}\Big|_{v_p\to\infty}(T) = -24\sqrt{2}\pi^2 d_h^3\frac{\hbar\omega}{h}\left|\frac{r_{\rm e}}{d_h}\right|^2\left[{\rm Im}\left(\frac{d_h}{r_{\rm e}}\right) + 2{\rm Im}\left(-\frac{r_{\rm e}}{r_{\rm e}^*}\frac{d_h^3}{v_p}\right)\frac{1}{k_F^2 d_h^2}\frac{T_F}{T}\right]. \tag{5.44}$$

where $k_F = (2M\omega/\hbar)^{1/2}(3N^{\rm trap})^{1/6}$, $T_F = (\hbar\omega/k_B)(3N^{\rm trap})^{1/3}$, and $d_h = [\hbar/(M\omega)]^{1/2}$.

### 5.D Measure microscopic parameters in a two-body system

In this section, we provide a means of measuring the microscopic parameters $\kappa_\nu$ using a two-body system. In a two-body system, $\partial_t N$ is determined by ${\rm Im}(\epsilon)$. To be more explicit, we can rewrite Equation (  ) as $\partial_t N = -[(\hbar C_1)/(8\pi^2 M)][\kappa_1 + 2{\rm Re}(q_\epsilon^2)\kappa_2]/[1 + C_1\kappa_3/(16\pi^2)]$. Since the contact $C_1$ and the real part of the energy can be measured from the momentum

distribution and a spectroscopy measurement, respectively, $\kappa_{1,2,3}$ can be accessed from the experimental data of the decay rate.

# 6. ANALOGUE BLACK HOLES IN REACTIVE MOLECULES

*This chapter is based on and modified from the article [ ] by R. Zhang, C. Lv, and Q. Zhou, Analogue Black Holes in Reactive Molecules, arXiv preprint arXiv:2204.04595, (2022)*

The previous chapter shows that contacts, the central quantities in dilute quantum systems, capture the two-body loss and deliver various universal relations that correlate two-body physics and many-body correlation in reactive polar molecules. This chapter presents another result brought by the dissipation and the controllability of reactive molecules, a simulator of black hole physics. The unit reaction rate at short inter-molecular distances acts as an event horizon. It leads to one-way traffic for matter-wave passing through the potential barrier when two molecules interact by higher partial wave scattering or dipole-dipole interactions. When the incident relative energy gets close to the maximum of the interaction potential barrier, the scattering rate exhibits a thermal distribution in the same manner as a scalar field scatters with a black hole. While the thermal distribution of scattering rate is ready to be observed in the two-body loss rate, a non-unit reaction rate at short distances allows us to study imperfect horizons in AMO setups.

## 6.1 Introduction

Black holes give rise to a variety of intriguing phenomena in our universe. The event horizon provides a perfect absorption for any objects traveling towards it. As such, once a matter or gravitational wave passes through a barrier produced by the black hole spacetime outside the event horizon, it must propagate in a one-way traffic without returning. The potential barrier itself is responsible for producing quasi-normal modes and black hole ringdown [ ]–[ ]. Near its maximum, the potential barrier can be well approximated by an inverted parabola. The resultant transmission and reflection rate exhibit thermal-like behaviors similar to a quantum mechanical problem of a particle scattered with an inverted harmonic potential [ ]–[ ]. The effective temperature in this thermal-like scattering encodes the mass of the black hole. Interestingly, the inverted harmonic oscillator (IHO) also underlies the profound Hawking-Unruh radiation [ ], [ ]–[ ]. Both the dynamics near the event horizon and in the accelerating reference frame can be mapped to IHOs.

While significant progress has been made in observational astronomy in the study of black holes in the past few decades [ ], [ ], there have been long-term efforts of exploring analogue black holes in laboratories. Therein, the spacetime metrics of black holes can be synthesized using a variety of platforms, such as supersonic fluid [ ]–[ ], Bose-Einstein condensates [ ]–[ ], metamaterials [ ]–[ ], and superconductor circuits [ ]. In parallel, it has been found that certain quantum systems can be used to simulate scatterings problems of black holes. For instance, when quantum Hall states are subject to saddle potentials, an effective inverted harmonic potential arises, and the transmission and reflection rate become thermal-like [ ], [ ], [ ].

In this chapter, we point out that reactive molecules with a unit probability of reaction at a short distance provide a natural simulator to study scattering problems in black holes. While the long-range part of the interaction between two molecules is a van der Waals potential, chemical reactions occur or two molecules form long-lived complexes in the short range [ ], [ ], [ ]. Some molecules like KRb have a unit probability of reaction such that whenever the separation between two molecules decreases down to a certain short length, chemical reactions occur with 100% probability [ ], [ ]. In other words, the incident wave moves towards the origin in the relative motion coordinates without returning. This one-way traffic is reminiscent of what happens to matter or gravitational waves traveling towards the event horizon of a black hole. Moreover, when molecules interact with high partial-wave scatterings or dipole-dipole interactions, a potential barrier arises. Near its maximum, the potential barrier is well approximated by an inverted parabola, similar to the barrier outside of the event horizon of a black hole. Therefore, reactive molecules could serve as a natural quantum simulator of relevant black hole physics, as shown in Fig. .

## 6.2 Black Hole Physics and Inverted Harmonic Oscillators

Before moving into simulating black hole physics in the reactive molecules, we first discuss some basics of black hole scatterings. Black hole scatterings are a fundamental property of black holes. Unlike the common thought that once a black hole is formed, anything will be absorbed into it and nothing can escape from it, carefully solving the Einstein equations

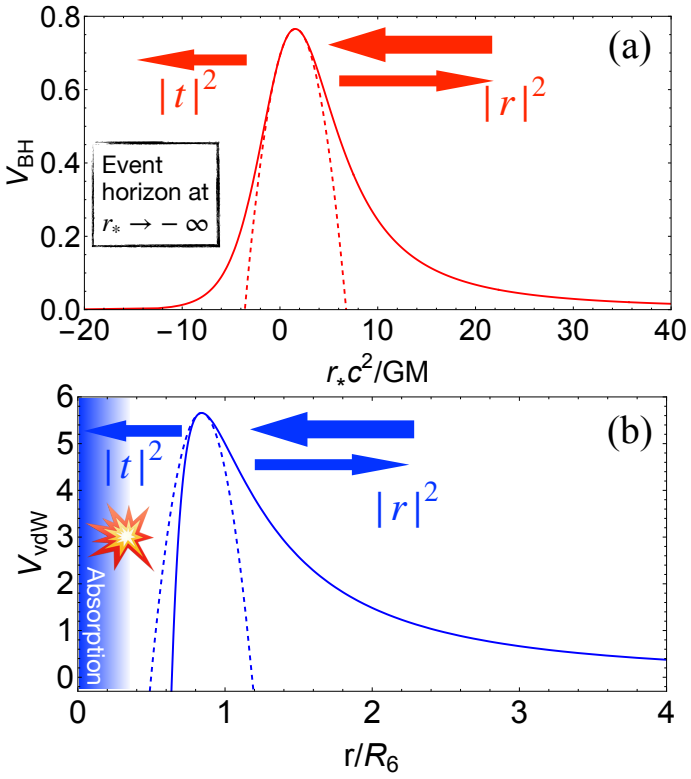


**Figure 6.1.** (a): The potential barrier (solid curves) outside the event horizon of the Schwarzschild black hole. (b): The interaction between two molecules with high partial-wave scattering or dipole-dipole interactions. At short distance, the unit probability of reaction leads to an absorbing boundary condition that mimics the event horizon. In both (a) and (b), $|r|^2$ and $|t|^2$ denote the reflection and transmission rate, respectively, and dashed curves denote the IHO approximation.

shows that both matter fields and perturbations of gravitational fields moving towards the black hole could be reflected back due to an effective barrier outside the event horizon. Moreover, the effective potential barrier features eigenstates with complex energies. Such eigenstates are termed the quasi-normal modes, whose eigenenergies determine the properties of the reflected waves. To be more precise, these eigenenergies provide the ringdown frequency and amplitude of gravitational waves emitted from black holes [ ]. While in the scattering of ultracold atoms, we are familiar with the higher partial wave scatterings where a potential barrier at $r_{\rm pb}$ may also occur, the near threshold phase shift is determined by the short-range physics $r \lesssim r_{\rm pb}$. Such a phenomenon where the reflected gravitational waves are only captured by the potential barrier relies on the very fact that the presence of an event horizon replaces the short-range physics directly by an absorption boundary condition.

An IHO serves as a minimal example in studying the scattering behavior of a potential barrier. Its quasi-normal modes actually well capture the behavior of black hole scattering in the eikonal limit with $\ell \gg 1$, where $\ell$ denotes the partial wave [ ]. In this section, we also discuss some analytical results on IHOs and show how it is correlated to black hole physics.

### 6.2.1 Black hole scatterings

The spacetime metric of a Schwarzschild black hole is written as

$$ds^2 = f(r)d(ct)^2 - f(r)^{-1}dr^2 - r^2 d\theta^2 - r^2 \sin^2\theta d\varphi^2, \tag{6.1}$$

where $f(r) \equiv (1 - r_s/r)$, and $r_s = 2GM/c^2$ denotes the Schwarzschild radius with $G$ being the gravitational constant, $M$ the black hole mass and $c$ the speed of light. The event horizon is located where $f(r) = 0$, i.e., $r = r_s$. In the so-called "tortoise" coordinate $r_*$, $r_* = r + r_s \ln(r/r_s - 1)$, the event horizon is moved to $r_* = -\infty$. A scalar field $\Phi(t, r, \theta, \varphi)$ interacting with a Schwarzschild black hole satisfies

$$\left(-\frac{d^2}{dr_*^2} + V_{\rm blackhole}(\ell, r_*)\right)\psi_\lambda(r_*) = \frac{\lambda^2}{c^2}\psi_\lambda(r_*), \tag{6.2}$$

where we have defined the single mode field with angular momentum $\ell$ as

$$\psi_\lambda(r_*)Y_\ell^m(\theta,\varphi) = \mathrm{e}^{\mathrm{i}\lambda t} r\Phi(t, r_*, \theta, \varphi) \tag{6.3}$$

with $\lambda$ being the frequency and $Y_\ell^m(\theta,\varphi)$ the spherical harmonic function. Eq.(  ) is reminiscent of a stationary Schrödinger equation with potential $V_{\text{blackhole}}(\ell, r_*)$,

$$V_{\text{blackhole}}(\ell, r_*) = \left(1 - \frac{r_s}{r(r_*)}\right)\left(\frac{r_s}{r(r_*)^3} + \frac{\ell(\ell+1)}{r(r_*)^2}\right). \tag{6.4}$$

As shown in Fig.  (a), $V_{\text{blackhole}}(\ell, r_*)$ has a potential barrier outside of the event horizon. Near the maximum of the potential, it can be approximated by the IHO, where the Hamiltonian is written as

$$\hat{H} = -\frac{1}{2}\frac{d^2}{dr_*^2} - \frac{1}{2}\omega^2(r_* - r_*^{\max})^2 + \frac{1}{2}V_{\text{blackhole}}(r_*^{\max}), \tag{6.5}$$

where $\omega = \sqrt{-\frac{1}{2}\partial_{r_*}^2 V_{\text{blackhole}}(\ell, r_*)|_{r_*^{\max}}}$ and $r_*^{\max}$ is defined via $\partial_{r_*} V_{\text{blackhole}}(\ell, r_*)|_{r_*^{\max}} = 0$. The larger is $\ell$, the better is the approximation. We want to point out that this effective potential approach is generic, as it applies to other matter fields or blackholes under the Newman-Penrose formalism [  ].

### 6.2.2 Inverted harmonic oscillators

The IHO approximation leads to a Fermi-Dirac distribution of transmission probability with respect to the incident energy. Using the results in Appendix A, we obtain the approximated $S$ matrix of scattering from black hole as

$$S = \frac{\Gamma\left(\frac{1}{2} - \frac{\mathrm{i}E}{\omega}\right)}{\sqrt{2\pi}} \begin{pmatrix} -\mathrm{i}\mathrm{e}^{-\frac{\pi E}{2\omega}} & \mathrm{e}^{\frac{\pi E}{2\omega}} \\ \mathrm{e}^{\frac{\pi E}{2\omega}} & -\mathrm{i}\mathrm{e}^{-\frac{\pi E}{2\omega}} \end{pmatrix}, \tag{6.6}$$

where $E = (\lambda^2/c^2 - V_{\text{blackhole}*})/2$ is now measured from $V_{\text{blackhole}*}$. Therefore, the reflection and transmission rate can be written as

$$|r|^2_{\text{BH}} = \frac{1}{\mathrm{e}^{\frac{2\pi E}{\omega}} + 1}; \quad |t|^2_{\text{BH}} = \frac{1}{\mathrm{e}^{-\frac{2\pi E}{\omega}} + 1}, \tag{6.7}$$

respectively, where $|t|^2_{\text{BH}}$ follows a Fermi-Dirac distribution, with an effective inverse temperature $2\pi/\omega$. While $\omega$ is related to the Schwarzschild radius and the number of partial wave, the thermal-like tunneling unfolds the mass of black hole. When $\ell = 0$, the effective temperature is written as

$$T_{\text{eff}} = \frac{27}{1024\sqrt{2}} \frac{\hbar^2 c^4}{\pi k_B \tilde{\mu} M^2 G^2}. \tag{6.8}$$

Since $k_B T_{\text{eff}}$ determined from Eq.(  ) has the dimension $L^{-2}$, the same as $\omega$, we have added in Eq.(  ) an extra factor, $\hbar^2/\tilde{\mu}$, where $\tilde{\mu}$ is an arbitrary mass scale, to ensure that $T_{\text{eff}}$ has the same dimension as the temperature.

For another $\ell$, the corresponding $T_{\text{eff}}$ can be obtained in the same way. It should be noted that there is a difference between $V_{\text{blackhole}*}$ and $V_{\text{blackhole}}(r_*^{\max})$, a constant energy shift from the top of the IHO to the maximum of the realistic potential. Such a shift exists since the IHO is applied as an approximation for a generic potential barrier, such as the Pöschl-Teller potential that has analytical solutions [  ]. With increasing $\ell$, the IHO approximation becomes better in the sense that it describes the potential barrier in a wider range of energy and the percentage difference between $V_{\text{blackhole}*}$ and $V_{\text{blackhole}}(r_*^{\max})$ decreases.

### 6.3 Reactive Molecules

In the absence of an external electric field, two molecules interact via the van der Waals potential at large distance and the Hamiltonian of the relative motion is written as

$$\left[\frac{d^2}{dr^2} - \frac{\ell(\ell+1)}{r^2} + \frac{\beta_6^4}{r^6} + \frac{2\mu\epsilon}{\hbar^2}\right] u_\ell(r) = 0, \tag{6.9}$$

where $\mu$ is the reduced mass, $\beta_6$ is the characteristic length of the van der Waals potential, and $u_\ell(r) = r\psi_\ell(r)$ with $\psi_\ell(r)$ being the radial wave function of $\ell$-th partial wave. The

analytical solutions have been obtained by the quantum defect theory (QDT) [ ], [ ]. The van der Waals potential and the centrifugal potential lead to an effective potential that has a maximum. As illustrated in Fig. (b), near the potential maximum, the effective potential can be expanded as

$$V_{\rm vdW}(r) \approx -\frac{1}{2}\mu\omega^2\left(r - \frac{3^{1/4}\beta_6}{(\ell(\ell+1))^{1/4}}\right)^2 + V_{\rm max}, \tag{6.10}$$

where $\omega = 2\ell(\ell+1)\hbar/(\sqrt{3}\mu\beta_6^2)$, and the maximum of the potential is $V_{\rm max} = \hbar^2(\ell(\ell+1))^{3/2}/(3\sqrt{3}\mu\beta_6^2)$. As such, similar to scatterings of a scalar field by black hole, the high partial wave scattering of molecules can also be approximated by the IHO. The reaction with unit probability at short distance plays the role of an event horizon. Specifically, the asymptotic wave function at the short-range takes the following form

$$u_\ell(r\to 0) \propto \frac{r^{3/2}}{\beta_6}\exp\left[{\rm i}\left(\frac{\beta_6^2}{2r^2} - \frac{\nu_0\pi}{2} - \frac{\pi}{4}\right)\right], \tag{6.11}$$

where $\nu_0 = (2\ell+1)/4$. The absence of $\exp[-{\rm i}\beta_6^2/(2r^2)]$ in the wave function signifies unit probability of reaction such that there is no outgoing flux. As such, similar to the previously discussed black hole physics, the transmission and reflection rate become thermal-like when the incident energy is near the maximum of the potential barrier,

$$T_{\rm eff} = \frac{\ell(\ell+1)}{\sqrt{3}\pi}\frac{\hbar^2}{k_B\mu\beta_6^2}. \tag{6.12}$$

Comparing Eq.( ) and Eq.( ), we see that, if identifying $\mu$ and $\tilde{\mu}$, $\beta_6$ plays the role of the mass of a black hole, i.e., $\beta_6 \sim MG/c^2$.

The comparison between the exact results of the van der Waals potential and the result of IHO is shown in Fig. . Near the $V_{\rm max}$, an IHO well reproduces the result of the van der Waals potential. The slope of $\log(|t|^2/|r|^2)$ is given by the frequency of the IHO near the maximum of the barrier, as shown in Fig. (a,b). Similar to black hole scattering, there is a small difference between $V_{\rm max}^*$ and $V_{\rm max}$. We find $|V_{\rm max}^* - V_{\rm max}|/V_{\rm max} \approx 34\%$ for $\ell = 1$. We also find that with increasing $\ell$, the IHO approximation works well in a larger energy

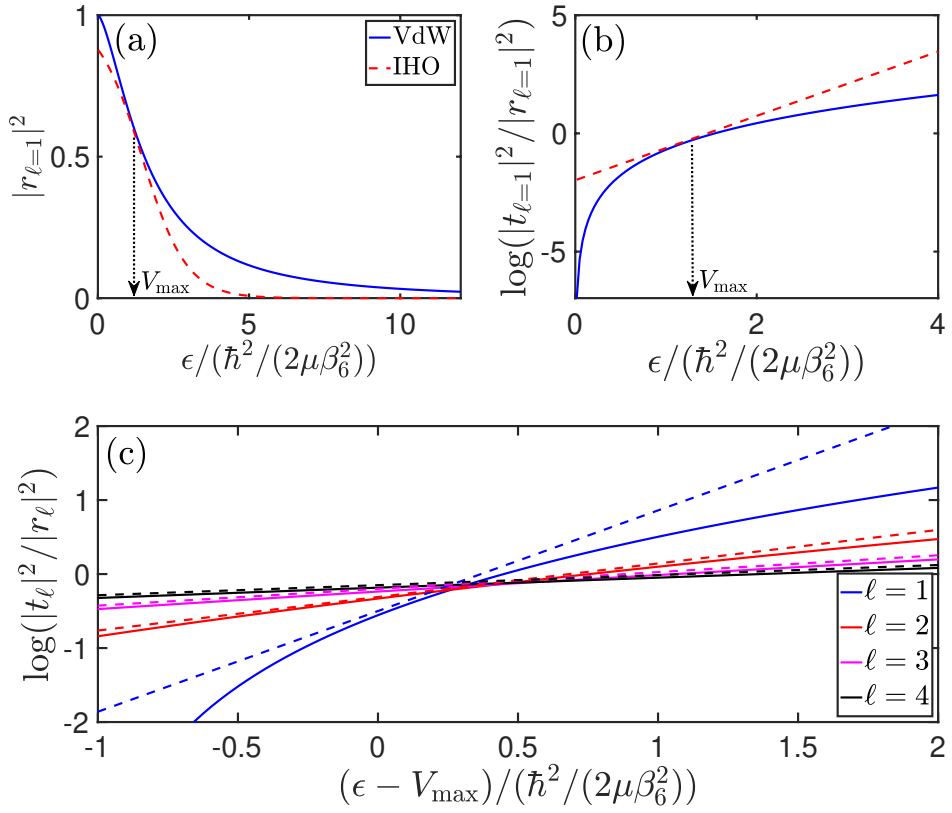


**Figure 6.2.** The reflection and transmission rate for high partial-wave scatterings at zero electric field. (a) and (b) depict the reflection rate $|r|^2$ and $\log(|t|^2/|r|^2)$ as a function of the energy for $p$-wave scattering. (c): $\log(|t|^2/|r|^2)$ for various high partial-wave scatterings. In (a,b,c), solid curves are results from the quantum defect theory. Dashed curves are results from the approximation using IHO, whose frequency is determined by the potential near the maximum of the potential barrier. With increasing $\ell$, the approximation using IHO covers a broader range of energy.

window near, as shown in Fig. (c). Meanwhile, $|V^*_{\max} - V_{\max}|/V_{\max}$ decreases. For $\ell = 4$, $|V^*_{\max} - V_{\max}|/V_{\max}$ is readily as small as 3%. Therefore, such thermal-like transmission and reflection become more evident in higher partial wave scatterings.

Whereas the energy-dependent transmission or reflection rate readily unfolds thermal-like scatterings in theory, it is not easy to prepare molecule pairs with given relative incident energy. What can be directly measured in experiments is the temperature-dependent two-body loss rate $\mathcal{K}^{\rm inel}_\ell(T)$, which is related to the transmission rate by a thermal average,

$$\mathcal{K}^{\rm inel}_\ell(T) = (2\ell+1)\frac{4\pi\hbar^2}{(2\mu)^{3/2}}\frac{\int_0^\infty \mathrm{e}^{-\frac{\epsilon}{k_B T}}|t|^2 d\epsilon}{\int_0^\infty \sqrt{\epsilon}\mathrm{e}^{-\frac{\epsilon}{k_B T}} d\epsilon}. \tag{6.13}$$

Using QDT, we can calculate both $t, r$ and $\mathcal{K}^{\rm inel}_\ell(T)$ explicitly [ ], [ ]. When the temperature is much smaller than the maximum of the barrier, we find that the loss rate is a constant and linearly dependent on $T$ for the $s$ and $p$-wave scatterings, respectively, i.e., $\mathcal{K}^{\rm inel}_{\ell=0} \approx 4h\bar{a}/\mu$ and $\mathcal{K}^{\rm inel}_{\ell=1} \approx 1512.58\bar{a}^3 k_B T/h$ with $\bar{a} = 2\pi\beta_6/\Gamma(1/4)^2$ and $h$ being the Planck constant, which are consistent with the results previously obtained in Ref. [ ], [ ], [ ], [ ], as shown in Fig. (a).

Here, we are interested in the high-temperature regime of the order of $\mu$K, which is comparable to the typical value of the potential barrier maximum from the van der Waals interaction and the centrifugal potential. The scatterings near the maximum of the barrier thus become relevant. In Fig. (a), we show the two-body loss rate as a function of temperature for $p$ and $d$-wave scatterings. Though this thermal average convolutes the previously discussed thermal-like quantum tunnelings near the maximum of the potential barrier with scatterings at other energies, Eq.( ) shows that such a thermal average is in fact a Laplace transform of the energy-dependent tunneling rate. An inverse Laplace transform thus could recover the energy-dependent reflection and transmission rate from the thermal averaged value. We have numerically confirmed that standard numerical techniques of the inverse Laplace transform are readily capable of recovering the thermal-like quantum tunneling from the thermally averaged decay rate. As shown in Fig. (b), using Talbot's method, we could reproduce energy-dependent reflection and transmission rates from 20 data points of the thermal averaged decay rate around $T = 4\hbar^2/(2\mu\beta_6^2 k_B)$. This method works so

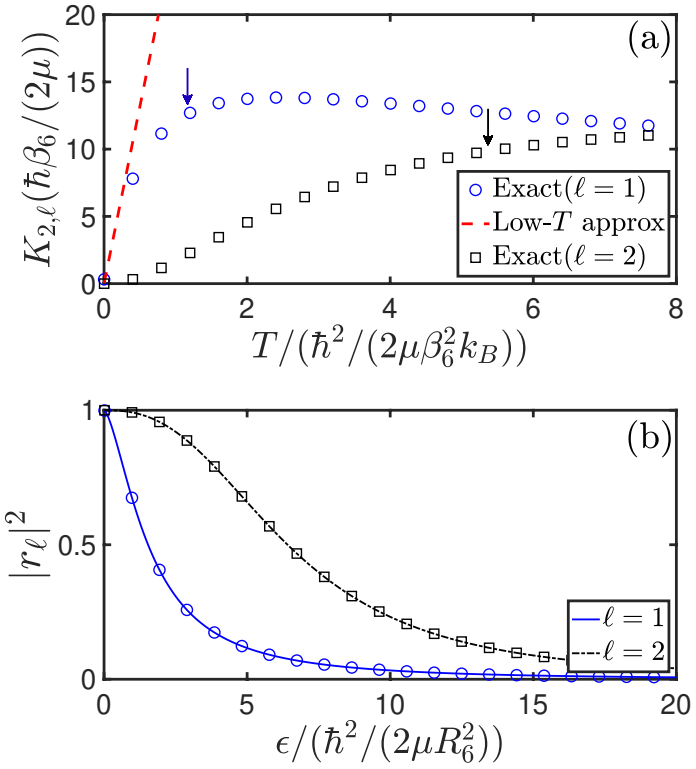


**Figure 6.3.** (a) Two-body loss rates $K_{2,\ell}$ of $p$ (circle) and $d$-wave (square) scatterings. The blue and black arrows indicate the characteristic temperature that corresponds to the maximum of the potential barrier of $p$ and $d$-wave scattering, respectively. The Red dashed line depicts the low-temperature approximation of the $p$ wave scattering. (b) Markers are the results from an inverse Laplace transform of (a). Twenty temperature points in the $T$-axis have been used. It recovers the transmission rate as a function of the energy (solid and dash-dotted curves).

well that the results by inverse Laplace transformation (markers) are indistinguishable from that given by QDT.

### 6.3.1 Dipole-dipole interaction

When an electric field is turned on, a dipole-dipole interaction between molecules is induced. Whereas such an interaction is anisotropic in three dimensions, to simplify discussions, we consider two dimensions and the electric field is perpendicular to the plane [ ], [ ]. As a result, an isotropic dipole-dipole repulsion creates a potential barrier even for $s$-wave scatterings. The dipole-dipole interaction depends on the electric field, providing

another knob to control the thermal-like tunnelings. The Schrödinger equation along the radial direction reads,

$$\left(\frac{d^2}{d\rho^2} - \frac{m^2 - 1/4}{\rho^2} + \frac{\beta_6^4}{\rho^6} - \frac{2\mu d^2}{4\pi\hbar^2\varepsilon_0\rho^3} + \frac{2\mu\epsilon}{\hbar^2}\right) u_m(\rho) = 0, \tag{6.14}$$

where $\varepsilon_0$ is vacuum permittivity, and $d$ is the induced electric dipole moment that depends on the electric field. $m$ is the quantum number of the angular momentum about the normal direction of the plane. Since there is no simple analytical solution to Eq.( ), we numerically solve it and extract the scattering properties.

Fig. shows the log of $|t_m|^2/|r_m|^2$ with a varying electric dipole moment for the $s$-wave and $p$-wave scattering. In most current experiments, the trapping potential height is around a van der Waals energy $\hbar^2/(2\mu\beta_6^2)$. We thus consider incident energies smaller than $\hbar^2/(2\mu\beta_6^2)$. By increasing the dipole moment, the IHO approximation works better and better. Even for the $s$-wave scattering, thermal scattering can be observed. In other words, the linear region near $V_{\max}$ becomes broader and broader by increasing the electric field, which is hopefully to be observed in current experiments.

### 6.4 Imperfect Event Horizon

Whereas we have been focusing on unit reaction probabilities at a short distance, it is worth considering smaller reaction probabilities. The reactive rate is characterized by a dimensionless "quantum-defect" parameter $0 \leq y \leq 1$ [ ]. $y = 1$ and $y = 0$ indicate that the molecule collision at a short range is complete lossy and elastic, respectively. Experiments have reported $y = 0.26, 1.0$ for RbCs, KRb [ ], [ ]. Recent experiments have further shown that $y$ can be manipulated by the external magnetic or electric field, which offers an unprecedented means to tune the boundary condition from a perfect event horizon to an imperfect one that partially or totally reflects the incident wave [ ]–[ ]. The latter case mimics matter waves bouncing back and forth between the potential barrier and the imperfect event horizon. A schematic plot of this process is shown in Fig. . Again, near the maximum of the potential barrier, such a multiple scattering problem of IHO (Appendix A) well captures the exact result which is obtained by QDT, as shown in Fig.

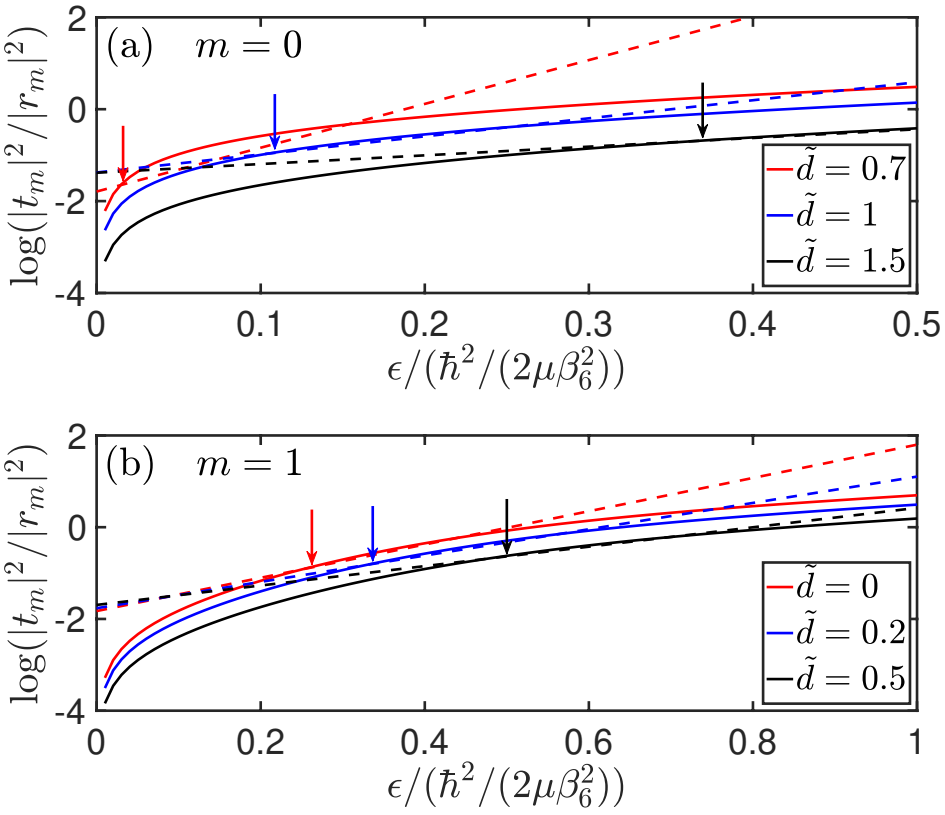


**Figure 6.4.** $\log(|t|^2/|r|^2)$ as a function of the incident energy in the presence of an external electric field in 2D. (a) and (b) are results of $m = 0$ and $m = 1$, respectively. $\tilde{d} = 2\mu d/(4\pi\hbar^2\epsilon_0)$ denotes electric field induced dipole moment. Solid curves are results from the quantum defect theory. Dashed curves are the results from the approximation using IHO. Arrows indicate the energy of the potential maximum $V_{\max}$.

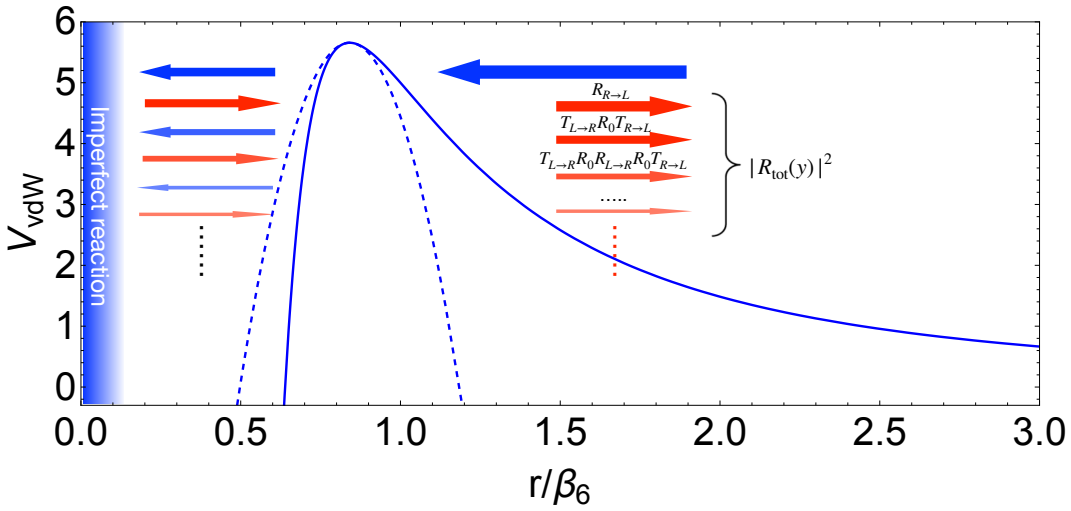


**Figure 6.5.** A schematic of multiple scatterings caused by an imperfect event horizon. $R_{R(L)\to L(R)}$ and $T_{R(L)\to L(R)}$ indicate the reflection and transmission amplitude for the "right(left) to left(right)" scattering. $R_{\rm tot}(y)$ denotes the total reflection amplitude with generic "quantum defect" parameter $y$. It can be obtained by summing over such an infinite series of scatterings. Blue and red arrows denote the left and right moving waves. The solid and dashed curves depict the interaction between two molecules with high partial-wave scatterings (or dipole-dipole interactions) and the IHO approximation, respectively.

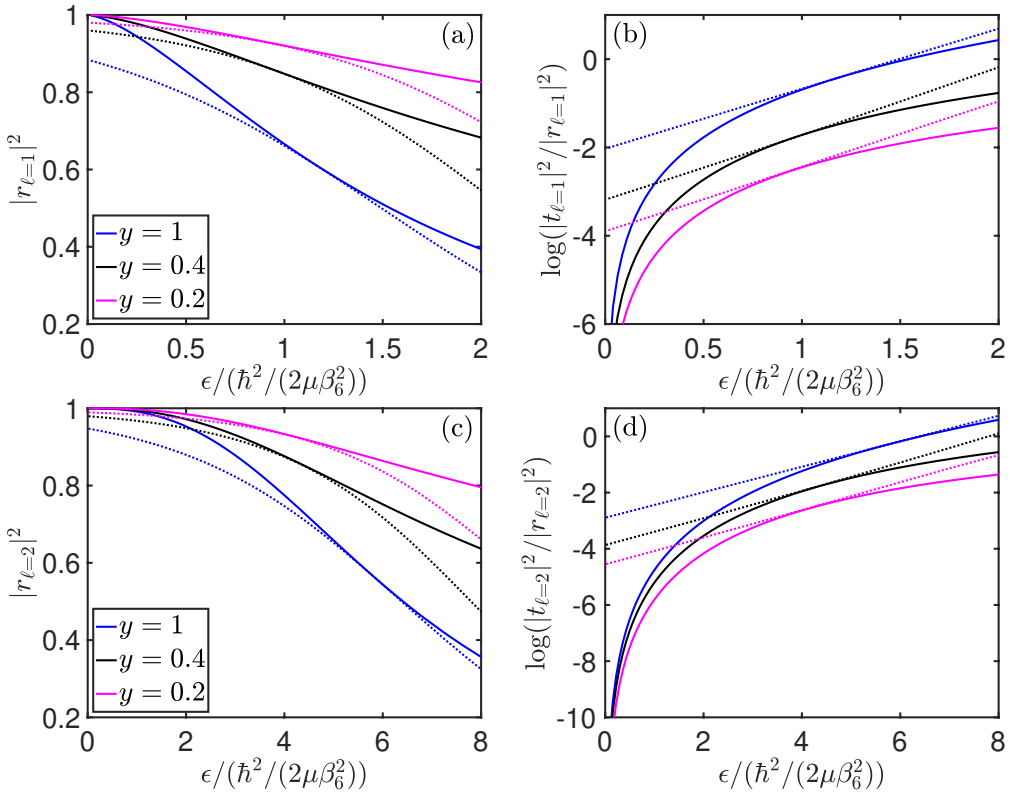


**Figure 6.6.** Reflection rate $|r_\ell|^2$ and $\log(|t_\ell|^2/|r_\ell|^2)$ of reactive molecule under imperfect absorbing boundary condition for $p$-wave (a,b) and $d$-wave (c,d) scattering.The solid curves depict the results of van der Waals potential and the dashed curves show the results of IHO.

## 6.A Scattering and multi-scattering from an inverted harmonic oscillator

We consider the Schrodinger equation

$$\left[\frac{d^2}{dr^2}+\frac{1}{\hbar^2}\mu^2\omega^2r^2+\frac{2\mu\epsilon}{\hbar^2}\right]u_l(r)=0, \tag{6.15}$$

which can be further simplified as

$$\left[\frac{d^2}{dr^2}+r^2+\epsilon\right]u_l(r)=0, \tag{6.16}$$

by choosing the harmonic length $\sqrt{\hbar/(\mu\omega)}$ and energy $\hbar\omega$ as unit. The generic solution reads

$$u(r)=c_1U\left(\frac{1}{2}\mathrm{i}\epsilon,(1+\mathrm{i})r\right)+c_2U\left(-\frac{1}{2}\mathrm{i}\epsilon,-(1-\mathrm{i})r\right), \tag{6.17}$$

where $U$ is Weber parabolic cylinder function. $U(a,z)$ has the asymptotic behavior at large $|z|$ as

$$\begin{aligned}
&U(a,z\to\infty)=\mathrm{e}^{-z^2/4}z^{-(a+1/2)},\quad |\mathrm{Arg}(z)|<\frac{3}{4}\boldsymbol{\pi}-\delta,\\
&U(a,z\to\infty)=\mathrm{e}^{-z^2/4}z^{-(a+1/2)}\pm\mathrm{i}\frac{\sqrt{2\boldsymbol{\pi}}}{\Gamma(a+1/2)}\mathrm{e}^{\mp\mathrm{i}\boldsymbol{\pi}a}\mathrm{e}^{z^2/4}z^{a-1/2},\quad \frac{1}{4}\boldsymbol{\pi}+\delta\le\pm\mathrm{Arg}(z)<\frac{5}{4}\boldsymbol{\pi}-\delta,
\end{aligned} \tag{6.18}$$

for infinitesimal $\delta$. We have following the asymptotic behavior of $U\left(\frac{1}{2}\mathrm{i}\epsilon,(1+\mathrm{i})r\right)$

$$\begin{aligned}
&U\left(\frac{1}{2}\mathrm{i}\epsilon,(1+\mathrm{i})r\right)=_{r\to\infty}\mathrm{e}^{-\mathrm{i}r^2/2}(\sqrt{2}|r|)^{-\frac{1}{2}(\mathrm{i}\epsilon+1)}\alpha,\\
&U\left(\frac{1}{2}\mathrm{i}\epsilon,(1+\mathrm{i})r\right)=_{r\to-\infty}\mathrm{e}^{-\mathrm{i}r^2/2}(\sqrt{2}|r|)^{-\frac{1}{2}(\mathrm{i}\epsilon+1)}\beta+\mathrm{e}^{\mathrm{i}r^2/2}(\sqrt{2}|r|)^{-\frac{1}{2}(-\mathrm{i}\epsilon+1)}\gamma.
\end{aligned} \tag{6.19}$$

we have defined

$$\alpha=\mathrm{e}^{-\mathrm{i}\boldsymbol{\pi}/8}\mathrm{e}^{\epsilon\boldsymbol{\pi}/8},\quad \beta=\mathrm{e}^{\mathrm{i}3\boldsymbol{\pi}/8}\mathrm{e}^{-3\epsilon\boldsymbol{\pi}/8},\quad \gamma=\mathrm{e}^{-\mathrm{i}\boldsymbol{\pi}/8}\mathrm{e}^{-\epsilon\boldsymbol{\pi}/8}\frac{\sqrt{2\boldsymbol{\pi}}}{\Gamma((\mathrm{i}\epsilon+1)/2)}. \tag{6.20}$$

Similarly, for $U\left(-\frac{1}{2}\mathrm{i}\epsilon, -(1-\mathrm{i})r\right)$,

$$\begin{aligned} U\left(-\frac{1}{2}\mathrm{i}\epsilon, -(1-\mathrm{i})r\right) &=_{r\to\infty} \mathrm{e}^{\mathrm{i}r^2/2}(\sqrt{2}|r|)^{-\frac{1}{2}(-\mathrm{i}\epsilon+1)}\beta^* + \mathrm{e}^{-\mathrm{i}r^2/2}(\sqrt{2}|r|)^{-\frac{1}{2}(\mathrm{i}\epsilon+1)}\gamma^*, \\ U\left(-\frac{1}{2}\mathrm{i}\epsilon, -(1-\mathrm{i})r\right) &=_{r\to-\infty} \mathrm{e}^{\mathrm{i}r^2/2}(\sqrt{2}|r|)^{-\frac{1}{2}(-\mathrm{i}\epsilon+1)}\alpha^*. \end{aligned} \tag{6.21}$$

To construct a scattering state, we take

$$\begin{aligned} u_+(r) &= -\mathrm{e}^{\mathrm{i}\pi/4}\mathrm{e}^{-\epsilon\pi/4}\frac{\sqrt{2\pi}}{\Gamma((-\mathrm{i}\epsilon+1)/2)}U\left(\frac{1}{2}\mathrm{i}\epsilon, (1+\mathrm{i})r\right) + U\left(-\frac{1}{2}\mathrm{i}\epsilon, -(1-\mathrm{i})r\right) \\ &= -\frac{\gamma^*}{\alpha}U\left(\frac{1}{2}\mathrm{i}\epsilon, (1+\mathrm{i})r\right) + U\left(-\frac{1}{2}\mathrm{i}\epsilon, -(1-\mathrm{i})r\right) \end{aligned} \tag{6.22}$$

Another state with incoming state from $+\infty$ reads

$$u_-(r) = -\frac{\gamma^*}{\alpha}U\left(\frac{1}{2}\mathrm{i}\epsilon, -(1+\mathrm{i})r\right) + U\left(-\frac{1}{2}\mathrm{i}\epsilon, (1-\mathrm{i})r\right) = u_+(-r), \tag{6.23}$$

such that $u_+$ and $u_-$ only have transmitted wave at $+\infty$ and $-\infty$, respectively. We obtain the elements of $S$ matrix,

$$t = \frac{\beta^*\alpha}{-\gamma^*\beta} = \mathrm{e}^{\epsilon\pi/4}\frac{\Gamma((-\mathrm{i}\epsilon+1)/2)}{\sqrt{2\pi}}, \tag{6.24}$$

$$r = \frac{-|\gamma|^2+|\alpha|^2}{-\gamma^*\beta} = -\mathrm{e}^{\mathrm{i}\pi/2}\frac{\mathrm{e}^{\epsilon\pi/4}}{1+\mathrm{e}^{\epsilon\pi}}\frac{\sqrt{2\pi}}{\Gamma((\mathrm{i}\epsilon+1)/2)}. \tag{6.25}$$

and the transmission and reflection rate,

$$T = |t|^2 = \frac{1}{1+\mathrm{e}^{-\epsilon\pi}}, R = |r|^2 = \frac{1}{1+\mathrm{e}^{\epsilon\pi}} = \frac{\mathrm{e}^{-\epsilon\pi}}{1+\mathrm{e}^{-\epsilon\pi}}. \tag{6.26}$$

$T$ exhibits a Fermi-Dirac distribution with inverse temperature $\beta = \pi$.

With finite flux reflected from $\pm\infty$, the boundary condition at large distance becomes

$$u\left(r\to+\infty\right) \propto \mathrm{e}^{\mathrm{i}r^2/2}(\sqrt{2}|r|)^{-\frac{1}{2}(-\mathrm{i}\epsilon+1)} + \mathrm{e}^{-\mathrm{i}r^2/2}(\sqrt{2}|r|)^{-\frac{1}{2}(\mathrm{i}\epsilon+1)}R_0. \tag{6.27}$$

where $R_0$ is related to the quantum defect parameter $y$ by $R_0 = -(1-y)/(1+y)$. By matching the boundary condition using a linear combination of $u_\pm$, we find

$$t(R_0) = \frac{\beta^*\alpha}{R_0|\beta|^2 - \gamma^*\beta}, \quad r(R_0) = \frac{R_0\beta^*\gamma - |\gamma|^2 + |\alpha|^2}{R_0|\beta|^2 - \gamma^*\beta}. \tag{6.28}$$

The reflection amplitude can be understood as a multi-scattering process,

$$r(R_0) = \frac{|\gamma|^2 - |\alpha|^2}{\beta\gamma^*} + \left(-\frac{|\alpha|^2}{\beta\gamma^*}\right)\sum_{n=1}^{\infty}\left(\frac{\beta^*}{\gamma^*}R_0\right)^n = r + t^2\frac{R_0}{1 - rR_0}. \tag{6.29}$$

The reflection rate becomes

$$R = |r|^2 = \frac{1 + R_0^2(1+\mathrm{e}^{\epsilon\pi}) + R_0\mathrm{e}^{-\epsilon\pi/4}(1+\mathrm{e}^{\epsilon\pi})\sqrt{2/\pi}\mathrm{Im}(\Gamma(1/2+\mathrm{i}\epsilon/2))}{(1 + R_0^2 + \mathrm{e}^{\epsilon\pi}) + R_0\mathrm{e}^{-\epsilon\pi/4}(1+\mathrm{e}^{\epsilon\pi})\sqrt{2/\pi}\mathrm{Im}(\Gamma(1/2+\mathrm{i}\epsilon/2))}. \tag{6.30}$$

# 7. SUMMARY

In this dissertation, we discussed the interplay between symmetry, geometry, dissipation, and quantum dynamics in ultracold systems. When certain dynamical symmetry is preserved in quantum dynamics, the structure of the symmetry group provides us with a geometrical approach to describe and coherently control the quantum system. Defining costs of quantum gates leads to a metric tensor, which delivers a method in simulations of curved spacetimes and fast transportation of quantum systems. The highly controllable interactions in ultracold AMO platforms allow the realizations of the group theoretical methods in various systems and provide us a means to simulate quantum dynamics in curved spaces without physical distortions. Simulating hyperbolic space on a lattice system leads to a funneling effect that attracts any initial wavepacket to the funneling mouth, equating hyperbolic space and the lattice system gives us an unprecedented duality between non-Hermitian models with intrinsic dissipations and curved spaces. While dissipation is undesired in conventional systems, manipulating dissipation in a controllable manner supplies experimentalists means to study quantum dynamics in curved spaces. We also apply contacts, a central quantity in ultracold dilute systems, to the non-Hermitian regime in the presence of dissipation. We show universality exists and correlates two-body loss rate, momentum distribution, and density correlation functions. These relations are valid for arbitrary microscopic parameters and therefore deliver a unique tool to explore interacting non-Hermitian many-body systems and engineer ultracold molecules. Meanwhile, reactive molecules to the universal limit also provide a platform for studying black hole physics.

In Chapter 2, we considered the quantum dynamics in weakly interacting Bose gases with time-dependent interaction strength and that in scale-invariant quantum systems in a harmonic potential with time-dependent frequency. Both cases are characterized by a dynamical group, the $SU(1,1)$ group. Using the underlying group structure, we can correlate the quantum dynamics to trajectories on a single or multiple Poincaré disks. Such a geometrical approach provides us with means of quantum control, the $SU(1,1)$ echoes, as an analog of the spin echo on the Bloch sphere. With this driving scheme, we can reverse the quantum dynamics of a many-body system with $SU(1,1)$ symmetry. In the situation where some

perturbations break the $SU(1,1)$ symmetry, the imperfect revival could potentially provide us with a means to detect symmetry-breaking terms in the same spirit of using spin echoes.

In Chapter 3, the same dynamical symmetry is considered. We implement the cost function, a continuous version of circuit depth that characterizes cost for each quantum gate, to derive a metric. This approach equals the time spent in laboratories to either the proper distance or proper time in curved spacetime. Using this method, we can minimize the total time transporting one state to another by moving the quantum system along the light cone or the geodesics. As some gates might be easier or more difficult to be implemented than others in certain systems, we show an inhomogeneous or anisotropic cost function leads to spacetimes with more interesting structures.

Chapter 4 moves on to the simulation of synthetic curved space in laboratories. We show the simulation of a quantum particle moving on any Riemann surface using a lattice system with tunable tunneling amplitudes. Using the hyperbolic space as an example, we find the Efimov-like state and funneling effect on the corresponding lattice system. We also propose a duality between generic non-Hermitian one-dimensional lattice models and two-dimensional curved spaces. This duality provides us not only with a coherent picture of understanding peculiar non-Hermitian physics but also an experimental method for simulating quantum dynamics on curved spaces using dissipations or exploring non-Hermitian phenomena in curved spaces.

In Chapter 5, we turn to the dilute ultracold reactive molecules. We systematically studied the universal relations for quantum gases with $p$-wave collision and complex interactions. We show that both scattering volume and effective range become complex in the presence of non-Hermiticity. Moreover, to capture the loss rate in the presence of bound states, we introduce a new microscopic two-body parameter $\kappa_3$. $\kappa_{1,2,3}$ obtained from two-body physics, and the contacts captured by many-body physics together determine the loss rate. To concretize our discussion, we consider an exact solvable two-body quantum system as an example and obtain a finite temperature result using the virial expansion.

In the last chapter, we continue the investigation of reactive molecules. Using exact calculations, we demonstrate the reactive molecules allow physicists to simulate scatterings from black holes, and the unit probability of reaction acts as an event horizon. Tuning inter-

molecular interaction provides us with different temperatures of thermal-like scattering rates. The ability to manipulate quantum defect parameters delivers a unique means to tune the boundary condition from a perfect event horizon to an imperfect one. With a time-dependent resolution of the two-body reaction process, reactive molecules are also promising candidates for studying other profound features of black holes, such as quasi-normal modes and black hole ringdown. Therefore, the dissipation in reactive molecules offers us an unprecedented playground for studying black hole physics.

In conclusion, the coherent, highly controllable ultracold platforms provide us with a unique means of studying the interplay between geometry and quantum dynamics. Exploring the AMO toolbox has pushed the quantum simulation in laboratories to new regimes. While there are numerous developments in this direction, and we only introduced a few, we hope our works will stimulate more interest in implementing the geometric approach to quantum dynamics and exploring the coherent control and universality in the presence of dissipation.

# REFERENCES


[1] P. A. M. Dirac, *The principles of quantum mechanics*. Oxford university press, 1981.

[2] H. Feshbach, "Unified theory of nuclear reactions," *Annals of Physics*, vol. 5, no. 4, pp. 357–390, 1958.

[3] H. Feshbach, "A unified theory of nuclear reactions. ii," *Annals of Physics*, vol. 19, no. 2, pp. 287–313, 1962.

[4] H.-P. Breuer, F. Petruccione, *et al.*, *The theory of open quantum systems*. Oxford University Press on Demand, 2002.

[5] M. H. Anderson, J. R. Ensher, M. R. Matthews, C. E. Wieman, and E. A. Cornell, "Observation of bose-einstein condensation in a dilute atomic vapor," *Science*, vol. 269, no. 5221, pp. 198–201, Jul. 1995. DOI: . [Online]. Available: .

[6] K. B. Davis, M. .-.-O. Mewes, M. R. Andrews, N. J. van Druten, D. S. Durfee, D. M. Kurn, and W. Ketterle, "Bose-einstein condensation in a gas of sodium atoms," *Phys. Rev. Lett.*, vol. 75, pp. 3969–3973, 22 Nov. 1995. DOI: . [Online]. Available: .

[7] C. C. Bradley, C. A. Sackett, J. J. Tollett, and R. G. Hulet, "Evidence of bose-einstein condensation in an atomic gas with attractive interactions," *Phys. Rev. Lett.*, vol. 75, pp. 1687–1690, 9 Aug. 1995. DOI: . [Online]. Available: .

[8] T. Weber, J. Herbig, M. Mark, H.-C. Nägerl, and R. Grimm, "Bose-einstein condensation of cesium," *Science*, vol. 299, no. 5604, pp. 232–235, Jan. 2003. DOI: . [Online]. Available: .

[9] S. Jochim, M. Bartenstein, A. Altmeyer, G. Hendl, S. Riedl, C. Chin, J. H. Denschlag, and R. Grimm, "Bose-einstein condensation of molecules," *Science*, vol. 302, no. 5653, pp. 2101–2103, Dec. 2003. DOI: . [Online]. Available: .

[10] J. Kasprzak, M. Richard, S. Kundermann, A. Baas, P. Jeambrun, J. M. J. Keeling, F. M. Marchetti, M. H. Szymańska, R. André, J. L. Staehli, V. Savona, P. B. Littlewood, B. Deveaud, and L. S. Dang, "Bose–einstein condensation of exciton polaritons," *Nature*, vol. 443, no. 7110, pp. 409–414, Sep. 2006. DOI: . [Online]. Available: .

[11] A. Görlitz, J. M. Vogels, A. E. Leanhardt, C. Raman, T. L. Gustavson, J. R. Abo-Shaeer, A. P. Chikkatur, S. Gupta, S. Inouye, T. Rosenband, and W. Ketterle, "Realization of bose-einstein condensates in lower dimensions," *Phys. Rev. Lett.*, vol. 87, p. 130 402, 13 Sep. 2001. DOI: . [Online]. Available: .

[12] C. J. Pethick and H. Smith, *Bose-Einstein condensation in dilute gases*. Cambridge university press, 2008.

[13] L. D. Marco, G. Valtolina, K. Matsuda, W. G. Tobias, J. P. Covey, and J. Ye, "A degenerate fermi gas of polar molecules," *Science*, vol. 363, no. 6429, pp. 853–856, Jan. 2019. DOI: . [Online]. Available: .

[14] H. P. Büchler, E. Demler, M. Lukin, A. Micheli, N. Prokof'ev, G. Pupillo, and P. Zoller, "Strongly correlated 2d quantum phases with cold polar molecules: Controlling the shape of the interaction potential," *Phys. Rev. Lett.*, vol. 98, p. 060 404, 6 Feb. 2007. DOI: . [Online]. Available: .

[15] N. R. Cooper and G. V. Shlyapnikov, "Stable topological superfluid phase of ultracold polar fermionic molecules," *Phys. Rev. Lett.*, vol. 103, p. 155 302, 15 Oct. 2009. DOI: . [Online]. Available: .

[16] N. Y. Yao, A. V. Gorshkov, C. R. Laumann, A. M. Läuchli, J. Ye, and M. D. Lukin, "Realizing fractional chern insulators in dipolar spin systems," *Phys. Rev. Lett.*, vol. 110, p. 185 302, 18 Apr. 2013. DOI: . [Online]. Available: .

[17] S. V. Syzranov, M. L. Wall, V. Gurarie, and A. M. Rey, "Spin–orbital dynamics in a system of polar molecules," *Nature Communications*, vol. 5, no. 1, Nov. 2014. DOI: . [Online]. Available: .

[18] V. V. Albert, J. P. Covey, and J. Preskill, "Robust encoding of a qubit in a molecule," *Phys. Rev. X*, vol. 10, p. 031 050, 3 Sep. 2020. DOI: . [Online]. Available: .

[19] J. F. E. Croft and J. L. Bohn, "Long-lived complexes and chaos in ultracold molecular collisions," *Phys. Rev. A*, vol. 89, p. 012 714, 1 Jan. 2014. DOI: . [Online]. Available: .

[20] M.-G. Hu, Y. Liu, D. D. Grimes, Y.-W. Lin, A. H. Gheorghe, R. Vexiau, N. Bouloufa-Maafa, O. Dulieu, T. Rosenband, and K.-K. Ni, "Direct observation of bimolecular reactions of ultracold krb molecules," *Science*, vol. 366, no. 6469, pp. 1111–1115, 2019. DOI: . eprint: . [Online]. Available: .

[21] R. D. Levine, *Molecular reaction dynamics*. Cambridge University Press, 2009.

[22] M. Mayle, G. Quéméner, B. P. Ruzic, and J. L. Bohn, "Scattering of ultracold molecules in the highly resonant regime," *Phys. Rev. A*, vol. 87, p. 012 709, 1 Jan. 2013. DOI: . [Online]. Available: .

[23] R. C. T. da Costa, "Quantum mechanics of a constrained particle," *Phys. Rev. A*, vol. 23, pp. 1982–1987, 4 Apr. 1981. DOI: . [Online]. Available: .

[24] S. M. Carroll, *Spacetime and geometry*. Cambridge University Press, 2019.

[25] V. Bargmann, "Irreducible unitary representations of the lorentz group," *Annals of Mathematics*, pp. 568–640, 1947.

[26] A. Perelomov, *Generalized coherent states and their applications*. Springer Science & Business Media, 2012.

[27] R. Gilmore, *Lie Groups, Physics, and Geometry: An Introduction for Physicists, Engineers and Chemists*. Cambridge University Press, 2008. DOI: .

[28] S. Tan, "Large momentum part of a strongly correlated fermi gas," *Annals of Physics*, vol. 323, no. 12, pp. 2971–2986, Dec. 2008. DOI: . [Online]. Available: .

[29] F. Werner and Y. Castin, "General relations for quantum gases in two and three dimensions: Two-component fermions," *Phys. Rev. A*, vol. 86, p. 013 626, 1 Jul. 2012. DOI: . [Online]. Available: .

[30] F. Werner and Y. Castin, "General relations for quantum gases in two and three dimensions. ii. bosons and mixtures," *Phys. Rev. A*, vol. 86, p. 053 633, 5 Nov. 2012. DOI: . [Online]. Available: .

[31] S.-L. Zhang, M. He, and Q. Zhou, "Contact matrix in dilute quantum systems," *Phys. Rev. A*, vol. 95, p. 062 702, 6 Jun. 2017. DOI: . [Online]. Available: .

[32] E. Braaten, D. Kang, and L. Platter, "Universal relations for identical bosons from three-body physics," *Phys. Rev. Lett.*, vol. 106, p. 153 005, 15 Apr. 2011. DOI: . [Online]. Available: .

[33] D. H. Smith, E. Braaten, D. Kang, and L. Platter, "Two-body and three-body contacts for identical bosons near unitarity," *Phys. Rev. Lett.*, vol. 112, p. 110 402, 11 Mar. 2014. DOI: . [Online]. Available: .

[34] C. Lyu, C. Lv, and Q. Zhou, "Geometrizing quantum dynamics of a bose-einstein condensate," *Phys. Rev. Lett.*, vol. 125, p. 253 401, 25 Dec. 2020. DOI: . [Online]. Available: .

[35] C. Lv, R. Zhang, and Q. Zhou, "$SU(1,1)$ echoes for breathers in quantum gases," *Phys. Rev. Lett.*, vol. 125, p. 253 002, 25 Dec. 2020. DOI: . [Online]. Available: .

[36] J. Maldacena, "The large-N limit of superconformal field theories and supergravity," *International Journal of Theoretical Physics*, vol. 38, no. 4, pp. 1113–1133, Apr. 1999. [Online]. Available: .

[37] S. Sachdev, *From Gravity to Thermal Gauge Theories: The AdS/CFT Correspondence*. Springer Berlin Heidelberg, 2011, pp. 273–311. DOI: .

[38] S. Chapman, J. Eisert, L. Hackl, M. P. Heller, R. Jefferson, H. Marrochio, and R. C. Myers, "Complexity and entanglement for thermofield double states," *SciPost Physics*, vol. 6, no. 3, Mar. 2019. [Online]. Available: .

[39] R. A. Jefferson and R. C. Myers, "Circuit complexity in quantum field theory," *Journal of High Energy Physics*, vol. 10, no. 10, p. 107, Oct. 2017. [Online]. Available: .

[40] J. Maldacena and L. Susskind, "Cool horizons for entangled black holes," *Fortschritte der Physik*, vol. 61, no. 9, pp. 781–811, Aug. 2013. [Online]. Available: .

[41] J. Maldacena, "Eternal black holes in anti-de sitter," *Journal of High Energy Physics*, vol. 04, no. 04, pp. 021–021, Apr. 2003. [Online]. Available: .

[42] F. Pastawski, B. Yoshida, D. Harlow, and J. Preskill, "Holographic quantum error-correcting codes: Toy models for the bulk/boundary correspondence," *Journal of High Energy Physics*, vol. 2015, no. 6, Jun. 2015. DOI: . [Online]. Available: .

[43] M. Nozaki, S. Ryu, and T. Takayanagi, "Holographic geometry of entanglement renormalization in quantum field theories," *Journal of High Energy Physics*, vol. 10, no. 10, p. 193, Oct. 2012. [Online]. Available: .

[44] B. Swingle, "Entanglement renormalization and holography," *Phys. Rev. D*, vol. 86, p. 065 007, 6 Sep. 2012. DOI: . [Online]. Available: .

[45] M. Miyaji, T. Numasawa, N. Shiba, T. Takayanagi, and K. Watanabe, "Continuous multiscale entanglement renormalization ansatz as holographic surface-state correspondence," *Phys. Rev. Lett.*, vol. 115, p. 171 602, 17 Oct. 2015. [Online]. Available: .

[46] E. L. Hahn, "Spin echoes," *Phys. Rev.*, vol. 80, pp. 580–594, 4 Nov. 1950. [Online]. Available: .

[47] H. Bluhm, S. Foletti, I. Neder, M. Rudner, D. Mahalu, V. Umansky, and A. Yacoby, "Dephasing time of GaAs electron-spin qubits coupled to a nuclear bath exceeding 200 $\mu$s," *Nature Physics*, vol. 7, no. 2, pp. 109–113, Dec. 2010. DOI: . [Online]. Available: .

[48] E. L. Hahn and D. E. Maxwell, "Spin echo measurements of nuclear spin coupling in molecules," *Phys. Rev.*, vol. 88, pp. 1070–1084, 5 Dec. 1952. DOI: . [Online]. Available: .

[49] L. G. Rowan, E. L. Hahn, and W. B. Mims, "Electron-spin-echo envelope modulation," *Phys. Rev.*, vol. 137, A61–A71, 1A Jan. 1965. DOI: . [Online]. Available: .

[50] P. F. Liao and S. R. Hartmann, "Determination of cr-al hyperfine and electric quadrupole interaction parameters in ruby using spin-echo electron-nuclear double resonance," *Phys. Rev. B*, vol. 8, pp. 69–80, 1 Jul. 1973. DOI: . [Online]. Available: .

[51] W. Yao, R.-B. Liu, and L. J. Sham, "Theory of electron spin decoherence by interacting nuclear spins in a quantum dot," *Phys. Rev. B*, vol. 74, p. 195 301, 19 Nov. 2006. DOI: . [Online]. Available: .

[52] A. W. Kinross, M. Fu, T. J. Munsie, H. A. Dabkowska, G. M. Luke, S. Sachdev, and T. Imai, "Evolution of quantum fluctuations near the quantum critical point of the transverse field ising chain system conb2o6," *Phys. Rev. X*, vol. 4, p. 031 008, 3 Jul. 2014. DOI: . [Online]. Available: .

[53] C. Chin, R. Grimm, P. Julienne, and E. Tiesinga, "Feshbach resonances in ultracold gases," *Rev. Mod. Phys.*, vol. 82, pp. 1225–1286, 2 Apr. 2010. [Online]. Available: .

[54] E. A. Donley, N. R. Claussen, S. L. Cornish, J. L. Roberts, E. A. Cornell, and C. E. Wieman, "Dynamics of collapsing and exploding Bose–Einstein condensates," *Nature*, vol. 412, no. 6844, pp. 295–299, Jul. 2001. [Online]. Available: .

[55] C. C. Bradley, C. A. Sackett, J. J. Tollett, and R. G. Hulet, "Evidence of Bose-Einstein condensation in an atomic gas with attractive interactions," *Phys. Rev. Lett.*, vol. 75, pp. 1687–1690, 9 Aug. 1995. [Online]. Available: .

[56] J. Mun, P. Medley, G. K. Campbell, L. G. Marcassa, D. E. Pritchard, and W. Ketterle, "Phase diagram for a Bose-Einstein condensate moving in an optical lattice," *Phys. Rev. Lett.*, vol. 99, p. 150 604, 15 Oct. 2007. [Online]. Available: .

[57] C.-A. Chen and C.-L. Hung, "Observation of universal quench dynamics and townes soliton formation from modulational instability in two-dimensional bose gases," *Phys. Rev. Lett.*, vol. 125, p. 250 401, 25 Dec. 2020. DOI: . [Online]. Available: .

[58] M. Novaes, "Some basics of *su*(1, 1)," *Revista Brasileira de Ensino de Física*, vol. 26, no. 4, pp. 351–357, Dec. 2004. [Online]. Available: .

[59] Y.-Y. Chen, P. Zhang, W. Zheng, Z. Wu, and H. Zhai, "Many-body echo," *Phys. Rev. A*, vol. 102, p. 011 301, 1 Jul. 2020. DOI: . [Online]. Available: .

[60] L.-Y. Chih and M. Holland, "Driving quantum correlated atom-pairs from a bose–einstein condensate," *New J. Phys.*, vol. 22, no. 3, p. 033 010, Mar. 2020. DOI: . [Online]. Available: .

[61] B. Yurke, S. L. McCall, and J. R. Klauder, "SU(2) and SU(1,1) interferometers," *Phys. Rev. A*, vol. 33, pp. 4033–4054, 6 Jun. 1986. DOI: . [Online]. Available: .

[62] D. Linnemann, H. Strobel, W. Muessel, J. Schulz, R. J. Lewis-Swan, K. V. Kheruntsyan, and M. K. Oberthaler, "Quantum-enhanced sensing based on time reversal of nonlinear dynamics," *Phys. Rev. Lett.*, vol. 117, p. 013 001, 1 Jun. 2016. DOI: . [Online]. Available: .

[63] Y. Cheng and Z.-Y. Shi, "Many-body dynamics with time-dependent interaction," *Phys. Rev. A*, vol. 104, p. 023 307, 2 Aug. 2021. DOI: . [Online]. Available: .

[64] J. Maldacena, S. H. Shenker, and D. Stanford, "A bound on chaos," *Journal of High Energy Physics*, vol. 08, no. 08, p. 106, Aug. 2016. [Online]. Available: .

[65] S. H. Shenker and D. Stanford, "Black holes and the butterfly effect," *Journal of High Energy Physics*, vol. 03, no. 03, p. 67, Mar. 2014. [Online]. Available: .

[66] M. O. Scully and M. S. Zubairy, *Quantum optics*. Cambridge University Press, 1997.

[67] C. C. Gerry, "Correlated two-mode SU(1, 1) coherent states: Nonclassical properties," *Journal of the Optical Society of America B*, vol. 8, no. 3, p. 685, Mar. 1991. DOI: . [Online]. Available: .

[68] S. W. Hawking, "Black hole explosions?" *Nature*, vol. 248, no. 5443, pp. 30–31, Mar. 1974. [Online]. Available: .

[69] W. G. Unruh, "Notes on black-hole evaporation," *Phys. Rev. D*, vol. 14, pp. 870–892, 4 Aug. 1976. [Online]. Available: .

[70] M. M. Wilde, *Quantum information theory*. Cambridge University Press, 2013.

[71] S. Chapman, M. P. Heller, H. Marrochio, and F. Pastawski, "Toward a definition of complexity for quantum field theory states," *Phys. Rev. Lett.*, vol. 120, p. 121 602, 12 Mar. 2018. DOI: . [Online]. Available: .

[72] Y.-Y. Chen, P. Zhang, W. Zheng, Z. Wu, and H. Zhai, "Many-body echo," *Phys. Rev. A*, vol. 102, p. 011 301, 1 Jul. 2020. DOI: . [Online]. Available: .

[73] J. Maki and F. Zhou, "Quantum many-body conformal dynamics: Symmetries, geometry, conformal tower states, and entropy production," *Phys. Rev. A*, vol. 100, p. 023 601, 2 Aug. 2019. DOI: . [Online]. Available: .

[74] J. Hu, L. Feng, Z. Zhang, and C. Chin, "Quantum simulation of Unruh radiation," *Nature Physics*, vol. 15, no. 8, pp. 785–789, May 2019. [Online]. Available: .

[75] E. L. Hahn, "Spin echoes," *Phys. Rev.*, vol. 80, pp. 580–594, 4 Nov. 1950. [Online]. Available: .

[76] E. L. Hahn and D. E. Maxwell, "Spin echo measurements of nuclear spin coupling in molecules," *Phys. Rev.*, vol. 88, pp. 1070–1084, 5 Dec. 1952. DOI: . [Online]. Available: .

[77] E. O. Stejskal and J. E. Tanner, "Spin diffusion measurements: Spin echoes in the presence of a time-dependent field gradient," *The Journal of Chemical Physics*, vol. 42, no. 1, pp. 288–292, 1965. DOI: . [Online]. Available: .

[78] N. Bogoliubov, "On the theory of superfluidity," *J. Phys*, vol. 11, no. 1, p. 23, 1947.

[79] S. Stringari, "Collective excitations of a trapped bose-condensed gas," *Phys. Rev. Lett.*, vol. 77, pp. 2360–2363, 12 Sep. 1996. DOI: . [Online]. Available: .

[80] M. R. Matthews, B. P. Anderson, P. C. Haljan, D. S. Hall, C. E. Wieman, and E. A. Cornell, "Vortices in a bose-einstein condensate," *Phys. Rev. Lett.*, vol. 83, pp. 2498–2501, 13 Sep. 1999. DOI: . [Online]. Available: .

[81] V. Gritsev, P. Barmettler, and E. Demler, "Scaling approach to quantum non-equilibrium dynamics of many-body systems," *New Journal of Physics*, vol. 12, no. 11, p. 113 005, Nov. 2010. DOI: . [Online]. Available: .

[82] A. Griffin, W.-C. Wu, and S. Stringari, "Hydrodynamic modes in a trapped bose gas above the bose-einstein transition," *Phys. Rev. Lett.*, vol. 78, pp. 1838–1841, 10 Mar. 1997. DOI: . [Online]. Available: .

[83] H. Heiselberg, "Collective modes of trapped gases at the bec-bcs crossover," *Phys. Rev. Lett.*, vol. 93, p. 040 402, 4 Jul. 2004. DOI: . [Online]. Available: .

[84] J. Kinast, S. L. Hemmer, M. E. Gehm, A. Turlapov, and J. E. Thomas, "Evidence for superfluidity in a resonantly interacting fermi gas," *Phys. Rev. Lett.*, vol. 92, p. 150 402, 15 Apr. 2004. DOI: . [Online]. Available: .

[85] A. Turlapov, J. Kinast, B. Clancy, L. Luo, J. Joseph, and J. E. Thomas, "Is a gas of strongly interacting atomic fermions a nearly perfect fluid?" *Journal of Low Temperature Physics*, vol. 150, no. 3-4, pp. 567–576, Nov. 2007. DOI: . [Online]. Available: .

[86] J. Kinast, A. Turlapov, and J. E. Thomas, "Breakdown of hydrodynamics in the radial breathing mode of a strongly interacting fermi gas," *Phys. Rev. A*, vol. 70, p. 051 401, 5 Nov. 2004. DOI: . [Online]. Available: .

[87] A. Altmeyer, S. Riedl, M. J. Wright, C. Kohstall, J. H. Denschlag, and R. Grimm, "Dynamics of a strongly interacting fermi gas: The radial quadrupole mode," *Phys. Rev. A*, vol. 76, p. 033 610, 3 Sep. 2007. DOI: . [Online]. Available: .

[88] L. P. Pitaevskii and A. Rosch, "Breathing modes and hidden symmetry of trapped atoms in two dimensions," *Physical Review A*, vol. 55, no. 2, R853–R856, Feb. 1997. [Online]. Available: .

[89] M. Holten, L. Bayha, A. C. Klein, P. A. Murthy, P. M. Preiss, and S. Jochim, "Anomalous breaking of scale invariance in a two-dimensional fermi gas," *Phys. Rev. Lett.*, vol. 121, p. 120 401, 12 Sep. 2018. DOI: . [Online]. Available: .

[90] T. Peppler, P. Dyke, M. Zamorano, I. Herrera, S. Hoinka, and C. J. Vale, "Quantum anomaly and 2d-3d crossover in strongly interacting fermi gases," *Phys. Rev. Lett.*, vol. 121, p. 120 402, 12 Sep. 2018. DOI: . [Online]. Available: .

[91] M. Olshanii, H. Perrin, and V. Lorent, "Example of a quantum anomaly in the physics of ultracold gases," *Phys. Rev. Lett.*, vol. 105, p. 095 302, 9 Aug. 2010. DOI: . [Online]. Available: .

[92] C. Gao and Z. Yu, "Breathing mode of two-dimensional atomic fermi gases in harmonic traps," *Phys. Rev. A*, vol. 86, p. 043 609, 4 Oct. 2012. DOI: . [Online]. Available: .

[93] K. Merloti, R. Dubessy, L. Longchambon, M. Olshanii, and H. Perrin, "Breakdown of scale invariance in a quasi-two-dimensional bose gas due to the presence of the third dimension," *Phys. Rev. A*, vol. 88, p. 061 603, 6 Dec. 2013. DOI: . [Online]. Available: .

[94] J. Hofmann, "Quantum anomaly, universal relations, and breathing mode of a two-dimensional fermi gas," *Phys. Rev. Lett.*, vol. 108, p. 185 303, 18 May 2012. DOI: . [Online]. Available: .

[95] Y. Kagan, E. L. Surkov, and G. V. Shlyapnikov, "Evolution of a bose-condensed gas under variations of the confining potential," *Phys. Rev. A*, vol. 54, R1753–R1756, 3 Sep. 1996. DOI: . [Online]. Available: .

[96] F. Chevy, V. Bretin, P. Rosenbusch, K. W. Madison, and J. Dalibard, "Transverse breathing mode of an elongated bose-einstein condensate," *Phys. Rev. Lett.*, vol. 88, p. 250 402, 25 Jun. 2002. DOI: . [Online]. Available: .

[97] E. Vogt, M. Feld, B. Fröhlich, D. Pertot, M. Koschorreck, and M. Köhl, "Scale invariance and viscosity of a two-dimensional fermi gas," *Phys. Rev. Lett.*, vol. 108, p. 070 404, 7 Feb. 2012. DOI: . [Online]. Available: .

[98] R. Saint-Jalm, P. C. M. Castilho, É. Le Cerf, B. Bakkali-Hassani, J.-L. Ville, S. Nascimbene, J. Beugnon, and J. Dalibard, "Dynamical symmetry and breathers in a two-dimensional bose gas," *Phys. Rev. X*, vol. 9, p. 021 035, 2 May 2019. [Online]. Available: .

[99] Z.-Y. Shi, C. Gao, and H. Zhai, "Ideal-gas approach to hydrodynamics," *Phys. Rev. X*, vol. 11, p. 041 031, 4 Nov. 2021. DOI: . [Online]. Available: .

[100] R. R. Puri, *Mathematical methods of quantum optics*. Springer, 2001.

[101] F. Werner and Y. Castin, "Unitary gas in an isotropic harmonic trap: Symmetry properties and applications," *Phys. Rev. A*, vol. 74, p. 053 604, 5 Nov. 2006. DOI: . [Online]. Available: .

[102] C. Lv and Q. Zhou, *Emergent spacetimes from hermitian and non-hermitian quantum dynamics*, 2022. DOI: . [Online]. Available: .

[103] J. Maldacena, "The large $N$ limit of superconformal field theories and supergravity," *Advances in Theoretical and Mathematical Physics*, vol. 2, no. 2, pp. 231–252, 1998. DOI: . [Online]. Available: .

[104] S. Gubser, I. Klebanov, and A. Polyakov, "Gauge theory correlators from non-critical string theory," *Physics Letters B*, vol. 428, no. 1-2, pp. 105–114, May 1998. DOI: . [Online]. Available: .

[105] E. Witten, "Anti de sitter space and holography," *Advances in Theoretical and Mathematical Physics*, vol. 2, no. 2, pp. 253–291, 1998. DOI: . [Online]. Available: .

[106] G. Vidal, "Entanglement renormalization," *Phys. Rev. Lett.*, vol. 99, p. 220 405, 22 Nov. 2007. DOI: . [Online]. Available: .

[107] B. Swingle, "Entanglement renormalization and holography," *Phys. Rev. D*, vol. 86, p. 065 007, 6 Sep. 2012. DOI: . [Online]. Available: .

[108] X.-L. Qi, *Exact holographic mapping and emergent space-time geometry*, 2013. DOI: . [Online]. Available: .

[109] M. A. Nielsen, *A geometric approach to quantum circuit lower bounds*, 2005. DOI: . [Online]. Available: .

[110] M. A. Nielsen, M. R. Dowling, M. Gu, and A. C. Doherty, "Quantum computation as geometry," *Science*, vol. 311, no. 5764, pp. 1133–1135, Feb. 2006. DOI: . [Online]. Available: .

[111] M. Guo, J. Hernandez, R. C. Myers, and S.-M. Ruan, "Circuit complexity for coherent states," *Journal of High Energy Physics*, vol. 2018, no. 10, Oct. 2018. DOI: . [Online]. Available: .

[112] A. R. Brown and L. Susskind, "Complexity geometry of a single qubit," *Phys. Rev. D*, vol. 100, p. 046 020, 4 Aug. 2019. DOI: . [Online]. Available: .

[113] U. Sood and M. Kruczenski, "Circuit complexity near critical points," *Journal of Physics A: Mathematical and Theoretical*, vol. 55, no. 18, p. 185 301, Apr. 2022. DOI: . [Online]. Available: .

[114] Y.-Y. Chen, P. Zhang, W. Zheng, Z. Wu, and H. Zhai, "Many-body echo," *Phys. Rev. A*, vol. 102, p. 011 301, 1 Jul. 2020. DOI: . [Online]. Available: .

[115] J. Zhang, X. Yang, C. Lv, S. Ma, and R. Zhang, *Quantum dynamics of cold atomic gas with $SU(1,1)$ symmetry*, 2022. DOI: . [Online]. Available: .

[116] R. R. Puri, *Mathematical methods of quantum optics*. Springer Science & Business Media, 2001, vol. 79.

[117] I. Bengtsson and P. Sandin, "Anti-de sitter space, squashed and stretched," *Classical and Quantum Gravity*, vol. 23, no. 3, pp. 971–986, Jan. 2006. DOI: . [Online]. Available: .

[118] F. Calogero, "Solution of the one-dimensional $N$-body problems with quadratic and/or inversely quadratic pair potentials," *Journal of Mathematical Physics*, vol. 12, no. 3, pp. 419–436, Mar. 1971. DOI: . [Online]. Available: .

[119] B. Sutherland, "Quantum many-body problem in one dimension: Ground state," *Journal of Mathematical Physics*, vol. 12, no. 2, pp. 246–250, Feb. 1971. DOI: . [Online]. Available: .

[120] A. del Campo, "Exact quantum decay of an interacting many-particle system: The calogero–sutherland model," *New Journal of Physics*, vol. 18, no. 1, p. 015 014, Jan. 2016. DOI: . [Online]. Available: .

[121] J. Hu, L. Feng, Z. Zhang, and C. Chin, "Quantum simulation of unruh radiation," *Nature Physics*, vol. 15, no. 8, pp. 785–789, May 2019. DOI: . [Online]. Available: .

[122] K. Kim, J. Hur, S. Huh, S. Choi, and J.-y. Choi, "Emission of spin-correlated matter-wave jets from spinor bose-einstein condensates," *Phys. Rev. Lett.*, vol. 127, p. 043 401, 4 Jul. 2021. DOI: . [Online]. Available: .

[123] B. Mukherjee, A. Shaffer, P. B. Patel, Z. Yan, C. C. Wilson, V. Crépel, R. J. Fletcher, and M. Zwierlein, "Crystallization of bosonic quantum hall states in a rotating quantum gas," *Nature*, vol. 601, no. 7891, pp. 58–62, Jan. 2022. DOI: . [Online]. Available: .

[124] C. V. Parker, L.-C. Ha, and C. Chin, "Direct observation of effective ferromagnetic domains of cold atoms in a shaken optical lattice," *Nature Physics*, vol. 9, no. 12, pp. 769–774, Oct. 2013. [Online]. Available: .

[125] J. H. V. Nguyen, D. Luo, and R. G. Hulet, "Formation of matter-wave soliton trains by modulational instability," *Science*, vol. 356, no. 6336, pp. 422–426, Apr. 2017. DOI: . [Online]. Available: .

[126] K. Wintersperger, M. Bukov, J. Näger, S. Lellouch, E. Demler, U. Schneider, I. Bloch, N. Goldman, and M. Aidelsburger, "Parametric instabilities of interacting bosons in periodically driven 1d optical lattices," *Phys. Rev. X*, vol. 10, p. 011 030, 1 Feb. 2020. DOI: . [Online]. Available: .

[127] C.-A. Chen and C.-L. Hung, "Observation of universal quench dynamics and townes soliton formation from modulational instability in two-dimensional bose gases," *Phys. Rev. Lett.*, vol. 125, p. 250 401, 25 Dec. 2020. DOI: . [Online]. Available: .

[128] B. Lapierre, K. Choo, C. Tauber, A. Tiwari, T. Neupert, and R. Chitra, "Emergent black hole dynamics in critical floquet systems," *Phys. Rev. Research*, vol. 2, p. 023 085, 2 Apr. 2020. DOI: . [Online]. Available: .

[129] B. Lapierre and P. Moosavi, "Geometric approach to inhomogeneous floquet systems," *Phys. Rev. B*, vol. 103, p. 224 303, 22 Jun. 2021. DOI: . [Online]. Available: .

[130] R. Fan, Y. Gu, A. Vishwanath, and X. Wen, "Floquet conformal field theories with generally deformed Hamiltonians," *SciPost Phys.*, vol. 10, p. 49, 2 2021. DOI: . [Online]. Available: .

[131] J. Wiersig, "Enhancing the sensitivity of frequency and energy splitting detection by using exceptional points: Application to microcavity sensors for single-particle detection," *Phys. Rev. Lett.*, vol. 112, p. 203 901, 20 May 2014. DOI: . [Online]. Available: .

[132] J. Wiersig, "Sensors operating at exceptional points: General theory," *Phys. Rev. A*, vol. 93, p. 033 809, 3 Mar. 2016. DOI: . [Online]. Available: .

[133] Z.-P. Liu, J. Zhang, Ş. K. Özdemir, B. Peng, H. Jing, X.-Y. Lü, C.-W. Li, L. Yang, F. Nori, and Y.-x. Liu, "Metrology with $\mathcal{PT}$-symmetric cavities: Enhanced sensitivity near the $\mathcal{PT}$-phase transition," *Phys. Rev. Lett.*, vol. 117, p. 110 802, 11 Sep. 2016. DOI: . [Online]. Available: .

[134] H. Hodaei, A. U. Hassan, S. Wittek, H. Garcia-Gracia, R. El-Ganainy, D. N. Christodoulides, and M. Khajavikhan, "Enhanced sensitivity at higher-order exceptional points," *Nature*, vol. 548, no. 7666, pp. 187–191, Aug. 2017. DOI: . [Online]. Available: .

[135] W. Chen, Ş. K. Özdemir, G. Zhao, J. Wiersig, and L. Yang, "Exceptional points enhance sensing in an optical microcavity," *Nature*, vol. 548, no. 7666, pp. 192–196, Aug. 2017. DOI: . [Online]. Available: .

[136] H.-K. Lau and A. A. Clerk, "Fundamental limits and non-reciprocal approaches in non-hermitian quantum sensing," *Nature Communications*, vol. 9, no. 1, Oct. 2018. DOI: . [Online]. Available: .

[137] M. Zhang, W. Sweeney, C. W. Hsu, L. Yang, A. D. Stone, and L. Jiang, "Quantum noise theory of exceptional point amplifying sensors," *Phys. Rev. Lett.*, vol. 123, p. 180 501, 18 Oct. 2019. DOI: . [Online]. Available: .

[138] M. P. Hokmabadi, A. Schumer, D. N. Christodoulides, and M. Khajavikhan, "Non-hermitian ring laser gyroscopes with enhanced sagnac sensitivity," *Nature*, vol. 576, no. 7785, pp. 70–74, Dec. 2019. DOI: . [Online]. Available: .

[139] Y.-H. Lai, Y.-K. Lu, M.-G. Suh, Z. Yuan, and K. Vahala, "Observation of the exceptional-point-enhanced sagnac effect," *Nature*, vol. 576, no. 7785, pp. 65–69, Dec. 2019. DOI: . [Online]. Available: .

[140] E. Torrontegui, S. Ibáñez, S. Martínez-Garaot, M. Modugno, A. del Campo, D. Guéry-Odelin, A. Ruschhaupt, X. Chen, and J. G. Muga, "Shortcuts to adiabaticity," in *Advances In Atomic, Molecular, and Optical Physics*, Elsevier, 2013, pp. 117–169. DOI: . [Online]. Available: .

[141] A. Reiserer, S. Ritter, and G. Rempe, "Nondestructive detection of an optical photon," *Science*, vol. 342, no. 6164, pp. 1349–1351, Nov. 2013. DOI: . [Online]. Available: .

[142] M. Cetina, M. Jag, R. S. Lous, I. Fritsche, J. T. M. Walraven, R. Grimm, J. Levinsen, M. M. Parish, R. Schmidt, M. Knap, and E. Demler, "Ultrafast many-body interferometry of impurities coupled to a fermi sea," *Science*, vol. 354, no. 6308, pp. 96–99, Oct. 2016. DOI: . [Online]. Available: .

[143] Y. Yan and Q. Zhou, *Manipulating anyons in quantum hall droplets of light using dissipations*, 2021. DOI: . [Online]. Available: .

[144] G. 't Hooft, "Magnetic monopoles in unified theories," *Nucl. Phys. B*, vol. 79, no. CERN-TH-1876, pp. 276–284, 1974.

[145] A. Polyakov, "Particle spectrum in the quantum field theory," *Journal of Experimental and Theoretical Physics Letters (JETP Letters)*, vol. 20, no. 6, pp. 194–195, 1974.

[146] R. Auzzi, S. Baiguera, A. Legramandi, G. Nardelli, P. Roy, and N. Zenoni, "On subregion action complexity in AdS3 and in the BTZ black hole," *Journal of High Energy Physics*, vol. 2020, no. 1, Jan. 2020. DOI: . [Online]. Available: .

[147] A. P. Reynolds and S. F. Ross, "Complexity of the AdS soliton," *Classical and Quantum Gravity*, vol. 35, no. 9, p. 095 006, Mar. 2018. DOI: . [Online]. Available: .

[148] R. Zhang, C. Lv, Y. Yan, and Q. Zhou, "Efimov-like states and quantum funneling effects on synthetic hyperbolic surfaces," *Science Bulletin*, vol. 66, no. 19, pp. 1967–1972, Oct. 2021. DOI: . [Online]. Available: .

[149] C. Lv, R. Zhang, Z. Zhai, and Q. Zhou, "Curving the space by non-hermiticity," *Nature Communications*, vol. 13, no. 1, Apr. 2022. DOI: . [Online]. Available: .

[150] N. Hatano and D. R. Nelson, "Localization transitions in non-hermitian quantum mechanics," *Phys. Rev. Lett.*, vol. 77, pp. 570–573, 3 Jul. 1996. DOI: . [Online]. Available: .

[151] I. Bloch, J. Dalibard, and W. Zwerger, "Many-body physics with ultracold gases," *Rev. Mod. Phys.*, vol. 80, pp. 885–964, 3 Jul. 2008. DOI: . [Online]. Available: .

[152] I. M. Georgescu, S. Ashhab, and F. Nori, "Quantum simulation," *Rev. Mod. Phys.*, vol. 86, pp. 153–185, 1 Mar. 2014. DOI: . [Online]. Available: .

[153] N. Goldman, J. C. Budich, and P. Zoller, "Topological quantum matter with ultracold gases in optical lattices," *Nature Physics*, vol. 12, no. 7, pp. 639–645, Jun. 2016. DOI: . [Online]. Available: .

[154] C. Gross and I. Bloch, "Quantum simulations with ultracold atoms in optical lattices," *Science*, vol. 357, no. 6355, pp. 995–1001, Sep. 2017. DOI: . [Online]. Available: .

[155] N. R. Cooper, J. Dalibard, and I. B. Spielman, "Topological bands for ultracold atoms," *Rev. Mod. Phys.*, vol. 91, p. 015 005, 1 Mar. 2019. DOI: . [Online]. Available: .

[156] I. Carusotto, A. A. Houck, A. J. Kollár, P. Roushan, D. I. Schuster, and J. Simon, "Photonic materials in circuit quantum electrodynamics," *Nature Physics*, vol. 16, no. 3, pp. 268–279, Mar. 2020. DOI: . [Online]. Available: .

[157] P. O. Fedichev and U. R. Fischer, "Gibbons-hawking effect in the sonic de sitter space-time of an expanding bose-einstein-condensed gas," *Phys. Rev. Lett.*, vol. 91, p. 240 407, 24 Dec. 2003. DOI: . [Online]. Available: .

[158] S. Batz and U. Peschel, "Linear and nonlinear optics in curved space," *Phys. Rev. A*, vol. 78, p. 043 821, 4 Oct. 2008. DOI: . [Online]. Available: .

[159] I. I. Smolyaninov and E. E. Narimanov, "Metric signature transitions in optical metamaterials," *Phys. Rev. Lett.*, vol. 105, p. 067 402, 6 Aug. 2010. DOI: . [Online]. Available: .

[160] F. Caravelli, A. Hamma, F. Markopoulou, and A. Riera, "Trapped surfaces and emergent curved space in the bose-hubbard model," *Phys. Rev. D*, vol. 85, p. 044 046, 4 Feb. 2012. DOI: . [Online]. Available: .

[161] R. Bekenstein, R. Schley, M. Mutzafi, C. Rotschild, and M. Segev, "Optical simulations of gravitational effects in the newton–schrödinger system," *Nature Physics*, vol. 11, no. 10, pp. 872–878, Aug. 2015. DOI: . [Online]. Available: .

[162] R. Bekenstein, Y. Kabessa, Y. Sharabi, O. Tal, N. Engheta, G. Eisenstein, A. J. Agranat, and M. Segev, "Control of light by curved space in nanophotonic structures," *Nature Photonics*, vol. 11, no. 10, pp. 664–670, Sep. 2017. DOI: . [Online]. Available: .

[163] Z.-Y. Shi and H. Zhai, "Emergent gauge field for a chiral bound state on curved surface," *Journal of Physics B: Atomic, Molecular and Optical Physics*, vol. 50, no. 18, p. 184 006, Sep. 2017. DOI: . [Online]. Available: .

[164] J. Zhang and T.-L. Ho, "Potential scattering on a spherical surface," *Journal of Physics B: Atomic, Molecular and Optical Physics*, vol. 51, no. 11, p. 115 301, May 2018. DOI: . [Online]. Available: .

[165] R. Bekenstein, Y. Kabessa, Y. Sharabi, O. Tal, N. Engheta, G. Eisenstein, A. J. Agranat, and M. Segev, "Control of light by curved space in nanophotonic structures," *Nature Photonics*, vol. 11, no. 10, pp. 664–670, Sep. 2017. DOI: . [Online]. Available: .

[166] X.-F. Zhou, C. Wu, G.-C. Guo, R. Wang, H. Pu, and Z.-W. Zhou, "Synthetic landau levels and spinor vortex matter on a haldane spherical surface with a magnetic monopole," *Phys. Rev. Lett.*, vol. 120, p. 130 402, 13 Mar. 2018. DOI: . [Online]. Available: .

[167] S. Eckel, A. Kumar, T. Jacobson, I. B. Spielman, and G. K. Campbell, "A rapidly expanding bose-einstein condensate: An expanding universe in the lab," *Phys. Rev. X*, vol. 8, p. 021 021, 2 Apr. 2018. DOI: . [Online]. Available: .

[168] A. J. Kollár, M. Fitzpatrick, and A. A. Houck, "Hyperbolic lattices in circuit quantum electrodynamics," *Nature*, vol. 571, no. 7763, pp. 45–50, Jul. 2019. DOI: . [Online]. Available: .

[169] N. Schine, M. Chalupnik, T. Can, A. Gromov, and J. Simon, "Electromagnetic and gravitational responses of photonic landau levels," *Nature*, vol. 565, no. 7738, pp. 173–179, Jan. 2019. DOI: . [Online]. Available: .

[170] I. Boettcher, P. Bienias, R. Belyansky, A. J. Kollár, and A. V. Gorshkov, "Quantum simulation of hyperbolic space with circuit quantum electrodynamics: From graphs to geometry," *Phys. Rev. A*, vol. 102, p. 032 208, 3 Sep. 2020. DOI: . [Online]. Available: .

[171] C. Viermann, M. Sparn, N. Liebster, M. Hans, E. Kath, Á. Parra-López, M. Tolosa-Simeón, N. Sánchez-Kuntz, T. Haas, H. Strobel, S. Floerchinger, and M. K. Oberthaler, *Quantum field simulator for dynamics in curved spacetime*, 2022. DOI: . [Online]. Available: .

[172] M. Tolosa-Simeón, Á. Parra-López, N. Sánchez-Kuntz, T. Haas, C. Viermann, M. Sparn, N. Liebster, M. Hans, E. Kath, H. Strobel, M. K. Oberthaler, and S. Floerchinger, *Curved and expanding spacetime geometries in bose-einstein condensates*, 2022. DOI: . [Online]. Available: .

[173] N. Syassen, D. M. Bauer, M. Lettner, T. Volz, D. Dietze, J. J. García-Ripoll, J. I. Cirac, G. Rempe, and S. Dürr, "Strong dissipation inhibits losses and induces correlations in cold molecular gases," *Science*, vol. 320, no. 5881, pp. 1329–1331, 2008, ISSN: 0036-8075. DOI: . eprint: . [Online]. Available: .

[174] A. Regensburger, C. Bersch, M.-A. Miri, G. Onishchukov, D. N. Christodoulides, and U. Peschel, "Parity–time synthetic photonic lattices," *Nature*, vol. 488, no. 74-10, pp. 167–171, Aug. 2012. DOI: . [Online]. Available: .

[175] L. Feng, Z. J. Wong, R.-M. Ma, Y. Wang, and X. Zhang, "Single-mode laser by parity-time symmetry breaking," *Science*, vol. 346, no. 6212, pp. 972–975, Oct. 2014. DOI: . [Online]. Available: .

[176] S. Longhi, D. Gatti, and G. D. Valle, "Robust light transport in non-hermitian photonic lattices," *Scientific Reports*, vol. 5, no. 1, Aug. 2015. DOI: . [Online]. Available: .

[177] J. Li, A. K. Harter, J. Liu, L. de Melo, Y. N. Joglekar, and L. Luo, "Observation of parity-time symmetry breaking transitions in a dissipative floquet system of ultracold atoms," *Nature Communications*, vol. 10, no. 1, Feb. 2019. DOI: . [Online]. Available: .

[178] W. Gou, T. Chen, D. Xie, T. Xiao, T.-S. Deng, B. Gadway, W. Yi, and B. Yan, "Tunable nonreciprocal quantum transport through a dissipative aharonov-bohm ring in ultracold atoms," *Phys. Rev. Lett.*, vol. 124, p. 070 402, 7 Feb. 2020. DOI: . [Online]. Available: .

[179] S. Weidemann, M. Kremer, T. Helbig, T. Hofmann, A. Stegmaier, M. Greiter, R. Thomale, and A. Szameit, "Topological funneling of light," *Science*, vol. 368, no. 6488, pp. 311–314, Mar. 2020. DOI: . [Online]. Available: .

[180] T. Helbig, T. Hofmann, S. Imhof, M. Abdelghany, T. Kiessling, L. W. Molenkamp, C. H. Lee, A. Szameit, M. Greiter, and R. Thomale, "Generalized bulk–boundary correspondence in non-hermitian topolectrical circuits," *Nature Physics*, vol. 16, no. 7, pp. 747–750, Jun. 2020. DOI: . [Online]. Available: .

[181] S. Yao and Z. Wang, "Edge states and topological invariants of non-hermitian systems," *Phys. Rev. Lett.*, vol. 121, p. 086 803, 8 Aug. 2018. DOI: . [Online]. Available: .

[182] F. K. Kunst, E. Edvardsson, J. C. Budich, and E. J. Bergholtz, "Biorthogonal bulk-boundary correspondence in non-hermitian systems," *Phys. Rev. Lett.*, vol. 121, p. 026 808, 2 Jul. 2018. DOI: . [Online]. Available: .

[183] V. M. Martinez Alvarez, J. E. Barrios Vargas, and L. E. F. Foa Torres, "Non-hermitian robust edge states in one dimension: Anomalous localization and eigenspace condensation at exceptional points," *Phys. Rev. B*, vol. 97, p. 121 401, 12 Mar. 2018. DOI: . [Online]. Available: .

[184] C. H. Lee and R. Thomale, "Anatomy of skin modes and topology in non-hermitian systems," *Phys. Rev. B*, vol. 99, p. 201 103, 20 May 2019. DOI: . [Online]. Available: .

[185] D. S. Borgnia, A. J. Kruchkov, and R.-J. Slager, "Non-hermitian boundary modes and topology," *Phys. Rev. Lett.*, vol. 124, p. 056 802, 5 Feb. 2020. DOI: . [Online]. Available: .

[186] K. Zhang, Z. Yang, and C. Fang, "Correspondence between winding numbers and skin modes in non-hermitian systems," *Phys. Rev. Lett.*, vol. 125, p. 126 402, 12 Sep. 2020. DOI: . [Online]. Available: .

[187] N. Okuma, K. Kawabata, K. Shiozaki, and M. Sato, "Topological origin of non-hermitian skin effects," *Phys. Rev. Lett.*, vol. 124, p. 086 801, 8 Feb. 2020. DOI: . [Online]. Available: .

[188] C. M. Bender and S. Boettcher, "Real spectra in non-hermitian hamiltonians having PT symmetry," *Phys. Rev. Lett.*, vol. 80, pp. 5243–5246, 24 Jun. 1998. DOI: . [Online]. Available: .

[189] A. Mostafazadeh, "Pseudo-hermiticity versus PT symmetry: The necessary condition for the reality of the spectrum of a non-hermitian hamiltonian," *Journal of Mathematical Physics*, vol. 43, no. 1, pp. 205–214, Jan. 2002. DOI: . [Online]. Available: .

[190] Y. Ashida, Z. Gong, and M. Ueda, "Non-hermitian physics," *Advances in Physics*, vol. 69, no. 3, pp. 249–435, Jul. 2020. DOI: . [Online]. Available: .

[191] E. J. Bergholtz, J. C. Budich, and F. K. Kunst, "Exceptional topology of non-hermitian systems," *Rev. Mod. Phys.*, vol. 93, p. 015 005, 1 Feb. 2021. DOI: . [Online]. Available: .

[192] Y. Xiong, "Why does bulk boundary correspondence fail in some non-hermitian topological models," *Journal of Physics Communications*, vol. 2, no. 3, p. 035 043, Mar. 2018. DOI: . [Online]. Available: .

[193] N. Okuma and M. Sato, "Topological phase transition driven by infinitesimal instability: Majorana fermions in non-hermitian spintronics," *Phys. Rev. Lett.*, vol. 123, p. 097 701, 9 Aug. 2019. DOI: . [Online]. Available: .

[194] K. Kawabata, K. Shiozaki, M. Ueda, and M. Sato, "Symmetry and topology in non-hermitian physics," *Phys. Rev. X*, vol. 9, p. 041 015, 4 Oct. 2019. DOI: . [Online]. Available: .

[195] J. Y. Lee, J. Ahn, H. Zhou, and A. Vishwanath, "Topological correspondence between hermitian and non-hermitian systems: Anomalous dynamics," *Phys. Rev. Lett.*, vol. 123, p. 206 404, 20 Nov. 2019. DOI: . [Online]. Available: .

[196] H. Zhou and J. Y. Lee, "Periodic table for topological bands with non-hermitian symmetries," *Phys. Rev. B*, vol. 99, p. 235 112, 23 Jun. 2019. DOI: . [Online]. Available: .

[197] L. Xiao, T. Deng, K. Wang, G. Zhu, Z. Wang, W. Yi, and P. Xue, "Non-hermitian bulk–boundary correspondence in quantum dynamics," *Nature Physics*, vol. 16, no. 7, pp. 761–766, 2020. DOI: . [Online]. Available: .

[198] M. C. Gutzwiller, *Chaos in classical and quantum mechanics*. Springer Science & Business Media, 2013, vol. 1.

[199] N. Balazs and A. Voros, "Chaos on the pseudosphere," *Physics Reports*, vol. 143, no. 3, pp. 109–240, Nov. 1986. DOI: . [Online]. Available: .

[200] V. Efimov, "Energy levels arising from resonant two-body forces in a three-body system," *Physics Letters B*, vol. 33, no. 8, pp. 563–564, Dec. 1970. DOI: . [Online]. Available: .

[201] D. R. Nelson and V. M. Vinokur, "Boson localization and correlated pinning of superconducting vortex arrays," *Phys. Rev. B*, vol. 48, pp. 13 060–13 097, 17 Nov. 1993. DOI: . [Online]. Available: .

[202] A. Mostafazadeh, "Pseudo-Hermitian Representation of Quantum Mechanics," *International Journal of Geometric Methods in Modern Physics*, vol. 07, no. 07, pp. 1191–1306, Nov. 2010. DOI: . [Online]. Available: .

[203] A. Comtet, "On the landau levels on the hyperbolic plane," *Annals of Physics*, vol. 173, no. 1, pp. 185–209, Jan. 1987. DOI: . [Online]. Available: .

[204] X. G. Wen and A. Zee, "Shift and spin vector: New topological quantum numbers for the hall fluids," *Phys. Rev. Lett.*, vol. 69, pp. 953–956, 6 Aug. 1992. DOI: . [Online]. Available: .

[205] K. Yokomizo and S. Murakami, "Non-bloch band theory of non-hermitian systems," *Phys. Rev. Lett.*, vol. 123, p. 066 404, 6 Aug. 2019. DOI: . [Online]. Available: .

[206] Z. Yang, K. Zhang, C. Fang, and J. Hu, "Non-hermitian bulk-boundary correspondence and auxiliary generalized brillouin zone theory," *Phys. Rev. Lett.*, vol. 125, p. 226 402, 22 Nov. 2020. DOI: . [Online]. Available: .

[207] M. He, C. Lv, H.-Q. Lin, and Q. Zhou, "Universal relations for ultracold reactive molecules," *Science Advances*, vol. 6, no. 51, Dec. 2020. DOI: . [Online]. Available: .

[208] D. DeMille, "Quantum computation with trapped polar molecules," *Phys. Rev. Lett.*, vol. 88, p. 067 901, 6 Jan. 2002. DOI: . [Online]. Available: .

[209] S. F. Yelin, K. Kirby, and R. Côté, "Schemes for robust quantum computation with polar molecules," *Phys. Rev. A*, vol. 74, p. 050 301, 5 Nov. 2006. DOI: . [Online]. Available: .

[210] S. Ospelkaus, K.-K. Ni, D. Wang, M. H. G. de Miranda, B. Neyenhuis, G. Quemener, P. S. Julienne, J. L. Bohn, D. S. Jin, and J. Ye, "Quantum-state controlled chemical reactions of ultracold potassium-rubidium molecules," *Science*, vol. 327, no. 5967, pp. 853–857, Feb. 2010. DOI: . [Online]. Available: .

[211] P. D. Gregory, M. D. Frye, J. A. Blackmore, E. M. Bridge, R. Sawant, J. M. Hutson, and S. L. Cornish, "Sticky collisions of ultracold RbCs molecules," *Nature Communications*, vol. 10, no. 1, Jul. 2019. DOI: . [Online]. Available: .

[212] X. Ye, M. Guo, M. L. González-Martínez, G. Quéméner, and D. Wang, "Collisions of ultracold 23na87rb molecules with controlled chemical reactivities," *Science Advances*, vol. 4, no. 1, eaaq0083, Jan. 2018. DOI: . [Online]. Available: .

[213] Z. Idziaszek and P. S. Julienne, "Universal rate constants for reactive collisions of ultracold molecules," *Phys. Rev. Lett.*, vol. 104, p. 113 202, 11 Mar. 2010. DOI: . [Online]. Available: .

[214] E. Braaten and H.-W. Hammer, "Universal relation for the inelastic two-body loss rate," *Journal of Physics B: Atomic, Molecular and Optical Physics*, vol. 46, no. 21, p. 215 203, Oct. 2013. DOI: . [Online]. Available: .

[215] S. Laurent, M. Pierce, M. Delehaye, T. Yefsah, F. Chevy, and C. Salomon, "Connecting few-body inelastic decay to quantum correlations in a many-body system: A weakly coupled impurity in a resonant fermi gas," *Phys. Rev. Lett.*, vol. 118, p. 103 403, 10 Mar. 2017. DOI: . [Online]. Available: .

[216] K.-K. Ni, S. Ospelkaus, M. H. G. de Miranda, A. Pe'er, B. Neyenhuis, J. J. Zirbel, S. Kotochigova, P. S. Julienne, D. S. Jin, and J. Ye, "A high phase-space-density gas of polar molecules," *Science*, vol. 322, no. 5899, pp. 231–235, Oct. 2008. DOI: . [Online]. Available: .

[217] S. M. Yoshida and M. Ueda, "Universal high-momentum asymptote and thermodynamic relations in a spinless fermi gas with a resonant $p$-wave interaction," *Phys. Rev. Lett.*, vol. 115, p. 135 303, 13 Sep. 2015. DOI: . [Online]. Available: .

[218] Z. Yu, J. H. Thywissen, and S. Zhang, "Universal relations for a fermi gas close to a $p$-wave interaction resonance," *Phys. Rev. Lett.*, vol. 115, p. 135 304, 13 Sep. 2015. DOI: . [Online]. Available: .

[219] M. He, S. Zhang, H. M. Chan, and Q. Zhou, "Concept of a contact spectrum and its applications in atomic quantum hall states," *Phys. Rev. Lett.*, vol. 116, p. 045 301, 4 Jan. 2016. DOI: . [Online]. Available: .

[220] C. Luciuk, S. Trotzky, S. Smale, Z. Yu, S. Zhang, and J. H. Thywissen, "Evidence for universal relations describing a gas with p-wave interactions," *Nature Physics*, vol. 12, no. 6, pp. 599–605, Feb. 2016. DOI: . [Online]. Available: .

[221] H. Friedrich, *Scattering theory*. Springer, 2013, vol. 872.

[222] S. M. Yoshida and M. Ueda, "$p$-wave contact tensor: Universal properties of axisymmetry-broken $p$-wave fermi gases," *Phys. Rev. A*, vol. 94, p. 033 611, 3 Sep. 2016. DOI: . [Online]. Available: .

[223] S. Dürr, J. J. García-Ripoll, N. Syassen, D. M. Bauer, M. Lettner, J. I. Cirac, and G. Rempe, "Lieb-liniger model of a dissipation-induced tonks-girardeau gas," *Phys. Rev. A*, vol. 79, p. 023 614, 2 Feb. 2009. DOI: . [Online]. Available: .

[224] J. J. García-Ripoll, S. Dürr, N. Syassen, D. M. Bauer, M. Lettner, G. Rempe, and J. I. Cirac, "Dissipation-induced hard-core boson gas in an optical lattice," *New Journal of Physics*, vol. 11, no. 1, p. 013 053, Jan. 2009. DOI: . [Online]. Available: .

[225] R. Zhang, C. Lv, and Q. Zhou, *Analogue black holes in reactive molecules*, 2022. DOI: . [Online]. Available: .

[226] C. V. Vishveshwara, "Scattering of gravitational radiation by a schwarzschild black-hole," *Nature*, vol. 227, no. 5261, pp. 936–938, 1970. DOI: . [Online]. Available: .

[227] H.-P. Nollert, "Quasinormal modes: The characteristic sound of black holes and neutron stars," *Class. Quantum Grav.*, vol. 16, no. 12, R159–R216, Nov. 1999. DOI: . [Online]. Available: .

[228] E. Berti, V. Cardoso, and A. O. Starinets, "Quasinormal modes of black holes and black branes," *Class. Quantum Grav.*, vol. 26, no. 16, p. 163 001, Jul. 2009. DOI: . [Online]. Available: .

[229] R. A. Konoplya and A. Zhidenko, "Quasinormal modes of black holes: From astrophysics to string theory," *Rev. Mod. Phys.*, vol. 83, pp. 793–836, 3 Jul. 2011. DOI: . [Online]. Available: .

[230] L. Landau and E. Lifshitz, "Chapter vii - the quasi-classical case," in *Quantum Mechanics (Third Edition)*, L. Landau and E. Lifshitz, Eds., Pergamon, 1977, ISBN: 978-0-08-020940-1. DOI: . [Online]. Available: .

[231] S. Chandrasekhar and S. Chandrasekhar, *The mathematical theory of black holes*. Oxford university press, 1998, vol. 69.

[232] S. Iyer and C. M. Will, "Black-hole normal modes: A wkb approach. i. foundations and application of a higher-order wkb analysis of potential-barrier scattering," *Phys. Rev. D*, vol. 35, pp. 3621–3631, 12 Jun. 1987. DOI: . [Online]. Available: .

[233] W. G. Unruh, "Notes on black-hole evaporation," *Phys. Rev. D*, vol. 14, pp. 870–892, 4 Aug. 1976. DOI: . [Online]. Available: .

[234] L. Susskind and J. Lindesay, "An introduction to black holes, information and the string theory revolution," in. World Scientific, 2004.

[235] V. Mukhanov and S. Winitzki, *Introduction to Quantum Effects in Gravity*. Cambridge University Press, 2007. DOI: .

[236] P. Betzios, N. Gaddam, and O. Papadoulaki, "The black hole s-matrix from quantum mechanics," *J. High Energy Phys.*, vol. 2016, no. 11, p. 131, 2016. DOI: . [Online]. Available: .

[237] S. S. Hegde, V. Subramanyan, B. Bradlyn, and S. Vishveshwara, "Quasinormal modes and the hawking-unruh effect in quantum hall systems: Lessons from black hole phenomena," *Phys. Rev. Lett.*, vol. 123, p. 156 802, 15 Oct. 2019. DOI: . [Online]. Available: .

[238] B. P. Abbott and *et. al.*, "Observation of gravitational waves from a binary black hole merger," *Phys. Rev. Lett.*, vol. 116, p. 061 102, 6 Feb. 2016. DOI: . [Online]. Available: .

[239] B. P. Abbott and *et. al.*, "Gw170817: Observation of gravitational waves from a binary neutron star inspiral," *Phys. Rev. Lett.*, vol. 119, p. 161 101, 16 Oct. 2017. DOI: . [Online]. Available: .

[240] W. G. Unruh, "Experimental black-hole evaporation?" *Phys. Rev. Lett.*, vol. 46, pp. 1351–1353, 21 May 1981. DOI: . [Online]. Available: .

[241] W. G. Unruh, "Sonic analogue of black holes and the effects of high frequencies on black hole evaporation," *Phys. Rev. D*, vol. 51, pp. 2827–2838, 6 Mar. 1995. DOI: . [Online]. Available: .

[242] S. Weinfurtner, E. W. Tedford, M. C. J. Penrice, W. G. Unruh, and G. A. Lawrence, "Measurement of stimulated hawking emission in an analogue system," *Phys. Rev. Lett.*, vol. 106, p. 021 302, 2 Jan. 2011. DOI: . [Online]. Available: .

[243] F. Michel and R. Parentani, "Probing the thermal character of analogue hawking radiation for shallow water waves?" *Phys. Rev. D*, vol. 90, p. 044 033, 4 Aug. 2014. DOI: . [Online]. Available: .

[244] L.-P. Euvé, F. Michel, R. Parentani, and G. Rousseaux, "Wave blocking and partial transmission in subcritical flows over an obstacle," *Phys. Rev. D*, vol. 91, p. 024 020, 2 Jan. 2015. DOI: . [Online]. Available: .

[245] A. Coutant and S. Weinfurtner, "The imprint of the analogue hawking effect in subcritical flows," *Phys. Rev. D*, vol. 94, p. 064 026, 6 Sep. 2016. DOI: . [Online]. Available: .

[246] M. Visser, "Acoustic black holes: Horizons, ergospheres and hawking radiation," *Class. Quantum Grav.*, vol. 15, no. 6, pp. 1767–1791, Jun. 1998. DOI: . [Online]. Available: .

[247] S. Giovanazzi, "Hawking radiation in sonic black holes," *Phys. Rev. Lett.*, vol. 94, p. 061 302, 6 Feb. 2005. DOI: . [Online]. Available: .

[248] G. Rousseaux, C. Mathis, P. Maïssa, T. G. Philbin, and U. Leonhardt, "Observation of negative-frequency waves in a water tank: A classical analogue to the hawking effect?" *New J. Phys.*, vol. 10, no. 5, p. 053 015, May 2008. DOI: . [Online]. Available: .

[249] O. Lahav, A. Itah, A. Blumkin, C. Gordon, S. Rinott, A. Zayats, and J. Steinhauer, "Realization of a sonic black hole analog in a bose-einstein condensate," *Phys. Rev. Lett.*, vol. 105, p. 240 401, 24 Dec. 2010. DOI: . [Online]. Available: .

[250] J. Steinhauer, "Observation of quantum hawking radiation and its entanglement in an analogue black hole," *Nat. Phys.*, vol. 12, no. 10, pp. 959–965, 2016. DOI: . [Online]. Available: .

[251] J. R. Muñoz de Nova, K. Golubkov, V. I. Kolobov, and J. Steinhauer, "Observation of thermal hawking radiation and its temperature in an analogue black hole," *Nature*, vol. 569, no. 7758, pp. 688–691, 2019. DOI: . [Online]. Available: .

[252] L. J. Garay, J. R. Anglin, J. I. Cirac, and P. Zoller, "Sonic analog of gravitational black holes in bose-einstein condensates," *Phys. Rev. Lett.*, vol. 85, pp. 4643–4647, 22 Nov. 2000. DOI: . [Online]. Available: .

[253] I. Carusotto, S. Fagnocchi, A. Recati, R. Balbinot, and A. Fabbri, "Numerical observation of hawking radiation from acoustic black holes in atomic bose–einstein condensates," *New J. Phys.*, vol. 10, no. 10, p. 103 001, Oct. 2008. DOI: . [Online]. Available: .

[254] T. G. Philbin, C. Kuklewicz, S. Robertson, S. Hill, F. König, and U. Leonhardt, "Fiber-optical analog of the event horizon," *Science*, vol. 319, no. 5868, pp. 1367–1370, 2008. DOI: . eprint: . [Online]. Available: .

[255] J. Drori, Y. Rosenberg, D. Bermudez, Y. Silberberg, and U. Leonhardt, "Observation of stimulated hawking radiation in an optical analogue," *Phys. Rev. Lett.*, vol. 122, p. 010 404, 1 Jan. 2019. DOI: . [Online]. Available: .

[256] C. Sheng, H. Liu, Y. Wang, S. N. Zhu, and D. A. Genov, "Trapping light by mimicking gravitational lensing," *Nat. Photon.*, vol. 7, no. 11, pp. 902–906, 2013. DOI: . [Online]. Available: .

[257] Y.-H. Shi, R.-Q. Yang, Z. Xiang, Z.-Y. Ge, H. Li, Y.-Y. Wang, K. Huang, Y. Tian, X. Song, D. Zheng, K. Xu, R.-G. Cai, and H. Fan, *On-chip black hole: Hawking radiation and curved spacetime in a superconducting quantum circuit with tunable couplers*, 2021. arXiv: .

[258] M. Stone, "An analogue of hawking radiation in the quantum hall effect," *Class. Quantum Grav.*, vol. 30, no. 8, p. 085 003, Mar. 2013. DOI: . [Online]. Available: .

[259] H. A. Fertig and B. I. Halperin, "Transmission coefficient of an electron through a saddle-point potential in a magnetic field," *Phys. Rev. B*, vol. 36, pp. 7969–7976, 15 Nov. 1987. DOI: . [Online]. Available: .

[260] M. A. Nichols, Y.-X. Liu, L. Zhu, M.-G. Hu, Y. Liu, and K.-K. Ni, "Detection of long-lived complexes in ultracold atom-molecule collisions," *Phys. Rev. X*, vol. 12, p. 011 049, 1 Mar. 2022. DOI: . [Online]. Available: .

[261] V. Ferrari and B. Mashhoon, "New approach to the quasinormal modes of a black hole," *Phys. Rev. D*, vol. 30, pp. 295–304, 2 Jul. 1984. DOI: . [Online]. Available: .

[262] V. Subramanyan, S. S. Hegde, S. Vishveshwara, and B. Bradlyn, "Physics of the inverted harmonic oscillator: From the lowest landau level to event horizons," *Annals of Physics*, vol. 435, p. 168 470, 2021, Special issue on Philip W. Anderson, ISSN: 0003-4916. DOI: . [Online]. Available: .

[263] B. Gao, "Solutions of the schrödinger equation for an attractive $1/r^6$ potential," *Phys. Rev. A*, vol. 58, pp. 1728–1734, 3 Sep. 1998. DOI: . [Online]. Available: .

[264] B. Gao, "Quantum-defect theory of atomic collisions and molecular vibration spectra," *Phys. Rev. A*, vol. 58, pp. 4222–4225, 5 Nov. 1998. DOI: . [Online]. Available: .

[265] K. Jachymski, M. Krych, P. S. Julienne, and Z. Idziaszek, "Quantum-defect model of a reactive collision at finite temperature," *Phys. Rev. A*, vol. 90, p. 042 705, 4 Oct. 2014. DOI: . [Online]. Available: .

[266] M. H. G. de Miranda, A. Chotia, B. Neyenhuis, D. Wang, G. Quéméner, S. Ospelkaus, J. L. Bohn, J. Ye, and D. S. Jin, "Controlling the quantum stereodynamics of ultracold bimolecular reactions," *Nat. Phys.*, vol. 7, no. 6, pp. 502–507, 2011. DOI: . [Online]. Available: .

[267] G. Valtolina, K. Matsuda, W. G. Tobias, J.-R. Li, L. De Marco, and J. Ye, "Dipolar evaporation of reactive molecules to below the fermi temperature," *Nature*, vol. 588, no. 7837, pp. 239–243, 2020. DOI: . [Online]. Available: .

[268] K. Matsuda, L. D. Marco, J.-R. Li, W. G. Tobias, G. Valtolina, G. Quéméner, and J. Ye, "Resonant collisional shielding of reactive molecules using electric fields," *Science*, vol. 370, no. 6522, pp. 1324–1327, 2020. DOI: . eprint: . [Online]. Available: .

[269] J.-R. Li, W. G. Tobias, K. Matsuda, C. Miller, G. Valtolina, L. De Marco, R. R. W. Wang, L. Lassablière, G. Quéméner, J. L. Bohn, and J. Ye, "Tuning of dipolar interactions and evaporative cooling in a three-dimensional molecular quantum gas," *Nat. Phys.*, vol. 17, no. 10, pp. 1144–1148, 2021. DOI: . [Online]. Available: .

[270] H. Son, J. J. Park, Y.-K. Lu, A. O. Jamison, T. Karman, and W. Ketterle, "Control of reactive collisions by quantum interference," *Science*, vol. 375, no. 6584, pp. 1006–1010, 2022. DOI: . eprint: . [Online]. Available: .

# VITA

**Education**

- Aug 2017 - Aug 2022, Doctor of Philosophy, Physics
  Department of Physics and Astronomy, Purdue University
  West Lafayette, Indiana, USA
  Advisor: Professor Qi Zhou

- Sep 2013 - Jun 2017: Bachelor of Science, Physics (with Honours, First Class)
  The Chinese University of Hong Kong
  Hong Kong, China

**Awards**

- Karl Lark-Horovitz Award, Department of Physics and Astronomy,
  Purdue University, May. 2022.

**Publications**(†equal contributions)

- An eternal discrete time crystal beating the Heisenberg limit
  Changyuan Lyu, Sayan Choudhury, **Chenwei Lv**, Yangqian Yan,
  and Qi Zhou
  Physical Review Research, 2(3), 033070

- Geometrizing quantum dynamics of a Bose-Einstein Condensate
  Changyuan Lyu†, **Chenwei Lv**†, and Qi Zhou
  Physical Review Letters, 125(25), 253401

- SU(1,1) Echoes for Breathers in Quantum Gases
  **Chenwei Lv**†, Ren Zhang†, and Qi Zhou
  Physical Review Letters 125 (25), 253002

- Universal relations for ultracold reactive molecules
  Mingyuan He†, **Chenwei Lv**†, Hai-Qing Lin, and Qi Zhou
  Science Advances, 6(51), eabd4699

- Efimov-like states and quantum funneling effects on synthetic hyperbolic surfaces
  Ren Zhang†, **Chenwei Lv**†, Yangqian Yan, and Qi Zhou
  Science Bulletin 66 (19), 1967-1972

- Curving the space by non-Hermiticity
  **Chenwei Lv**†, Ren Zhang†, Zhengzheng Zhai, and Qi Zhou
  Nature Communications 13 (1), 1-6

- Losses, Many-Body Correlations, and Universality in Ultracold Molecules
  Mingyuan He†, **Chenwei Lv**†, and Qi Zhou
  Advanced Quantum Technologies 5 (4), 2100117

- Quantum Dynamics of Cold Atomic Gas with $SU(1,1)$ Symmetry
  Jing Zhang, Xiaoyi Yang, **Chenwei Lv**, Shengli Ma, and Ren Zhang
  arXiv preprint arXiv:2201.04304

- Analogue Black Holes in Reactive Molecules
  Ren Zhang†, **Chenwei Lv**†, and Qi Zhou
  arXiv preprint arXiv:2204.04595

- Universal relations for dilute systems with two-body decays in reduced dimensions
  Mingyuan He, **Chenwei Lv**, and Qi Zhou
  arXiv preprint arXiv:2204.13300

- Emergent spacetimes from Hermitian and non-Hermitian quantum dynamics
  **Chenwei Lv** and Qi Zhou
  arXiv preprint arXiv:2205.07429